Precambrian Research 377 (2022) 106691

Contents lists available at ScienceDirect

Precambrian Research

journal homepage: www.elsevier.com/locate/precamres

A microfossil assemblage from the Ediacaran Doushantuo Formation in the Shennongjia area (Hubei Province, South China): Filling critical paleoenvironmental and biostratigraphic gaps

Qin Ye [a,b,*], Jiaqi Li [a], Jinnan Tong [a], Zhihui An [c], Jun Hu [a], Shuhai Xiao [d,*]

[a] State Key Laboratory of Biogeology and Environmental Geology, School of Earth Sciences, China University of Geosciences, Wuhan 430074, China
[b] State Key Laboratory of Palaeobiology and Stratigraphy (Nanjing Institute of Geology and Palaeontology, CAS), Nanjing 210008, China
[c] Hubei Key Laboratory of Paleontology and Geological Environment Evolution, Wuhan Center of China Geological Survey, Wuhan 430205, China
[d] Department of Geosciences, Virginia Tech, Blacksburg, VA 24061, USA

ARTICLE INFO

Keywords:
Acanthomorphic acritarchs
Multicellular algae
Carbon isotopes
Ediacaran biostratigraphy
Shennongjia area
South China

ABSTRACT

Microfossils of the Ediacaran Doushantuo Formation in South China provide an important window onto the rapid diversification of marine eukaryotes after the terminal Cryogenian global glaciation. They also offer key data in the biostratigraphic subdivision and correlation of the lower–middle Ediacaran System. Previously published Doushantuo microfossils in South China were mostly from intra-shelf facies in the Yangtze Gorges area, shelf margin facies in the Weng'an area, and upper slope facies in the Zhangjiajie area, whereas paleontological data from shallow-water inner shelf facies have been rarely documented. In addition, previous data from South China leave a "barren zone" associated with the negative $\delta^{13}C_{carb}$ excursion EN2 that impedes biostratigraphic correlation. To address these environmental and stratigraphic gaps, we conducted an integrated chemostratigraphic and biostratigraphic analysis of the Doushantuo Formation at the inner shelf Lianhuacun section in the eastern Shennongjia area of Hubei Provence, South China. The Lianhuacun fossils are preserved in chert nodules/bands of the lower Doushantuo Formation, precisely in a chemostratigraphic interval identified as EN2, indicating that the so-called "barren zone" is likely a taphonomic artifact. A total of 33 genera and 82 species are identified, including a new genus (*Duospinosphaera* gen. nov.) and seven new species (*Duospinosphaera shennongjiaensis* sp. nov., *D. biformis* sp. nov., *Jixiania retorta* sp. nov., *Mengeosphaera mamma* sp. nov., *Sinosphaera exilis* sp. nov., *Tanarium columnatum* sp. nov., and *Weissiella concentrica* sp. nov.). The Lianhuacun acanthomorphic acritarchs can be broadly assigned to the third microfossil assemblage zone (i.e., the *Tanarium conoideum* – *Cavaspina basiconica* Assemblage Zone) recognized on the basis of the Weng'an biota that is correlated with upper Member II of Doushantuo Formation in the Yangtze Gorges area, consistent with chemostratigraphic correlation between the Shennongjia and Yangtze Gorges areas. Thus, the so-called "barren zone" may be a poorly preserved part of the third microfossil assemblage zone. Alternatively, it may represent a new and yet unnamed microfossil assemblage zone between the third and the overlying *Tanarium pycnacanthum* – *Ceratosphaeridium glaberosum* Assemblage Zone. Regardless, the new data presented here fill important gaps in the geographical, paleoenvironmental, and stratigraphic distributions of Ediacaran acanthomorphic acritarchs in South China. As such, they facilitate integrative chemostratigraphic and biostratigraphic correlation of Ediacaran strata at regional and global scales.

1. Introduction

Ediacaran eukaryotic life diversified in the wake of the terminal Cryogenian snowball Earth glaciation (Cohen and Macdonald, 2015). Of central importance to the paleontological record of this diversification event is a group of early Ediacaran eukaryotic microfossils known as acanthomorphs acritarchs, which are also emerging as an indispensable tool for Ediacaran biostratigraphic correlation (Xiao and Narbonne, 2020). In South China, relatively large acanthomorphic acritarchs (tens to hundreds μm in diameter) appear in the geological record shortly

* Corresponding authors.
E-mail addresses: yeqin@cug.edu.cn (Q. Ye), xiao@vt.edu (S. Xiao).

https://doi.org/10.1016/j.precamres.2022.106691
Received 15 November 2021; Received in revised form 10 February 2022; Accepted 21 April 2022

after the terminal Cryogenian or Marinoan glaciation (Ouyang et al., 2021; Zhou et al., 2007). They then rapidly radiated worldwide as recorded in many Ediacaran successions, including those in South China (e.g., Liu and Moczydłowska, 2019; Liu et al., 2014a; Ouyang et al., 2021; Xiao et al., 2014), Australia (Grey, 2005; Willman and Moczydłowska, 2008, 2011; Willman et al., 2006; Zang and Walter, 1992a), Siberia (Golubkova et al., 2010; Moczydłowska, 2005; Moczydłowska and Nagovitsin, 2012; Moczydłowska et al., 1993; Sergeev et al., 2011; Vorob'eva and Petrov, 2020; Vorob'eva et al., 2008), the East European Platform (Golubkova et al., 2015; Veis et al., 2006; Vorob'eva et al., 2009a, b), India (Joshi and Tiwari, 2016; Prasad and Asher, 2016; Shukla and Tiwari, 2014; Tiwari and Knoll, 1994; Xiao et al., 2022), Svalbard (Knoll, 1984, 1992; Knoll et al., 1991), and Southern Norway (Vidal, 1990), although some taxa may extend to the Cambrian Period (Anderson et al., 2017a, 2019; Anttila and Macdonald, 2020; Grazhdankin et al., 2020). Together with other Ediacaran eukaryotic fossils, acanthomorphs help us to better understand the tempo and mode of post-Cryogenian evolution and the diversification of eukaryotes (e.g., Chen et al., 2014; Cohen et al., 2009; Moczydłowska and Willman, 2009; Xiao et al., 1998; Yin et al., 2007b) and to improve early–middle Ediacaran biostratigraphic subdivision and global correlation (e.g., Grey, 2005; Liu and Moczydłowska, 2019; Liu et al., 2013, 2014a, b; McFadden et al., 2009; Xiao et al., 2014, 2016; Yin et al., 2009b).

Over the past three decades, diverse microfossils have been recovered from chert nodules and phosphorites of the Ediacaran Doushantuo Formation deposited in different paleogeographic and sedimentary environments of South China (Fig. 1A–B; Jiang et al., 2011; Muscente et al., 2015). The best-known and most-studied Doushantuo microfossils are the silicified microfossils from the Yangtze Gorges area in western Hubei Province (e.g., Liu and Moczydłowska, 2019; Liu et al., 2014a; Ouyang et al., 2021; Xiao et al., 2012) and phosphatized microfossils from the Weng'an area in central Guizhou Province (e.g., Xiao et al., 2014; Yuan and Hofmann, 1998; Zhang et al., 1998a). Less celebrated assemblages of silicified microfossils have also been reported from several other localities (red circles in Fig. 1B), including the Changyang section in western Hubei Province (Liu et al., 2021), the Liujing section in northwestern Guizhou Province (Shang et al., 2019), as well as the Siduping, Tianping, and Lujiayuanzi sections in the Zhangjiajie area of Hunan Province (Hawkins et al., 2017; Nie et al., 2017; Ouyang et al., 2017; Shang and Liu, 2020). Additionally, a number of minor assemblages of phosphatized microfossils are known from several additional localities in South China (blue triangles in Fig. 1A–C), including the Chadian section in southern Shanxi Province (Chen and Liu, 1986; Xiao et al., 1999), the Chaoyang section in eastern Jiangxi Province (Zhou et al., 2002), as well as the Baizhu section (Yang et al., 2020; Yin et al., 2009c; Zhou et al., 2001, 2004) and the Zhangcunping section (Liu et al., 2009b; Ye et al., 2015; Zhou et al., 2005) in western Hubei Province. Mainly based on data from the Yangtze Gorges area, several different schemes of acanthomorph biostratigraphic zonation have been proposed (Liu and Moczydłowska, 2019; Liu et al., 2014a; McFadden et al., 2009). However, their application in biostratigraphic correlation around and beyond the Yangtze Gorges area in South China has met with limited success.

Currently available micropaleontological data of the Doushantuo Formation mostly come from cherts and phosphorites in strata deposited in the intra-shelf, shelf margin, and upper slope facies (Fig. 1A–B; Jiang et al., 2011; Muscente et al., 2015). In comparison, Doushantuo strata deposited in an inner shelf setting have not been as thoroughly explored for microfossils. In addition, because of preservational biases associated with silicification and phosphatization (Xiao et al., 2012, 2014), stratigraphic distribution of Doushantuo microfossils is not continuous. Indeed, a biostratigraphic "barren zone" has been known from many Doushantuo sections in the Yangtze Gorges area (Liu and Moczydłowska, 2019; Liu et al., 2013, 2014a; McFadden et al., 2009). This "barren zone" represents a significant gap hampering a full view of biostratigraphic zonation. To fill these knowledge gaps and to achieve a better

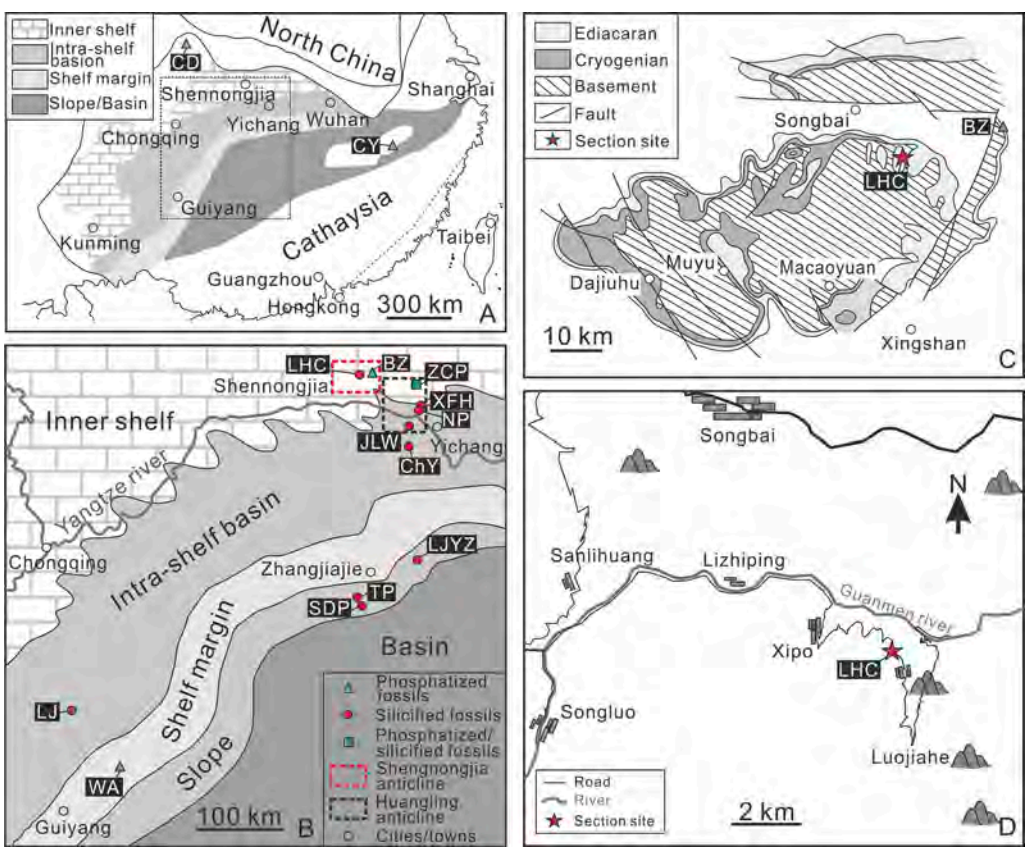

Fig. 1. Paleogeographic, geological, and section locality maps. (A) Paleogeographic map of the Yangtze block in the Ediacaran Period. Patterns and different shades of gray denote different facies. (B) Magnified view of area marked by rectangle in (A), showing approximate location of fossiliferous sections mentioned in the text. (A–B) Modified from Jiang et al. (2011). The Doushantuo Formation at eastern Shennongjia area was deposited in an inner shelf setting (Gu et al., 2021). Red and black rectangles in (B) mark location of the Shennongjia and Huangling anticlines, respectively, with the Yangtze Gorges area located in the southeastern quarter of the Huangling anticline. (C) Magnified view of area marked by red rectangle in (B), showing a simplified geological map of the Shennongjia area, the location of the studied Lianhuacun section (star), as well as the location of the nearby Baizhu section (triangle). (D) Locality map of the Lianhuacun section (star) in the eastern Shennongjia area. Abbreviations of section localities: BZ: Baizhu; CD, Chadian; ChY: Changyang; CY: Chaoyang; JLW, Jiulongwan; LHC: Lianhuacun; LJYZ: Lujiayuanzi; LJ: Liujing; NP: Niuping; SDP, Siduping; TP, Tianping; WA, Weng'an; XF, Xiaofenghe; ZCP, Zhangcunping.

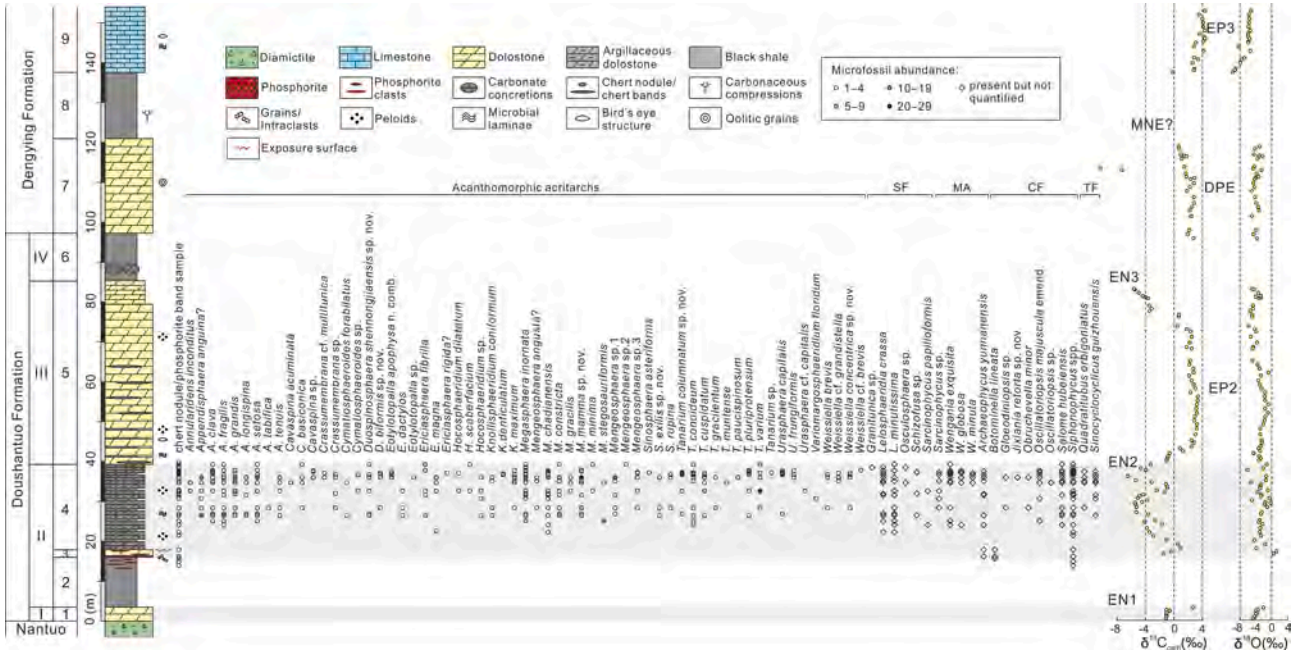

Fig. 2. Lithostratigraphy, sampling horizons, microfossils distribution, and chemostratigraphy of the Lianhuacun section. Stratigraphic units 1–9 and stratigraphic heights (in meters) are marked. The subdivision of the Doushantuo Formation into four members follows An et al. (2015) and Gu et al. (2021). Abbreviations: CF: cyanobacterial fossils; MA: multicellular algae; SF: spheroidal microfossils; TF: tubular microfossils.

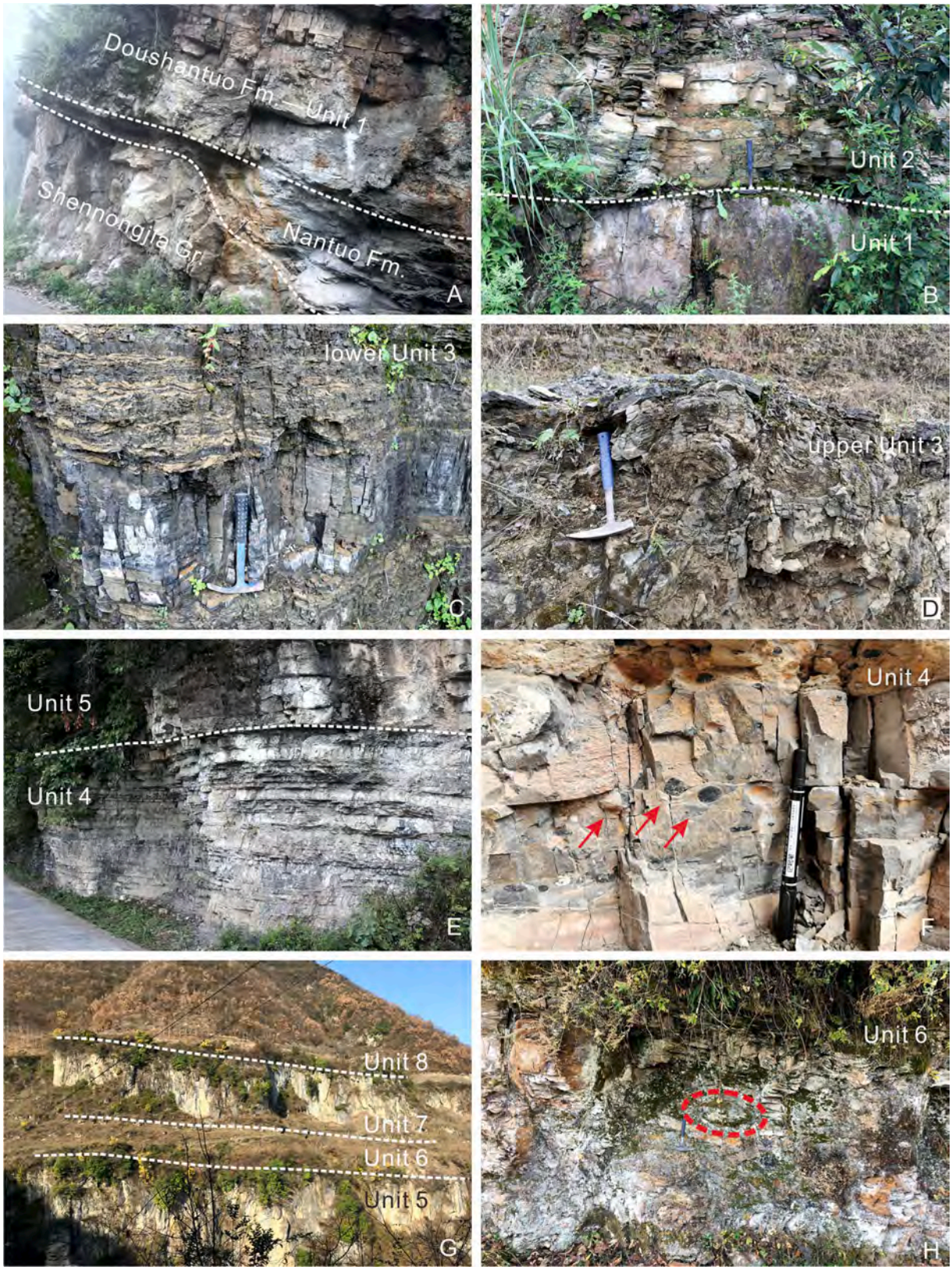

Fig. 3. Field photographs of the Shennongjia Group and Nantuo–Doushantuo–Dengying formations at the Lianhuacun section. (A) Outcrop showing stratigraphic contacts between dolostone of the Shennongjia Group, diamictite of the Nantuo Formation, and the cap dolostone (Unit 1) of the basal Doushantuo Formation. (B) Unit 1 (cap dolostone) and Unit 2 (black shale). (C) Lower phosphorite unit and phosphatic argillaceous dolostone of Unit 3. (D) Uneven surface on top of Unit 3, interpreted to be a subaerial exposure or erosional surface. (E) Unit 4 (dark-colored, thin-bedded dolostone intercalated with shale) and Unit 5 (light-colored medium- to thick-bedded dolostone). (F) Unit 4 with abundant chert nodules (red arrows) in argillaceous dolostone. (G) Distant view of units 6–9, with the Doushantuo–Dengying boundary placed between Unit 6 and Unit 7. (H) Black shale with carbonate concretions (red circle) in Unit 6.

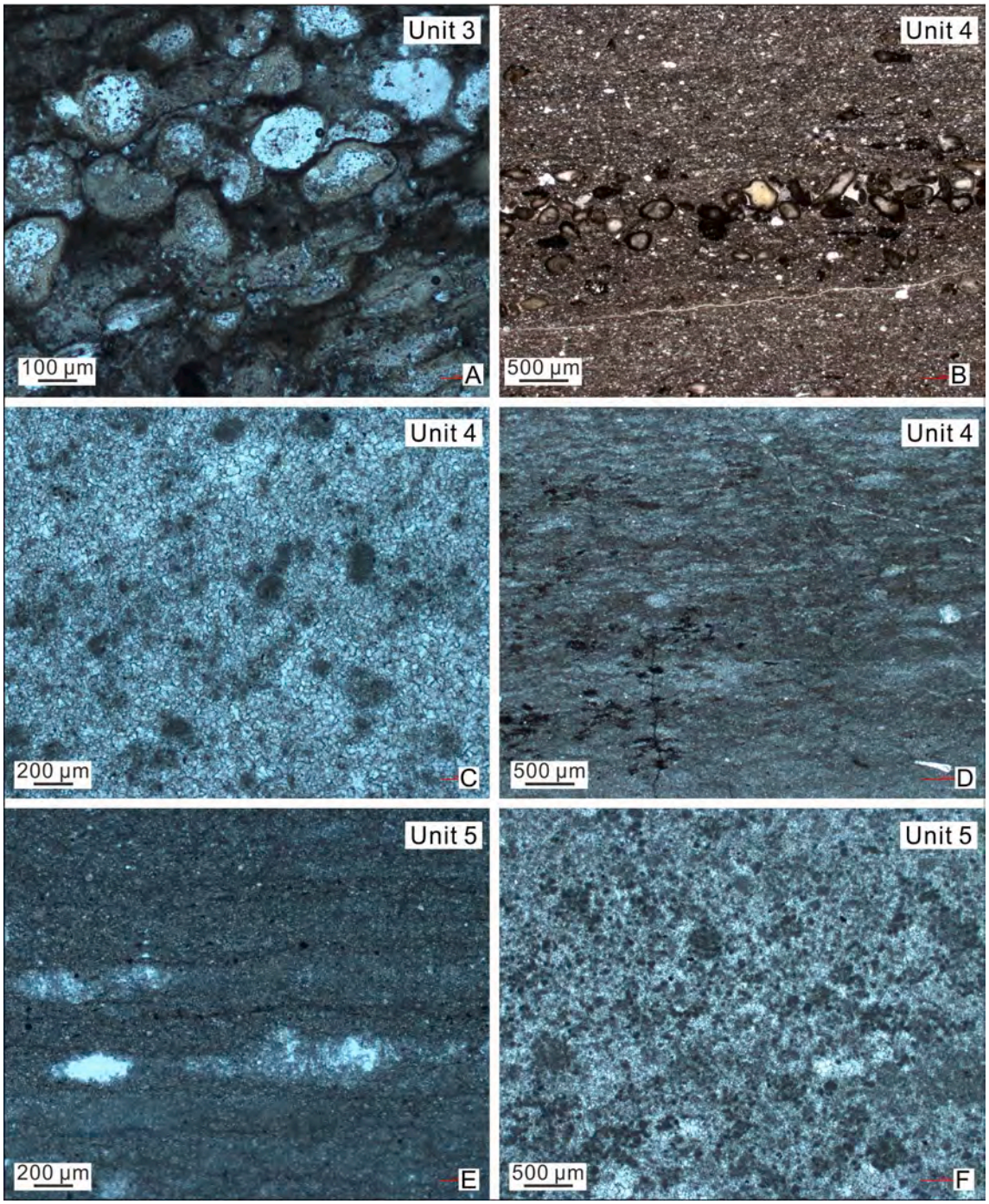

Fig. 4. Representative thin-section petrographic photomicrographs (plane-polarized light) of the Doushantuo Formation at the Lianhuacun Section in eastern Shennongjia area. (A) Granular phosphorite, Unit 3. (B) Micritic dolostone with phosphatic grains, lower Unit 4. (C) Dolomicrosparite with peloids, lower-middle Unit 4. (D) Dolomicrite with crinkled microbial laminae, upper Unit 4. (E) Bird's-eye structures in dolomicrite, Unit 5. (F) Peloidal dolomicrite, Unit 5. All photographs are courtesy of Haodong Gu.

understanding of the spatial and temporal distribution of Doushantuo microfossils, we carried out an integrated lithostratigraphic, carbon isotope chemostratigraphic, and paleontological investigation of the Doushantuo Formation in inner shelf facies at the Lianhuacun section of the Shennongjia area in western Hubei Province, South China (Gu et al., 2021). The new data not only expand the paleogeographical range of the Ediacaran microfossils, but also demonstrate the presence of acanthomorphs in the $\delta^{13}C_{carb}$ chemostratigraphic interval EN2—previously regarded as a biostratigraphically "barren zone", thus providing key biostratigraphic data for regional correlation of Ediacaran successions in South China.

2. Geological background

The Ediacaran succession in South China was deposited in a passive continental margin setting on the Yangtze block with mixed siliciclastic and carbonate rocks (Jiang et al., 2011). It consists of Doushantuo and Dengying formations that overlie the terminal Cryogenian glacial diamictites of the Nantuo Formation and are overlain by basal Cambrian strata. The Shennongjia area is located in the northern part of the

Yangtze block, ~18 km northwest of the Huangling anticline (Fig. 1A–B), and it was paleogeographically located in the inner shelf facies in the Ediacaran Period (Gu et al., 2021). Here, the Mesoproterozoic Shennongjia Group forms the core of the Shennongjia anticline and is surrounded by late Neoproterozoic to Phanerozoic strata (Fig. 1C). Phosphorite and chert nodules/bands in the Doushantuo Formation in the Shennongjia area have not been explored for microfossils, although microfossils have been discovered in similar lithofacies in Doushantuo phosphorites in the nearby Baizhu area (Yang et al., 2020; Yin et al., 2009c; Zhou et al., 2001, 2004). In this study, we logged and sampled the Doushantuo Formation and part of the Dengying Formation at the Lianhuacun section (31°40′57.37″N, 110°42′45.58″E, Fig. 1D, 2) in the eastern Shennongjia area for $\delta^{13}C_{carb}$ chemostratigraphic and microfossil analyses.

The logged Doushantuo-Dengying formations at the Lianhuacun section can be subdivided into nine lithostratigraphic units (Fig. 2). At the base is Unit 1 (~3.5 m thick), which directly overlies the Cryogenian Nantuo Formation diamictites (Fig. 3A) or the Mesoproterozoic Shennongjia Group dolostones where the Nantuo Formation is missing. This unit is characterized by thick-bedded dolostone (Fig. 3A–B) and is considered as the basal Ediacaran cap dolostone. The overlying Unit 2 (~12.5 m thick) consists of black shale with phosphorite clasts at the top (Fig. 3B). Unit 3 is an ore-grade phosphorite unit, consisting of phosphorite bands intercalated with phosphatic argillaceous dolostone (Fig. 3C). Phosphorite is granular and consists of ellipsoidal to irregularly shaped phosphatic grains (Fig. 4A), indicating that the phosphorite was reworked from a pristine phosphorite (Schwid et al., 2020). The thickness of this unit varies from ~ 0.4 m to ~ 6.3 m (Gu et al., 2021), and this variation is partly due to the local presence of an uneven surface (likely a subaerial exposure surface or an erosional surface) atop this unit (Fig. 3D). Unit 4 (~21.4 m thick) is characterized by alternating thinly bedded dolostone and black shale with abundant pea-sized phosphatic chert nodules (Fig. 3E–F). It also contains phosphatic grains (Fig. 4B), as well as peloids (Fig. 4C) and crinkled microlaminae (Fig. 4D) that may represent microbial laminae. Unit 5 (~46.0 m thick) is composed of medium to thick-bedded dolostone with chert bands at the base (Fig. 3G). Bird's-eye structures (Fig. 4E) and peloids (Fig. 4F) are common in this unit. The lithostratigraphic boundary between Unit 4 and Unit 5 is easily recognizable in the eastern Shennongjia area, and can be used for local stratigraphic correlation (Fig. 3E). Above Unit 5, there are two black shale intervals separated by a dolostone unit (Fig. 3G), which are regarded as Unit 6, Unit 7, and Unit 8, respectively (Fig. 2). Unit 6 is about 12.0 m thick and consists of shales with decimeter-sized carbonate concretions (Fig. 3H), lithologically similar to Member IV of the uppermost Doushantuo Formation in the Yangtze Gorges area (Dong et al., 2008). Unit 7 is composed of ~ 23.7 m of light grey, thick-bedded dolostones with abundant oolitic and intraclastic grains (see Fig. 4g of Gu et al., 2021). Unit 8 consists of ~ 16.6 m of black shales and contains abundant macroscopic carbonaceous compression fossils which are taxonomically similar to the Miaohe biota (Xiao et al., 2002; Ye et al., 2019). Unit 8 is overlain by Unit 9, which consists of dark grey, thin-bedded argillaceous limestone with bird's-eye structures and microbial laminae (see Fig. 4h of Gu et al., 2021). The occurrence of microbial laminae, phosphatic grains, peloids, and bird's-eye structures in Doushantuo carbonates at the Lianhuacun section (Fig. 4) indicates deposition in a generally shallow-water environment, consistent with the inner shelf facies as inferred from a paleogeographic reconstruction proposed by Jiang et al. (2011).

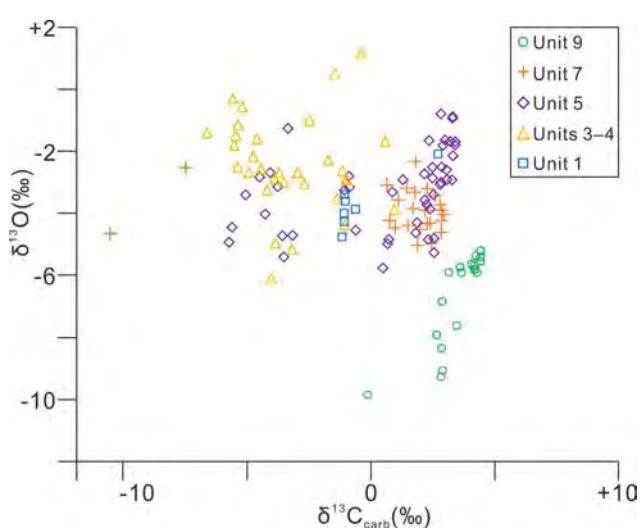

Fig. 5. Cross-plots of $\delta^{13}C$ and $\delta^{18}O$ data for different lithostratigraphic units of the Doushantuo and Dengying formations at the Lianhuacun section.

3. Material and methods

Phosphorite clasts, phosphorites, and chert nodules in units 2–4 were intensively sampled for micropaleontological analysis (Fig. 2). Only one horizon of chert nodules was obtained from Unit 5 because of poor accessibility on a steep cliff (Fig. 3G). Totally, there were 35 sampled horizons, including 5 phosphorite and 30 chert nodule/band horizons. All samples were cut both perpendicular and parallel to the bedding plane, and a total of 1034 petrographic thin sections—each approximately 50 μm in thickness—were prepared for microfossil observation. Microfossils were examined and photographed under a transmitted light microscope. Measurements were made on photomicrographs using Image J (http://imagej.nih.gov/ij). All rock samples and thin sections are reposited at the China University of Geosciences (Wuhan), China.

A total of 129 carbonate samples were collected from the Lianhuacun section for carbon and oxygen isotope analysis (Figs. 2, 5). Powders were micro-drilled from these samples and isotopic analysis was performed in the State Key Lab of Biogeology and Environmental Geology (BGEG) at the China University of Geosciences (Wuhan). About 100–300 μg powder of each sample was loaded into a 10 mL Na-glass vial, sealed with a butyl rubber septum, and allowed to react with 100% phosphoric acid at 72 °C after flushing with helium. The evolved CO_2 gas was subsequently introduced into a MAT 253 isotope ratio mass-spectrometer via a Finnigan GasBench II interface for isotopic analysis. $\delta^{13}C$ and $\delta^{18}O$ are expressed as per mil (‰) relative to the Vienna Pee Dee Belemnite (VPDB) standard with an analytical precision better than ± 0.1‰, as monitored by duplicate analyses of two laboratory standards (GBW 04416 and GBW 04417).

4. Results

4.1. Paleontological data

Stratigraphic occurrences of microfossils from the Lianhuacun section are shown in Fig. 2 and Table 1 (Supplementary Table). Composite stratigraphic ranges of the Lianhuacun taxa, on the basis of published data (see occurrence information in Systematic Paleontology; Table 2) and new data reported in this paper, are compiled from South China and projected to the Doushantuo stratocolumn in the Yangtze Gorges area as represented by the Jiulongwan section (Fig. 6).

At the Lianhuacun section, only coccoidal and filamentous microfossils (e.g., *Archaeophycus yunnanensis*, *Botominella lineata*, and *Siphonophycus* spp.), but no acanthomorphs, were recovered from Units 2–3 phosphorite samples. In contrast, abundant microfossils are present in Unit 4 chert nodules, and these include large acanthomorphic acritarchs (Figs. 7–50), sphaeromorphic acritarchs (Fig. 51A–C, E–K), multicellular thalli (Fig. 52B–K, 53), coccoidal and filamentous cyanobacteria (Fig. 51D, 52A, 54), and tubular fossils (Fig. 55). These silicified microfossils were recovered from chert nodules (Fig. 3F) that were formed during early diagenesis (Xiao et al., 2010). Overall, the

Table 2
Acanthomorph taxa in the Lianhuacun assemblage and their distribution in other Ediacaran successions. Abbreviations stand for: YG, the Yangtze Gorges area; II and III, members II and III of the Doushantuo Formation, respectively; WA, Weng'an area; BK, Baokang area; ZJJ, Zhangjiajie area; SL, Songlin area; SR, Shangrao area; MX, Mianxian area. Black: absent. See occurrences in Systematic Paleontology for source of data.

Species of acritarchs	number of specimens @ Lianhuacun	South China								Siberia	East European Platform	Australia	India	Mongolia	Svalbard
		YG		WA	BK	ZJJ	SR	MX	SL						
		Member II	Member III												
Annularidens inconditus	2	○													
Appendisphaera anguina?	29		○									○			
Appendisphaera clava	23	○	○							○			○		
Appendisphaera fragilis	48	○		○					○	○		○	○	○	
Appendisphaera grandis	54	○	○	○		○			○	○		○	○	○	
Appendisphaera longispina	8	○	○						○				○		
Appendisphaera setosa	32	○	○						○	○			○		
Appendisphaera tabifica	4	○	○							○	○	○	○		
Appendisphaera tenuis	12	○	○	○		○			○	○		○	○	○	
Cavaspina acuminata	1	○	○	○		○			○	○	○	○	○		
Cavaspina basiconica	6		○	○		○			○	○		○	○	○	
Cavaspina sp.	3														
Crassimembrana cf. *multitunica*	2	○													
Crassimembrana sp.	12														
Cymatiosphaeroides forabilatus	3	○							○				○		
Cymatiosphaeroides sp.	2														
Duospinosphaera shennongjiaensis sp. nov.	17														
Duospinosphaera biformis sp. nov.	8														
Eotylotopalla apophysa n. comb.	8										○				
Eotylotopalla dactylos	4	○	○	○									○		
Eotylotopalla sp.	1		○												
Ericiasphaera fibrilla	26	○							○						
Ericiasphaera magna	10	○	○	○		○									
Ericiasphaera rigida?	1	○													
Hocosphaeridium dilatatum	2		○												
Hocosphaeridium scaberfacium	4		○	○								○			
Hocosphaeridium sp.	5														
Knollisphaeridium coniformum	6	○													
Knollisphaeridium denticulatum	2		○						○						
Knollisphaeridium maximum	13	○	○	○	○	○				○		○	○		○
Megasphaera inornata	75	○		○	○	○	○		○					○	
Mengeosphaera angusta ?	4		○												
Mengeosphaera chadianensis	51	○	○	○	○		○	○	○						
Mengeosphaera constricta	16		○												
Mengeosphaera gracilis	3	○	○			○			○				○		
Mengeosphaera mamma sp. nov.	43	○													
Mengeosphaera minima	2	○	○												
Mengeosphaera stegosauriformis	18		○												
Mengeosphaera sp. 1	21														
Mengeosphaera sp. 2	1														
Mengeosphaera sp. 3	8														
Sinosphaera asteriformis	1	○	○												
Sinosphaera exilis sp. nov.	3														
Sinosphaera rupina	5		○												
Tanarium columnatum sp. nov.	18														
Tanarium conoideum	22		○	○					○	○					
Tanarium cuspidatum	17	○	○			○			○						
Tanarium gracilentum	2	○					○								
Tanarium muntense	1	○	○							○		○			
Tanarium paucispinosum	1	○	○									○			

(*continued on next page*)

Table 2 (*continued*)

Species of acritarchs	number of specimens @ Lianhuacun	South China							Siberia	East European Platform	Australia	India	Mongolia	Svalbard
		YG		WA	BK	ZJJ	SR	MX	SL					
		Member II	Member III											
Tanarium pluriprotensum	8	○							○	○				
Tanarium varium	37	○	○			○					○			
Tanarium sp.	1													
Urasphaera capitalis	11									○				
Urasphaera cf. *capitalis*	1													
Urasphaera fungiformis	5		○			○								
Variomargosphaeridium floridum	1		○							○				
Weissiella brevis	3	○		○					○			○		
Weissiella cf. *brevis*	1													
Weissiella cf. *grandistella*	4	○	○											
Weissiella concentrica sp. nov.	4													

Lianhuacun microfossils are relatively well preserved, although some acanthomorphic species are deformed and fragmented.

Acanthomorphs are abundant and taxonomically diverse. A total of 17 genera and 61 species are described. The top three most speciose genera are *Mengeosphaera* (Figs. 31–38), *Tanarium* (Figs. 41–46), and *Appendisphaera* (Fig. 7D–K, 8–12), which contain 27 species (four unnamed species included). They are also the top three most abundant genera, accounting for 65.8% of the acanthomorph specimens in our collection. A new genus (*Duospinosphaera* gen. nov.) and its two constituent species (*Duospinosphaera shennongjiaensis* sp. nov. and *D. biformis* sp. nov.; Figs. 18–22) are described. This new genus is characterized by two types of hollow processes (bimorphic), with small cylindrical processes hanging on the inner surface of the vesicle wall whereas large conical or biform processes are irregularly distributed on the outer surface of the vesicle wall. In comparison, *Sinosphaera exilis* sp. nov. (Fig. 40), a new species also characterized by biform processes, has long and slender conical processes sparsely interspersed among short and small processes, and both types of its processes are distributed on the outer surface of the vesicle wall. Three additional new acanthomorph species are described. *Mengeosphaera mamma* sp. nov. has distinct biform processes with a strongly inflated basal expansion and a relatively short broad apical spine with a blunt tip (Figs. 35–36). *Tanarium columnatum* sp. nov. is characterized by densely arranged, basally connected, large, and long conical processes (Fig. 41). The characteristic features of *Weissiella concentrica* sp. nov. are its conical processes with transverse cross-walls and spheroidal vesicle with concentric double walls (Fig. 50).

Simple sphaeromorphic acritarchs sparsely occur in the chert nodules and they are assigned to *Leiosphaeridia* spp., *Granitunica* sp., *Osculosphaera* sp., and *Schizofusa* sp. They are characterized by a smooth vesicle wall (*Leiosphaeridia*; Fig. 51A–C, E–F), or a thick-walled vesicle with granular texture (*Granitunica*; Fig. 51G–I), or a vesicle with one or two apertures (*Osculosphaera*; Fig. 51K), or a vesicle with a slitlike medial split and an outer membrane (*Schizofusa*; Fig. 51J).

Multicellular thalli were also recovered from Lianhuacun chert nodules, including two genera and five species. The genus *Wengania* is characterized by a spherical thallus with tightly packed spheroidal to cuboidal cells (Fig. 53), whereas *Sarcinophycus* is recognized by its irregular thallus with cell packets arranged in rows and sometimes with morphologically distinct peripheral cells (Fig. 52B–K).

Coccoidal and filamentous cyanobacterial fossils are common in our collection and they occur individually, in clusters, or in fragments of microbial mats. Coccoidal cyanobacteria include *Archaeophycus yunnanensis* (Fig. 52A) and *Gloeodiniopsis* sp. (Fig. 51D), whereas filamentous cyanobacteria are represented by *Botominella lineata* (Fig. 54G), *Jixiania retorta* sp. nov. (Fig. 54A–D), *Obruchevella minor* (Fig. 54K), *Oscillatoriopsis* spp. (Fig. 54E–F, J), *Salome hubeiensis* (Fig. 54H–I), *Siphonophycus* spp. (Fig. 54L–M), and some unidentifiable tubular fragments. Of these, the first five taxa are typically preserved individually, whereas *Siphonophycus* mainly occurs in aggregates and represents tubular sheaths tightly intertwined to form microbial mats (Fig. 54L–M). The new species, *Jixiania retorta* sp. nov., is a tubular structure with numerous closely arranged longitudinal striations (Fig. 54A–D).

Two species of tubular fossils have been found and are here referred to as *Quadratitubus orbigoniatus* and *Sinocyclocyclicus guizhouensis* based on the presence of interspersed complete and incomplete cross-walls with a square transverse cross-section or a cylindrical tube (Fig. 55).

4.2. Carbon isotope chemostratigraphic data

$\delta^{13}C$ data from the Doushantuo and lower Dengying formations at the Lianhuacun section are presented in Figs. 2, 5–6, and Table 3. $\delta^{13}C$ values of Unit 1 (the cap dolostone) are almost exclusively negative (between –1.2‰ and –0.6‰), with only one positive value (+2.7‰) at the topmost cap dolostone. Units 3–4 also yield negative $\delta^{13}C$ values, with a nadir of –6.6‰ at 36.1 m above the base of the Doushantuo

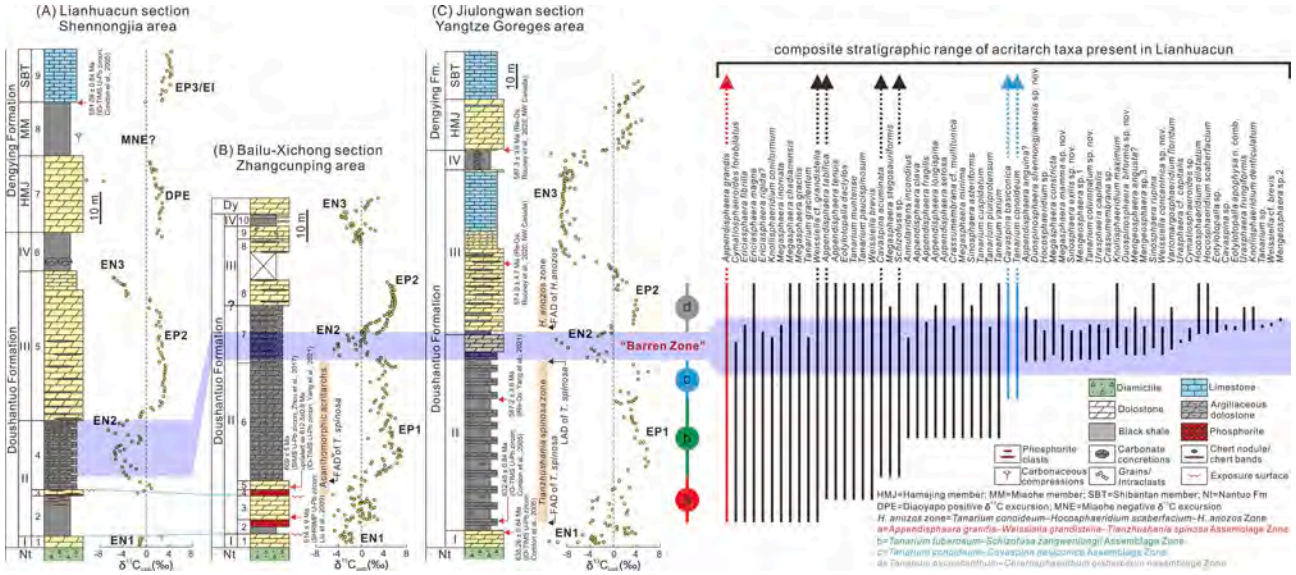

Fig. 6. Integrated $\delta^{13}C$ chemostratigraphic and acritarch biostratigraphic correlation among the (A) Lianhuacun section (eastern Shennongjia area), (B) Bailu and Xichong sections (Zhangcunping area), and the (C) Jilulongwan section (Yangtze Gorges area). $\delta^{13}C$ data for the Bailu, Xichong, and Jiulongwan sections are from Wang et al. (2017), Ouyang et al. (2019), and Jiang et al. (2007) plus An et al. (2015), respectively. Radiometric ages are from Condon et al. (2005), Liu et al. (2009b), Rooney et al. (2020), Yang et al. (2021), and Zhou et al. (2017b). Biostratigraphic data of Bailu-Xichong and Jiulongwan sections are from Ouyang et al. (2019). Solid vertical lines show composite stratigraphic range of Lianhuacun acritarch taxa projected on the Jiulongwan section in the Yangtze Gorges area (see occurrence information in Systematic Paleontology and Table 2; Liu et al., 2014a; Liu and Moczydłowska, 2019). Several species may extend above EN3, as shown by dashed vertical arrows. Important zonal taxa are colored code according to the four acritarch assemblage zones (marked as a, b, c, d) recognized in the Yangtze Gorges area (Liu and Moczydłowska, 2019), where a "barren zone" is present, likely due to taphonomic or environmental biases.

Table 3
Carbon and oxygen isotopic data of the Doushantuo and Dengying formations at the Lianhuacun section.

Sample	Height (m)	Unit	$\delta^{13}C$(‰)	$\delta^{18}O$(‰)
LHC-SBT + 16.4 *m*	152.8	9	4.4	−5.2
LHC-SBT + 15.4 *m*	151.8	9	3.6	−5.7
LHC-SBT + 14.4 *m*	150.8	9	4.1	−5.6
LHC-SBT + 13.4 *m*	149.8	9	4.2	−5.7
LHC-SBT + 12.4 *m*	148.8	9	4.2	−5.8
LHC-SBT + 11.4 *m*	147.8	9	4.4	−5.4
LHC-SBT + 10.6 *m*	147	9	3.7	−5.9
LHC-SBT + 9.9 *m*	146.3	9	4.3	−5.9
LHC-SBT + 9.4 *m*	145.8	9	4.4	−5.5
LHC-SBT + 8.7 *m*	145.1	9	4.2	−5.8
LHC-SBT + 8.4 *m*	144.8	9	3.1	−5.9
LHC-SBT + 7.4 *m*	143.8	9	2.9	−8.3
LHC-SBT + 6.3 *m*	142.7	9	4.3	−5.4
LHC-SBT + 4.6 *m*	141	9	2.9	−6.8
LHC-SBT + 4.2 *m*	140.6	9	3.5	−7.6
LHC-SBT + 3.3 *m*	139.7	9	2.7	−7.9
LHC-SBT + 1.8 *m*	138.2	9	2.9	−9.1
LHC-SBT + 1.5 *m*	137.9	9	2.8	−9.3
LHC-SBT + 1 *m*	137.4	9	−0.1	−9.8
LHC-HMJ-1 *m*	118.8	7	0.7	−3.1
LHC-HMJ-1.6 *m*	118.2	7	0.8	−4.2
LHC-HMJ-3 *m*	116.8	7	1.0	−4.5
LHC-HMJ-3.3 *m*	116.5	7	1.5	−3.2
LHC-HMJ-3.5 *m*	116.3	7	1.8	−2.3
LHC-HMJ-4.1 *m*	115.7	7	1.1	−3.6
LHC-HMJ-6.1 *m*	113.7	7	1.5	−4.4
LHC-HMJ-6.6 *m*	113.2	7	−10.5	−4.6
LHC-HMJ-6.9 *m*	112.9	7	−7.5	−2.5
LHC-HMJ-7.8 *m*	112	7	1.7	−3.8
LHC-HMJ-8.6 *m*	111.2	7	1.8	−3.3
LHC-HMJ-8.9 *m*	110.9	7	2.9	−4.0
LHC-HMJ-9.2 *m*	110.6	7	2.4	−4.3
LHC-HMJ-10.2 *m*	109.6	7	2.8	−4.6
LHC-HMJ-11.2 *m*	108.6	7	2.3	−4.3
LHC-HMJ-12.2 *m*	107.6	7	1.9	−5.0
LHC-HMJ-13.7 *m*	106.1	7	2.9	−4.2
LHC-HMJ-15.2 *m*	104.6	7	2.9	−3.9
LHC-HMJ-16.2 *m*	103.6	7	2.6	−3.4
LHC-HMJ-17 *m*	102.8	7	2.3	−3.2
LHC-HMJ-18.5 *m*	101.3	7	2.5	−5.0
LHC-HMJ-22 *m*	97.8	7	2.2	−3.9
LHC-HMJ-23 *m*	96.8	7	2.0	−4.5
LHC-HMJ-24 *m*	95.8	7	2.8	−3.7
LHC-D3-1 *m*	83.1	5	−5.7	−4.9
LHC-D3-1.2 *m*	82.9	5	−5.6	−4.4
LHC-D3-2 *m*	82.1	5	−5.1	−3.4
LHC-D3-2.8 *m*	81.3	5	−4.5	−2.8
LHC-D3-3 *m*	81.1	5	−4.3	−4.0
LHC-D3-3.2 *m*	80.9	5	−4.1	−2.7
LHC-D3-3.4 *m*	80.7	5	−3.7	−3.1
LHC-D3-5.2 *m*	78.9	5	−3.6	−4.7
LHC-D3-6 *m*	78.1	5	−3.2	−4.7
LHC-D3-6.5 *m*	77.6	5	−3.5	−5.4
LHC-D3-7.5 *m*	76.6	5	0.7	−4.8
LHC-D3-8 *m*	76.1	5	0.7	−5.0
LHC-D3-10.3 *m*	73.8	5	0.5	−5.8
LHC-D3-11.1 *m*	73	5	1.9	−4.3
LHC-D3-11.7 *m*	72.4	5	2.4	−3.9
LHC-D3-13 *m*	71.1	5	2.6	−5.3
LHC-D3-14.5 *m*	69.6	5	2.3	−3.7
LHC-D3-15.6 *m*	68.5	5	1.8	−4.6
LHC-D3-16 *m*	68.1	5	2.5	−4.8
LHC-D3-19 *m*	65.1	5	2.3	−4.8
LHC-D3-20 *m*	64.1	5	2.2	−3.6
LHC-D3-21 *m*	63.1	5	2.8	−3.1
Sample	Height (m)	Unit	$\delta^{13}C$(‰)	$\delta^{18}O$(‰)
21LHC-1-10*m*	62.1	5	2.8	−0.8
21-LHC-1–10.8*m*	61.3	5	2.2	−2.7
21-LHC-1-12*m*	60.1	5	2.5	−3.4
21LHC-1-13*m*	59.1	5	2.8	−3.0
21-LHC-1-14*m*	58.1	5	3.1	−2.6
21-LHC-1-15*m*	57.1	5	2.3	−1.6
21-LHC-1-16*m*	56.1	5	3.4	−1.8

(*continued on next page*)

Table 3 (*continued*)

Sample	Height (m)	Unit	$\delta^{13}C$(‰)	$\delta^{18}O$(‰)
21LHC-1-17*m*	55.1	5	3.4	−1.7
21-LHC-1-18*m*	54.1	5	3.3	−0.9
21LHC-1-19*m*	53.1	5	3.2	−1.7
21-LHC-1–20.1*m*	52	5	3.3	−0.9
21LHC-1-21*m*	51.1	5	3.0	−1.6
21-LHC-1-22*m*	50.1	5	2.9	−1.8
21-LHC-1-23*m*	49.1	5	3.3	−2.1
21-LHC-1-24*m*	48.1	5	3.3	−2.9
21LHC-1–25.5*m*	46.6	5	3.1	−2.9
21-LHC-1-27*m*	45.1	5	2.5	−2.5
21-LHC-1–27.6*m*	44.5	5	2.9	−2.5
21LHC-1–28.5*m*	43.6	5	2.5	−2.9
21-LHC-1-29*m*	43.1	5	0.9	−3.3
21-LHC-1–29.7*m*	42.4	5	1.3	−2.9
21-LHC-1–30.2*m*	41.9	5	−0.6	−4.5
21LHC-1-31*m*	41.1	5	−0.9	−3.2
21LHC-1–31.5*m*	40.6	5	−0.9	−2.8
21-LHC-1-32*m*	40.1	5	−1.1	−3.2
21-LHC-1-33*m*	39.1	4	−3.3	−1.3
21-LHC-1-34*m*	38.1	4	−4.7	−2.2
21LHC-1–34.4*m*	37.7	4	−4.0	−6.1
21LHC-1-36*m*	36.1	4	−6.6	−1.4
21LHC-1-37*m*	35.1	4	−5.5	−1.5
21LHC-1–37.5*m*	34.6	4	−3.2	−5.2
21LHC-1-38*m*	34.1	4	−1.1	−2.6
21LHC-1–38.5*m*	33.6	4	−1.0	−2.9
21-LHC-1-39*m*	33.1	4	−0.9	−2.9
21-LHC-1–39.5*m*	32.6	4	−2.5	−1.0
21-LHC-1-40*m*	32.1	4	−1.4	−3.5
21-LHC-1–40.6*m*	31.5	4	−4.4	−2.6
21-LHC-1-41*m*	31.1	4	−4.9	−2.7
21-LHC-1–41.5*m*	30.6	4	−5.2	−0.5
21-LHC-1-42*m*	30.1	4	−3.8	−5.0
21LHC-1–42.5*m*	29.6	4	−4.6	−1.6
21LHC-1–42.7*m*	29.4	4	−5.6	−0.3
21-LHC-1-43*m*	29.1	4	−5.5	−1.8
21-LHC-1–43.7*m*	28.4	4	−5.4	−1.1
21-LHC-1-45*m*	27.1	4	−5.4	−2.5
21-LHC-1–45.5*m*	26.6	4	−3.7	−2.7
21-LHC-1-47*m*	25.1	4	−2.7	−3.0
21-LHC-1–47.5*m*	24.6	4	−4.2	−3.2
21-LHC-1-48*m*	24.1	4	−1.7	−2.3
21-LHC-1-49*m*	23.1	4	−3.9	−2.9
21-LHC-1-50*m*	22.1	4	−3.5	−3.0
21LHC-1–50.9*m*	21.2	4	−3.0	−2.7
21LHC-1-52*m*	20.1	4	−1.1	−4.4
21-LHC-1-53*m*	19.1	4	0.6	−1.7
21-LHC-1-54*m*	18.1	4	1.0	−3.9
21-LHC-1–54.8*m*	17.3	3	−0.4	1.2
21-LHC-1–55.4*m*	16.7	3	−1.5	0.5
LHC-DST-cap+3.2*m*	3.2	1	2.7	−2.1
LHC-DST-cap+2.6*m*	2.6	1	−1.1	−3.4
LHC-DST-cap+2.4*m*	2.4	1	−0.6	−3.9
LHC-DST-cap+1.9*m*	1.9	1	−1.0	−3.6
LHC-DST-cap+1.6*m*	1.6	1	−1.1	−4.0
LHC-DST-cap+1*m*	1	1	−1.1	−4.3
LHC-DST-cap+50cm	0.5	1	−1.2	−4.8

Formation. $\delta^{13}C$ values increase and become positive in the lower part of Unit 5, which is largely characterized by positive $\delta^{13}C$ values between + 0.5‰ and 3.3‰ (averaging around + 2.5‰), except the top ~ 8.7 m of Unit 5 where $\delta^{13}C$ values drop to –5.7‰. In Unit 7 and Unit 9 of the Dengying Formation, $\delta^{13}C$ values are mostly positive, between + 0.7‰ and + 4.5‰, with the exception of three negative values.

There is no strong correlation between $\delta^{13}C$ and $\delta^{18}O$ values from the Doushantuo and Dengying formations at the Lianhuacun section (Fig. 5). The lack of correlation and the generally high $\delta^{18}O$ values (particularly for the Doushantuo Formation) indicate that $\delta^{13}C$ values have not been strongly modified by meteoric diagenesis. Moreover, no co-variation between $\delta^{13}C$ and $\delta^{18}O$ is observed for individual stratigraphic units, with the exception of Unit 9 of the Dengying Formation. Thus, we regard the $\delta^{13}C$ values of the Doushantuo Formation as largely primary signals reflecting the carbon isotopic compositions of coeval seawaters. As a result, the Doushantuo $\delta^{13}C$ profile at the Lianhuacun section reveals three negative excursions in Unit 1 (cap carbonate), units 3–4, and upper Unit 5 (Fig. 2), and these excursions can be used for chemostratigraphic correlation.

5. Discussion

5.1. Correlation between the Shennongjia and Zhangcunping areas: Recognizing stratigraphic gaps

Litho- and chemostratigraphy of the Doushantuo Formation are similar between the Shennongjia and Zhangcunping areas (Fig. 6A–B; Gu et al., 2021). Fig. 6 illustrates the stratigraphic correlation between these two areas, using a composite stratigraphic section published in Wang et al. (2017) and Ouyang et al. (2019) to represent the

Doushantuo litho- and chemostratigraphic sequence in the Zhangcunping area. In both Shennongjia and Zhangcunping areas, the Doushantuo Formation begins with the basal Ediacaran cap dolostone (Unit 1, with the chemostratigraphic feature EN1), which is succeeded by a unit of black shale and phosphorite (Unit 2, no $\delta^{13}C$ data available due to inappropriate lithology), and then a karstified dolostone (Unit 3, with highly variable $\delta^{13}C$ values). In the Zhangcunping area, the karstified surface atop Unit 3 is overlain by another phosphorite and then a dolostone unit and an argillaceous dolostone unit with chert nodules and glendonite (An et al., 2018; Wang et al., 2017); together, these Zhangcunping units (units 4–6 of Wang et al., 2017) record a positive $\delta^{13}C$ excursion (EP1; Wang et al., 2017) and preserve an acritarch assemblage with abundant occurrences of *Tianzhushania spinosa* (Ouyang et al., 2019). These units seem to be missing from the Lianhuacun section in the Shennongjia area. Overlying strata in both Shennongjia and Zhangcunping areas are characterized by argillaceous dolostones and dolomitic shale interbeds that record a positive $\delta^{13}C$ excursion (EP2) and then the declining arm of a negative $\delta^{13}C$ excursion (EN3). The Doushantuo Formation in both areas ends by black shales of Member IV (according to stratigraphic nomenclature of An et al., 2015).

The correlation model proposed here implies that much of EP1, which is roughly equivalent to the second acritarch assemblage zone of Liu and Moczydłowska (2019) and the middle Member II in the Yangtze Gorges area, may be missing from the Lianhuacun section. The missing strata is represented by a subaerial exposure surface atop Unit 3 at Lianhuacun, suggesting that resumption of sedimentation above the subaerial exposure surface is asynchronous at a regional scale. The correlation model also implies that, while the Lianhuacun section can help fill one stratigraphic gap, it also has its own gaps, highlighting the need to piece together multiple sections in order to develop a more complete understanding of biological and environmental evolution.

5.2. Correlation between the Shennongjia and Yangtze Gorges areas: Lianhuacun acritarchs and EN2

Lithostratigraphic correlation of the Doushantuo Formation between the Shennongjia and Yangtze Gorges areas is rather straightforward (Figs. 2, 6A, C; Gu et al., 2021). Units 1, 2–4, and 5 at the Lianhuacun section can be correlated with, respectively, Member I (cap dolostone), II (black shales and dolostones), III (dolostone and limestone) of the Doushantuo Formation in the Yangtze Gorges area of southern Huangling anticline (McFadden et al., 2008). Units 6–8 (two black shale intervals separated by a dolostone unit) can be correlated with, respectively, the lower black shale unit, upper dolostone unit, and Miaohe Member in the western Huangling anticline (An et al., 2015; Zhou et al., 2017a), where the Miaohe Member hosts the famous Miaohe Biota (Xiao et al., 2002; Ye et al., 2019). However, it is a matter of debate whether units 7–8 in the Shennongjia area (i.e., the upper dolostone unit and the Miaohe Member in western Huangling anticline) are correlated with the Hamajing and lower Shibantan members of the Dengying Formation (An et al., 2015) or partly with Member IV of the uppermost Doushantuo Formation in the southeastern Huangling anticline (Zhou et al., 2017a). Here we followed An et al. (2015) and consider units 7–9 as part of the Dengying Formation, with the implication that the Miaohe biota is part of the Dengying Formation. Because the focus of this study is on units 3–4, where all the microfossils described in this paper came from, our main conclusions are independent of whether units 7–9 are correlated with Doushantuo or Dengying Formation, as long as the correlation between units 1–5 at Lianhuacun and Member I–III of the Doushantuo Formation in the Yangtze Gorges area is robust.

Chemostratigraphic correlation of the Doushantuo Formation has largely been guided by data from the Yangtze Gorges areas. Three negative $\delta^{13}C$ excursions and two positive excursions have been reported from the Doushantuo Formation in the Yangtze Gorges area (e.g., Jiang et al., 2007, 2011; McFadden et al., 2008; Zhou and Xiao, 2007), although there may be additional minor excursions (An et al., 2015; Zhou et al., 2017a; Zhu et al., 2007, 2013; Yang et al., 2021). Zhou and Xiao (2007) first identified several major excursions in the Yangtze Gorges area, including a negative excursion (EN1) in the cap dolostone, a positive excursion (EP1) in Member II, a negative excursion (EN2) around the Member II/III boundary, a positive excursion (EP2) in the lower Member III, and a pronounced negative excursion (EN3) in the upper Member III as well as carbonate concretions in Member IV. Above the Doushantuo Formation, a positive excursion (EP3), a stable plateau (EI), and a negative excursion (EN4) have been recognized in the lower Denying Formation, middle–upper Denying Formation, and strata near the Ediacaran-Cambrian boundary, respectively. Other minor and often regionally inconsistent excursions include a negative excursion known as WANCE in lower Member II or between EN1 and EN2 (Chen et al., 2022; Zhu et al., 2007, 2013), as well as a positive excursion known as DPE (Diaoyapo Positive Excursion, in upper dolostone unit of Zhou et al., 2017a) followed by a negative excursion known as MNE (Miaohe Negative Excursion in the Miaohe Member) above EN3 (An et al., 2015; Zhou et al., 2017a; Yang et al., 2021).

The $\delta^{13}C$ profile of the Doushantuo and Dengying formations at Lianhuacun, although discontinuous and incomplete due to the lack of carbonate lithologies in several units (e.g., units 2, 6, 8), can be readily correlated with those in the Yangtze Gorges area. Consistent with the lithostratigraphic correlation model proposed above, the negative $\delta^{13}C$ excursions in Unit 1, upper Unit 4, and upper Unit 5 at Lianhuacun are regarded as equivalents of EN1, EN2, and EN3 that occur in Member I (cap dolostone), upper Member II (or near the Member II/III), and upper Member III of the Doushantuo Formation in the Yangtze Gorges area (Figs. 2, 6). There is also a negative trend of $\delta^{13}C$ values around Unit 8, which may be correlated with MNE of Zhou et al. (2017a). Accordingly, the positive $\delta^{13}C$ excursions in units 5, 7, and 9 would be correlated with the $\delta^{13}C$ features EP2, DPE, and EP3 (or EI) that occur in the lower Member III, upper dolostone unit of Zhou et al. (2017a), and the Dengying Formation in the Yangtze Gorges area. Overall, our correlation model is consistent with those proposed by Zhu et al. (2013), Wang et al. (2017), and Ouyang et al. (2019) for the correlation of the Doushantuo Formation in South China, except that EP1 and WANCE are either truncated or not recorded due to the erosional surface atop Unit 3 and the lack of carbonate in Unit 2 at the Lianhuacun section.

Accepting the chemostratigraphic correlations described above, the acanthomorphs described in this paper are in stratigraphic association with the negative $\delta^{13}C$ excursion EN2. This association is important because in the Yangtze Gorges area, strata hosting EN2 are devoid of acanthomorphs (Liu and Moczydłowska, 2019; Liu et al., 2013, 2014a, b; Yin et al., 2011a). This discrepancy may reflect a taphonomic bias because Doushantuo fossil preservation in the Yangtze Gorges area is strongly controlled by early diagenetic chert nodules (Xiao et al., 2012, 2014). Indeed, early diagenetic chert nodules are rare in strata hosting EN2, probably related to a myriad of depositional and diagenetic factors such as sedimentation rates and redox conditions in bottom waters and pore waters (Muscente et al., 2015; Xiao et al., 2010). Alternatively, this discrepancy may be related to environmental difference between inner shelf facies at Lianhuacun and intra-shelf basin facies in the Yangtze Gorges area. Regardless, the Lianhuacun acritarchs help to fill a gap of biozonation associated with EN2 in the Yangtze Gorges area.

5.3. Biostratigraphic correlation of the Lianhuacun assemblage

Acanthomorphic acritarchs are important in the subdivision and correlation of the Ediacaran System (Narbonne et al., 2012; Xiao et al., 2016; Xiao and Narbonne, 2020). Grey (2005) first applied Ediacaran acritarchs in biostratigraphic correlation and proposed four acanthomorph assemblage zones in Australia. Subsequently, recognizing differences among different regions, several schemes of Ediacaran acanthomorph biozonations have been developed (e.g., Liu and Moczydłowska, 2019; Liu et al., 2013, 2014a; McFadden et al., 2009; Moczydłowska and Nagovitsin, 2012; Willman and Moczydłowska, 2008;

Xiao et al., 2014; Yin et al., 2009b). In the Yangtze Gorges area of South China, earlier studies revealed two acanthomorph biozones in the Doushantuo Formation: the *Tianzhushania spinosa* biozone in Member II that is characterized by the positive $\delta^{13}C$ feature EP1, and the *Tanarium conoideum – Hocosphaeridium scaberfacium – Hocosphaeridium anozos* biozone in Member III characterized by the positive $\delta^{13}C$ feature EP2 (Fig. 6C; Liu et al., 2013, 2014a, b; Yin et al., 2011a). These two biozones are separated by a "barren zone" characterized by a negative $\delta^{13}C$ excursion (EN2). However, with more acritarch data from the Yangtze Gorges area and elsewhere in South China, it has become increasingly clear that two of the eponymous fossils, *Tianzhushania spinosa* and *Hocosphaeridium anozos*, overlap in stratigraphic distribution (Hawkins et al., 2017; Liu and Moczydłowska, 2019; Xiao et al., 2014). Thus, it is essential to explore the "barren zone" or the EN2 interval at multiple stratigraphic sections in order to fill this biostratigraphic gap and to improve acanthomorphic biozonation. Toward this goal, Hawkins et al. (2017) first demonstrated the presence of acanthomorphic acritarchs in the EN2 interval of the Doushantuo Formation deposited in upper slope facies at the Siduping section in South China, and they also showed that *H. anozos* extends to Member II of the Doushantuo Formation and co-exists with *Tianzhushania spinosa*, an observation subsequently confirmed in the Yangtze Gorges area (Liu and Moczydłowska, 2019).

Recently, Liu and Moczydłowska (2019) integrated previously published and new biostratigraphic data from the Doushantuo Formation in the Yangtze Gorges and Weng'an areas in South China and proposed four acanthomorphs biozones. These biozones are, in ascending order, the *Appendisphaera grandis – Weissiella grandistella – Tianzhushania spinosa*, *Tanarium tuberosum – Schizofusa zangwenlongii*, *Tanarium conoideum – Cavaspina basiconica*, and *Tanarium pycnacanthum – Ceratosphaeridium glaberosum* Assemblage Zones. The first three are recorded in Member II of the Doushantuo Formation, thus roughly equivalent to the *Tianzhushania spinosa* biozone of Liu et al. (2014a), whereas the fourth occurs in Member III of the Doushantuo Formation and is separated from the third microfossil assemblage zone by a "barren zone" near the Member II–III boundary of the Doushantuo Formation. They further estimated the age of the lower boundary of the four microfossil assemblage zones to be ~ 633 Ma, ~620 Ma, ~610 Ma, and shortly after ~ 580 Ma, respectively. More recently, Ouyang et al. (2021) carried out a comprehensive microfossil study of the lower Member II of the Doushantuo Formation in the Yangtze Gorges area, and they identified two waves of first appearances of acanthomorphs. The first wave ushered in many acanthomorphic species, including *Appendisphaera grandis*, *Dicrospinasphaera improcera*, *Knollisphaeridium coniformum*, *Tianzhushania polysiphonia*, *Tianzhushania spinosa*, and *Yinitianzhushania tuberifera*. In the second wave, additional acanthomorphs appeared, including *Appendisphaera heliaca*, *Cavaspina acuminata*, and *Ericiasphaera fibrilla*. The correlation between Liu and Moczydłowska's (2019) first three microfossil assemblage zones and Ouyang et al.'s (2021) two waves, however, remains unclear. Furthermore, it is uncertain whether the "barren zone" of Liu and Moczydłowska (2019) masks additional acanthomorphic biozones or represents a taphonomically infertile interval of adjacent biozones that have already been recognized.

The Lianhuacun microfossils described here can help to illuminate the biostratigraphic questions discussed above. As most acanthomorph species described from Lianhuacun have been previously recognized from the Doushantuo Formation in South China and Ediacaran successions in other sedimentary basins (Table 2), they facilitate first-order biostratigraphic correlation. We propose that the Lianhuacun acanthomorph assemblage is part of the *Tanarium conoideum – Cavaspina basiconica* Assemblage Zone or the third microfossil assemblage zone of Liu and Moczydłowska (2019) based on the following considerations. First, it contains both *Tanarium conoideum* and *Cavaspina basiconica*, which are the nominal taxa of the third microfossil assemblage zone of Liu and Moczydłowska (2019), as well as many other species (e.g., *Appendisphaera grandis*, *A. tabifica*, *A. tenuis*, *Cavaspina acuminata*, *Eotylotopalla dactylos*, *Ericiasphaera magna*, *Mengeosphaera chadianensis*, *M. gracilis*, *Tanarium cuspidatum*, *T. muntense*, *T. paucispinosum*, and *Weissiella* cf. *grandistella*) that are commonly present in this biozone. Second, neither of the eponymous taxa of the fourth microfossil assemblage zone (i.e., the *Tanarium pycnacanthum – Ceratosphaeridium glaberosum* Assemblage Zone) are present in the Lianhuacun acanthomorphic assemblage. Third, *Tianzhushania spinosa*, the eponymous species of the first microfossil assemblage zone of Liu and Moczydłowska (2019) and a numerically dominant species in the lower Member II (Ouyang et al., 2021), has not been recovered from the Lianhuacun section.

We note that the microfossil assemblage zones of Liu and Moczydłowska (2019) were defined at their lower boundaries using the first appearance datum (FADs) of eponymous species. As such, it is possible that the stratigraphic range of *Tianzhushania spinosa* extends above the first microfossil assemblage zone of Liu and Moczydłowska (2019; see their Fig. 15). In fact, *Tianzhushania spinosa* does occurs sparsely in the third assemblage biozone or the *Tanarium conoideum – Cavaspina basiconica* Assemblage Zone, the reference section of which is unit 4A of the Doushantuo Formation at Weng'an, where *Tanarium conoideum*, *Cavaspina basiconica*, and *Tianzhushania spinosa* co-occur (Xiao et al. 2014). Thus, in principle, the lack of *Tianzhushania spinosa* in the Lianhuacun assemblage may be taken as evidence for a correlation with the fourth microfossil assemblage zone of Liu and Moczydłowska (2019). However, considering that (1) the abundance of *Tianzhushania spinosa* decreases sharply in the upper Member II in the Yangtze Gorges area (Ouyang et al., 2021), and (2) eponymous taxa of the third assemblage biozone are positively identified but those of the fourth assemblage biozone are not found in the Lianhuacun assemblage, we favor the correlation that places the Lianhuacun assemblage as part of the third rather than the fourth microfossil assemblage zone of Liu and Moczydłowska (2019). It is important to emphasize that our favored biostratigraphic correlation model is consistent with independently derived lithostratigraphic and chemostratigraphic correlations (Fig. 6; see sections 5.1 and 5.2). We would also like to point out that, although we favor the interpretation that the Lianhuacun assemblage is part (and likely the upper part) of the third microfossil assemblage zone of Liu and Moczydłowska (2019), we cannot rule out the possibility that the Lianhuacun assemblage may represent a new and yet unnamed biozone between the third and the fourth microfossil assemblage zones of Liu and Moczydłowska (2019). This is because the Lianhuacun assemblage occurs in the EN2 interval, which represents the "barren zone" between the third and fourth assemblage zones in the Yangtze Gorges area. As a result, the Lianhuacun assemblage or the "barren zone" can either be part of the third assemblage zone or a new biozone between the third and fourth assemblage zone, but it cannot be part of the fourth assemblage zone because of the lack of eponymous taxa of the fourth zone. This possibility of a new assemblage zone needs to be investigated in the future and if confirmed, nominal taxa need to be carefully chosen to maximize correlation potential.

The age of the Lianhuacun assemblage can be constrained by radiometric dates from the Yangtze Gorges and Zhangcunping areas through correlations proposed above. The fossiliferous Unit 4 at the Lianhuacun section is lithostratigraphically correlated with the upper Member II of Doushantuo Formation in the Yangtze Gorges area (An et al., 2018; Gu et al., 2021), both preserving the negative $\delta^{13}C_{carb}$ excursion EN2 and the third acritarch assemblage biozone of Liu and Moczydłowska (2019) (Fig. 6). Accepting this correlation, the Lianhuacun assemblage must be younger than 612.5 ± 0.9 Ma based on correlation with the Doushantuo Formation in the Zhangcunping area (Fig. 6; Yang et al., 2021; Zhou et al., 2017b). It would also be younger than 587.2 ± 3.6 Ma, a Re-Os age from a horizon 58 m above the base of the Doushantuo Formation in the Yangtze Gorges area and correlated with the boundary between the second and the third assemblage zones (Yang et al., 2021). The minimum age constraint for the Lianhuacun assemblage comes from EN3, which occurs in upper Unit 5 at Lianhuacun (Fig. 6). EN3 is regarded as an equivalent of the Shuram negative

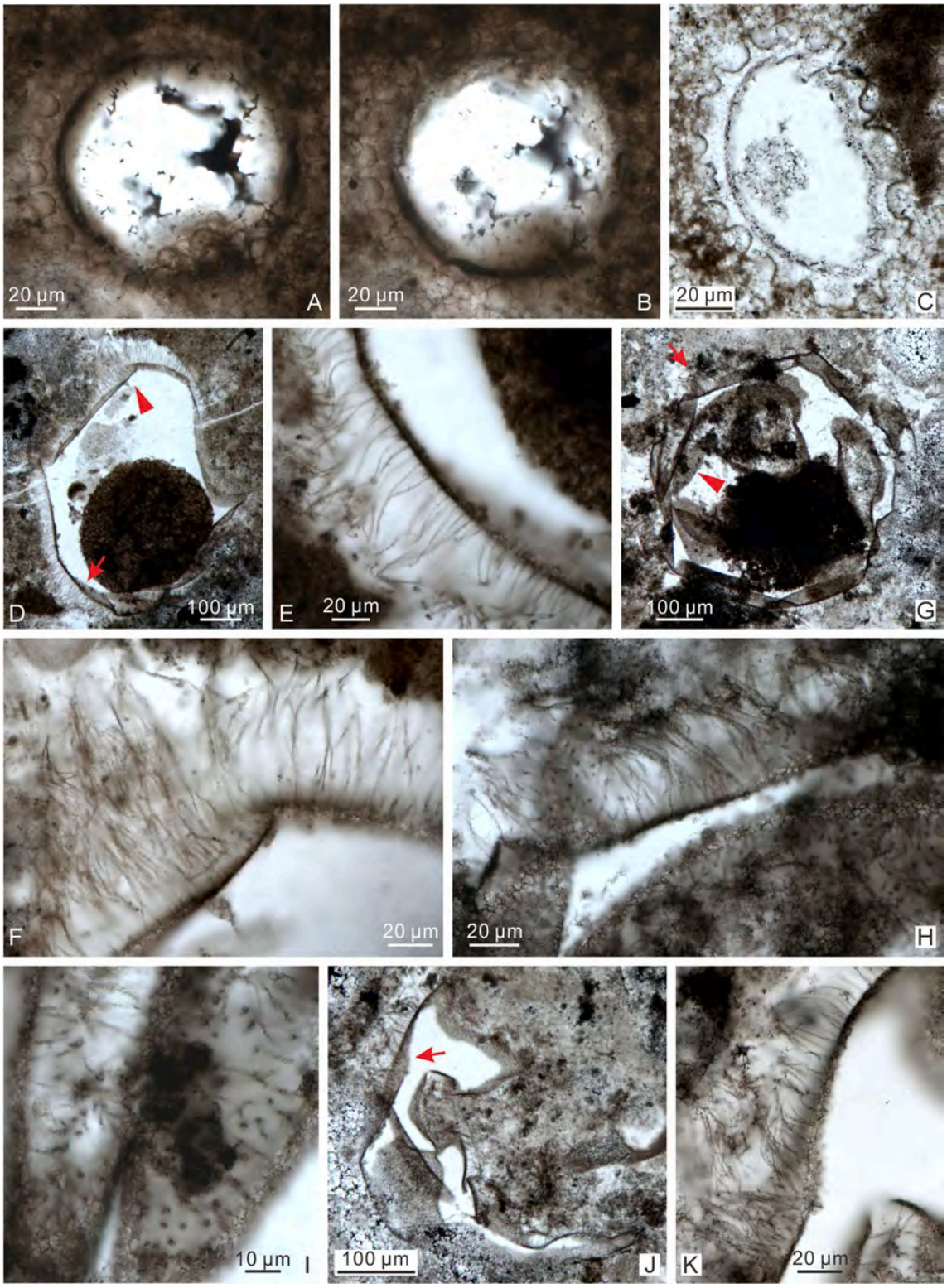

Fig. 7. (A–C) *Annularidens inconditus* Ouyang et al., 2021. (A–B) 21LHC-1–39.5 m-2p-7 (9 × 105), showing same specimen at different focal levels. (C) 21LHC-1–37.4 m-1p-3 (9 × 85). (D–K) *Appendisphaera anguina*? Grey, 2005. (D–F) 21LHC-1–45.6 m-3p-3 (9.5 × 98.8). (E–F) Magnified views of areas in (D) marked by arrow and arrowhead, respectively. (G–I) 21LHC-1–36.1 m-6p-15 (10 × 94.5). (H–I) Magnified views of areas in (G) marked by arrow and arrowhead, respectively. (J–K) 21LHC-1–36.1 m-6p-20 (13 × 100). (K) Magnified view of area marked by arrow in (J).

excursion, which has been bracketed between 574.0 ± 4.7 Ma and 567.3 ± 3.0 Ma based on Re-Os ages from northwestern Canada (Rooney et al., 2020). Thus, the Lianhuacun microfossil assemblage, as well as EN2 and the third acritarch assemblage biozone of Liu and Moczydłowska (2019), are constrained between 587.2 ± 3.6 Ma and 574.0 ± 4.7 Ma.

The correlation model presented in Fig. 6 also raises important questions about Ediacaran biostratigraphic gaps. As discussed above, such gaps can result from missing strata related to unconformities or

subaerial erosional surfaces. In addition, they can result from environmental or taphonomic biases. Environmental controls on the distribution of Ediacaran acanthomorphs have not been investigated in details, but the distribution of Mesoproterozoic acanthomorphs do appear to have been controlled by facies and they tend to be biased toward nearshore facies (Butterfield and Chandler, 1992; Javaux et al., 2001). Taphonomic factors can also place key controls on the preservation of Ediacaran acritarchs. Total organic content, for example, can bias the preservation quality and abundance of Proterozoic acritarchs in fine-grained siliciclastic rocks (Woltz et al., 2021). In the Doushantuo Formation, acritarchs are preserved in phosphorite or chert nodules, both of which are controlled by local depositional and diagenetic environments. For example, Doushantuo phosphorites tend to occur in shallow-water facies in inner shelf and shelf margin settings, where the Fe shuttle operates at the redox boundary near the water–sediment interface to aid the delivery of phosphate to the pore waters (Muscente et al., 2015). Additionally, sedimentary processes in shallow-water environments facilitate the secondary concentration of phosphatic grains through the reworking and winnowing of pristine phosphorite (Xiao et al., 1999; Muscente et al., 2015; Zhang et al., 2019). In contrast, early diagenetic chert nodules in the Doushantuo Formation likely formed near or underlying ferruginous waters where localized decrease in pH promoted SiO_2 precipitation (Xiao et al., 2010). Thus, there are a myriad of sedimentary, environmental, and early diagenetic factors controlling the preservation of acritarchs in shales, phosphorites, and chert nodules. Any one of these factors may cause the non-preservation of acanthomorphs in the EN2 interval.

The Lianhuacun assemblage offers new insights into the evolution of acanthomorph diversity at the Doushantuo Member II-III transition in South China. It was previously perceived that acanthomorphs are taxonomically more diverse in Member III than in Member II of Doushantuo Formation (Liu et al., 2014a). As new data become available, however, this simplistic view warrants a reassessment. For example, on the basis of a regional review, Liu and Moczydłowska (2019; their table 1 and Fig. 15) listed 49 acanthomorph species in Member II and 81 in Member III (with 20 species shared between the two members), whereas Ouyang et al. (2021) described 69 acanthomorph species from Member II at three stratigraphic sections in the Yangtze Gorges area alone, some of which were new or previously only know from Member III. The Lianhuacun assemblage described here adds additional species richness of acanthomorphs to Member II. Among all taxonomically described acanthomorph species from Lianhuacun, nearly one third of them (19 in 61) occur in both Member II and III in the Yangtze Gorges (Table 2). However, twelve species (*Appendisphaera anguina*?, *Cavaspina basiconica*, *Hocosphaeridium dilatatum*, *H. scaberfacium*, *Knollisphaeridium denticulatum*, *Mengeosphaera angusta*?, *M. constricta*, *M. stegosauriformis*, *Sinosphaera rupina*, *Tanarium conoideum*, *Urasphaera fungiformis*, and *Variomargosphaeridium floridum*), as well as the genus *Granitunica*, were previously reported from Member III but unknown from Member II in the Yangtze Gorges area; indeed, the *Tanarium conoideum* – *Cavaspina basiconica* Assemblage Zone was established on the basis of microfossils from Weng'an and correlated with upper Member II of the Doushantuo Formation in the Yangtze Gorges area (Liu and Moczydłowska, 2019), but in the Yangtze Gorges area both eponymous species are only found in Member III. The Lianhuacun assemblage also includes two species—*Eotylotopalla apophysa* (Vorob'eva et al., 2009b) n. comb. and *Urasphaera capitalis*—that are recorded for the first time from the Yangtze craton. In addition, two species of tubular fossil–*Quadratitubus orbigoniatus* and *Sinocyclocyclicus guizhouensis*, which have been previously described in the Weng'an biota and in Member III of Yangtze Gorges area (Liu et al., 2010; 2014a), are recovered from the Lianhuacun section. These new occurrences, together with the new species from the Lianhuacun assemblage (*Duospinosphaera shennongjiaensis* sp. nov., *D. biformis* sp. nov., *Mengeosphaera mamma* sp. nov., *Sinosphaera exilis* sp. nov., *Tanarium columnatum* sp. nov., and *Weissiella concentrica* sp. nov.), expand the paleoenvironmental distribution of Ediacaran acanthomorphs, add to Member II diversity, and bridge a biostratigraphic gap (previously known as the "barren zone") between Member II and Member III of the Doushantuo Formation, thus facilitating the development of continuous biostratigraphic zonation and evolutionary pattern of Doushantuo acanthomorphs.

6. Conclusions

A taxonomically diverse microfossil assemblage is reported from chert nodules of the lower Doushantuo Formation at the Lianhuacun section in the Shennongjia area, Hubei Province, South China. In total, 33 genera (including one new genus) and 82 species (including seven new species) are described. The Lianhuacun microfossils include acanthomorphic acritarchs, filamentous and coccoidal cyanobacteria, multicellular algal thalli, and tubular microfossils. The fossiliferous strata were deposited in an inner shelf facies and are associated with a negative $\delta^{13}C$ excursion correlated with EN2. Because previously published paleontological data were scarce in inner shelf facies and nearly absent from strata hosting EN2 (formerly regarded as a "barren zone" in terms of acanthomorphs), the Lianhuacun fossils fill two critical environmental and stratigraphic gaps in Doushantuo paleontology, broaden the environmental and stratigraphic distribution of a number of Doushantuo microfossil taxa, add to the taxonomic diversity of Ediacaran eukaryotes, and facilitate the biostratigraphic correlation of the Ediacaran System in South China and beyond.

Based on integrated chemostratigraphic and biostratigraphic correlations, we propose that the Lianhuacun microfossil assemblage is likely part of (and probably equivalent to the upper part of) the *Tanarium conoideum* – *Cavaspina basiconica* Assemblage Zone recognized in the Doushantuo Formation at Weng'an and correlated with the lower Doushantuo Formation (upper Member II) in the Yangtze Gorges area of South China (Liu and Moczydłowska, 2019). We also note the possibility that the Lianhuacun assemblage may represent a new and yet unnamed microfossil assemblage zone between the third and fourth microfossil assemblage zones of Liu and Moczydłowska (2019). Regardless, the "barren zone" in the Yangtze Gorges area apparently results from taphonomic or environmental biases. At a regional scale, the "barren zone" and the chemostratigraphic interval EN2 may actually be correlated with the upper part of the *Tanarium conoideum* – *Cavaspina basiconica* Assemblage Zone or a new assemblage zone to be defined in the future.

Our correlation model indicates that EN2 and the *Tanarium conoideum* – *Cavaspina basiconica* assemblage zone in South China is constrained between 587.2 ± 3.6 Ma and 574.0 ± 4.7 Ma. It also implies that the first two acritarch assemblage zones in the Doushantuo Formation, as recognized by Liu and Moczydłowska (2019), are not preserved at the Lianhuacun section, due to missing strata, unfitting environments, or inappropriate taphonomic conditions. This study highlights the fragmentary nature of microfossil sequence preserved in the Doushantuo Formation and emphasizes the need to combine data from multiple localities, facies, and taphonomic modes in order to reconstruct a complete and continuous set of Ediacaran microfossil biozones.

7. Appendix: Systematic paleontology

All illustrated microfossils were observed in petrographic thin sections, which are reposited at the China University of Geosciences (CUG), Wuhan, China. Microfossils were positioned using the coordinate system of a Zeiss AxioScope.A1 microscope. Unfortunately, some specimens are beyond the range of one or both coordinates, in which case the unrecorded coordinates are registered as "NR" (not recorded) in the figure captions. Descriptive terminology follows that of Xiao et al. (2014).

Group Acritarcha Evitt, 1963.

Genus *Annularidens* Ouyang et al., 2021.

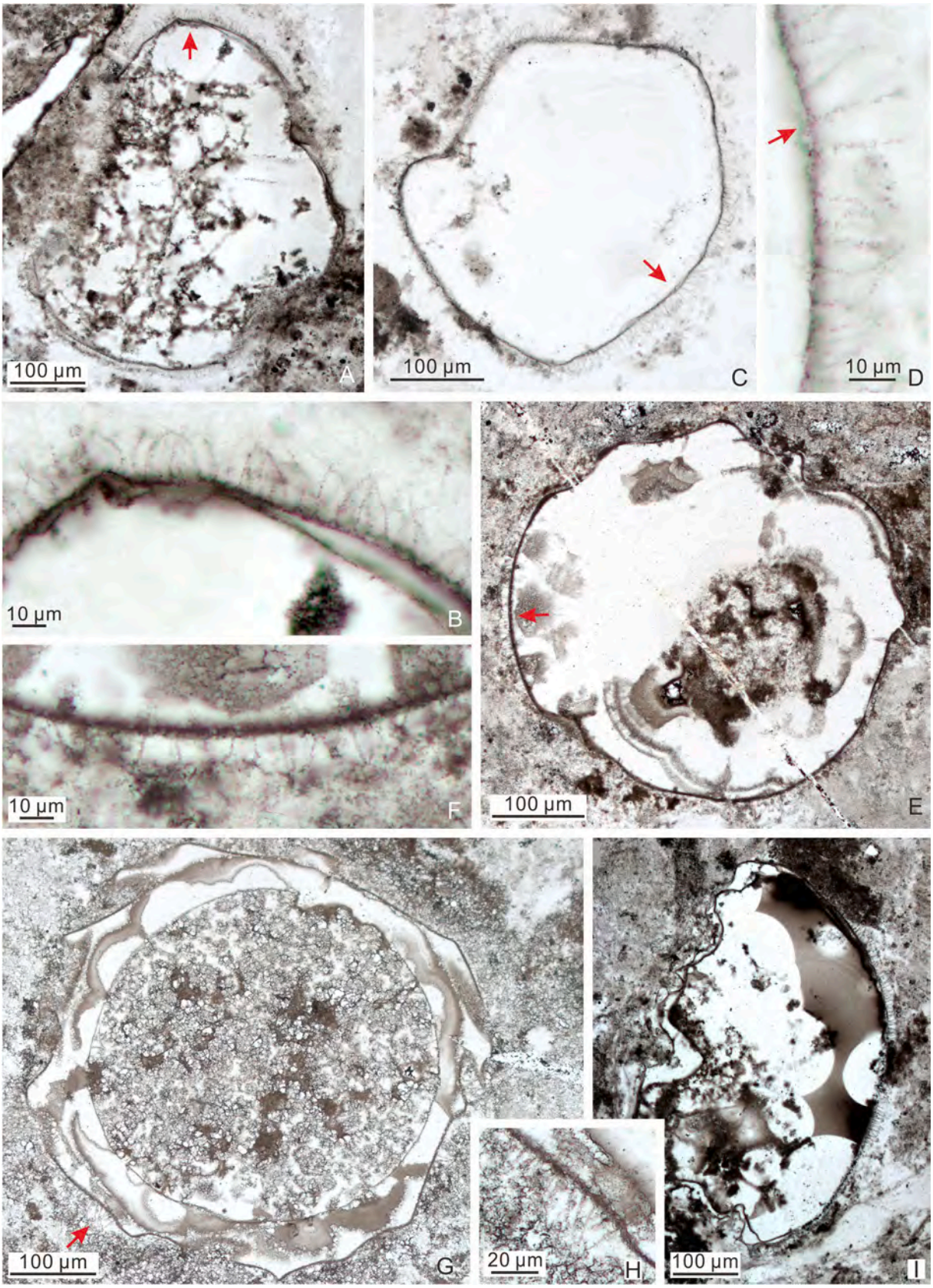

Fig. 8. *Appendisphaera clava* Liu et al., 2014a. (A–B) LHG-d2-3.4 m-3p-1 (29.6 × 72). (B) Magnified view of area marked by arrow in (A). (C–D) LHG-d2-3.4 m-3p-11 (31.8 × 69.3). (D) Magnified view of area marked by arrow in (C), with arrow denoting a small basal expansion. (E–F) LHG-d2-3.4 m-2–5 (15.7 × 69.5). (F) Magnified view of area marked by arrow in (E). (G–H) LHG2-d2-2.1 m-3–2 (20.7 × 81.3). (H) Magnified view of area marked by arrow in (G). (I) LHG-d3 + 30 cm-1–1 (25.1 × 64).

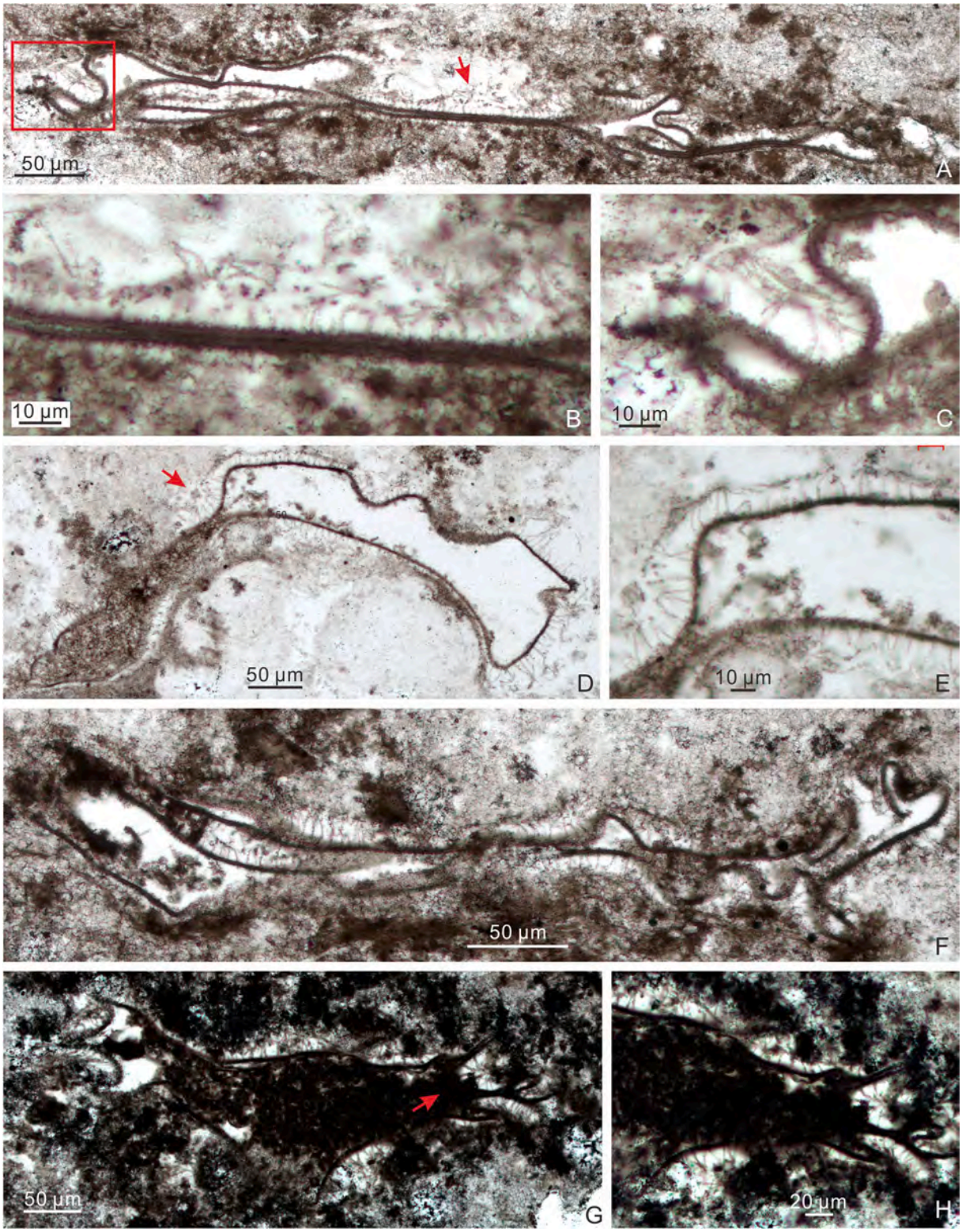

Fig. 9. *Appendisphaera fragilis* Moczydłowska et al., 1993, emend. Moczydłowska, 2005. (A–C) LHG-d2-3.4 m-1–29 (33.8 × 77). (B–C) Magnified views of areas in (A) marked by arrow and rectangle, respectively. (D–E) LHG-d2-3.4 m-5–1 (32 × 77). (E) Magnified view of area marked by arrow in (D). (F) LHG-d2-3.4 m-1–2 (31.6 × 70). (G–H) LHG-d2-60 cm-10–17 (23.8 × 70.3). (H) Magnified view of area marked by arrow in (G).

Type species: *Annularidens inconditus* Ouyang et al., 2021.

Annularidens inconditus Ouyang et al., 2021.

Fig. 7A–C.

Synonymy:

2021 *Annularidens inconditus* Ouyang et al., p. 21, Fig. 10C–E, H–I.

Material: Two adequately preserved specimens.

Description: Small to medium-sized spheroidal vesicle enveloped by membraneous outer wall that bears a moderate number of evenly distributed processes. Processes hollow, broad cylindrical, basally deflated, and distally rounded, blunt or truncated. They are uniform in

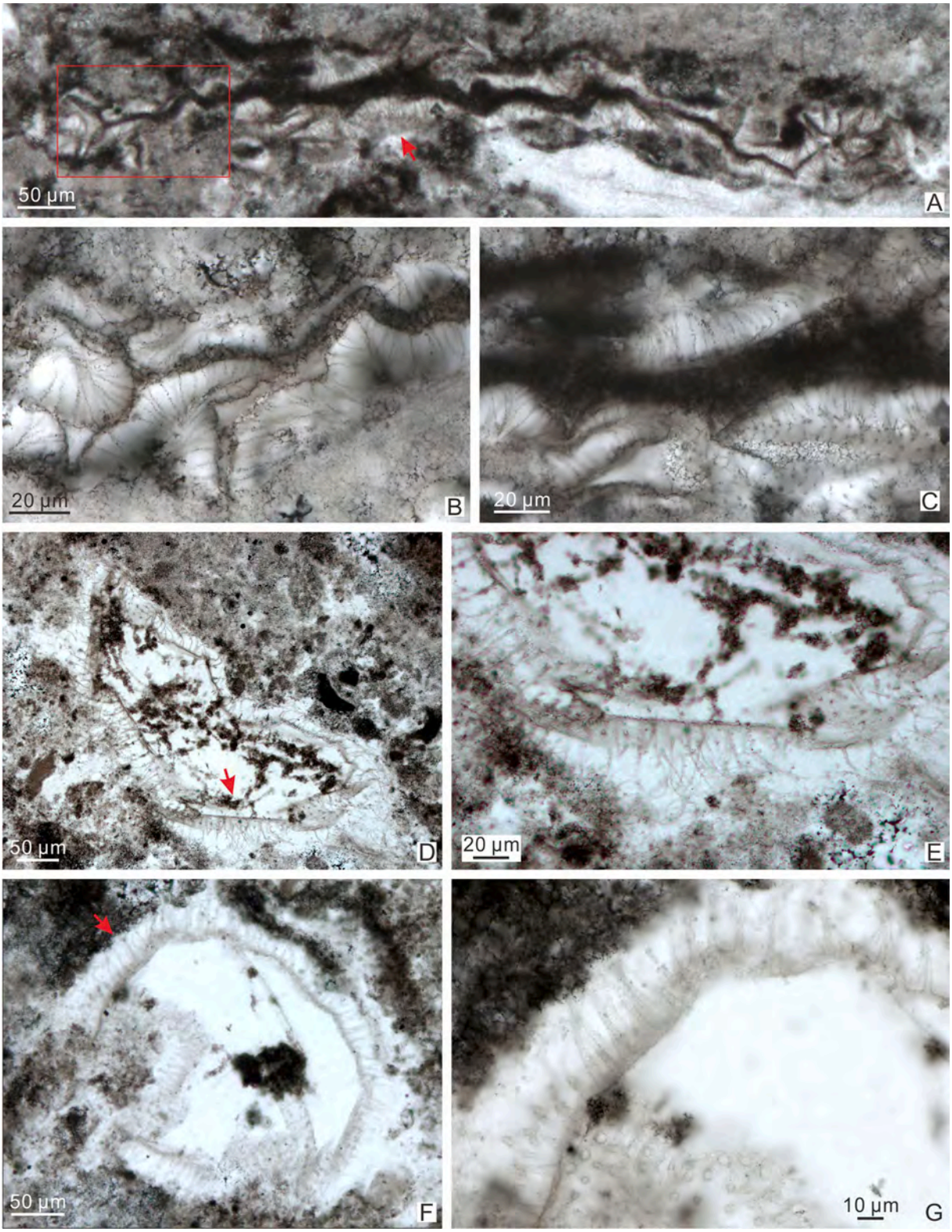

Fig. 10. *Appendisphaera grandis* Moczydłowska et al., 1993, emend. Moczydłowska, 2005. (A–C) 21LHC-1–45.2 m-4c-5 (11 × 96). (B–C) Magnified views of areas in (A) marked by rectangle and arrow, respectively. (D–E) LHG2-d2-3.1 m-2p-9 (23.6 × 79.2). (E) Magnified view of area marked by arrow in (D). (F–G) 21LHC-1–36.1 m-1p-1 (3.5 × 98). (G) Magnified view of area marked by arrow in (F).

length but variable in width.

Dimensions: Specimen illustrated in Fig. 7A–B: vesicle diameter 110.6 μm; membrane thickness ~ 5.7 μm; process length 7.2–7.8 μm; process terminal width 2.3–15.0 μm; process spaced distance 7.3–11.5 μm. Specimen illustrated in Fig. 7C: vesicle diameter 65.2 μm (calculated from circumference measurement); membrane thickness 2.8–5.6 μm; process length 7.0–8.5 μm; process terminal width 1.6–8.5 μm; process spaced distance 4.7–11.1 μm.

Remarks: The current specimens resemble *A. inconditus* in their overall morphology and size dimensions.

Occurrence: The Ediacaran Doushantuo Formation in the Shennongjia (this paper) and Three Gorges areas (Ouyang et al., 2021) of Hubei Province, South China.

Genus *Appendisphaera* Moczydłowska et al., 1993, emend. Moczydłowska, 2005.

Type species: *Appendisphaera grandis* Moczydłowska et al., 1993, emend. Moczydłowska, 2005.

Appendisphaera anguina? Grey, 2005.

Fig. 7D–K.

Synonymy:

? 2005 *Appendisphaera anguina* Grey, pp. 206–209, Fig. 43C, 88A, 90A–C, 91.

? 2009b *Appendisphaera* aff. *anguina* Grey; Vorob'eva et al., p.175, figs. 9.9, 9.9a.

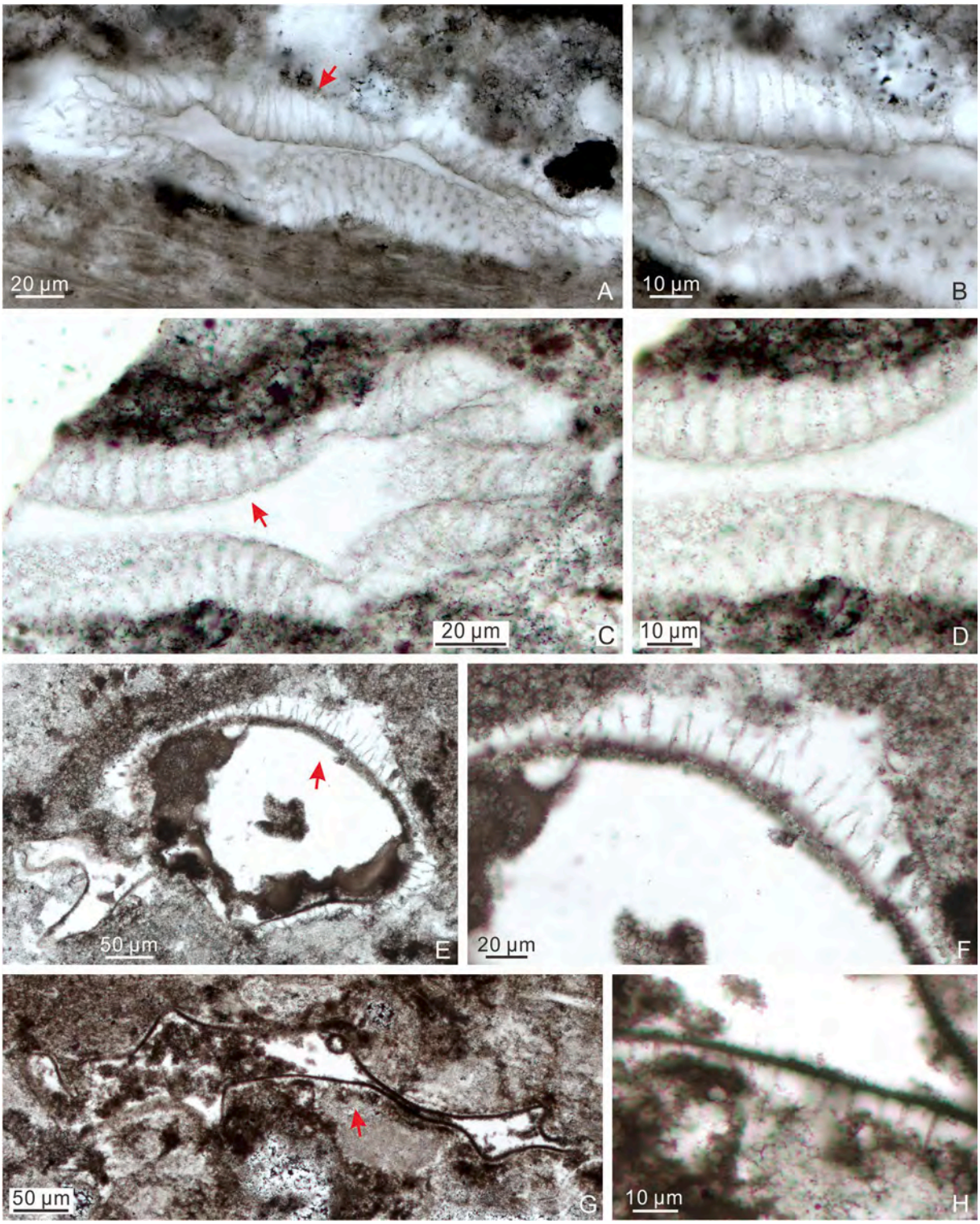

Fig. 11. (A–D) *Appendisphaera longispina* Liu et al., 2014a. (A–B) 21LHC-1–45.6 m-3c-8 (11.4 × 107.8). (B) Magnified view of area marked by arrow in (A). (C–D) LHG-d2-3.4 m-3c-1 (25 × 76.2). (D) Magnified view of area marked by arrow in (C). (E–H) *Appendisphaera setosa* Liu et al., 2014a. (E–F) LHG-d2-4.3 m-5–13 (30.3 × 77.7). (F) Magnified view of area marked by arrow in (E). (G–H) LHG-d2-3.4 m-1–24 (22.5 × 76.2). (H) Magnified view of area marked by arrow in (G).

? 2014a *Appendisphaera anguina* Grey; Liu et al., p. 11, Fig. 5.1A–B, 6.1–6.8.

non 2016 *Appendisphaera* aff. *anguina* Grey; Prasad and Asher, p. 40, pl. I, Figs. 3–4. (=*Appendisphaera tenuis*).

2019 *Appendisphaera anguina*?; Ouyang et al., Fig. 8A–B.

Material: Fifteen adequately preserved specimens and 14 poorly preserved specimens.

Description: Large spheroidal vesicle bearing abundant, densely distributed, basally separated, cylindrical processes. Processes long, very thin, highly flexible, and often tangled and bent. Processes hollow and freely communicate with the vesicle cavity.

Dimensions: Vesicle diameter 301.6–637.7 μm; estimated process length 49.7–95.8 μm; process width about 0.5–1.0 μm; ratio of process length to vesicle diameter about 9.8–16.7%.

Remarks: The specimens described here are similar to *A. anguina* based on their very large vesicle and their long, thin, flexible, and cylindrical processes. However, our specimens are larger in vesicle size and thus show relatively shorter processes (49.7–95.8 μm or typically < 20% of vesicle diameter) than the holotype (vesicle diameter ~ 224 μm and process length ~ 100 μm; Grey, 2005) and other published specimens of *A. anguina*, whose process length is 25–45% or typically greater than 20% of vesicle diameter (Grey, 2005; Liu et al., 2014a; Vorob'eva et al., 2009b), although the process length of our specimens may be underestimated because the processes may be broken off or not fully captured in the thin section. Thus, the identification of our specimens is provisional.

Our material is somewhat similar to *A. tabifica* (and *A. barbata* which has been synonymized with *A. tabifica* by Liu and Moczydłowska, 2019), but the latter has more densely arranged (often coalesced) processes and much smaller vesicles. One incomplete specimen illustrated as *Appendisphaera anguina*? in Ouyang et al. (2019; their Fig. 8A–B) contains long, thin, and very flexible processes, which are similar to the processes of our specimens. Two specimens illustrated as *Appendisphaera* aff. *anguina* in Prasad and Asher (2016; their pl. I, Figs. 3–4) are better assigned to *A. tenuis* because of their relatively smaller vesicles and shorter processes relative to *A. anguina*.

Occurrence: The Ediacaran Doushantuo Formation in the Shennongjia (this paper) and Zhangcunping areas (Ouyang et al., 2019) of Hubei Province, South China.

Appendisphaera clava Liu et al., 2014a.

Fig. 8.

Synonymy:

2013 Unnamed (E); Liu et al., Fig. 12A–B.

2014a *Appendisphaera clava* Liu et al., pp. 12, 17, figs. 5.4, 8.1–8.5, 9.1–9.7.

non 2019 *Appendisphaera clava* Liu et al.; Ouyang et al., Fig. 8E–F.

2019 *Appendisphaera clava* Liu et al.; Ouyang et al., Fig. 8G–H.

2020 *Appendisphaera clava* Liu et al.; Grazhdankin et al., Fig. 3C.

2021 *Appendisphaera clava* Liu et al.; Ouyang et al., Fig. 10*K*–L.

2022 *Appendisphaera clava* Liu et al.; Xiao et al., Figs. 5–6.

Material: Five well-preserved and 18 poorly preserved specimens.

Description: Large spheroidal vesicle bearing abundant processes of a more or less uniform length. Processes short, hollow, thin, densely and evenly spaced. Processes occasionally show a small expansion at base and openly communicate with the vesicle cavity.

Dimensions: Vesicles 365.8–670.8 μm in diameter. Processes 11.6–24.3 μm in length, generally ~ 1 μm wide at base but some with a basal expansion up to ~ 2.2 μm wide and ~ 1.3 μm high, and typically < 1 μm at tips. Spacing distance of processes ~ 1.0–4.1 μm. The ratio of process length to vesicle diameter 2.7–6.6%.

Remarks: The main features of the present specimens conform to the diagnostic features of *A. clava* (Liu et al., 2014a). Two specimens described here consist of an expanded base and a slender distal part with a sharply pointed tip (Fig. 8B, D), which are somewhat similar to *Cavaspina basiconica*, although the latter species generally has a smaller vesicle (but some specimens identified as *C. basiconica* have vesicles up to 385 μm in diameter; Liu and Moczydłowska, 2019; Liu et al., 2014a) and a lower density of processes. Two specimens in our collection contain a large spheroidal internal body (Fig. 8G), which is rarely reported in this species. One deformed specimen illustrated as *Appendisphaera clava* in Ouyang et al. (2019; their Fig. 8E–F) contains abundant thin, slender, flexible, ciliate processes, which are more akin to the processes of *A. anguina* or *A. grandis*.

Occurrences: The Ediacaran Doushantuo Formation in the Shennongjia (this paper), Zhangcunping (Ouyang et al., 2019), and Yangtze Gorges areas (Liu et al., 2013, 2014a; Ouyang et al., 2021) of Hubei Province, South China; Ediacaran Krol A Formation in northern India (Xiao et al., 2022); and possibly the Cambrian Oppokun Formation in central Arctic Siberia (Grazhdankin et al., 2020).

Appendisphaera fragilis Moczydłowska et al., 1993, emend. Moczydłowska, 2005.

Fig. 9.

Synonymy:

1993 *Appendisphaera fragilis* Moczydłowska et al., p. 505, text-Fig. 6A–B.

2015 *Appendisphaera* sp.; Ouyang et al., p. 216. pl. I, Figs. 6–8.

2019 *Appendisphaera fragilis* Moczydłowska et al., 1993, emend. Moczydłowska, 2005; Shang et al., pp. 5–6, Fig. 2B–E, and synonyms therein.

Material: Fifteen well-preserved specimens and 33 poorly preserved specimens.

Description: Deformed vesicle (originally spheroidal) bearing numerous widely and evenly spaced processes. Processes hollow, relatively long, slender, and sometimes twisted. Processes are cylindrical in shape and directly communicate with the vesicle interior.

Dimensions: Process length cannot be precisely measured as the apical end is often poorly preserved, but the preserved processes are as much as 13.4–40.2 μm in length, ~1.1–1.9 μm in width, and 3.7–10.7 μm in spacing distance.

Remarks: Moczydłowska et al. (1993) established the species *A. fragilis* and later emended its diagnosis of bearing hollow and widely spaced processes (Moczydłowska, 2005). This species is similar to *A. setosa* because both of them have relatively wide process spacing distance. However, the processes of the latter are shorter, more rigid, and straighter than those in *A. fragilis*. The specimen identified as *Appendisphaera* sp. by Ouyang et al. (2015; their pl. I, Figs. 6–8) is here placed in *A. fragilis*, since it has widely distributed cylindrical processes (3.3–7.1 μm).

Occurrence: The Doushantuo Formation in the Shennongjia (this paper) and Yangtze Gorges areas (Ouyang et al., 2015) of Hubei Province, and the Weng'an (Yin et al., 2011b) and Songlin area (Shang et al., 2019) of Guizhou Province, South China; Ediacaran successions in Siberia (Moczydłowska, 2005; Moczydłowska et al., 1993), Australia (Grey, 2005; Grey and Willman, 2009) and possibly India (Sharma et al., 2016; Shukla and Tiwari, 2014 but see Shang et al., 2019). *A. fragilis* has also been reported from the uppermost Khesen Formation in northern Mongolia (Anderson et al., 2019), but this taxonomic identification is regarded tentative (Shang et al., 2019) and the uppermost Khesen Formation is considered terminal Ediacaran in age although it contains Cambrian-age detrital zircons (Anttila and Macdonald, 2020).

Appendisphaera grandis Moczydłowska et al., 1993, emend. Moczydłowska, 2005.

Fig. 10.

Synonymy:

1993 *Appendisphaera grandis* Moczydłowska et al., pp. 503–505, pl. 1, Figs. 1–2, text-Fig. 5.

1997 *Appendisphaera grandis* Moczydłowska et al.; Vidal and Moczydłowska-Vidal, Fig. 2A.

2015 *Appendisphaera grandis* Moczydłowska et al., 1993, emend. Moczydłowska, 2005; Nagovitsin and Kochnev, Fig. 4.I.1–4.I.2.

2017a *Appendisphaera grandis* Moczydłowska et al.; Anderson et al., Fig. 2B.

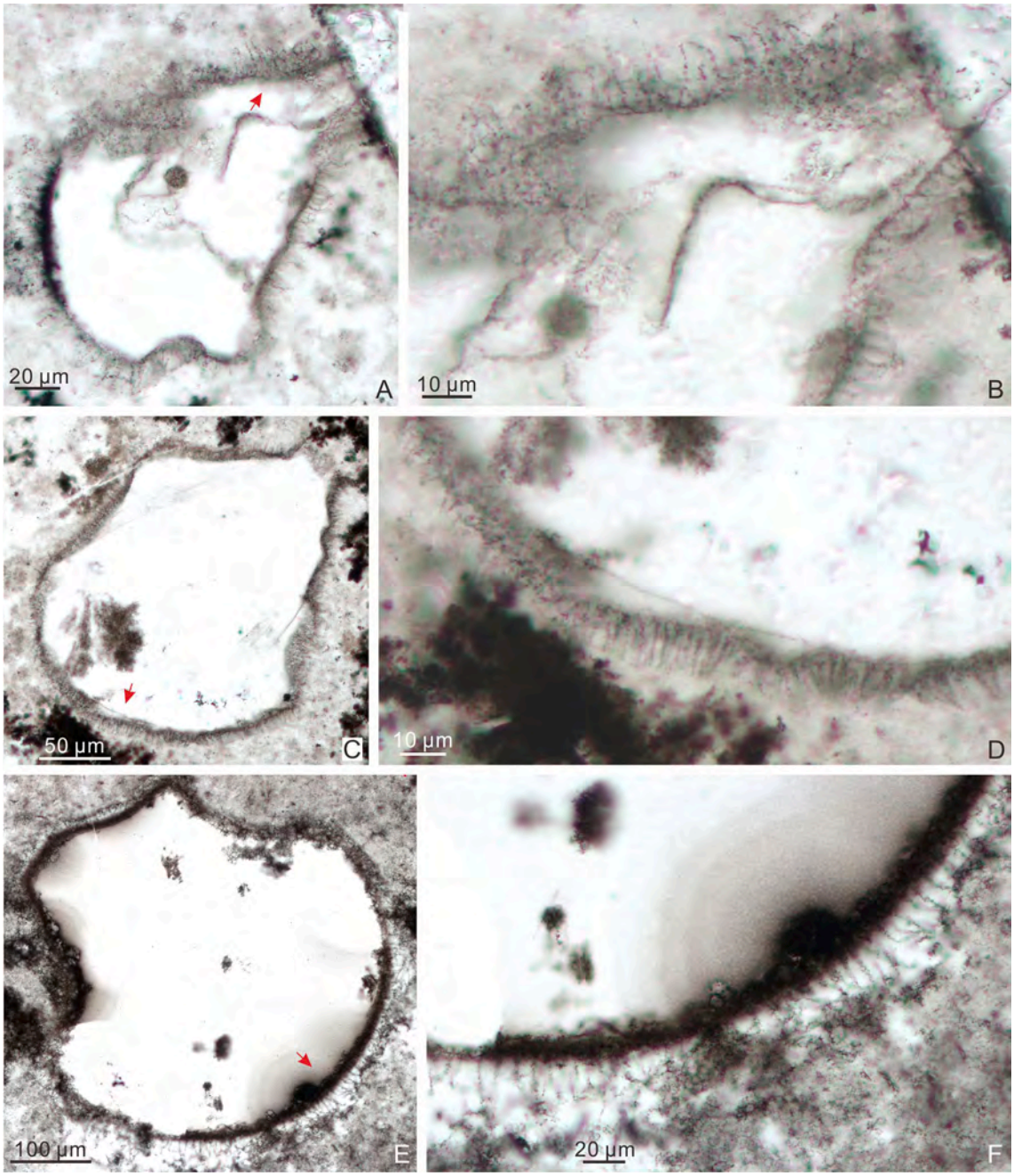

Fig. 12. (A–D) *Appendisphaera tabifica* Moczydłowska et al., 1993, emended. Liu and Moczydłowska, 2019. (A–B) LHG-UD-n-2–5 (24.5 × 76.5). (B) Magnified view of area marked by arrow in (A). (C–D) LHG-UD-n-2–8 (24.5 × 76.5). (D) Magnified view of area marked by arrow in (C). (E–F) *Appendisphaera tenuis* Moczydłowska et al., 1993, emend. Moczydłowska, 2005; LHG-d2-4.3 m-2–2 (21.5 × 72.6). (F) Magnified view of area marked by arrow in (E).

2019 *Appendisphaera grandis* Moczydłowska et al., 1993, emend. Moczydłowska, 2005; Anderson et al., pp. 507–509, Fig. 6A–D.

2019 *Appendisphaera grandis* Moczydłowska et al.; Ouyang et al., Fig. 8I–K.

2019 *Appendisphaera grandis* Moczydłowska et al., 1993, emend. Moczydłowska, 2005; Liu and Moczydłowska, pp. 48, 50–54, Figs. 21–23, and synonyms therein (except *Appendisphaera*? *hemisphaerica* illustrated in Fig. 9C–D of Hawkins et al., 2017).

2019 *Appendisphaera grandis* Moczydłowska et al., 1993, emend. Moczydłowska, 2005; Shang et al., p. 7, Fig. 3.

2020 *Appendisphaera grandis* Moczydłowska et al., 1993, emend. Moczydłowska, 2005; Shang and Liu, pp. 156–157, Fig. 4.

2021 *Appendisphaera grandis* Moczydłowska et al., 1993, emend. Moczydłowska, 2005; Ouyang et al., Fig. 10M–P.

2021 *Appendisphaera grandis* Moczydłowska et al.; Liu et al., fig. 5.4.

2022 *Appendisphaera grandis* Moczydłowska et al., 1993, emend. Moczydłowska, 2005; Xiao et al., Fig. 7.

Material: Seventeen relatively well-preserved specimens and 37 poorly preserved specimens.

Description: Large compressed vesicle (originally spheroidal) bearing abundant homomorphic processes that are long, thin, simple, and cylindrical in shape, and slightly widened at the base and gradually tapering to a sharp-pointed tip. Processes are evenly and densely distributed on vesicle wall but clearly basally separated. They are hollow and openly communicate with vesicle interior.

Dimensions: Vesicle diameter 249.4–526.3 μm; processes length 11.9–42.3 μm; ratio of process length to vesicle diameter 5.6–16.3%; basal width ~ 1.0–5.9 μm; distance between processes 1.9–8.1 μm.

Remarks: The overall morphology of the specimens described here is similar to the holotype in Siberia (Moczydłowska, 2005; Moczydłowska et al., 1993), although their vesicle size and process length are greater. We note that published specimens of *A. grandis* show considerable variations in vesicle size (50–812 μm) and process length (8–80 μm) (Liu and Moczydłowska, 2019), and our specimens can be accommodated considering these variations. *A. grandis* differs from *A. tenuis* in its longer and slightly flexible processes, and from *A. longispina* in that the latter has longer, wider, and basally joined processes with a well-defined basal expansion.

A specimen of *Appendisphaera*? *hemisphaerica* illustrated in Hawkins et al. (2017; their Fig. 9C–D) was transferred to *A. grandis* by Liu and Moczydłowska (2019). But Hawkins et al.'s (2017) specimen has biform processes with a distinct basal expansion, and is different from the holotype of *A. grandis*. Thus, this specimen is excluded from the synonymy list of *A. grandis*.

Occurrence: The Ediacaran Doushantuo Formation in the Shennongjia (this paper), Zhangcunping (Chen et al., 2010; Ouyang et al., 2019), Changyang (Liu et al., 2021), and Yangtze Gorges areas (Liu and Moczydłowska, 2019; Ouyang et al., 2021) of Hubei Province, the Zhangjiajie area of Hunan Province (Hawkins et al., 2017; Ouyang et al., 2017; Shang and Liu, 2020), the Weng'an (Xiao et al., 2014) and Songlin areas of Guizhou Province (Shang et al., 2019), South China; Ediacaran successions in Siberia (Golubkova et al., 2010; Moczydłowska, 2005; Moczydłowska et al., 1993; Nagovitsin and Kochnev, 2015), Australia (Willman and Moczydłowska, 2008), and India (Prasad and Asher, 2016; Xiao et al., 2022); the uppermost Khesen Formation in northern Mongolia (Anderson et al., 2017a, 2019), which is considered terminal Ediacaran in age although it contains Cambrian-age detrital zircons (Anttila and Macdonald, 2020).

Appendisphaera longispina Liu et al., 2014a.

Fig. 11A–D.

Synonymy:

2013 Unnamed (C); Liu et al., Fig. 12G–H.

2014a *Appendisphaera longispina* Liu et al., p. 21, figs. 5.7, 17.1–17.5, 18.1–18.6.

2014a *Appendisphaera crebra* (Zang *in* Zang and Walter, 1992a) Liu et al., p. 17, figs. 5.5, 10.1–10.6, 11.1–11.6.

2019 *Appendisphaera longispina* Liu et al.; Liu and Moczydłowska, pp. 54–55, Fig. 25.

2019 *Appendisphaera longispina* Liu et al.; Shang et al., pp. 8–10, Fig. 4C–D.

2021 *Appendisphaera longispina* Liu et al.; Ouyang et al., Fig. 11G–H.

2022 *Appendisphaera longispina* Liu et al.; Xiao et al., Figs. 13–14.

Material: Five moderately preserved specimens and three poorly preserved specimens.

Description: Collapsed vesicle (originally spheroidal) bearing abundant tightly distributed and basally joined processes. Processes are homomorphic and slightly biform, with a small and slightly deflated base that gradually transitions into a filamentous distal end. Processes are hollow and openly communicate with the vesicle cavity.

Dimensions: Overall process length 14.5–42.0 μm; process base 4.2–7.0 μm in width and 3.4–6.5 μm in height; process apical spine ~ 1.0–1.6 μm in width.

Remarks: Liu et al. (2014a) established *A. longispina* and commented on the similarities between *A. longispina* and *A. crebra*, the latter of which is a new combination that Liu et al. (2014a) created on the basis of *Goniosphaeridium crebum* Zang *in* Zang and Walter, 1992a. Liu and Moczydłowska (2019) noted that *G. crebum* should be transferred to a different genus, but they did not accept its transfer to the genus *Appendisphaera*. Liu and Moczydłowska (2019) argued that Doushantuo acanthomorphs from the Yangtze Gorges area described by Liu et al. (2014a) as *A. crebra* should be identified as *A. longispina*, as they are similar to *A. longispina* in their uniform, densely arranged, and gradually tapering processes with a conical base. Accepting Liu and Moczydłowska's (2019) proposition, *A. longispina* shows a wide range in vesicle size (100–370 μm) and process length (15–50 μm). Our specimens are morphologically and dimensionally comparable to *A. longispina*.

Occurrence: The Ediacaran Doushantuo Formation in the Shennongjia (this paper) and Yangtze Gorges areas (Liu and Moczydłowska, 2019; Liu et al., 2013, 2014a; Ouyang et al., 2021) of Hubei Province and the Songlin area of Guizhou Province (Shang et al., 2019), South China, as well as the Ediacaran Krol A Formation in northern India (Xiao et al., 2022).

Appendisphaera setosa Liu et al., 2014a.

Fig. 11E–H.

Synonymy:

2013 Unnamed (G); Liu et al., Fig. 12K–L.

2014a *Appendisphaera setosa* Liu et al., p. 31, figs. 5.9, 21.1–21.8, 22.1–22.9.

2019 *Appendisphaera setosa* Liu et al; Liu and Moczydłowska, pp. 56, 58, Fig. 27.

2019 *Appendisphaera setosa* Liu et al; Shang et al., p. 10, Fig. 4E–J.

? 2020 *Appendisphaera setosa* Liu et al; Grazhdankin et al., Fig. 3A.

2021 *Appendisphaera setosa* Liu et al; Ouyang et al., Fig. 11*K*–O.

2022 *Appendisphaera setosa* Liu et al; Xiao et al., Figs. 15–16.

Material: Four well-preserved specimens and 28 poorly preserved specimens.

Description: Large compressed vesicle (originally spheroidal) bearing abundant, evenly and widely distributed processes that are homomorphic, straight, thin, cylindrical, and slightly tapering toward to the tip. Processes are hollow and presumably communicate with the vesicle cavity.

Dimensions: Process length 12.7–27.1 μm; process basal width 1.1–2.1 μm; distance between processes 2.3–8.2 μm.

Remarks: Among all published species of *Appendisphaera*, *A. setosa* is similar to *A. clava*, but processes in the latter species tend to have an expanded base. *A. setosa* can be distinguished from other *Appendisphaera* species by its thin, rigid, widely and regularly arranged processes that lack a basal expansion. The specimen illustrated as *A. setosa* in Grazhdankin et al. (2020) have basally expanded processes and is better assigned to *A. tenuis*.

Occurrence: The Ediacaran Doushantuo Formation in the Shennongjia (this paper) and Yangtze Gorges areas (Liu and Moczydłowska, 2019; Liu et al., 2013, 2014a; Ouyang et al., 2021) of Hubei Province, and the Songlin area of Guizhou Province (Shang et al., 2019), South China; Ediacaran Krol A Formation in northern India (Xiao et al., 2022); and possibly the Cambrian-aged Oppokun Formation in central Arctic Siberia (Grazhdankin et al., 2020).

Appendisphaera tabifica Moczydłowska et al., 1993, emend. Liu and Moczydłowska, 2019.

Fig. 12A–D.

Synonymy:

1993 *Appendisphaera*? *tabifica* Moczydłowska et al., p. 508, text-Fig. 6C–D.

2015 *Appendisphaera tabifica* Moczydłowska et al.; Nagovitsin and Kochnev, Fig. 4.I.5.

2019 *Appendisphaera tabifica* Moczydłowska et al., 1993, emend. Liu and Moczydłowska, pp. 58, 61, Fig. 28, and synonyms therein.

2021 *Appendisphaera tabifica* Moczydłowska et al.; Ouyang et al., Fig. 11*L*–N, P.

Material: Two well-preserved specimens and two relatively poorly preserved specimens.

Description: Circular to deformed vesicle, originally spheroidal, medium to large in size, bearing numerous densely distributed homomorphic processes. Processes are thin and cylindrical in shape and have sharp-pointed tips. Processes are hollow and communicate freely with vesicle interior.

Dimensions: Vesicle diameter 162.3–215.5 μm; process length 9.5–15.9 μm; ratio of process length to vesicle diameter 4.4–10.9%; process width<1 μm.

Remarks: Liu and Moczydłowska (2019) revised this species and

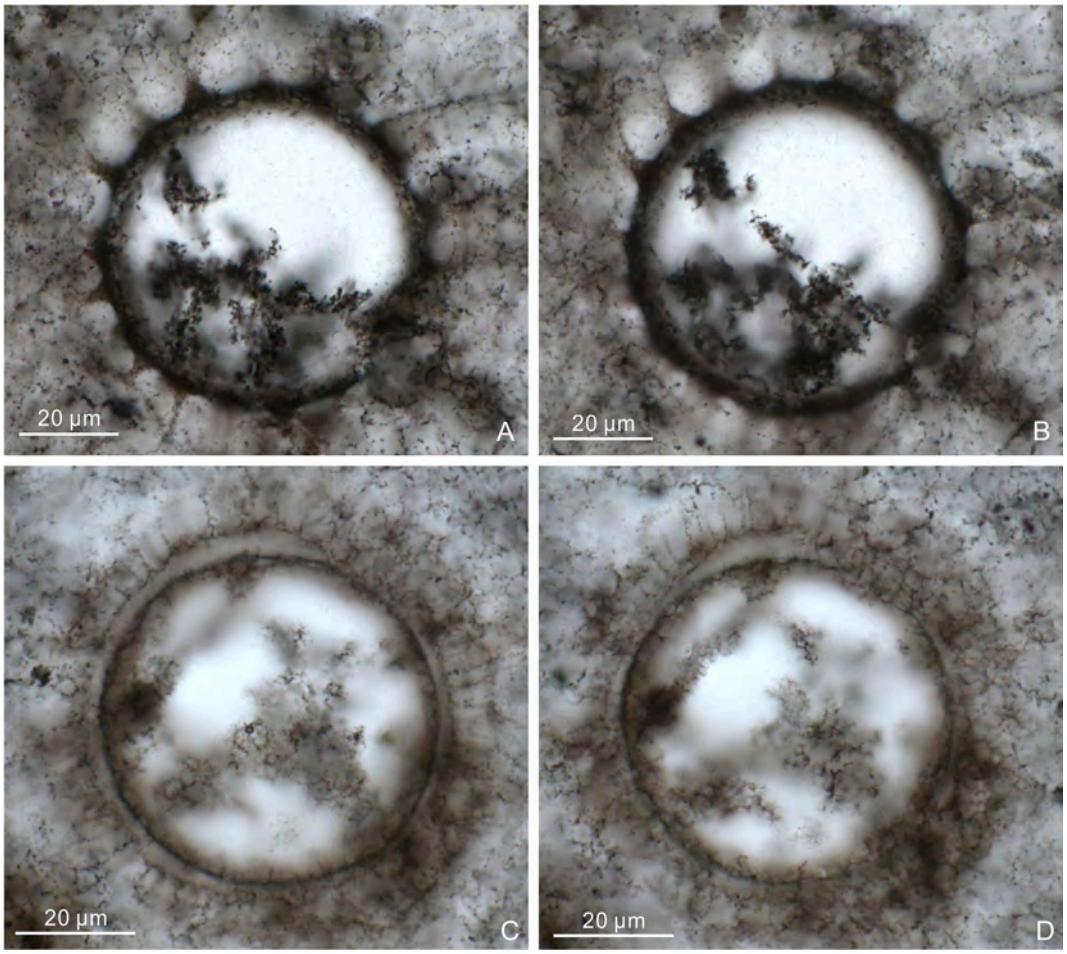

Fig. 13. (A–B) *Cavaspina acuminata* (Kolosova, 1991) Moczydłowska et al., 1993; 21LHC-1–37.4 m-3p-3 (10 × 106.5), showing same specimen at different focal levels. (C–D) *Cavaspina basiconica* Moczydłowska et al., 1993; 21LHC-1–37.4 m-10p-3 (13.3 × 93.6), showing same specimen at different focal levels.

regarded *A. barbata*, *A. centoreticulata*, *A. dilutopila*, and *A. minutiforma* to be junior synonyms of *A. tabifica*. These species are all characterized by abundant thin and flexible processes. The membrane-like structure and coalesced processes, which were part of the original diagnosis of *A. tabifica* (Moczydłowska et al., 1993), were regarded as taphonomic features and have been removed from the emended diagnosis (Liu and Moczydłowska, 2019). The specimens described here can be accommodated in the diagnosis of *A. tabifica* as emended by Liu and Moczydłowska (2019). We recognize that several *Appendisphaera* species (e.g., *A. anguina*, *A.*? *brevispina*, *A. clava*) are characterized by thin, homomorphic, and densely arranged processes, but *A. anguina* has a larger vesicle and much longer processes (holotype of *A. anguina*: 224 μm in vesicle diameter and 100 μm in process length; Grey, 2005), *A.*? *brevispina* and *A. clava* have larger vesicles and relatively shorter processes (holotype of *A.*? *brevispina*: 350 μm in vesicle diameter and 6 μm in process length; holotype of *A. clava*: 420 μm in vesicle diameter and 12 μm in process length; Liu et al., 2014a), which can be differentiate from *A. tabifica* (holotype of *A. tabifica*: 115 μm in vesicle diameter and 40–46 μm in process length; Moczydłowska et al., 1993).

Occurrence: The Ediacaran Doushantuo Formation in the Shennongjia (this paper) and Yangtze Gorges areas (Liu and Moczydłowska, 2019; Liu et al., 2014a; Ouyang et al., 2021) of Hubei Province, South China; and Ediacaran strata in Siberian (Moczydłowska and Nagovitsin, 2012; Moczydłowska et al., 1993; Nagovitsin and Kochnev, 2015), East European Platform (Veis et al., 2006), Australia (Grey, 2005; Willman and Moczydłowska, 2008; Willman et al., 2006; Zang and Walter, 1992a), and India (Prasad and Asher, 2016).

Appendisphaera tenuis Moczydłowska et al., 1993, emend. Moczydłowska, 2005.

Fig. 12E–F.

Synonymy:

1993 *Appendisphaera tenuis* Moczydłowska et al., pp. 506–508, text-Fig. 7.

2015 *Appendisphaera tenuis* Moczydłowska et al.; Nagovitsin and Kochnev, Fig. 4.I.3.

2015 *Appendisphaera tenuis* Moczydłowska et al.; Golubkova et al., Fig. 2a.

2019 *Appendisphaera tenuis* Moczydłowska et al., 1993, emend. Moczydłowska, 2005; Liu and Moczydłowska, pp. 61–65, Figs. 29–30, and synonyms therein.

2019 *Appendisphaera tenuis* Moczydłowska et al., 1993, emend. Moczydłowska, 2005; Anderson et al., p. 509, Fig. 6H–I.

2019 *Appendisphaera tenuis* Moczydłowska et al., 1993, emend. Moczydłowska, 2005; Shang et al., pp. 10–11, Fig. 5.

2020 *Appendisphaera tenuis* Moczydłowska et al., 1993, emend. Moczydłowska, 2005; Shang and Liu, p. 157, Fig. 5A–B.

2020 *Appendisphaera tenuis* Moczydłowska et al., 1993, emend. Moczydłowska, 2005; Vorob'eva and Petrov, pp. 370, 372, pl. I, Figs. 3–4.

2021 *Appendisphaera tenuis* Moczydłowska et al., 1993, emend. Moczydłowska, 2005; Ouyang et al., Fig. 11Q–R.

2022 *Appendisphaera tenuis* Moczydłowska et al., 1993, emend. Moczydłowska, 2005; Xiao et al., Fig. 17.

Material: One moderately preserved specimen and 11 poorly preserved specimens.

Description: Large spheroidal vesicle, bearing abundant evenly

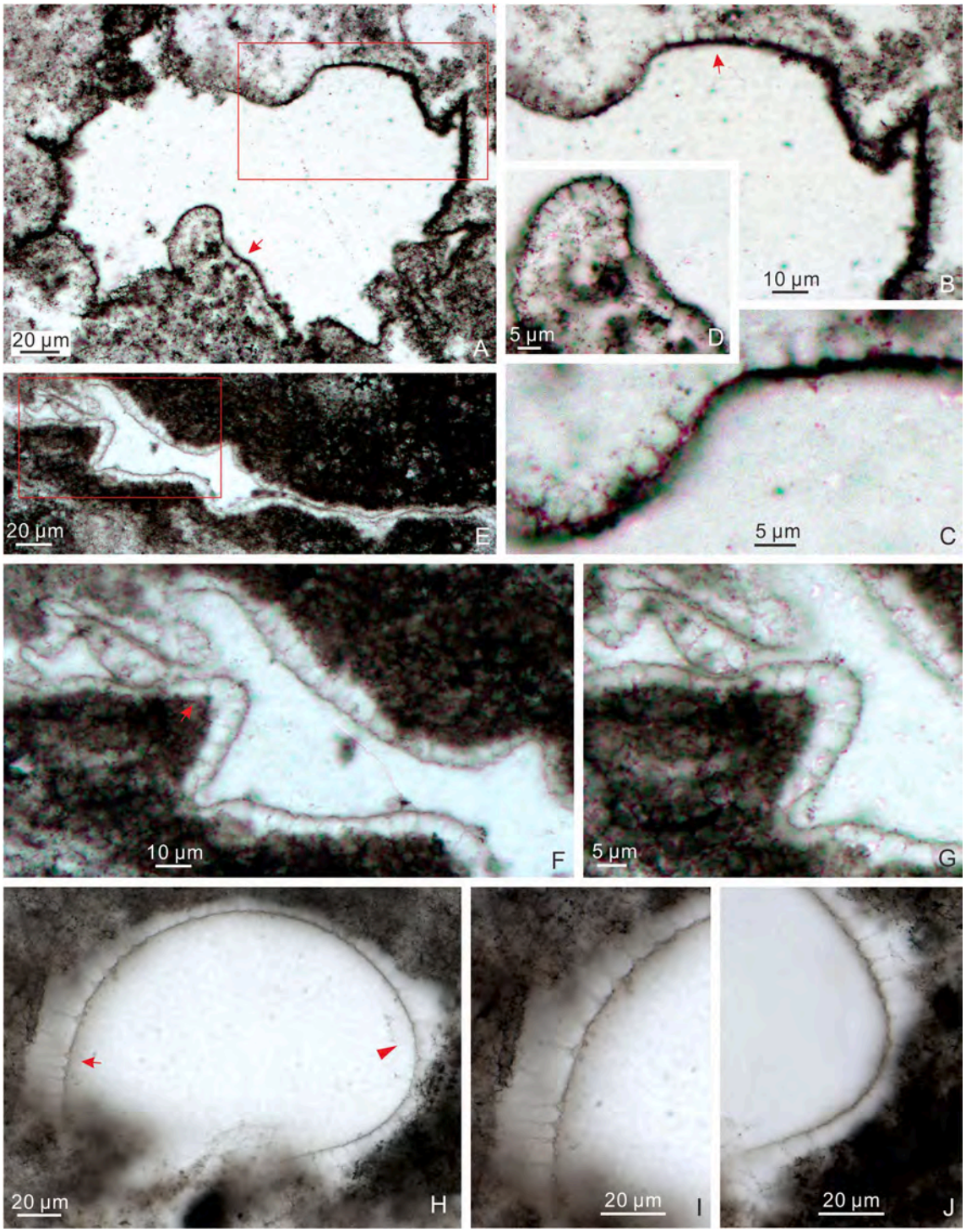

Fig. 14. (A–D) *Cavaspina* sp.; LHG-d3 + 30 cm-1–10 (19.9 × 67). (B, D) Magnified views of areas in (A) marked by rectangle and arrow, respectively. (C) Magnified view of area marked by arrow in (B). (E–J) *Cavaspina basiconica* Moczydłowska et al., 1993. (E–G) LHG2-d2-3.1 m-4c-19 (16.8 × 73.4). (F) Magnified view of area marked by rectangle in (E). (G) Magnified view of area marked by arrow in (F) at a different focal level. (H–J) 21LHC-1–36.1 m-17p-1 (15.6 × 108). (I) Magnified view of area marked by arrow in (H). (J) Magnified view of area marked by arrowhead in (H) at a different focal level.

distributed processes that are homomorphic, thin, slender, slightly expanded at base. They are hollow and communicate freely with vesicle interior.

Dimensions: Vesicle diameter 387.1–461.2 μm; process length 21.1–35.2 μm; ratio of process length to vesicle diameter 6.8–8.0%; process basal width ~ 3 μm.

Remarks: The specimens described here are characterized by their relatively short and slender processes with a slightly expanded base. *A. tenuis* is somewhat similar to *A. clava* but the latter has smaller ratio of process length to vesicle diameter (typical < 5%; Liu et al., 2014a).

Occurrence: The Ediacaran Doushantuo Formation in the Shennongjia (this paper) and Yangtze Gorges areas (Liu and Moczydłowska, 2019; Liu et al., 2014a; Ouyang et al., 2021) of Hubei Province, the Zhangjiajie area (Shang and Liu, 2020) of Hunan Province, the Weng'an (Xiao et al., 2014) and Songlin areas (Shang et al., 2019) of Guizhou Province, South China; Ediacaran successions in Siberia (Golubkova et al., 2010;

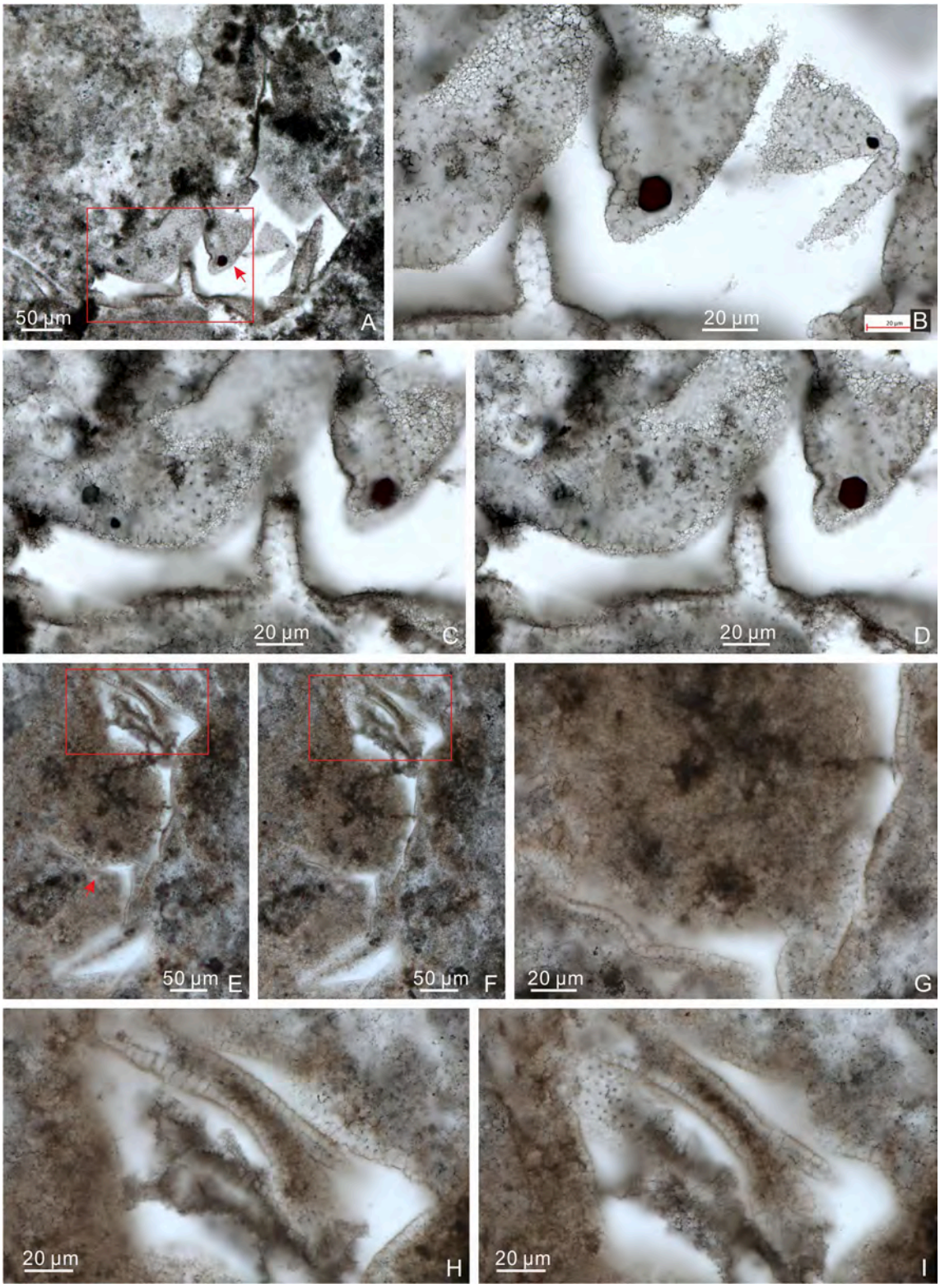

Fig. 15. *Cavaspina* sp. (A–D) 21LHC-1–36.1 m-8p-6 (22.3 × 89). (B–C) Magnified views of area marked by rectangle in (A) at different focal levels. (D) Magnified view of area marked by arrow in (A) at a different focal level. (E–I) 21LHC-1–34.4 m-4p-2 (15.7 × 105.7). (E–F) Different views of the same specimen. (G–H) Magnified views of areas in (E) marked by arrow and rectangle, respectively. (I) Magnified view of area marked by rectangle in (F).

Moczydłowska et al., 1993; Nagovitsin and Kochnev, 2015; Sergeev et al., 2011; Vorob'eva and Petrov, 2020; Vorob'eva et al., 2008), Australia (Grey, 2005; Willman and Moczydłowska, 2008), and India (Prasad and Asher, 2016; Shukla and Tiwari, 2014; Xiao et al., 2022); the uppermost Khesen Formation in northern Mongolia (Anderson et al., 2019), which is considered terminal Ediacaran in age although it contains Cambrian-age detrital zircons (Anttila and Macdonald, 2020).

Genus *Cavaspina* Moczydłowska et al., 1993.

Type species: *Cavaspina acuminata* (Kolosova, 1991) Moczydłowska et al., 1993.

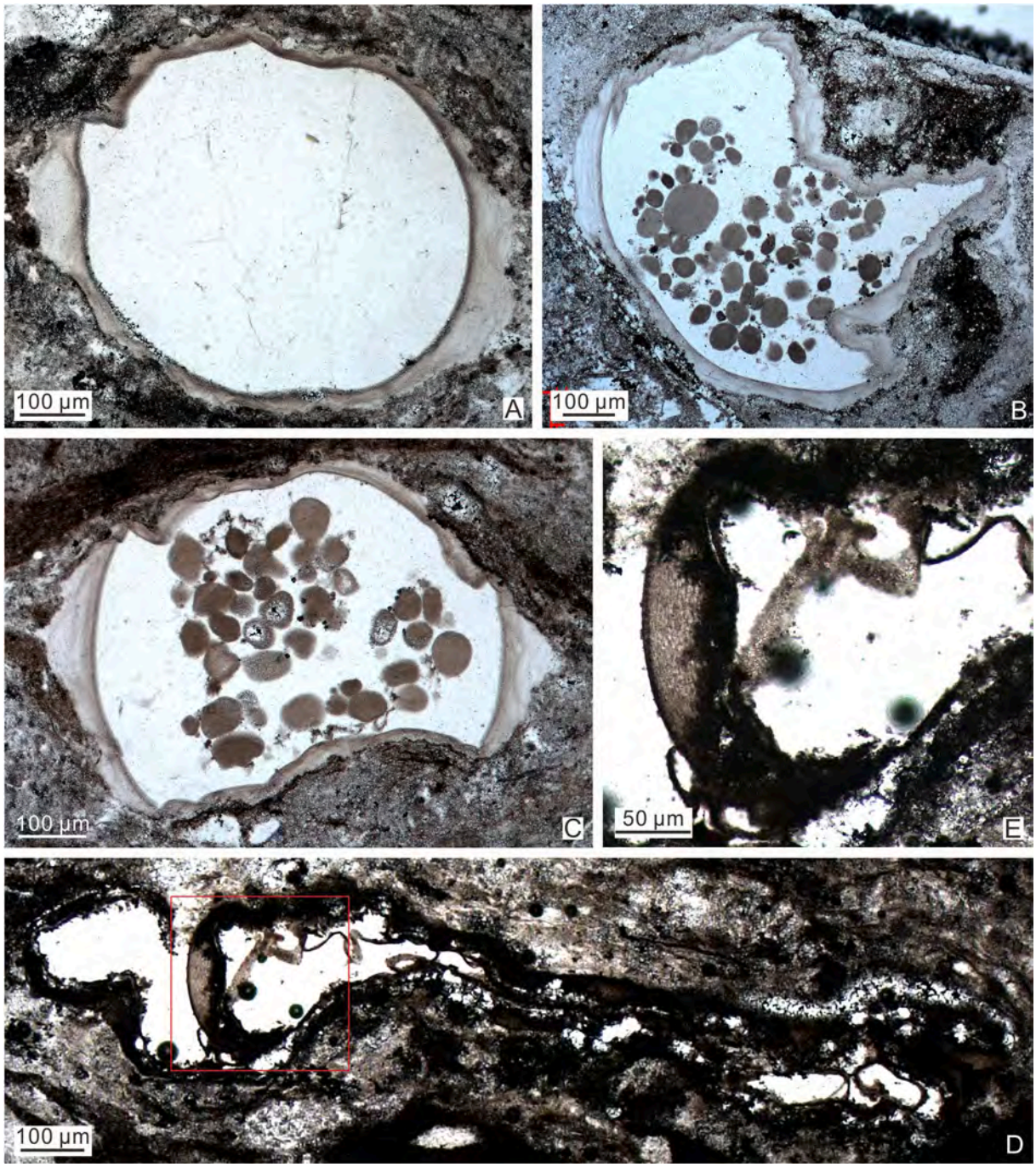

Fig. 16. (A–C) *Crassimembrana* sp. (A) LHG2-d2-3.1 m-4c-18 (18 × 74.7). (B) LHG2-d2-3.1 m-3p-22 (41.5 × 78.3). (C) LHG2-d2-3.1 m-3c-31 (20.8 × 77). (D–E) *Crassimembrana* cf. *multitunica* Ouyang et al., 2021; LHG2-d2-3.1 m-43–6 (47.0, NR). (E) Magnified view of area marked by rectangle in (D).

Cavaspina acuminata (Kolosova, 1991) Moczydłowska et al., 1993. Fig. 13A–B.

Synonymy:

1993 *Cavaspina acuminata* (Kolosova, 1991) Moczydłowska et al., pp. 509–510, text-Fig. 10A–B.

2017 *Cavaspina acuminata* (Kolosova, 1991) Moczydłowska et al.; Nie et al., p. 374, fig. 5.1–5.4.

2019 *Cavaspina acuminata* (Kolosova, 1991) Moczydłowska et al.; Liu and Moczydłowska, pp. 76–78, Fig. 38, and synonyms therein.

2019 *Cavaspina acuminata* (Kolosova, 1991) Moczydłowska et al.; Shang et al., pp. 19–21, Fig. 8A–D.

2020 *Cavaspina acuminata* (Kolosova, 1991) Moczydłowska et al.; Shang and Liu, pp. 157–158, Fig. 5D–H.

2021 *Cavaspina acuminata* (Kolosova, 1991) Moczydłowska et al.; Ouyang et al., Fig. 13A.

Material: One moderately preserved specimen.

Description: Small-sized spheroidal vesicle bearing small number of irregularly distributed processes. Processes are short, hollow, conical, and well communicate with vesicle interior.

Dimensions: Vesicle diameter ~ 68.9 μm; process length 8.4–14.4 μm that is 12.2–20.9% of vesicle diameter; process basal width 3.5–6.8 μm; process spaced at 2.3–12.5 μm.

Remarks: The genus *Cavaspina* is characterized by its relatively short conical processes and contains four recognized species, *C. acuminata*, *C. basiconica*, *C. conica*, and *C. uria*. *C. acuminata* differs from *C. basiconica* in that the latter has more closely and evenly distributed

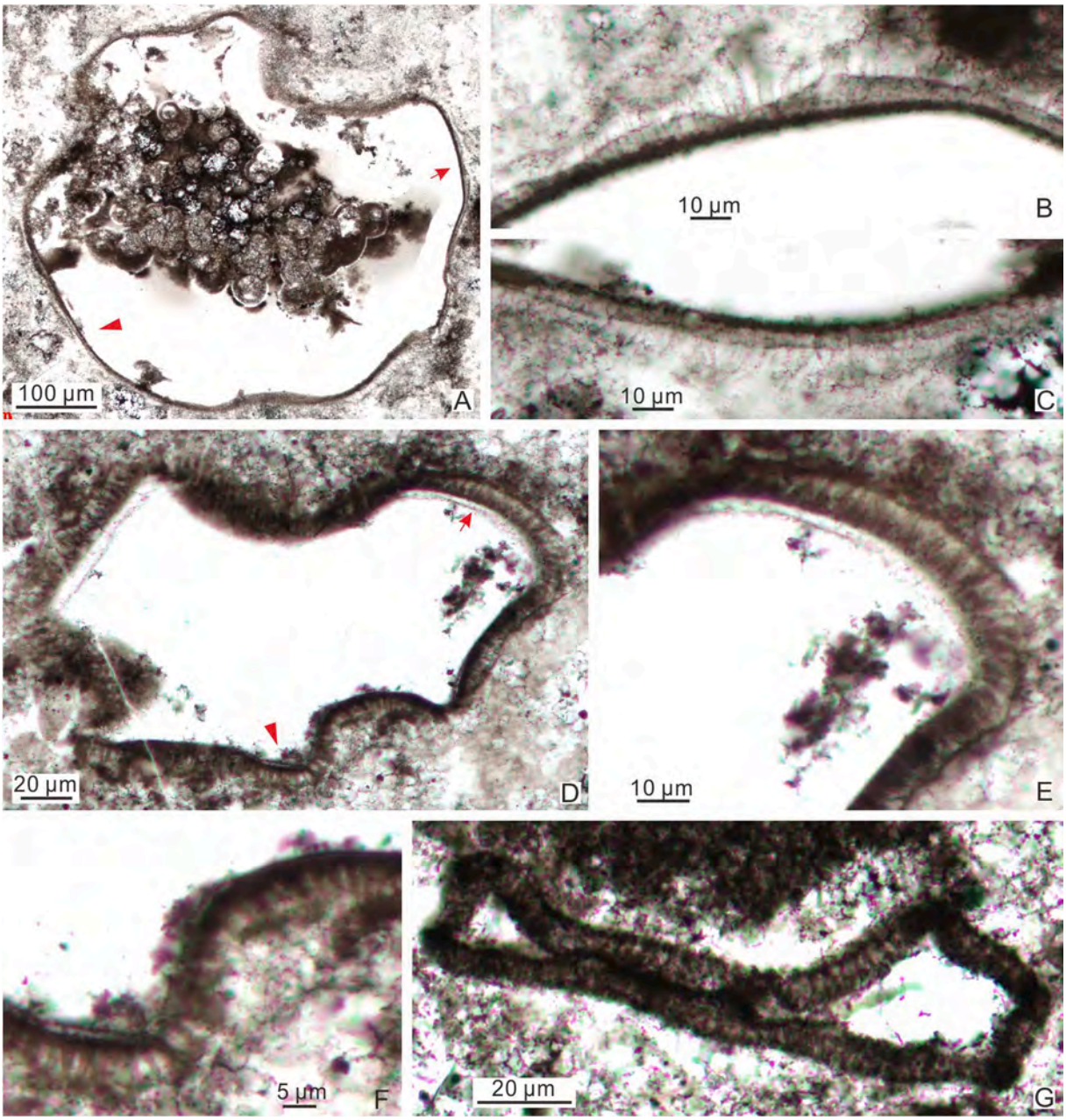

Fig. 17. (A–C) *Cymatiosphaeroides forabilatus* Liu and Moczydłowska, 2019, emend. Shang et al., 2019; LHG-d2-3.4 m-3p-20 (30.7 × 66). (B–C) Magnified views of areas in (A) marked by arrow and arrowhead, respectively. (D–G) *Cymatiosphaeroides* sp. (D–F) LHG-d2-4.3 m-5–1 (24 × 80.2). (E–F) Magnified views of areas in (D) marked by arrow and arrowhead, respectively. (G) LHG-d2-60 cm-1–3.

processes with a sharply pointed tip and a slightly widened base; from *C. conica* in that the latter has more densely and regularly arranged processes; and from *C. uria* in that the processes of the latter have an expanded base.

Occurrence: The Ediacaran Doushantuo Formation in the Shennongjia (this paper) and Yangtze Gorges areas (Liu and Moczydłowska, 2019; Liu et al., 2014a; Ouyang et al., 2021) of Hubei Province, the Zhangjiajie area of Hunan Province (Nie et al., 2017; Ouyang et al., 2017; Shang and Liu, 2020), the Weng'an (Xiao et al., 2014; Zhou et al., 2001) and Songlin areas (Shang et al., 2019) of Guizhou Province, South China; Ediacaran successions in Siberia (Moczydłowska, 2005; Moczydłowska et al., 1993; Moczydłowska and Nagovitsin, 2012), East European Platform (Veis et al., 2006; Vorob'eva et al., 2009a), Australia (Willman and Moczydłowska, 2008, 2011), and India (Prasad and Asher, 2016; Shukla and Tiwari, 2014).

Cavaspina basiconica Moczydłowska et al., 1993.

Fig. 13C–D, 14E–J.

Synonymy:

1993 *Cavaspina basiconica* Moczydłowska et al., pp. 510–512, text-Fig. 11.

? 2014 *Cavaspina acuminata* (Kolosova, 1991) Moczydłowska et al.; Shukla and Tiwari, p. 216, Fig. 5C–D.

2017 *Cavaspina basiconica* Moczydłowska et al.; Nie et al., pp. 374–375, fig. 5.5–5.6.

2019 *Cavaspina basiconica* Moczydłowska et al.; Liu and Moczydłowska, pp. 78–81, Fig. 39, and synonyms therein.

2019 *Cavaspina basiconica* Moczydłowska et al.; Anderson et al., pp. 509–510, Fig. 7A–F.

2019 *Cavaspina basiconica* Moczydłowska et al.; Shang et al., p. 21, Fig. 8E–G.

2020 *Cavaspina basiconica* Moczydłowska et al.; Vorob'eva and Petrov, p. 374, pl. II, Figs. 16–18.

Material: Three well-preserved specimens and three poorly preserved specimens.

Description: Large deformed vesicle (originally spheroidal) bearing numerous evenly distributed processes that are homomorphic, short, and separated by a small gap. Processes have a deflated basal expansion and taper rapidly from the base to a slender distal portion with a sharply pointed tip. Processes are hollow and freely communicate with vesicle cavity.

Dimensions: Vesicle 60.6–251.6 μm in diameter; processes 4.8–16.8 μm in length; process basal expansion 1.7–4.1 μm in width and ~

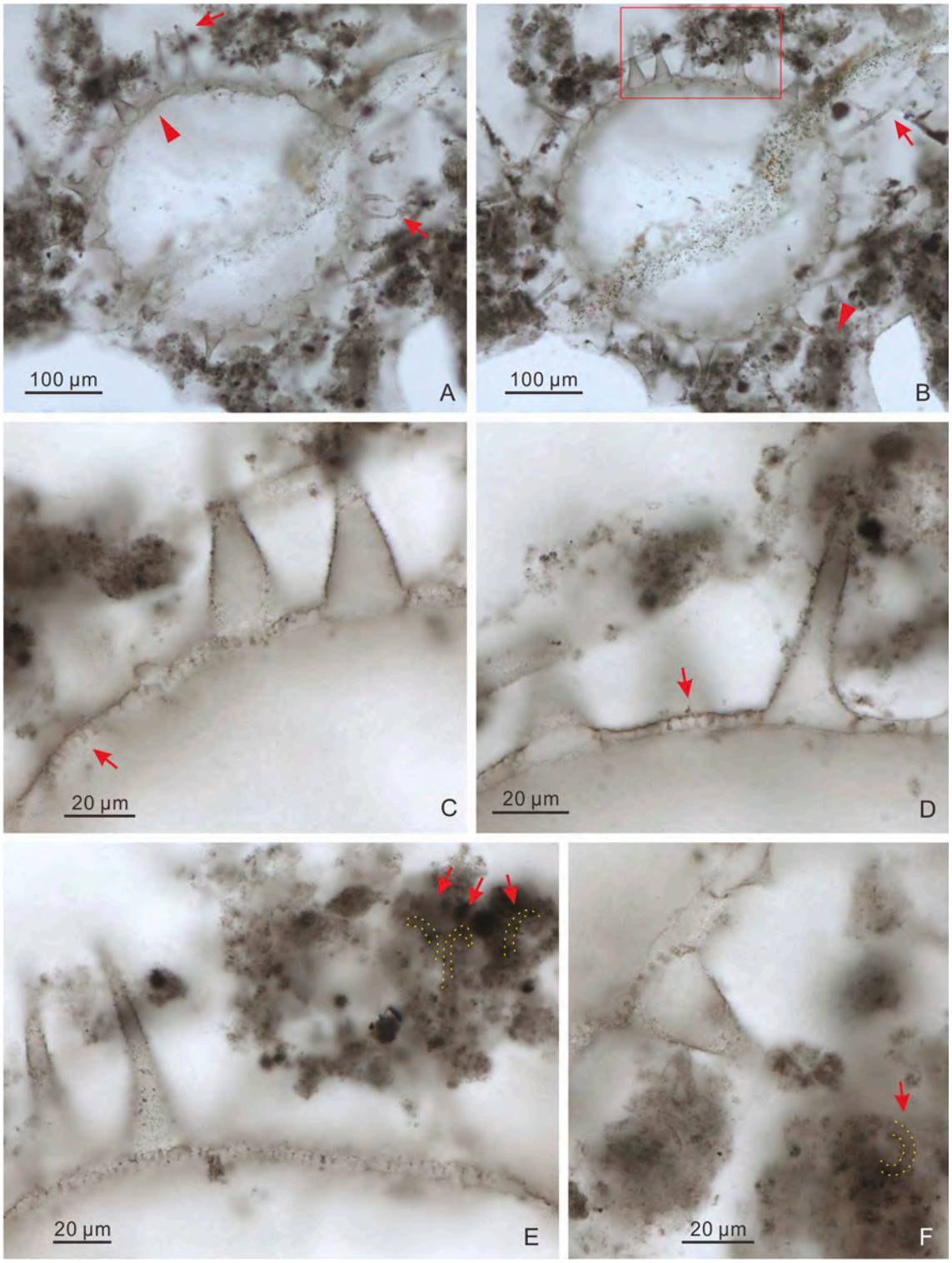

Fig. 18. *Duospinosphaera shennongjiaensis* sp. nov. holotype: 21LHC-1–45.6 m-1c-2 (18.5 × 94.8). (A–B) Different views of the same specimen, with arrows marking occasionally hooked tips of large processes. (C–D) Magnified views of area in (A) marked by arrowhead at different focal levels, with arrows denoting small cylindrical processes. (E–F) Magnified views of area in (B) marked by rectangle and arrowhead, respectively, with arrows denoting occasionally curved terminations of large processes.

1.0–3.5 μm in height; processes spaced at ~ 1.0–4.2 μm.

Remarks: Our specimens are very similar to *C. basiconica* and *Mengeosphaera*? *gracilis* (Liu et al., 2014a; their figs. 51.6, 60) in their basally expanded processes. However, our specimens have shorter, smaller, and relatively widely spaced (rather than basally joined) processes, which better conform to the diagnostic features of *C. basiconica*. One specimen described from the Outer Krol Belt of Lesser Himalaya in India is poorly preserved but its processes likely have distinct expanded bases (Shukla and Tiwari, 2014, Fig. 5C–D); we regard this specimen as a possible example of *C. basiconica*, but better-preserved specimens are needed to confirm this taxonomic identification.

Occurrence: The Ediacaran Doushantuo Formation in the Shennongjia (this paper) and Yangtze Gorges areas (Liu and Moczydłowska, 2019; Liu et al., 2014a) of Hubei Province, the Zhangjiajie area of Hunan Province (Nie et al., 2017; Ouyang et al., 2017), the Weng'an (Xiao et al., 2014; Zhou et al., 2001) and Songlin areas (Shang et al., 2019) of Guizhou Province, South China; Ediacaran successions in Siberia (Moczydłowska, 2005; Moczydłowska et al., 1993; Vorob'eva and Petrov, 2020), Australia (Grey, 2005; Willman and Moczydłowska, 2008, 2011; Willman et al., 2006; Zang and Walter, 1992a), and India (Prasad and Asher, 2016; Shukla and Tiwari, 2014); the uppermost Khesen Formation in northern Mongolia (Anderson et al., 2017a, 2019), which is considered terminal Ediacaran in age although it contains Cambrian-age detrital zircons (Anttila and Macdonald, 2020).

Cavaspina sp.

Fig. 14A–D, 15.

Material: Three adequately preserved specimens.

Description: Large oval vesicle, originally spheroidal, bearing a low density of evenly and regularly distributed processes. Processes homomorphic, conical, very short, and tapering distally. They are hollow and communicate openly with the vesicle interior. One specimen appears to have an outer membrane surrounding the vesicle with processes (Fig. 15E–I).

Dimensions: Vesicle ~ 280.8–491.6 μm in diameter (estimated from circumference measurement); processes 3.0–5.8.6 μm in length, 0.6–1.8 μm in basal width, and 3.1–7.0 μm in spacing.

Remarks: The hollow, short, thin, conical processes of our specimens identify them with the genus *Cavaspina*. They differ from *C. basiconica* and *C. uria* in the lack of an expanded or widened conical base in their processes. They can be differentiated from *C. conica* by their very sparsely distributed processes. These specimens show similarities with *C. acuminata* but the processes of the latter are often unevenly distributed on vesicle surface. Since all three specimens in our collection are poorly preserved, they are placed in an open nomenclature.

Occurrence: The Ediacaran Doushantuo Formation in the Shennongjia area of Hubei Province, South China (this paper).

Genus *Crassimembrana* Ouyang et al., 2021.

Type species: *Crassimembrana multitunica* Ouyang et al., 2021.

Crassimembrana cf. *multitunica* Ouyang et al., 2021.

Fig. 16D–E.

Material: Two moderately preserved specimens.

Description: Large collapsed (originally spheroidal) vesicle encompassed by a thick membrane. The membrane is composed of multiple thin, discontinuous, and tightly compacted laminae.

Dimensions: Vesicle diameter ~ 495.7–1146.5 μm (estimated from circumference measurement) and membrane thickness measured at ~ 50.0–62.5 μm.

Remarks: Our specimens resemble *C. multitunica* in having a thick laminated membrane. However, compared with the holotype of *C. multitunica*, the membrane in our specimens consists of discontinuous and more tightly arranged laminae. Thus, they are tentatively placed in an open nomenclature as *Crassimembrana* cf. *multitunica*.

Occurrence: The Ediacaran Doushantuo Formation in the Shennongjia area of Hubei Province, South China (this paper).

Crassimembrana sp.

Fig. 16A–C.

Material: Twelve adequately preserved specimens.

Description: Large spheroidal vesicle, surrounded by a thick outer membrane with variable thicknesses along the perimeter and a diffuse outer limit. The membrane consists of thin multilaminate layers. The laminae are poorly preserved but are discernable in the inner part of the membrane. They are curved and more or less continuous. The outer limit of the membrane is irregular, resulting in variable membrane thickness along the perimeter. Dark-colored spheroidal debris are preserved inside some vesicles.

Dimensions: Vesicle diameter 458.6–1390.3 μm; membrane thickness ranging from 15.2 to 94.4 μm.

Remarks: The irregular outer limit of laminated membrane is probably a taphonomic artifact due to poor preservation and vesicle deformation (Fig. 16B–C). The current specimens are characterized by large vesicles surrounded by thick multilaminate layers, which agree with the diagnosis of the genus *Crassimembrana*. However, they differ from *C. crispans* which is characterized by anastomosed multilaminate layers to form a spongy texture, and from *C. multitunica* which is characterized by regularly spaced and finely-laminated outer layers. Our specimens are also somewhat similar to *Tianzhushania spinosa* in the presence of a thick multilaminate wall, but they do not have the cylindrical processes typical of *T. spinosa*. Likewise, our specimens can be differentiated from the genus *Laminasphaera* by the lack of long thin filamentous processes.

Occurrence: The Ediacaran Doushantuo Formation in the Shennongjia area of Hubei Province, South China (this paper).

Genus *Cymatiosphaeroides* Knoll, 1984, emend. Shang et al., 2019.

Type species: *Cymatiosphaeroides kullingii* Knoll, 1984, emend. Shang et al., 2019.

Cymatiosphaeroides forabilatus Liu and Moczydłowska, 2019, emend. Shang et al., 2019.

Fig. 17A–C.

Synonymy:

2019 *Cymatiosphaeroides forabilatus* Liu and Moczydłowska, pp. 81, 84, Fig. 41.

2019 *Cymatiosphaeroides forabilatus* Liu and Moczydłowska, 2019, emend. Shang et al., p. 22, Fig. 9, 10A–C.

2022 *Cymatiosphaeroides forabilatus* Liu and Moczydłowska, 2019, emend. Shang et al., 2019; Xiao et al., Figs. 20–22, and synonyms therein.

Material: Two well-preserved specimens and one poorly preserved specimen.

Description: Large spheroidal vesicle consisting of two concentric walls: an inner thick wall bearing abundant cylindrical processes, and an outer wall which is thin, smooth, and single-layered. Processes are homomorphic, simple, thin, uniform in length, and distally tapering to sharp-pointed tips. Processes evenly arise from the inner wall surface and penetrate the outer wall at about one fourth to half length. Several spheroidal internal bodies are preserved in the vesicle cavity (Fig. 17A).

Dimensions: Inner wall diameter 519.4 μm; distance between the inner wall and outer membrane 2.9–8.9 μm; process length 16.6–18.2 μm; ratio of process length to vesicle diameter 3.2–3.5%; process width < 1 μm; distance between processes 1.5–1.7 μm; internal body diameter 23.2–47.6 μm.

Remarks: We were unable to ascertain whether the processes are hollow or solid, because they are too thin and none of them were cut transversely in thin section. As discussed in Shang et al. (2019), the processes may have been originally hollow but appear solid due to taphonomic accumulation of organic carbon on or within the processes. Although we consider this is likely the case for our specimen, it remains to be shown that the holotype of *C. forabilatus* has originally hollow processes. Our specimen shows some similarities to *Membranosphaera formosa* (Liu and Moczydłowska, 2019; their fig. 68), but the latter has two distinct types of membranes and processes.

Occurrence: The Ediacaran Doushantuo Formation in the Shennongjia (this paper) and Yangtze Gorges areas (Liu and Moczydłowska, 2019) of Hubei Province, and the Songlin area of Guizhou Province (Shang

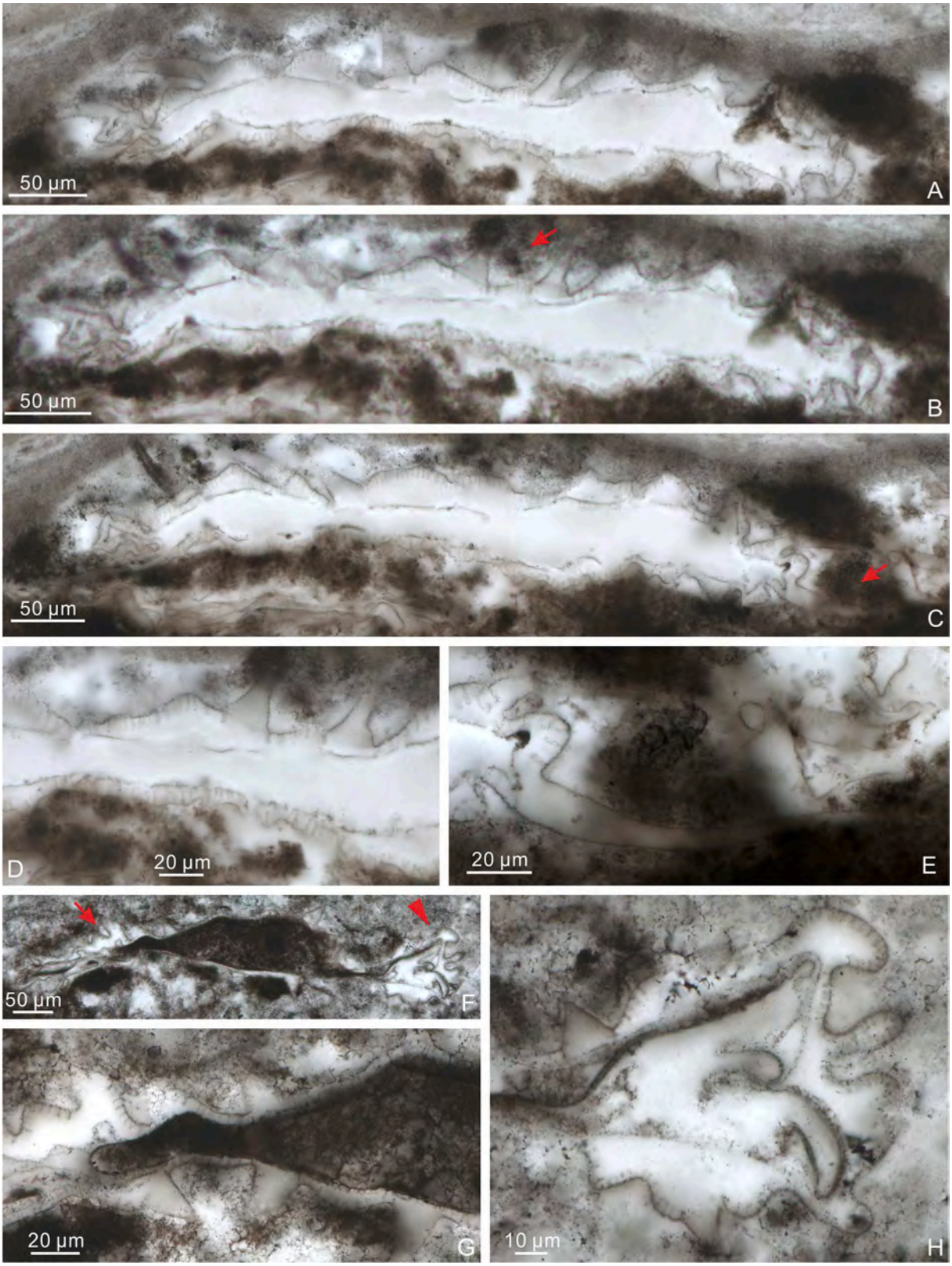

Fig. 19. *Duospinosphaera shennongjiaensis* sp. nov. (A–E) paratype, 21LHC-1–39.5 m-3c-30 (12 × 102.6). (A–C) Different views of the same specimen. (D–E) Magnified views of areas marked by arrows in (B–C), respectively. (F–H) 21LHC-1–45.2 m-4c-7 (12.4 × 106.4). (G–H) Magnified views of areas in (F) marked by arrow and arrowhead, respectively.

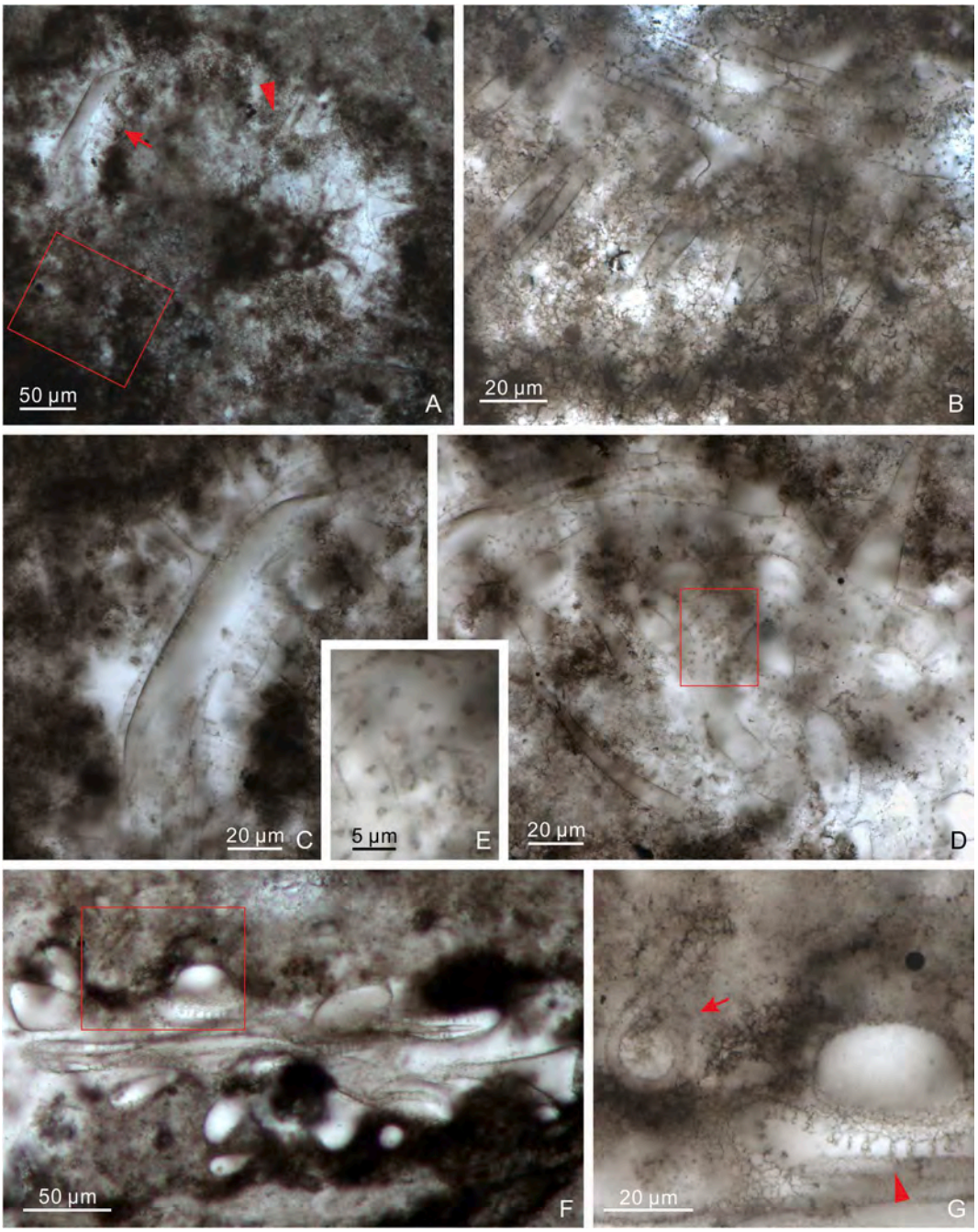

Fig. 20. *Duospinosphaera shennongjiaensis* sp. nov. (A–E) 21LHC-1–39.5 m-3p-4 (7.8 × 106). (B–D) Magnified views of areas in (A) marked by rectangle, arrow, and arrowhead, respectively. (E) Magnified view of area marked by rectangle in (D), showing transverse cross sections of hollow small processes. (F–G) 21LHC-1–45.6 m-3c-1 (19 × 93). (G) Magnified view of area marked by rectangle in (F), showing a large conical process with a curved termination (arrow) and small cylindrical hollow processes (arrowhead).

et al., 2019), South China; Ediacaran Krol A Formation in northern India (Xiao et al., 2022).

Cymatiosphaeroides sp.

Fig. 17D–G.

Material: One relatively well-preserved specimen and one moderately preserved specimen.

Description: Small to medium sized deformed vesicle, originally spheroidal, consisting of two concentric walls: an inner thick wall and a relatively thinner outer wall. The inner wall bears numerous densely and regularly arranged processes. Processes simple, apparently hollow, conical, short, similar in length, and sharply pointed at the distal ends. They support but do not penetrate the outer wall. Processes are basally joined or separated by a very small gap.

Dimensions: The first specimen (Fig. 17D–F): inner wall diameter ~ 185.9 μm (estimated from circumference measurement); process length 7.3–9.8 μm; process width 2.0–2.4 μm; ratio of process length to vesicle diameter 3.9–5.3%. The second specimen (Fig. 17G): inner wall diameter ~ 89.3 μm (estimated from circumference measurement); process length 5.7–7.4 μm; process width ~ 1.0 μm; ratio of process length to vesicle diameter 6.4–8.3%.

Remarks: The specimens described here are very similar to C. *kullingii* in overall shape and size range, but their processes are conical, have greater basal width, and are more densely distributed than those in C. *kullingii* (process basal width < 1.0 μm and process spacing 2–3 μm; Liu

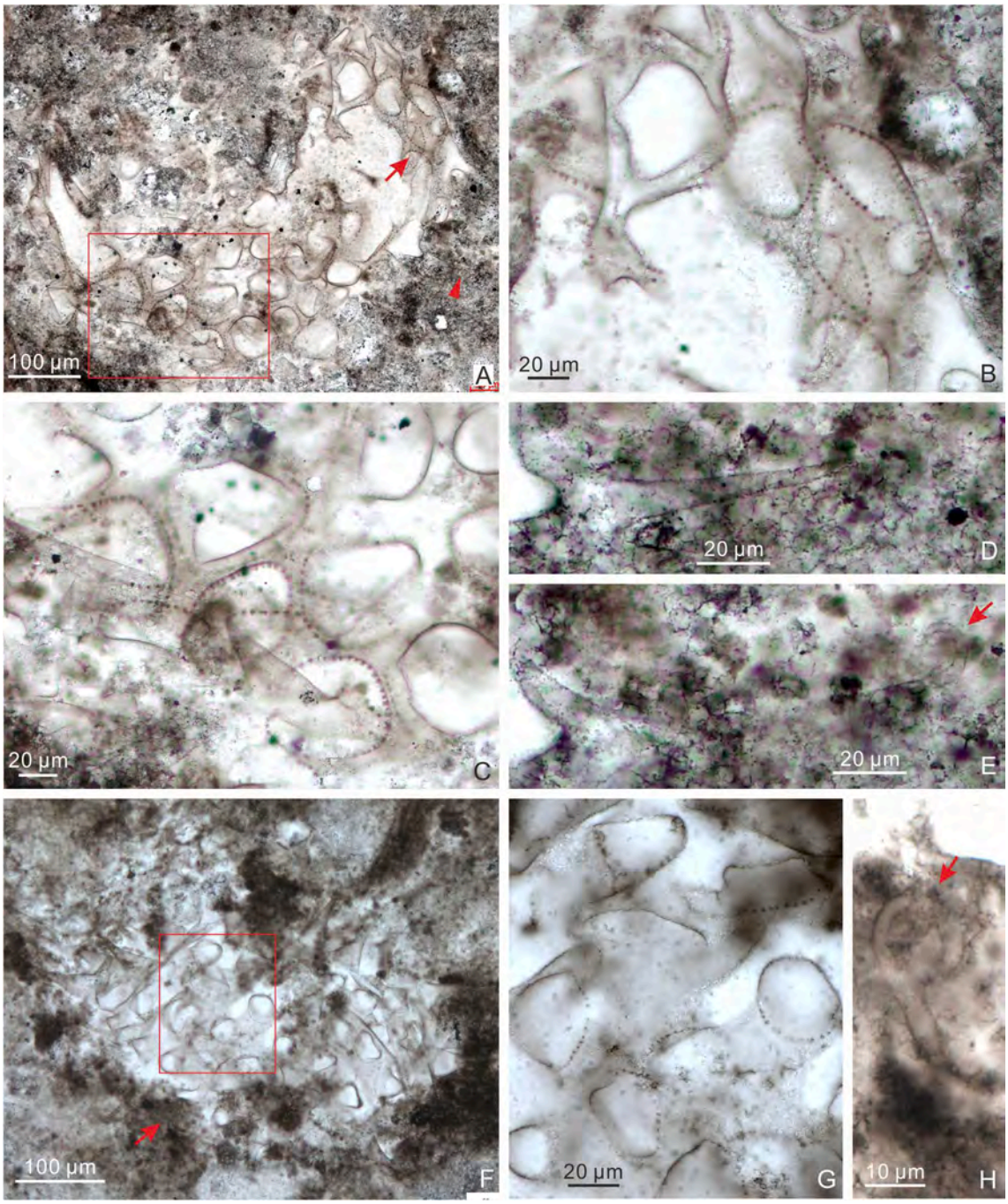

Fig. 21. *Duospinosphaera shennongjiaensis* sp. nov. (A–E) LHG-d2-90 cm-2p-1 (27.5 × 71.3). (B–C) Magnified views of areas in (A) marked by arrow and rectangle, respectively, showing small processes at different focal levels. (D–E) Magnified view of area marked by arrowhead in (A) at different focal levels, with arrow in (E) denoting a curved termination in a large conical process. (F–H) 21LHC-1–45.6 m-4p-1 (9 × 96). (G) Magnified view of area marked by rectangle in (F) at a different focal level, showing transverse cross sections of small processes. (H) Magnified view of area marked by arrow in (F), with arrow denoting a curved termination in a large conical process.

and Moczydłowska, 2019). Thus, they are tentatively placed in an open nomenclature of *Cymatiosphaeroides*.

Occurrence: The Ediacaran Doushantuo Formation in the Shennongjia area of Hubei Provinces, South China (this paper).

Genus *Duospinosphaera* gen. nov.

Type species: *Duospinosphaera shennongjiaensis* sp. nov., designated herein.

Derivation of name: From the Latin *duo-* and *spina*, and Greek *sphaîra*, with reference to the presence of two distinct types of processes (bimorphic processes) on a spheroidal vesicle.

Diagnosis: Large spheroidal vesicle with bimorphic processes. Small processes homomorphic, hollow, short, cylindrical, and densely and evenly distributed on the inner surface of vesicle wall, thus appearing like icicles hanging under the eaves. Large processes hollow, long, conical or biform, and unevenly spaced on the vesicle surface. Large processes communicate freely with the vesicle interior.

Remarks: There are five genera that are characterized by bimorphic processes, including *Bispinosphaera*, *Distosphaera*, *Duospinosphaera* gen. nov., *Sinosphaera*, and *Verrucosphaera*. These genera can be easily distinguished by their processes of different sizes and morphologies. In

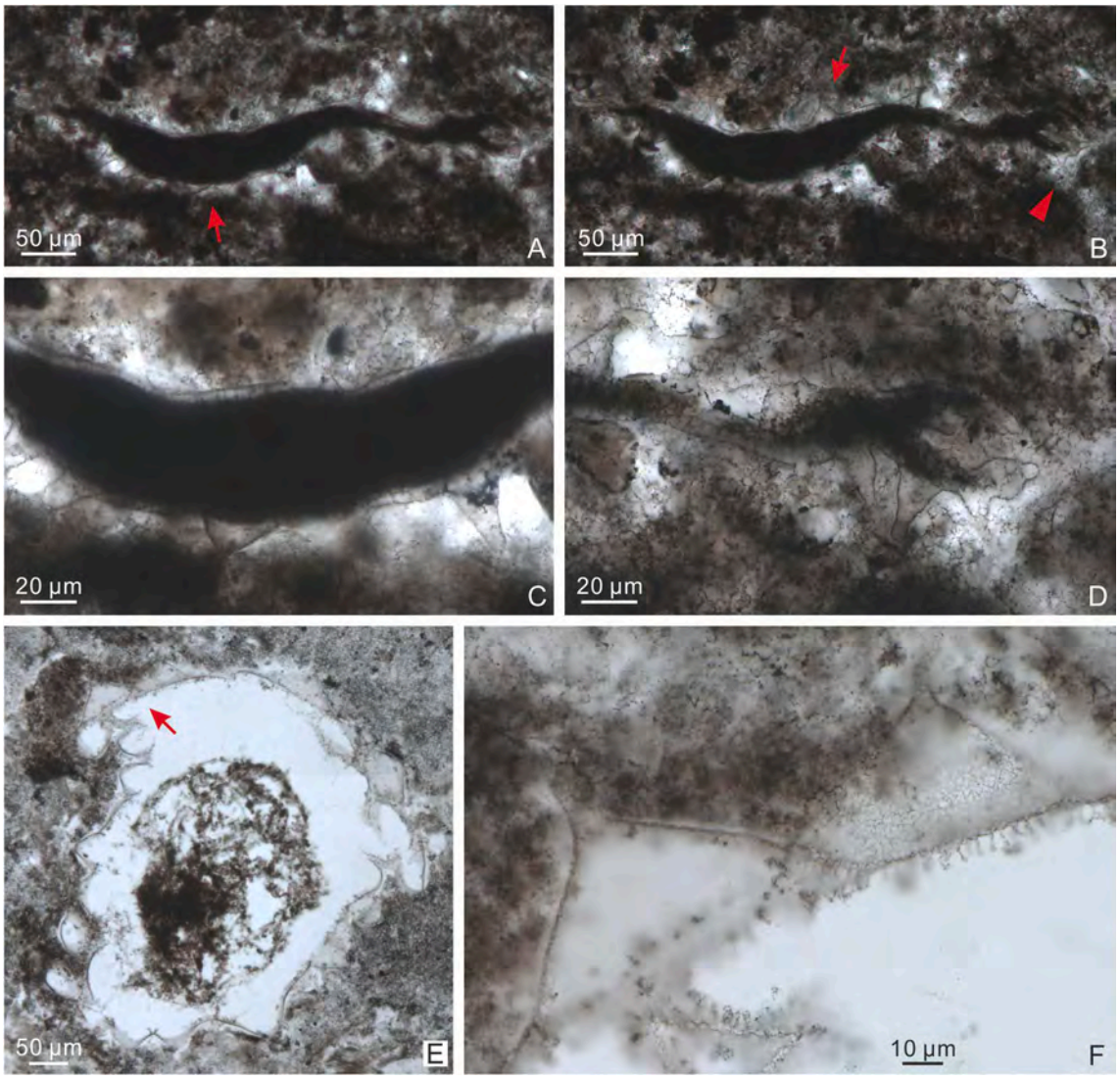

Fig. 22. *Duospinosphaera biformis* sp. nov. (A–D) 21LHC-1–43.7 m-22c-2 (9.5 × 98). (A–B) Different views of the same specimen, with arrow in (B) denoting a biform process. (C) Magnified view of area marked by arrow in (A). (D) Magnified view of area marked by arrowhead in (B) at a different focal level. (E–F) holotype, 21LHC-1–36.1 m-6p-19 (12 × 105). (F) Magnified view of area marked by arrow in (E), showing two types of processes.

Duospinosphaera, the small processes occur on the inner surface of the vesicle wall and they are hollow, short, and cylindrical, whereas the large processes on the outer surface are hollow and conical or biform. In *Bispinosphaera*, the small processes are solid and hair-like, whereas the large processes are hollow and conical (Ouyang et al., 2021), and may have internal cross-walls (Liu et al., 2014a). Both types of processes are hollow in *Duospinosphaera* and *Sinosphaera*, but the small processes in *Sinosphaera* are distributed on the outer surface of vesicles and they are generally conical or domal in shape (e.g., Liu et al., 2014a; Xiao et al., 2014). *Distosphaera* is characterized by an inner wall and an outer wall, with thin and hollow processes arising on the inner wall and supporting the outer wall, whereas broadly conical processes arise on the outer wall (see emended diagnosis in Liu and Moczydłowska, 2019). Finally, *Verrucosphaera* contains small solid spines that are located on the top of large hollow protrusions (Liu and Moczydłowska, 2019).

Duospinosphaera shennongjiaensis sp. nov.

Figs. 18–21.

Holotype: The specimen illustrated in Fig. 18, thin section 21LHC-1–45.6 m-1c-2 (18.5 × 94.8).

Paratype: The specimen illustrated in Fig. 19A–E, thin section 21LHC-1–39.5 m-3c-30 (12 × 102.6).

Etymology: In reference to the Shennongjia area where the described material was collected.

Locus typicus: The Ediacaran Doushantuo Formation at the Lianhuacun section, Shennongjia area of Hubei Province, South China.

Stratum typicum: Chert nodules in thin to medium bedded dolostones of unit 4, Doushantuo Formation.

Material: Seven adequately preserved specimens and 10 poorly preserved specimens.

Diagnosis: Large spheroidal vesicle bearing two types of hollow processes. Small processes are short, cylindrical, homomorphic, and regularly arranged on the inner surface of vesicle wall. Large processes elongate, conical, slightly expanded at the base, and gradually taper to a sharply-pointed termination that is occasionally but not consistently curved or hooked (e.g., Fig. 18E–F, 20G, 21E, H). Large processes unevenly distributed on the outer surface of vesicle wall and communicate with the vesicle interior. Two specimens have apparently solid small processes (e.g., Fig. 21B–C), which may be infilled with organic matter.

Dimensions: Holotype (Fig. 18): vesicle diameter 354.5 μm; small processes 3.8–4.0 μm in length, 0.9–1.5 μm in width, and spaced at 1.8–2.8 μm; large processes 119.2–123.5 μm in maximum length and 22.7–30.3 μm in basal width. Paratype (Fig. 19A–E): vesicle diameter 351.9 μm (estimated from circumference measurement); small processes 6.2–7.1 μm in length, ~1.0–1.1 μm in width, and spaced at 1.9–4.0 μm;

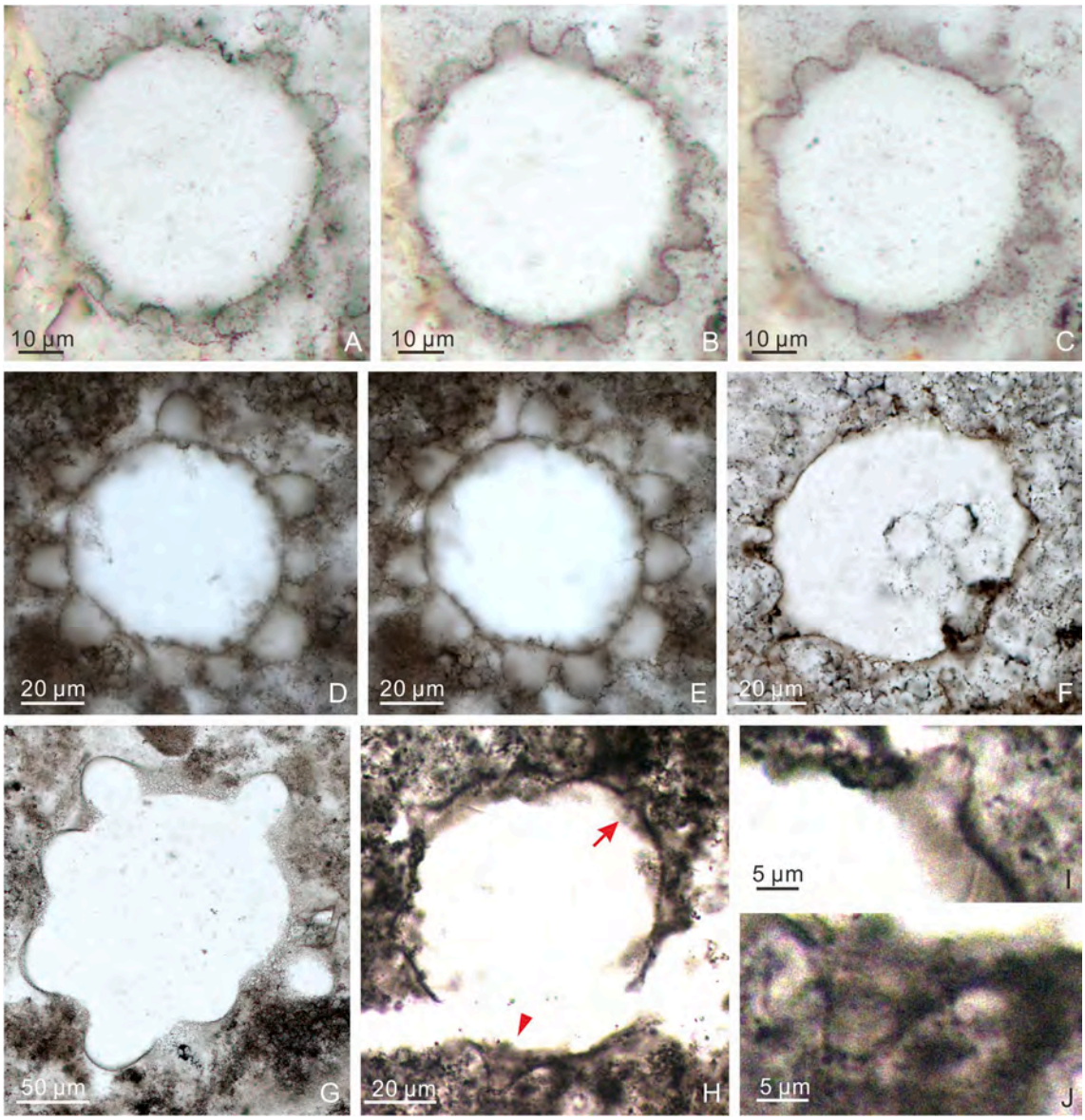

Fig. 23. (A–F) *Eotylotopalla dactylos* Zhang et al., 1998a. (A–C) LHG-d2-4.5 m-2–7 (32 × 66), different views of the same specimen. (D–E) 21LHC-1–45.6 m-10p-5 (13 × 97), different views of the same specimen. (F) 21LHC-1–43.7 m-1c-5 (9.3 × 109.5), showing cell-like inclusions in vesicle cavity. (G) *Eotylotopalla apophysa* (Vorob'eva et al., 2009b) n. comb. LHG2-d2-2 m-2–18 (25.6 × 70.5). (H–J) *Eotylotopalla* sp.; LHG2-d2-3.1 m-5-H-1 (39.2, NR). (I–J) Magnified views of areas in (H) marked by arrow and arrowhead, respectively.

large processes 39.2–132.5 μm in preserved length, and 11.4–20.6 μm in basal width. Other specimens: vesicle diameter 304.8–655.6 μm; small processes 2.5–5.1 μm in length, ~0.7–2.4 μm in width, and spaced at 2.1–3.8 μm; large processes 22.7–93.6 μm in preserved length (full length is difficult to measure because most processes are not fully captured in the thin section), 16.6–82.2 μm in basal width, with an apical spine ~ 3.9–11.0 μm in maximum width.

Occurrence: The Ediacaran Doushantuo Formation in the Shennongjia area of Hubei Provinces, South China (this paper).

Duospinosphaera biformis sp. nov.

Fig. 22.

Holotype: The specimen illustrated in Fig. 22E–F, thin section 21LHC-1–36.1 m-6p-19 (12 × 102.6).

Etymology: From Latin *bi-* and *formis*, with reference to biform large processes.

Locus typicus: The Ediacaran Doushantuo Formation at the Lianhuacun section, Shennongjia area of Hubei Province, South China.

Stratum typicum: Chert nodules in thin to medium bedded dolostones of unit 4, Doushantuo Formation.

Material: Three adequately preserved specimens and five poorly preserved specimens.

Diagnosis: Large spheroidal vesicle, bearing two types of hollow processes. Small processes are short, cylindrical, homomorphic, and regularly arranged on the inner surface of vesicle wall. Large processes heteromorphic, ranging from conical to biform in shape. Biform processes composed of a basal expansion and an apical spine. Basal expansion often obtusely conical. Apical spine short, acutely conical, and has a rounded termination.

Dimensions: Holotype (Fig. 22E–F): vesicle diameter 493.0 μm; small processes 4.0–4.5 μm in length, ~0.7–1.0 μm in width, and spaced at 1.8–3.8 μm; large processes 46.7–56.2 μm in maximum length; basal expansion 79.0–101.9 μm wide and 33.7–52.8 μm high; apical spine 2.7–2.9 μm in maximum width and 8.9–19.5 μm in maximum length. Other specimens: vesicle diameter 326.4–465.2 μm; small processes 4.5–6.1 μm in length, ~1.0 μm in width, and spaced at 3.0–5.5 μm; large processes 21.9–96.4 μm in preserved length; basal expansion 11.9–59.9

μm in width and 12.0–39.1 μm in height; apical spine 3.2–9.0 μm in maximum width and 12.4–42.6 μm in maximum length.

Remarks: Duospinosphaera biformis sp. nov. can be differentiated from *D. shennongjiaensis* sp. nov. by its large processes, which can be biform (Fig. 22F) or conical (Fig. 22C–D), hence heteromorphic.

Occurrence: The Ediacaran Doushantuo Formation in the Shennongjia area of Hubei Provinces, South China (this paper).

Genus *Eotylotopalla* Yin, 1987.

Type species: *Eotylotopalla delicata* Yin, 1987.

Synonymy:

2009b *Timanisphaera* Vorob'eva et al., p. 183.

Remarks: Eotylotopalla was first described by Yin (1987) based on its overall shape and rounded-conical processes. However, published *Eotylotopalla* species (e.g., *E. dactylos* Zhang et al., 1998a; *E. delicata* Yin, 1987; *E. quadrata* Liu and Moczydłowska, 2019; *E. strobilata* Sergeev et al., 2011) show greater variations in vesicle diameter, process length, process basal width, and number of processes than the holotype of *E. delicata*. Overall, the genus is characterized by small to large-sized spheroidal vesicle bearing sparse to densely distributed bulbous to hemispherical processes that are blunt or distally rounded. The genus

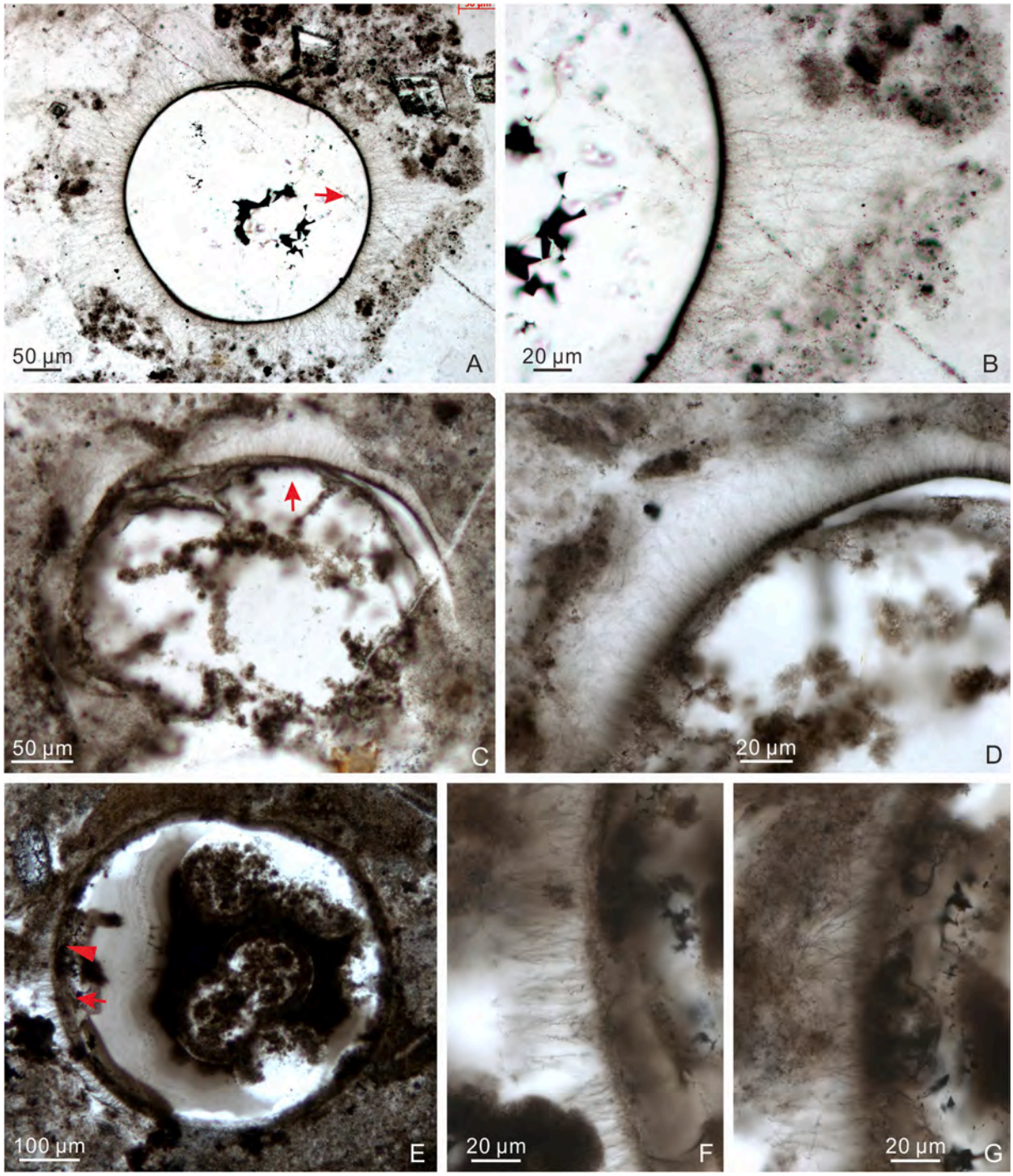

Fig. 24. *Ericiasphaera fibrilla* Liu and Moczydłowska, 2019. (A–B) LHG-d3 + 80 cm-6–1 (31.4 × 66.7). (B) Magnified view of area marked by arrow in (A). (C–D) 21LHC-1–32.8 m-5p-2 (14.8 × 109.3). (D) Magnified view of area marked by arrow in (C) with a rotation. (E–G) 21LHC-1–45.6 m-1c-13 (12 × 105). (F–G) Magnified views of areas in (E) marked by arrow and arrowhead, respectively.

Timanisphaera, which is typified by *Timanisphaera apophysa* Vorob'eva et al., 2009b and contains bluntly conoidal to hemispherical processes with distinctly rounded terminations (Vorob'eva et al., 2009b), can be accommodated in the diagnosis of *Eotylotopalla* and thus is here regarded as a junior synonym of *Eotylotopalla*.

Eotylotopalla apophysa (Vorob'eva et al., 2009b) n. comb.

Fig. 23G.

Synonymy:

2006 Vesicles with large hemispherical processes; Veis et al., pl. IV, Figs. 13, 24.

2006 *Pulvinosphaeridium* aff. *P. antiquum* Paskeviciene; Veis et al., pl. IV, Fig. 22.

2009a Unnamed form with hemispherical processes; Vorob'eva et al., Fig. 4 g.

2009b *Timanisphaera apophysa* Vorob'eva et al., p. 183, fig. 12.1–12.7, 12.9–12.10.

2013 *Eotylotopalla*? *grandis* Tang et al., p. 166, Fig. 12D–F.

Basionym: *Timanisphaera apophysa* Vorob'eva et al., 2009b, p. 183, fig. 12.1–12.7, 12.9–12.10.

Material: One well-preserved specimen and seven poorly preserved specimens.

Description: Medium-sized spheroidal vesicle bearing a small number of large hemispherical to cylindrical processes with distinctly rounded terminations. Processes are highly variable in length and width at the base, thus they change in shape at different focal levels when viewed in thin sections. They are sparsely arranged, hollow, and connect openly with vesicle cavity.

Dimensions: Vesicle diameter ~ 169.4 μm, processes 22.1–46.9 μm long or 13.1–23.6% of vesicle diameter and 31.6–53.8 μm wide at base, with seven processes in circumferential view.

Remarks: Timanisphaera and its type species *T. apophysa* were originally established by Vorob'eva et al. (2009b) and diagnosed with conical to hemispherical processes with distinctly rounded terminations. Tang et al. (2015) commented on the possible synonymy of *T. apophysa* and *Eotylotopalla*? *grandis* Tang et al., 2013, but they did not formally synonymize these two species. We concur with Tang et al. (2015) that the main features of *T. apophysa* can be accommodated in the diagnosis of *Eotylotopalla*. Thus, *T. apophysa* is here formally transferred to *Eotylotopalla* to become *Eotylotopalla apophysa* n. comb., and *Eotylotopalla*? *grandis* Tang et al., 2013 is here regarded as a junior synonym of *Eotylotopalla apophysa* n. comb. *Eotylotopalla apophysa* n. comb. can be differentiated from *E. dactylos* and *E. strobilata* by its large vesicle and low density of very large and robust processes. Liu and Moczydłowska (2019) listed *T. apophysa* as a junior synonym of *E. delicata*, but did not provide explanation or justification. In our opinion, *E. apophysa* n. comb. differs from *E. delicata* by its much larger vesicles (265–450 μm in *E. apophysa* n. comb.; Vorob'eva et al., 2009b *vs.* 35–42 μm in *E. delicata*; Yin, 1987) as well as larger processes (70–110 μm wide and 50–90 μm long in *E. apophysa* n. comb.; Vorob'eva et al., 2009b *vs.* 8.4–12.5 μm wide and 4.2–5.6 μm long in *E. delicata*; Yin, 1987; see also Fig. 16 of Tang et al., 2015). As discussed in Tang et al. (2015), *E. apophysa* is also somewhat similar to *Bacatisphaera baokangensis* (Xiao et al., 2014; Zhou et al., 2001). However, the processes of *B. baokangensis* are smaller and more densely distributed.

Specimens in our collection are smaller in vesicle diameter and process dimensions than the original material of *T. apophysa* described by Vorob'eva et al. (2009b, vesicle diameter 265–450 μm, process length 70–110 μm, and process basal width 50–90 μm), but their overall morphology and distinct hemispherical processes are similar.

Occurrence: The Ediacaran Doushantuo Formation in the

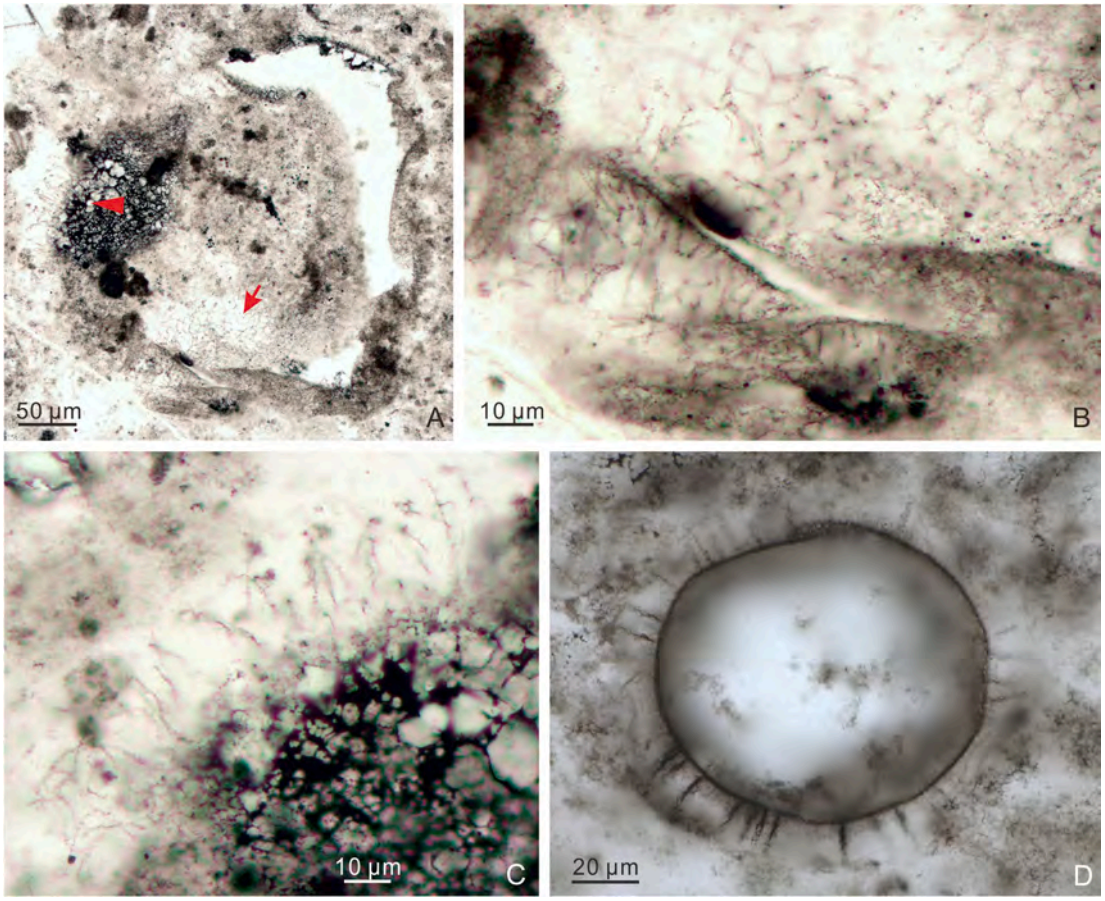

Fig. 25. (A–C) *Ericiasphaera magna* (Zhang, 1984a) Zhang et al., 1998a; LHG-d2-3.4 m-8–1 (22.5 × 70.8). (B–C) Magnified views of areas in (A) marked by arrow and arrowhead, respectively. (D) *Ericiasphaera rigida*? Zhang et al., 1998a; 21LHC-1–35 m-4p-4 (9.3 × 103.8).

Shennongjia area of Hubei Province, South China (this paper), Ediacaran strata in the East European Platform (Veis et al., 2006; Vorob'eva et al., 2009a, b), and the Tonian Liulaobei Formation in Huainan region of Anhui Province, North China (Tang et al., 2013).

Eotylotopalla dactylos Zhang et al., 1998a.

Fig. 23A–F.

Synonymy:

1998a *Eotylotopalla dactylos* Zhang et al., p. 26, fig. 7.8–7.9.

2014b *Eotylotopalla dactylos* Zhang et al.; Liu et al., Fig. 7B.

2014 *Eotylotopalla dactylos* Zhang et al.; Shukla and Tiwari, pp. 217, 219, Fig. 6A–B.

2015 *Eotylotopalla dactylos* Zhang et al.; Ouyang et al., p. 217, pl. I, Fig. 11.

2016 *Sinosphaera rupina* Zhang et al., 1998a, emend. Liu et al., 2014a; Prasad and Asher, p. 54, pl. VII, Figs. 3–5.

2019 *Eotylotopalla dactylos* Zhang et al.; Liu and Moczydłowska, pp. 95–96, Fig. 48, and synonyms therein.

2021 *Eotylotopalla dactylos* Zhang et al.; Ouyang et al., Fig. 14J–L.

2021 *Eotylotopalla dactylos* Zhang et al.; Liu et al., fig. 5.6–5.7.

Material: Four well-preserved specimens.

Description: Small spheroidal vesicle possessing a moderate number of robust, hollow, and regularly distributed processes. Processes are cylindrical or digitate in shape and slightly tapering towards a rounded or truncated tip. Processes hollow and freely communicate with vesicle interior. Vesicle may contain several cell-like structures (Fig. 23F).

Dimensions: Vesicle diameter 59.0–70.6 μm; processes 6.0–19.8 μm in length (or 10.2–22.2% of the vesicle diameter) and 6.3–15.7 μm in basal width; processes spaced at a distance of 4.1–6.2 μm, about one half of process basal width; 8–12 processes observed in circumferential view of vesicle.

Remarks: E. dactylos can be differentiated from all other *Eotylotopalla* species by its digitate process morphology. Published specimens of *E. dactylos* show a wide size range (35–200 μm in vesicle diameter, 6–30 μm in process length, and 5–23 μm in basal width of processes) relative to the original material of Zhang et al. (1998a; vesicle diameter 35–45 μm, process length 9–14 μm, and process basal width 6–8 μm). Our specimens morphologically resemble the holotype of *E. dactylos*, although their vesicles are slightly larger and processes are wider. A specimen of *E. dactylos* illustrated in Shukla and Tiwari (2014; their Fig. 6A–B) was said to have a thin transparent sheath covering some of its conical processes, but this feature is not clearly illustrated. Specimens described as *Sinosphaera rupina* in Prasad and Asher (2016, their pl. VII, Figs. 3–5) are here considered to be *E. dactylos*, as they have digitate processes with round terminations that characterize *E. dactylos*, rather than the bimorphic processes characteristic of *Sinosphaera*.

Occurrence: The Ediacaran Doushantuo Formation in the Shennongjia (this paper), Changyang (Liu et al., 2021), and Yangtze Gorges areas (Liu and Moczydłowska, 2019; Liu et al., 2014a, b; Ouyang et al., 2015, 2021; Zhang et al., 1998a) of Hubei Province, and the Weng'an area (Xiao et al., 2014) of Guizhou Province, South China; Ediacaran succession in India (Prasad and Asher, 2016; Shukla and Tiwari, 2014).

Eotylotopalla sp.

Fig. 23H–J.

Synonymy:

2014a *Eotylotopalla* sp.; Liu et al., pp. 61, 73, fig. 31.10–31.13.

Material: One moderately preserved specimen.

Description: Small spheroidal vesicle, bearing a small number of sparsely, unevenly spaced conical processes with a broad base and a rounded distal end. Processes hollow, generally wider than long, and openly communicate with vesicle interior.

Dimensions: Vesicle diameter 81.2 μm, processes 7.5–9.7 μm long and 9.2–14.4 μm wide at base, with six processes in an equatorial section.

Remarks: The present specimen is characterized by its slightly tapering cylindrical or conical processes, which fit the diagnosis of *Eotylotopalla*. However, it differs from *E. dactylos* by its distinctively smaller number of sparsely distributed processes. Thus, it is currently placed in an open nomenclature. Two specimens illustrated as *Eotylotopalla* sp. in Liu et al. (2014a; their fig. 31.10–31.13) are similar to our specimen in process morphology and overall dimensions.

Occurrence: The Ediacaran Doushantuo Formation in the Shennongjia (this paper) and Yangtze Gorges areas (Liu et al., 2014a) of Hubei Province, South China.

Genus *Ericiasphaera* Vidal, 1990, emend. Grey, 2005.

Type species: *Ericiasphaera spjeldnaesii* Vidal, 1990.

Ericiasphaera fibrilla Liu and Moczydłowska, 2019.

Fig. 24.

Synonymy:

2019 *Ericiasphaera fibrilla* Liu and Moczydłowska, p. 101, Fig. 52.

2019 *Ericiasphaera fibrilla* Liu and Moczydłowska; Shang et al., p. 23, Fig. 12B–C.

2021 *Ericiasphaera fibrilla* Liu and Moczydłowska; Ouyang et al., Fig. 12N–O.

Material: Seven relatively well-preserved specimens and 19 moderately preserved specimens.

Description: Large spheroidal vesicle possessing numerous hair-like processes on the vesicle surface. Processes long, thin, filamentous, solid, and very densely spaced.

Dimensions: One well-preserved specimen (Fig. 24A–B): vesicle ~ 313.0 μm in diameter; processes up to 134.3 μm in length (or 42.9% of vesicle diameter) and < 1 μm in width. Other specimens: vesicle diameter 233.1–323.9 μm; processes length 15.9–42.7 μm; ratio of process length to vesicle diameter ~ 6.0–11.3%.

Remarks: The size range compiled from previously known occurrences of this species is 72–500 μm in vesicle diameter and 16–50 μm in process length or 10–42.5% of vesicle diameter (Liu and Moczydłowska, 2019; Shang et al., 2019). One of our specimens (Fig. 24A–B) has extremely long processes but the proportions of process length relative to vesicle diameter is comparable to some previously described specimens (Liu and Moczydłowska, 2019).

Occurrence: The Ediacaran Doushantuo Formation in the Shennongjia (this paper) and Yangtze Gorges areas (Liu and Moczydłowska, 2019; Ouyang et al., 2021) of Hubei Province, and the Songlin area of Guizhou Province (Shang et al., 2019), South China.

Ericiasphaera magna (Zhang, 1984a) Zhang et al., 1998a.

Fig. 25A–C.

Synonymy:

1984a *Comasphaeridium magnum* Zhang, p. 98, pl. 1, Figs. 1–6.

1998a *Ericiasphaera magna* (Zhang, 1984a) Zhang et al., p. 28, fig. 8.1–8.2.

2015 *Ericiasphaera magna* (Zhang, 1984a) Zhang et al.; Ye et al., p. 49, pl. I, Figs. 6–8.

2019 *Ericiasphaera magna* (Zhang, 1984a) Zhang et al., 1988 (*sic*! It should be 1998); Liu and Moczydłowska, pp. 101, 103, Fig. 53, and synonyms therein.

2021 *Ericiasphaera magna* (Zhang, 1984a) Zhang et al.; Liu et al., fig. 4.5–4.6.

Material: Four moderately and six poorly preserved specimens.

Description: Large deformed vesicle (originally spheroidal) bearing abundant and densely arranged processes. Processes homomorphic, solid, flexible, cylindrical, terminated with a sharp-pointed or blunt tip.

Dimensions: Vesicle diameter of one of the better-preserved specimens ~ 310.5 μm; process length 13.2–34.4 μm; process width estimated < 0.5 μm; distance between processes 3.9–7.3 μm.

Remarks: Ericiasphaera differs from *Appendisphaera* in having solid processes. *E. magna* is different from other species of *Ericiasphaera* in its long, thin, flexible, and uniformly cylindrical processes.

Occurrence: The Ediacaran Doushantuo Formation in the Shennongjia (this paper), Changyang (Liu et al., 2021), and Yangtze Gorges areas (Liu and Moczydłowska, 2019; Liu et al., 2014a; Zhang et al., 1998a) of Hubei Province; the Zhangjiajie area of Hunan Province (Hawkins et al., 2017); and the Weng'an area of Guizhou Province (Xiao et al., 2014; Yuan and Hofmann, 1998; Zhang et al., 1998b), South China.

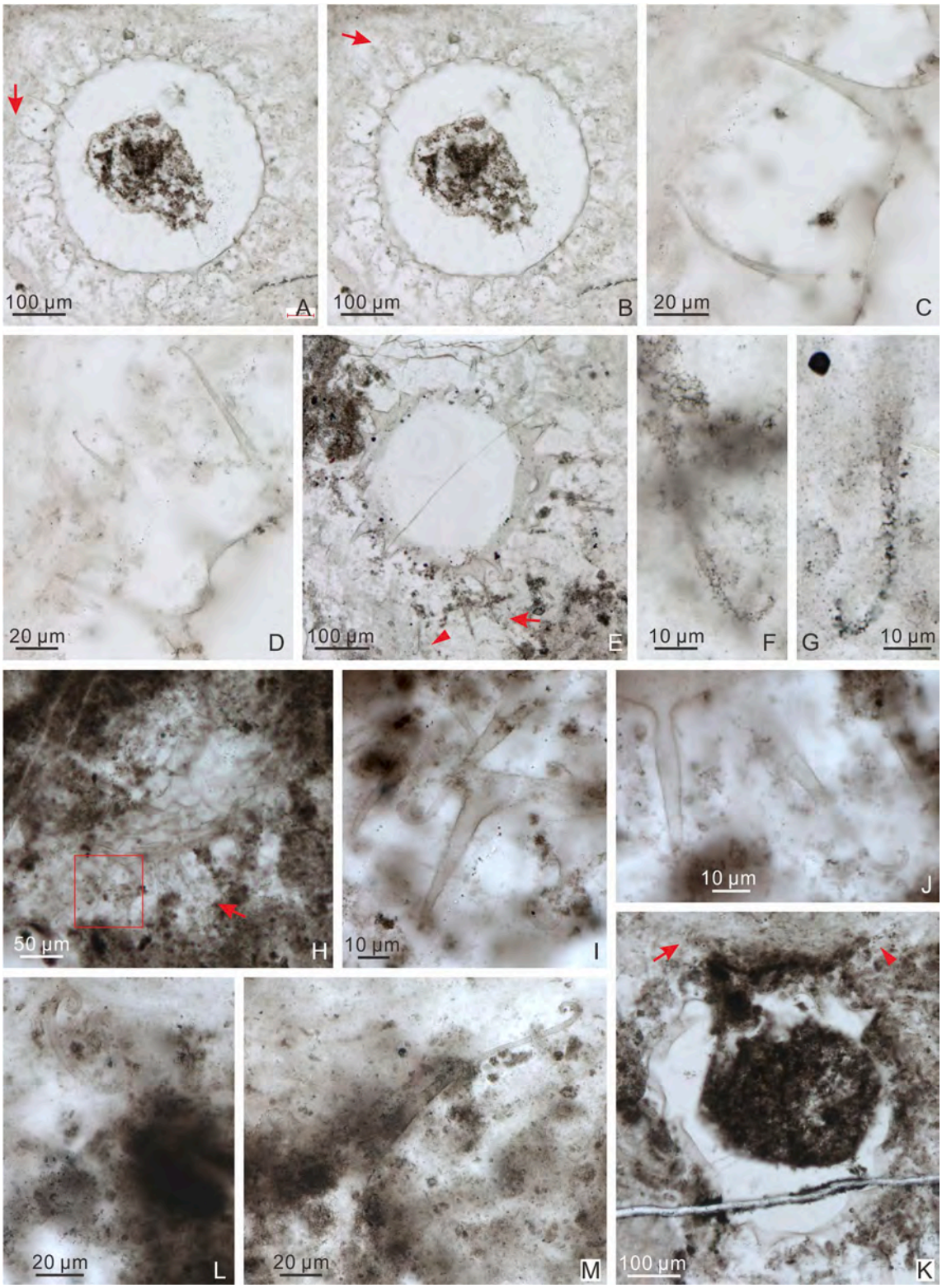

Fig. 26. (A–G) *Hocosphaeridium dilatatum* Liu et al., 2014a. (A–D) 21LHC-1–39.5 m-6p-13 (23.5 × 101). (A–B) Different views of the same specimen. (C–D) Magnified views of areas marked by arrows in (A–B), respectively. (E–G) 21LHC-1–35 m-1p-4 (21 × 87.8). (F–G) Magnified views of areas in (E) marked by arrow and arrowhead, respectively. (H–J) *Hocosphaeridium scaberfacium* (Zang *in* Zang and Walter, 1992a) emend. Liu et al., 2014a; 21LHC-1–39.5 m-6p-7 (2.2 × 102.4). (I–J) Magnified views of areas in (H) marked by rectangle and arrow, respectively. (K–M) *Hocosphaeridium* sp.; 21LHC-1–41.4 m-1p-4 (10.5 × 108). (L–M) Magnified views of areas in (K) marked by arrow and arrowhead, respectively.

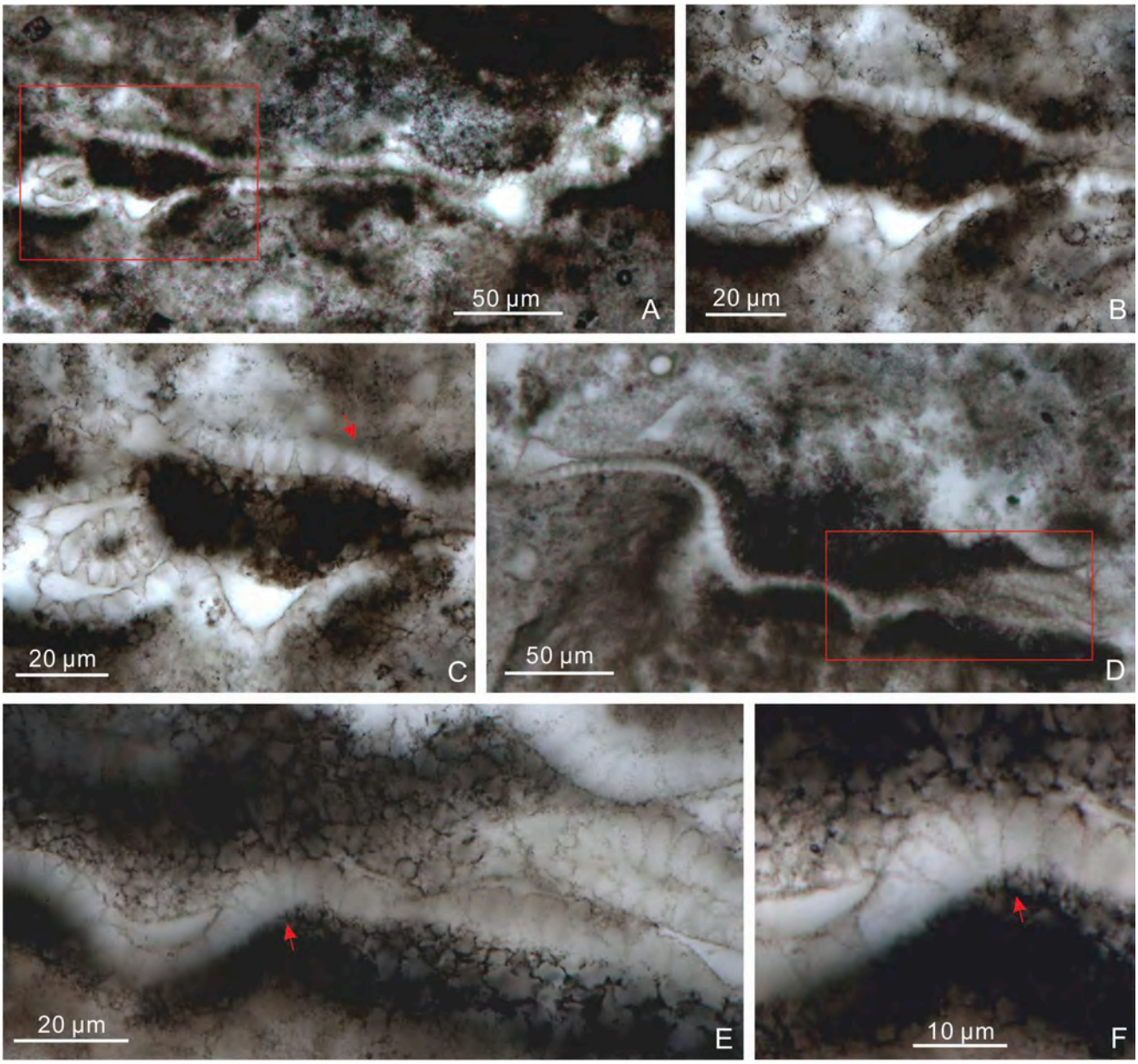

Fig. 27. *Knollisphaeridium coniformum* Liu and Moczydłowska, 2019. (A–C) 21LHC-1–43.7 m-2c-16 (15.3 × 97.5). (B–C) Magnified views of area marked by rectangle in (A) at different focal levels, with arrow in (C) denoting a sharp process tip. (D–F) 21LHC-1–43.7 m-5c-2 (10.5 × 92.7). (E) Magnified view of area marked by rectangle in (D). (F) Magnified view of area marked by arrow in (E), with arrow denoting sharp process tips.

Ericiasphaera rigida? Zhang et al., 1998a.

Fig. 25D.

Synonymy:

? 1998a *Ericiasphaera rigida* Zhang et al., p. 28, fig. 8.4–8.7.

? 2019 *Ericiasphaera rigida* Zhang et al.; Liu and Moczydłowska, p. 104, Figs. 53–54, and synonyms therein.

Material: One adequately preserved specimen.

Description: Small spheroidal vesicle bearing solid, short, cylindrical processes that taper gradually toward a blunt tip.

Dimensions: vesicle diameter 85.7 × 99.4 μm; processes ~ 7.8–14.9 μm in length (or 8.4–16.0% of the vesicle diameter) and 0.7–1.8 μm in width; processes spaced at ~ 2.8–27.5 μm.

Remarks: The current specimen is similar to *Ericiasphaera rigida* in overall morphology and size dimensions, but its processes are longer than those in the holotype of *E. rigida* (~6.2% of vesicle diameter; Zhang et al., 1998a, their fig. 8.6). In addition, processes in our specimen are variably preserved, with darker-colored processes better preserved and seemingly thicker than lighter-colored ones, giving an impression that the processes are unevenly distributed and variable in length. Thus, we tentatively identify our specimen as *Ericiasphaera rigida*?

Occurrence: The Ediacaran Doushantuo Formation in the Shennongjia area of Hubei Provinces, South China (this paper).

Genus *Hocosphaeridium* Zang *in* Zang and Walter, 1992a, emend. Xiao et al., 2014.

Type species: *Hocosphaeridium scaberfacium* (Zang *in* Zang and Walter, 1992a) emend. Liu et al., 2014a.

Hocosphaeridium dilatatum Liu et al., 2014a.

Fig. 26A–G.

Synonymy:

2014a *Hocosphaeridium dilatatum* Liu et al., pp. 77–78, figs. 39.2, 40.1–40.8.

Material: Two well preserved specimens.

Description: Large spheroidal vesicle with abundant closely spaced but basally separated, homomorphic, and distally hooked processes.

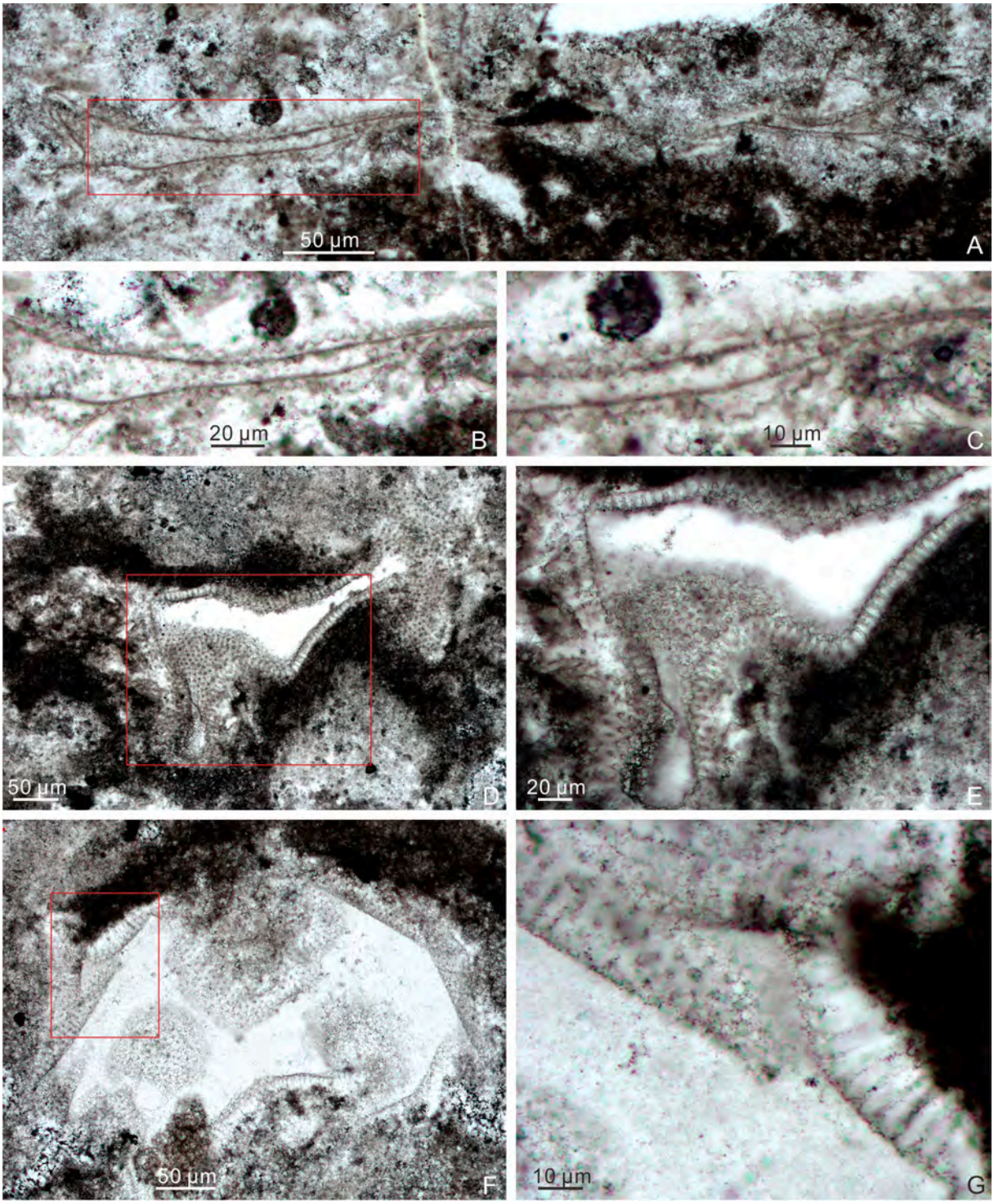

Fig. 28. (A–C) *Knollisphaeridium denticulatum* Liu et al., 2014a; LHG-d2-50 cm-2–13 (19.5 × 71.8). (B–C) Magnified views of area marked by rectangle in (A) at different magnifications. (D–G) *Knollisphaeridium maximum* (Yin, 1987) Willman and Moczydłowska, 2008, emended. Liu and Moczydłowska, 2019. (D–E) LHG-d2-2 m-6–1 (22.7 × 73.8). (F–G) LHG2-d2-3.1 m-3p-45 (31 × 76). (E, G) Magnified views of areas marked by rectangle in (D, F), respectively.

Processes have an expanded conical base that rapidly taper to a sharp tip. The end of the tip is consistently bent 180° or more. Processes hollow and communicate well with vesicle cavity.

Dimensions: Vesicle diameter 300.9–420.7 μm; processes 98.4–114.8 μm in length (or 23.4–38.2% of vesicle diameter), 17.6–40.1 μm in basal width, 24.1–27.8 μm in basal expansion height, and 2.0–30.4 μm in basal spacing; approximately 20–35 processes in circumferential view.

Remarks: The specimens described here are morphologically similar to the holotype of *H. dilatatum* (Liu et al., 2014a). However, in comparison to the specimens described from the Yangtze Gorges area of South China (125–165 μm in vesicle diameter, 55–65 μm in process total length, and 8–12 μm in process basal width; Liu et al., 2014a), our specimens are much larger in size dimensions. Nonetheless, we consider the size difference as intraspecific variation and identify the current specimens as *H. dilatatum*.

Occurrence: The Ediacaran Doushantuo Formation in the

Shennongjia (this paper) and Yangtze Gorges areas (Liu et al., 2014a) of Hubei Province, South China.

Hocosphaeridium scaberfacium (Zang *in* Zang and Walter, 1992a) emend. Liu et al., 2014a.

Fig. 26H–J.

Synonymy:

1992a *Hocosphaeridium scaberfacium* Zang *in* Zang and Walter, p. 61, Fig. 45A–45F (not 45G).

2014 *Hocosphaeridium scaberfacium* Zang *in* Zang and Walter; Xiao et al., pp. 27–28, and synonyms therein.

2014a *Hocosphaeridium scaberfacium* Zang *in* Zang and Walter, 1992a, emend. Liu et al., p. 78, figs. 39.3, 41.1–41.7, 42.1–42.5.

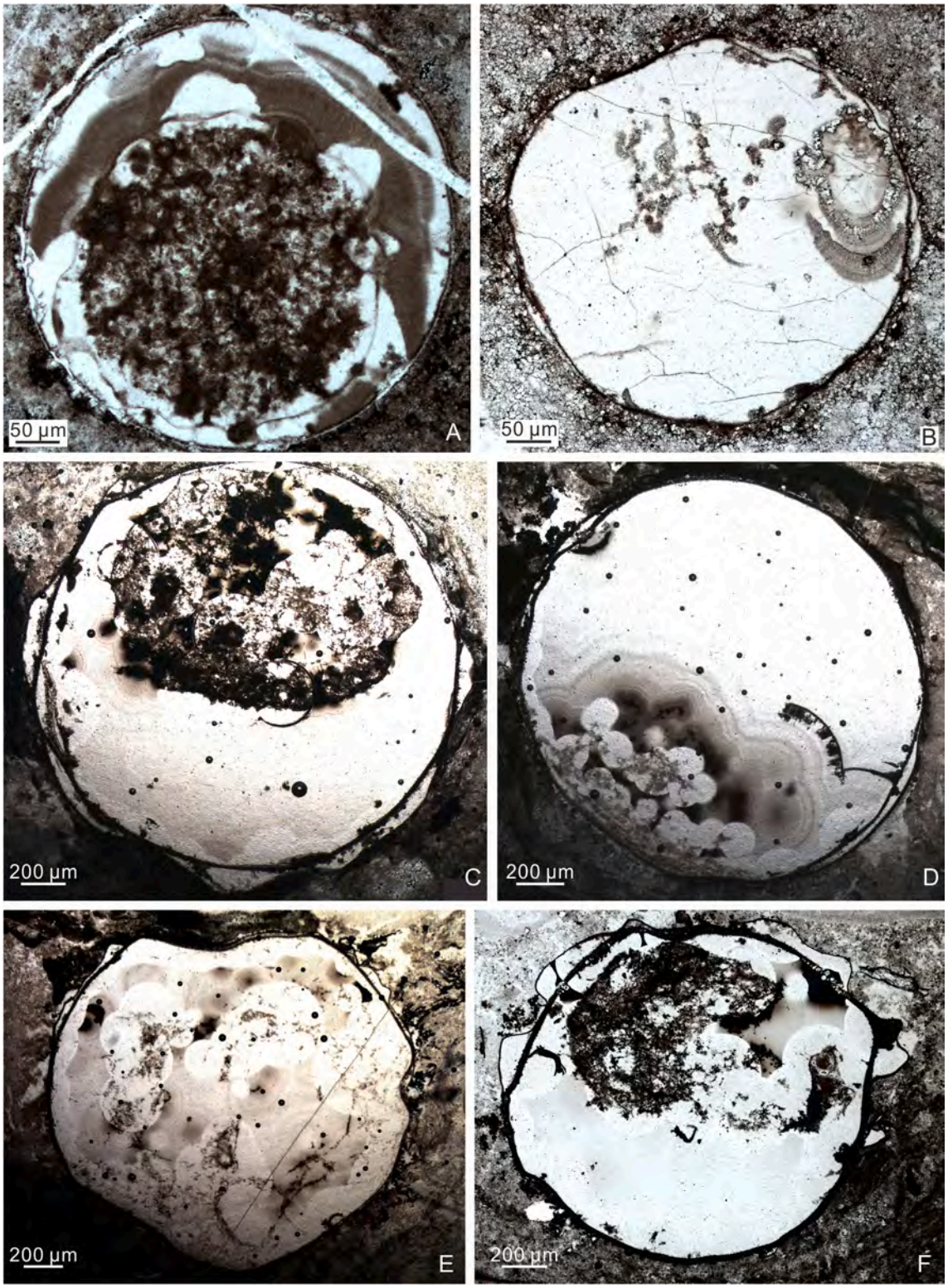

Fig. 29. *Megasphaera inornata* Chen and Liu, 1986, emend. Xiao et al., 2014. (A) LHG2-d2-3.1 m-7–1 (31.7 × 63.7). (B) LHG2-d2-3.1 m-4p-1 (39.8 × 85.7). (C) LHG2-d2-3.1 m-4-H-19 (38.2, NR). (D) LHG2-d2-3.1 m-4-Z-5 (32.9, NR). (E) LHG2-d2-3.1 m-4-Z-4 (30.7, NR). (F) LHG-d3 + 60 cm-2–1 (34.5 × 76.8).

2021 *Hocosphaeridium scaberfacium*; Liu et al., fig. 6.3–6.4.

Material: Two adequately and two poorly preserved specimens.

Description: Deformed spheroidal vesicle with a moderate number of apically hooked processes. Processes conical and gradually tapers from the base to the distal end. Processes hollow and freely communicate with vesicle interior.

Dimensions: Processes 41.0–74.0 μm in total length and 7.5–13.3 μm in basal width.

Remarks: The specimens described here are similar to *H. scaberfacium* based on their consistently hooked processes which are long, conical, and distally curved more than 180°. It is noted that our specimens have greater process density than the holotype of *H. scaberfacium*, however, this difference may be an intraspecific variation.

Occurrence: The Ediacaran Doushantuo Formation in the Shennongjia (this paper), Changyang (Liu et al., 2021), and Yangtze Gorges areas (Liu et al., 2010, 2012, 2013, 2014a) of Hubei Province, the Weng'an area of Guizhou Province (Xiao et al., 2014; Yuan et al., 2002; Zhang et al., 1998a), South China; Ediacaran successions in Siberia (Golubkova et al., 2010; Kolosova, 1991; Moczydłowska and Nagovitsin, 2012; Vorob'eva et al., 2008) and Australia (Grey, 2005; Willman and Moczydłowska, 2008; Willman et al., 2006; Zang and Walter, 1992a).

Hocosphaeridium sp.

Fig. 26K–M.

Material: One adequately and four poorly preserved specimens.

Description: Large spheroidal vesicle, bearing several hollow, widely distributed, extremely long, and distally hooked processes. Process consists of three parts: the basal part is conical and tapers rapidly to the middle part; the middle part is flexible, cylindrical, and tapers gradually to the distal end which is curved more than 180° and sometimes up to 360°. Processes open directly into vesicle cavity.

Dimensions: Vesicle 230.4–479.7 μm in diameter; processes 60.6–193.9 μm in total length (or 21.9–46.9% of vesicle diameter); conical base 22.0–70.4 μm in basal width and 23.9–52.3 μm in height; cylindrical tube 2.7–5.5 μm in maximum width; <10 processes in circumferential view.

Remarks: The consistently hooked processes of the current specimens identify them with the genus *Hocosphaeridium*. They differ from *H. anozos* and *H. scaberfacium* in having a distinct conical base and a cylindrical tube that gradually tapers to the apex, and from *H. dilatatum* in having much less process density. In addition, in comparison with previously published *Hocosphaeridium* material, the Lianhuacun specimens are much larger in vesicle diameter, process basal width, and process length. Thus, these specimens are placed in an open nomenclature.

Occurrence: The Ediacaran Doushantuo Formation in the Shennongjia (this paper) of Hubei Province, South China.

Genus *Knollisphaeridium* Willman and Moczydłowska, 2008, emend. Liu and Moczydłowska, 2019.

Type species: *Knollisphaeridium maximum* (Yin, 1987) Willman and Moczydłowska, 2008, emend. Liu and Moczydłowska, 2019.

Knollisphaeridium coniformum Liu and Moczydłowska, 2019.

Fig. 27.

Synonymy:

2019 *Knollisphaeridium coniformum* Liu and Moczydłowska, pp. 115–118, fig. 62.

2021 *Knollisphaeridium coniformum* Liu and Moczydłowska; Ouyang et al., Fig. 15A–E, H–J.

Material: Six adequately preserved specimens.

Description: Vesicle strongly deformed, originally spheroidal, large, bearing numerous evenly and closely distributed processes of uniform length. Processes comprise of a conical base and a filamentous distal part with a sharp-pointed tip. Processes hollow and communicate openly with vesicle interior.

Dimensions: Vesicle 221.7–449.0 μm in diameter (calculated from circumference measurement); processes 8.1–16.0 μm in total length or 3.6–4.7% of vesicle diameter; basal part of processes 2.7–4.3 μm wide and 3.0–3.2 μm long, and terminal part of processes < 1 μm wide; processes spaced at 1.0–2.8 μm.

Remarks: K. coniformum is most similar to *K. maximum*, but its processes have a widened conical base followed by a slender distal portion, whereas the processes of *K. maximum* are relatively narrower in process basal width and gradually taper from the base to the apex with pointed or blunt tips.

Occurrence: The Ediacaran Doushantuo Formation in the Shennongjia (this paper) and Yangtze Gorges areas (Liu and Moczydłowska, 2019; Ouyang et al., 2021) of Hubei Province, South China.

Knollisphaeridium denticulatum Liu et al., 2014a.

Fig. 28A–C.

Synonymy:

2014a *Knollisphaeridium denticulatum* Liu et al., pp. 82–83, figs. 43.1–43.9, 44.1.

2019 *Knollisphaeridium denticulatum* Liu et al.; Shang et al., p. 24, Fig. 13H–I.

Material: One adequately preserved specimen and one poorly preserved specimen.

Description: Large strongly compressed vesicle, originally spheroidal, bearing abundant, small, and short processes. Processes are generally conical in shape with a round distal end. Processes densely distributed and basally joined to form a serrate or denticulate pattern. They are hollow and freely communicate with the vesicle cavity. Process length more or less equals basal width.

Dimensions: Conical processes are 3.9–6.6 μm in length and 3.5–6.4 μm in basal width.

Remarks: K. denticulatum is characterized by its conical (or equilaterally triangular in profile view) and basally joined processes, which can be distinguished from other species of *Knollisphaeridium*. Present specimens morphologically resemble *K. denticulatum*, although there are rare biform processes among the predominantly conical processes.

Occurrence: The Ediacaran Doushantuo Formation in the Shennongjia (this paper) and Yangtze Gorges areas (Liu et al., 2014a) of Hubei Province, and the Songlin area of Guizhou Province (Shang et al., 2019), South China.

Knollisphaeridium maximum (Yin, 1987) Willman and Moczydłowska, 2008, emend. Liu and Moczydłowska, 2019.

Fig. 28D–G.

Synonymy:

1987 *Baltisphaeridium maximum* Yin, pp. 439, 440, pl. 14, Figs. 14–15.

2011 *Knollisphaeridium maximum* (Yin, 1987) Willman and Moczydłowska; Sergeev et al., p. 1004, fig. 7.5, 7.5a.

2014 *Knollisphaeridium maximum* (Yin, 1987) Willman and Moczydłowska; Xiao et al., p. 30, fig. 19.1–19.7.

2015 *Knollisphaeridium* sp.; Ouyang et al., p. 217, pl. II, Figs. 1–4.

2019 *Knollisphaeridium maximum* (Yin, 1987) Willman and Moczydłowska, 2008, emend. Liu and Moczydłowska, pp. 118, 122–123, figs. 64–65, and synonyms therein.

2019 *Knollisphaeridium maximum*; Ouyang et al., Fig. 13A–D.

2020 *Knollisphaeridium maximum* (Yin, 1987) emend. Willman and Moczydłowska; Vorob'eva and Petrov, p. 374, pl. II, Figs. 19–20.

Material: Eight well preserved specimens and five poorly preserved specimens.

Description: Large collapsed vesicle (originally spheroidal) bearing abundant, hollow, acutely conical processes. Processes homomorphic, uniform in length, and gradually taper to a pointed tip. Processes closely and evenly distributed, basally separated by a very small gap. Processes openly connect with the vesicle cavity.

Dimensions: Vesicle diameter of a well-preserved specimen (Fig. 28F) estimated to be 236.8 × 363.1 μm. Processes 2.2–4.7 μm in basal width, 10.5–20.9 μm in length, and spaced at a distance of 1.2–3.1 μm.

Remarks: K. maximum has been revised to accommodate the presence of an outer membrane surrounding the vesicle and occasionally bifurcating processes among homomorphic conical processes (Liu and

Table 4
Compilation of size range of illustrated specimens of *Megasphaera inornata* and *Megasphaera minuscula* from published literature.

Reference	Synonymy	Illustrated figure	Vesicle diameter (μm) stated by authors	Measurements based on illustrated firgures	Number of layers
Chen and Liu, 1986	*Megasphaera inornata*	pl.I, Fig. 4	500–800		1
Xue et al., 1995	*Parapandorina raphospissa*	pl. I, Fig. 1a, 1b, 2, 3	480–1200		1
Xue et al., 1995	*P. beidoushanensis*	pl. I, Fig. 6; pl. II, Figs. 1, 3–5b	480–560		1
Xue et al., 1995	*Parapandorina beidoushanensis* var. *cylindrica*	pl. II, Fig. 2	720–850		1
Xue et al., 1995	Megaclonophycus onustus	pl. III, Figs. 3–4, pl. IV, Figs. 1–6, pl. V, Figs. 2, 6–9	650–960		2
Xue et al., 1995	Colossotetrahedrion ovimpositum	pl. V, Figs. 3, 5			
Xiao and Knoll, 2000	Megaclonophycus onustus	Fig. 9.7–9.12	mean: 634		1
Xiao and Knoll, 2000	*Megaclonophycus onustus*	Fig. 9.7		588.0	
Xiao and Knoll, 2000	*Megaclonophycus onustus*	Fig. 9.8		534.0	
Xiao and Knoll, 2000	*Megaclonophycus onustus*	Fig. 9.9		660.0	
Xiao and Knoll, 2000	*Megaclonophycus onustus*	Fig. 9.11		684.0	
Xiao and Knoll, 2000	*Megaclonophycus onustus*	Fig. 9.12		638.0	
Xiao and Knoll, 2000	*Megasphaera inornata*	Fig. 3.1–3.2, 3.4–3.5, 3.7, 3.11	400–1100		1
Xiao and Knoll, 2000	*Megasphaera inornata*	Fig. 3.1		629.1	
Xiao and Knoll, 2000	*Megasphaera inornata*	Fig. 3.4		489.9	
Xiao and Knoll, 2000	*Megasphaera inornata*	Fig. 3.5		681.7	
Xiao and Knoll, 2000	*Megasphaera inornata*	Fig. 3.7		368.1	
Xiao and Knoll, 2000	*Megasphaera inornata*	Fig. 3.11		616.3	
Xiao and Knoll, 2000	*Parapandorina raphospissa*	Figs. 5.5–5.11, 7–8, 9.1–9.6	400–1100		1
Xiao and Knoll, 2000	*Parapandorina raphospissa*	Fig. 5.5		439.9	
Xiao and Knoll, 2000	*Parapandorina raphospissa*	Fig. 5.7		678.1	
Xiao and Knoll, 2000	*Parapandorina raphospissa*	Fig. 5.8		663.0	
Xiao and Knoll, 2000	*Parapandorina raphospissa*	Fig. 5.11		739.7	
Xiao and Knoll, 2000	*Parapandorina raphospissa*	Fig. 7.1		604.4	
Xiao and Knoll, 2000	*Parapandorina raphospissa*	Fig. 7.2		610.0	
Xiao and Knoll, 2000	*Parapandorina raphospissa*	Fig. 7.3		534.4	
Xiao and Knoll, 2000	*Parapandorina raphospissa*	Fig. 7.4		648.2	
Xiao and Knoll, 2000	*Parapandorina raphospissa*	Fig. 7.5		724.2	
Xiao and Knoll, 2000	*Parapandorina raphospissa*	Fig. 7.6		596.1	
Xiao and Knoll, 2000	*Parapandorina raphospissa*	Fig. 7.7		658.1	
Xiao and Knoll, 2000	*Parapandorina raphospissa*	Fig. 7.8		576.1	
Xiao and Knoll, 2000	*Parapandorina raphospissa*	Fig. 7.9		546.4	
Xiao and Knoll, 2000	*Parapandorina raphospissa*	Fig. 7.10		756.3	
Xiao and Knoll, 2000	*Parapandorina raphospissa*	Fig. 8.1		614.0	
Xiao and Knoll, 2000	*Parapandorina raphospissa*	Fig. 8.4		654.6	
Xiao and Knoll, 2000	*Parapandorina raphospissa*	Fig. 8.5		544.0	
Xiao and Knoll, 2000	*Parapandorina raphospissa*	Fig. 8.6		456.9	
Xiao and Knoll, 2000	*Parapandorina raphospissa*	Fig. 8.7		566.0	

(*continued on next page*)

Table 4 (*continued*)

Reference	Synonymy	Illustrated figure	Vesicle diameter (μm) stated by authors	Measurements based on illustrated firgures	Number of layers
Xiao and Knoll, 2000	*Parapandorina raphospissa*	Fig. 8.8		636.0	
Xiao and Knoll, 2000	*Parapandorina raphospissa*	Fig. 8.9		616.5	
Xiao and Knoll, 2000	*Parapandorina raphospissa*	Fig. 8.10		628.0	
Xiao and Knoll, 2000	*Parapandorina raphospissa*	Fig. 8.11		706.2	
Xiao and Knoll, 2000	*Parapandorina raphospissa*	Fig. 8.12		694.4	
Xiao and Knoll, 2000	*Parapandorina raphospissa*	Fig. 9.1		573.4	
Xiao and Knoll, 2000	*Parapandorina raphospissa*	Fig. 9.2		564.6	
Xiao and Knoll, 2000	*Parapandorina raphospissa*	Fig. 9.3		714.6	
Xiao and Knoll, 2000	*Parapandorina raphospissa*	Fig. 9.4		561.3	
Xiao and Knoll, 2000	*Parapandorina raphospissa*	Fig. 9.5		543.8	
Zhou et al., 2002	*Megasphaera inornata*	pl. II, Figs. 1–2	100–300		1
Zhou et al., 2002	*Megasphaera inornata*	pl. II, Fig. 1		357.5	
Zhou et al., 2002	*Megasphaera inornata*	pl. II, Fig. 2		133.8	
Zhou et al., 2004	*Parapandorina raphospissa*	pl. VI, Figs. 5–9	315.2–384.3		
Zhou et al., 2004	*Parapandorina raphospissa*	pl. VI, Fig. 5		386.3	
Zhou et al., 2004	*Parapandorina raphospissa*	pl. VI, Fig. 6		390.2	
Zhou et al., 2004	*Parapandorina raphospissa*	pl. VI, Fig. 7		810.3	
Zhou et al., 2004	*Parapandorina raphospissa*	pl. VI, Fig. 8		377.0	
Zhou et al., 2004	*Parapandorina raphospissa*	pl. VI, Fig. 9		476.2	
Zhou et al., 2004	*Megaclonophycus onustus*	pl. VI, Fig. 10	390.7	585.1	
Xie et al., 2008	*Megaclonophycus onustus*	pl. II, Figs. 5–6	~300	291.9	1
Xie et al., 2008	*Megasphaera ornata*	pl. I, Figs. 4–5 (*sci!* should be pl. I, Figs. 3–4)	600–1000	492.2	
Xie et al., 2008	*Parapandorina raphospissa*	pl. II, Fig. 4	~220	207.8	1
Yin et al., 2009c	*Megasphaera inornata*	Fig. 3a–b		394.9	
	Megaclonophycus onustus	Fig. 4b–d		302.9	
Liu et al., 2009a	*Phosphatized globular fossils*	Fig. 2	520–1030		
Liu et al., 2009a	*Phosphatized globular fossils*	Fig. 2a		776.4	
Liu et al., 2009a	*Phosphatized globular fossils*	Fig. 2b		624.7	
Liu et al., 2009a	*Phosphatized globular fossils*	Fig. 2c		739.8	
Liu et al., 2009a	*Phosphatized globular fossils*	Fig. 2d		771.2	
Liu et al., 2009a	*Phosphatized globular fossils*	Fig. 2e		733.4	
Liu et al., 2009a	*Phosphatized globular fossils*	Fig. 2f		725.3	
Liu et al., 2009a	*Phosphatized globular fossils*	Fig. 2g		964.6	
Liu et al., 2009a	*Phosphatized globular fossils*	Fig. 2h		938.6	
Liu et al., 2009a	*Phosphatized globular fossils*	Fig. 2i		958.7	
Liu et al., 2009a	*Phosphatized globular fossils*	Fig. 2j		629.5	
Liu et al., 2009a	*Phosphatized globular fossils*	Fig. 2k		988.4	
Liu et al., 2009a	*Phosphatized globular fossils*	Fig. 2l		1081.2	
Liu et al., 2009a	*Phosphatized globular fossils*	Fig. 2*m*		708.3	
Liu et al., 2009a	*Phosphatized globular fossils*	Fig. 2*n*		884.3	
Liu et al., 2009a	*Phosphatized globular fossils*	Fig. 2o		893.1	
Liu et al., 2009a	*Phosphatized globular fossils*	Fig. 2p		961.8	
Liu et al., 2009a	*Phosphatized globular fossils*	Fig. 2q		616.0	
Liu et al., 2009a	*Phosphatized globular fossils*	Fig. 2r		730.1	
Liu et al., 2009a	*Phosphatized globular fossils*	Fig. 2s		548.5	
Xiao and Schiffbauer, 2009	*Megasphaera inornata*	Fig. 2, 3A–E	400–1100		1–2
Xiao and Schiffbauer, 2009	*Megasphaera inornata*	Fig. 2A		909.5	
Xiao and Schiffbauer, 2009	*Megasphaera inornata*	Fig. 3A		400.3	
Xiao and Schiffbauer, 2009	*Megasphaera inornata*	Fig. 3C		577.9	
Xiao and Schiffbauer, 2009	*Parapandorina raphospissa*	Fig. 3F–H	400–1100		1
Xiao and Schiffbauer, 2009	*Parapandorina raphospissa*	Fig. 3G		775.8	
Xiao et al., 2014	*Megasphaera inornata*		400–1100		
Ye et al., 2015	*Megasphaera inornata*	pl. II, Figs. 1–13	100–800		
Ye et al., 2015	*Megasphaera inornata*	pl. II, Fig. 1		176.8	
Ye et al., 2015	*Megasphaera inornata*	pl. II, Fig. 2		267.8	
Ye et al., 2015	*Megasphaera inornata*	pl. II, Fig. 3		297.3	
Ye et al., 2015	*Megasphaera inornata*	pl. II, Fig. 4		549.6	
Ye et al., 2015	*Megasphaera inornata*	pl. II, Fig. 5		608.8	

(*continued on next page*)

Table 4 (*continued*)

Reference	Synonymy	Illustrated figure	Vesicle diameter (μm) stated by authors	Measurements based on illustrated firgures	Number of layers
Ye et al., 2015	*Megasphaera inornata*	pl. II, Fig. 6		567.2	
Ye et al., 2015	*Megasphaera inornata*	pl. II, Fig. 7		671.6	
Ye et al., 2015	*Megasphaera inornata*	pl. II, Fig. 8		364.0	
Ye et al., 2015	*Megasphaera inornata*	pl. II, Fig. 9		426.8	
Ye et al., 2015	*Megasphaera inornata*	pl. II, Fig. 11		309.0	
Ye et al., 2015	*Megasphaera inornata*	pl. II, Fig. 13		125.7	
Zhang and Zhang, 2017	*Megasphaera inornata*	Fig. 3c–g	200–1200		at least 2
Zhang and Zhang, 2017	*Megasphaera inornata*	Fig. 3c		411.6	
Zhang and Zhang, 2017	*Megasphaera inornata*	Fig. 3d		635.1	
Zhang and Zhang, 2017	*Megasphaera inornata*	Fig. 3e		656.4	
Zhang and Zhang, 2017	*Megasphaera inornata*	Fig. 3g		1071.6	
Nie et al., 2017	*Megasphaera inornata*	Fig. 10	100–400		
Nie et al., 2017	*Megasphaera inornata*	Fig. 10.1		344.2	
Nie et al., 2017	*Megasphaera inornata*	Fig. 10.2		381.5	
Nie et al., 2017	*Megasphaera inornata*	Fig. 10.5		502.1	
Nie et al., 2017	*Megasphaera inornata*	Fig. 10.6		433.8	
Nie et al., 2017	*Megasphaera inornata*	Fig. 10.7		444.0	
Ouyang et al., 2019	*Megasphaera inornata*	Fig. 9L.	714	742.4	1
Shang et al., 2019	*Megasphaera inornata*	Fig. 14A–B	300–650		1–2
Shang et al., 2019	*Megasphaera inornata*	Fig. 14A		667.6	
Shang et al., 2019	*Megasphaera inornata*	Fig. 14B		311.3	
Yang et al., 2020	*Megasphaera inornata*	Fig. 3	200–550		
Yang et al., 2020	*Megasphaera inornata*	Fig. 3a		616.3	
Yang et al., 2020	*Megasphaera inornata*	Fig. 3b		558.1	
Yang et al., 2020	*Megasphaera inornata*	Fig. 3c		586.4	
Yang et al., 2020	*Megasphaera inornata*	Fig. 3d		527.1	
Yang et al., 2020	*Megasphaera inornata*	Fig. 3e		492.0	
Yang et al., 2020	*Megasphaera inornata*	Fig. 3f		548.4	
Yang et al., 2020	*Megasphaera inornata*	Fig. 3g		496.2	
Yang et al., 2020	*Megasphaera inornata*	Fig. 3h		357.5	
Yang et al., 2020	*Megasphaera inornata*	Fig. 3i		235.6	
Shang et al., 2020	*Megasphaera inornata*	Fig. 5C	350	356.0	
Shang et al., 2020	Acritarcha gen. et sp. indet.	Fig. 6D–E	1800	1828.7	2
Ouyang et al., 2021	*Megasphaera inornata*	Fig. 16A–D	1000–2200		
Ouyang et al., 2021	*Megasphaera inornata*	Fig. 16A		661.2	
Ouyang et al., 2021	*Megasphaera inornata*	Fig. 16B		1592.5	
Ouyang et al., 2021	*Megasphaera inornata*	Fig. 16C		709.6	
Ouyang et al., 2021	*Megasphaera inornata*	Fig. 16D		634.5	
Current study	*Megasphaera inornata*	Fig. 27	129.8–2260.8		1–2
Current study	*Megasphaera inornata*	21LHC-1–32.8 m-3c-1		397.9	
Current study	*Megasphaera inornata*	21LHC-1–32.8 m-3c-4		465.1	
Current study	*Megasphaera inornata*	21LHC-1–32.8 m-9c-2		351.1	
Current study	*Megasphaera inornata*	21LHC-1–32.8 m-9c-4		174.1	
Current study	*Megasphaera inornata*	21LHC-1–33.6 m-4p-1		1745.2	
Current study	*Megasphaera inornata*	21LHC-1–33.6 m-4p-2		1220.5	
Current study	*Megasphaera inornata*	21LHC-1–33.6 m-5c-3		1764.7	
Current study	*Megasphaera inornata*	LHG-d3 + 60 cm-1–2		298.8	
Current study	*Megasphaera inornata*	LHG-d3 + 60 cm-1–5		191.0	
Current study	*Megasphaera inornata*	LHG-d3 + 60 cm-2–1		1657.6	
Current study	*Megasphaera inornata*	LHG-d3 + 70 cm-6–4		213.6	
Current study	*Megasphaera inornata*	LHG-d3 + 80 cm-6–26		513.2	
Current study	*Megasphaera inornata*	21LHC-1–34.4 m-1p-1		2260.8	
Current study	*Megasphaera inornata*	21LHC-1–34.4 m-1p-2		327.9	
Current study	*Megasphaera inornata*	21LHC-1–34.4 m-9c-2		284.1	
Current study	*Megasphaera inornata*	21LHC-1–35.2 m-3p-1		611.2	
Current study	*Megasphaera inornata*	21LHC-1–35.2 m-7p-1		758.2	
Current study	*Megasphaera inornata*	21LHC-1–35.4 m-8p-1		437.7	
Current study	*Megasphaera inornata*	21LHC-1–35.4 m-24p-4		259.8	
Current study	*Megasphaera inornata*	LHG2-d2-2.9 m-1–2		129.8	
Current study	*Megasphaera inornata*	21LHC-1–36.1 m-8c-4		518.3	
Current study	*Megasphaera inornata*	21LHC-1–36.1 m-13c-5		496.1	
Current study	*Megasphaera inornata*	LHG2-d2-3.1 m-4p-1		452.3	
Current study	*Megasphaera inornata*	LHG2-d2-3.1 m-7–1		508.8	
Current study	*Megasphaera inornata*	21LHC-1–37.0 m-10p-7		487.1	
Current study	*Megasphaera inornata*	21LHC-1–37.0 m-10p-8		432.4	
Current study	*Megasphaera inornata*	21LHC-1–37.0 m-14p-1		472.7	
Current study	*Megasphaera inornata*	21LHC-1–37.0 m-14p-2		434.5	
Current study	*Megasphaera inornata*	21LHC-1–37.0 m-15p-2		582.8	
Current study	*Megasphaera inornata*	21LHC-1–37.0 m-17p-1		1512.2	
Current study	*Megasphaera inornata*	LHG-d2-2 m-7–1		529.0	

(*continued on next page*)

Table 4 (*continued*)

Reference	Synonymy	Illustrated figure	Vesicle diameter (μm) stated by authors	Measurements based on illustrated firgures	Number of layers
Current study	*Megasphaera inornata*	LHG-d2-2 m-2–1		338.5	
Current study	*Megasphaera inornata*	LHG-D2-1.5 M−2−3		191.2	
Current study	*Megasphaera inornata*	LHG2-d2-2 m-5–7		277.2	
Current study	*Megasphaera inornata*	21LHC-1–37.4 m-1c-6		631.3	
Current study	*Megasphaera inornata*	21LHC-1–37.4 m-1p-9		1793.9	
Current study	*Megasphaera inornata*	21LHC-1–37.4 m-3c-2		493.4	
Current study	*Megasphaera inornata*	21LHC-1–37.4 m-3p-2		547.1	
Current study	*Megasphaera inornata*	21LHC-1–37.4 m-3p-4		387.7	
Current study	*Megasphaera inornata*	21LHC-1–37.4 m-7p-6		2096.4	
Current study	*Megasphaera inornata*	21LHC-1–37.4 m-10c-1		1660.7	
Current study	*Megasphaera inornata*	21LHC-1–39.5 m-5p-1		182.9	
Current study	*Megasphaera inornata*	LHG-d2-4.3 m-4–1		1608.1	
Current study	*Megasphaera inornata*	21LHC-1–40.1 m-1c-1		703.0	
Current study	*Megasphaera inornata*	21LHC-1–40.1 m-2c-1		1449.7	
Current study	*Megasphaera inornata*	21LHC-1–40.1 m-6c-1		1322.3	
Current study	*Megasphaera inornata*	21LHC-1–40.1 m-11p-1		1569.5	
Current study	*Megasphaera inornata*	21LHC-1–40.1 m-11p-2		1712.8	
Current study	*Megasphaera inornata*	21LHC-1–40.2 m-10c-1		1808.6	
Current study	*Megasphaera inornata*	21LHC-1–40.5 m-3p-1		374.7	
Current study	*Megasphaera inornata*	21LHC-1–40.5 m-10c-1		1434.8	
Current study	*Megasphaera inornata*	21LHC-1–40.5 m-11p-2		403.7	
Current study	*Megasphaera inornata*	21LHC-1–41.4 m-5p-4		418.5	
Current study	*Megasphaera inornata*	LHG-UD-n-3–2		825.4	
Current study	*Megasphaera inornata*	21LHC-1–45.2 m-1c-1		925.5	
Current study	*Megasphaera inornata*	21LHC-1–45.2 m-2c-5		433.3	
Current study	*Megasphaera inornata*	21LHC-1–45.2 m-7–2		574.0	
Current study	*Megasphaera inornata*	21LHC-1–45.2 m-10p-2		649.7	
Current study	*Megasphaera inornata*	21LHC-1–45.2 m-11p-5		625.2	
Current study	*Megasphaera inornata*	21LHC-1–45.2 m-11p-7		705.1	
Current study	*Megasphaera inornata*	21LHC-1–45.2 m-12p-1		603.2	
Current study	*Megasphaera inornata*	21LHC-1–45.2 m-12p-2		548.4	
Current study	*Megasphaera inornata*	21LHC-1–45.6 m-1c-12		627.2	
Current study	*Megasphaera inornata*	21LHC-1–45.6 m-1c-14		413.7	
Current study	*Megasphaera inornata*	21LHC-1–45.6 m-3p-9		571.9	
Current study	*Megasphaera inornata*	21LHC-1–45.6 m-4c-2		1938.2	
Current study	*Megasphaera inornata*	21LHC-1–45.6 m-12c-13		493.1	
Current study	*Megasphaera inornata*	21LHC-1–45.6 m-18c-1		1527.0	
Current study	*Megasphaera inornata*	21LHC-1–45.6 m-22c-5		457.0	
Current study	*Megasphaera inornata*	21LHC-1–47.0 m-3c-1		485.4	
Current study	*Megasphaera inornata*	21LHC-1–47.0 m-3c-3		618.8	
Current study	*Megasphaera inornata*	21LHC-1–47.0 m-4p-8		476.5	
Current study	*Megasphaera inornata*	21LHC-1–47.0 m-5p-3		640.7	
Current study	*Megasphaera inornata*	21LHC-1–47.0 m-17c-1		1663.0	
Current study	*Megasphaera inornata*	21LHC-1–47.0 m-19c-2		504.3	
Anderson et al., 2019	*Megasphaera minuscula*	Fig. 9A–M, 10A–J, 11A–J	76–325		
Anderson et al., 2019	*Megasphaera minuscula*	Fig. 9A		193.4	
Anderson et al., 2019	*Megasphaera minuscula*	Fig. 9C		158.4	
Anderson et al., 2019	*Megasphaera minuscula*	Fig. 9E		161.5	
Anderson et al., 2019	*Megasphaera minuscula*	Fig. 9G		188.5	
Anderson et al., 2019	*Megasphaera minuscula*	Fig. 9J		105.4	
Anderson et al., 2019	*Megasphaera minuscula*	Fig. 9L		146.6	
Anderson et al., 2019	*Megasphaera minuscula*	Fig. 10A		175.2	
Anderson et al., 2019	*Megasphaera minuscula*	Fig. 10B		178.2	
Anderson et al., 2019	*Megasphaera minuscula*	Fig. 10C		130.4	
Anderson et al., 2019	*Megasphaera minuscula*	Fig. 10D		158.2	
Anderson et al., 2019	*Megasphaera minuscula*	Fig. 10E		167.2	
Anderson et al., 2019	*Megasphaera minuscula*	Fig. 10F		134.9	
Anderson et al., 2019	*Megasphaera minuscula*	Fig. 10G		157.3	
Anderson et al., 2019	*Megasphaera minuscula*	Fig. 10*H*		125.5	
	Megasphaera minuscula	Fig. 10I		206.9	

(*continued on next page*)

Table 4 (*continued*)

Reference	Synonymy	Illustrated figure	Vesicle diameter (μm) stated by authors	Measurements based on illustrated firgures	Number of layers
Anderson et al., 2019					
Anderson et al., 2019	*Megasphaera minuscula*	Fig. 10J		177.7	
Anderson et al., 2019	*Megasphaera minuscula*	Fig. 11A		179.7	
Anderson et al., 2019	*Megasphaera minuscula*	Fig. 11B		150.8	
Anderson et al., 2019	*Megasphaera minuscula*	Fig. 11C		307.9	
Anderson et al., 2019	*Megasphaera minuscula*	Fig. 11D		131.7	
Anderson et al., 2019	*Megasphaera minuscula*	Fig. 11E		373.8	
Anderson et al., 2019	*Megasphaera minuscula*	Fig. 11F		400.0	
Anderson et al., 2019	*Megasphaera minuscula*	Fig. 11G		332.7	
Anderson et al., 2019	*Megasphaera minuscula*	Fig. 11*H*		515.7	
Anderson et al., 2019	*Megasphaera minuscula*	Fig. 11I		302.3	

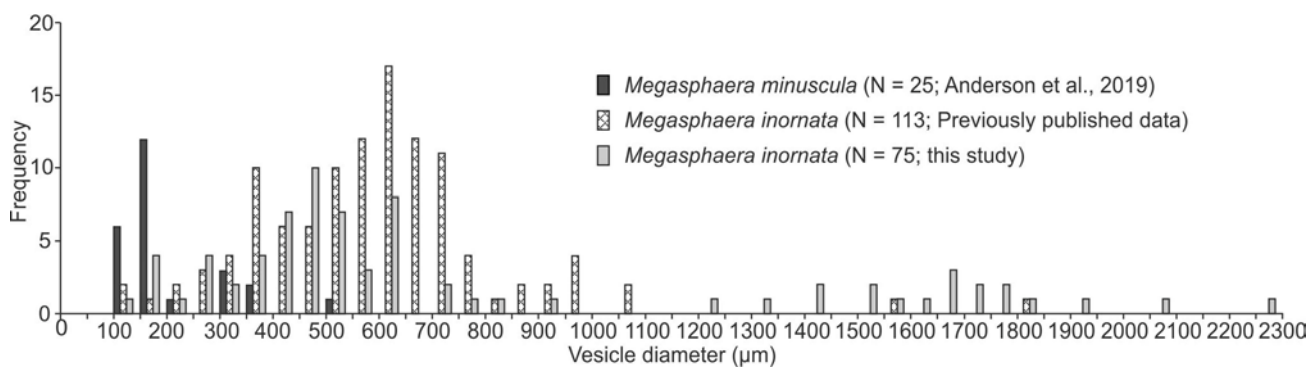

Fig. 30. Histogram showing size distribution of *Megasphaera inornata* and *M. minuscula*.

Moczydłowska, 2019). *Knollisphaeridium* sp. illustrated by Ouyang et al. (2015; their pl. II, Figs. 1–4) with a clearly bifurcating process fits the emended diagnosis and is here reassigned to *K. maximum*. Additionally, the vesicle size limit of *K. maximum* has been abandoned in the diagnosis emendation and the species is recognized as having two size classes with non-overlapping ranges of vesicle diameter (245–524 μm and 40–86 μm, respectively; Liu and Moczydłowska, 2019). Whether these two size groups with distinct vesicle size represent two different species can be disputed. Nonetheless, the current specimens belong to the larger size class, and their uniformly conical, short, hollow, densely and evenly distributed processes support their identification to *K. maximum*.

Occurrence: The Ediacaran Doushantuo Formation in the Shennongjia (this paper), Baokang area (Zhou et al., 2004), Zhangcunping (Ouyang et al., 2019), and Yangtze Gorges areas (Liu and Moczydłowska, 2019; Liu et al., 2014a; Ouyang et al., 2015; Zhang et al., 1998a) of Hubei Province, the Weng'an area of Guizhou Province (Xiao et al., 2014), and the Zhangjiajie area of Hunan Province (Ouyang et al., 2017), South China; Ediacaran successions in Svalbard (Knoll, 1992), Australia (Willman and Moczydłowska, 2008), India (Tiwari and Knoll, 1994; Tiwari and Pant, 2004), and Siberia (Sergeev et al., 2011; Vorob'eva and Petrov, 2020).

Genus *Megasphaera* Chen and Liu, 1986, emend. Xiao et al., 2014.

Type species: *Megasphaera inornata* Chen and Liu, 1986, emend. Xiao et al., 2014.

Megasphaera inornata Chen and Liu, 1986, emend. Xiao et al., 2014. Fig. 29.

Synonymy:

1986 *Megasphaera inornata* Chen and Liu, p. 51, pl. I, Fig. 4.

2004 *Megaclonophycus onustus* Xue et al.; Zhou et al., pl. VI, Fig. 10.

2004 *Parapandorina raphospissa* Xue et al.; Zhou et al., pl. VI, Figs. 5–9.

2009c *Megasphaera inornata* Chen and Liu; Yin et al., Fig. 3a–b.

2019 *Megasphaera inornata* Chen and Liu, 1986, emend. Xiao et al., 2014; Shang et al., pp. 24–25, Fig. 14A–B, and synonyms therein.

2020 *Megasphaera inornata* Chen and Liu, 1986, emend. Xiao et al., 2014; Yang et al., pp. 9–10, Fig. 3.

2020 *Megasphaera inornata* Chen and Liu, 1986, emend. Xiao et al., 2014; Shang and Liu, p. 158, Fig. 5C.

2020 Acritarcha gen. et sp. indet.; Shang and Liu, p. 159, Fig. 6D–E.

2021 *Megasphaera inornata* Chen and Liu, 1986, emend. Xiao et al., 2014; Ouyang et al., Fig. 16A–D.

Material: Seventy-five well-preserved specimens.

Dimensions: Vesicle diameter of specimens in our collection is 129.8–2260.8 μm. The total range of vesicle diameter compiled from previously published material is 100.0–2300.0 μm.

Remarks: Based on Xiao et al. (2014), large (400–1100 μm in diameter) and smooth spheroidal vesicles with one or more internal bodies are assigned to *M. inornata*. *Megasphaera minuscula* was erected to accommodate smooth spheroidal vesicles with smaller sizes (76–325 μm or < 400 μm; Anderson et al., 2019). However, previously reported specimens and our collection of *M. inornata* show a wide range of vesicle diameter (100.0–2300.0 μm; Table. 4; Fig. 30), which overlaps with that

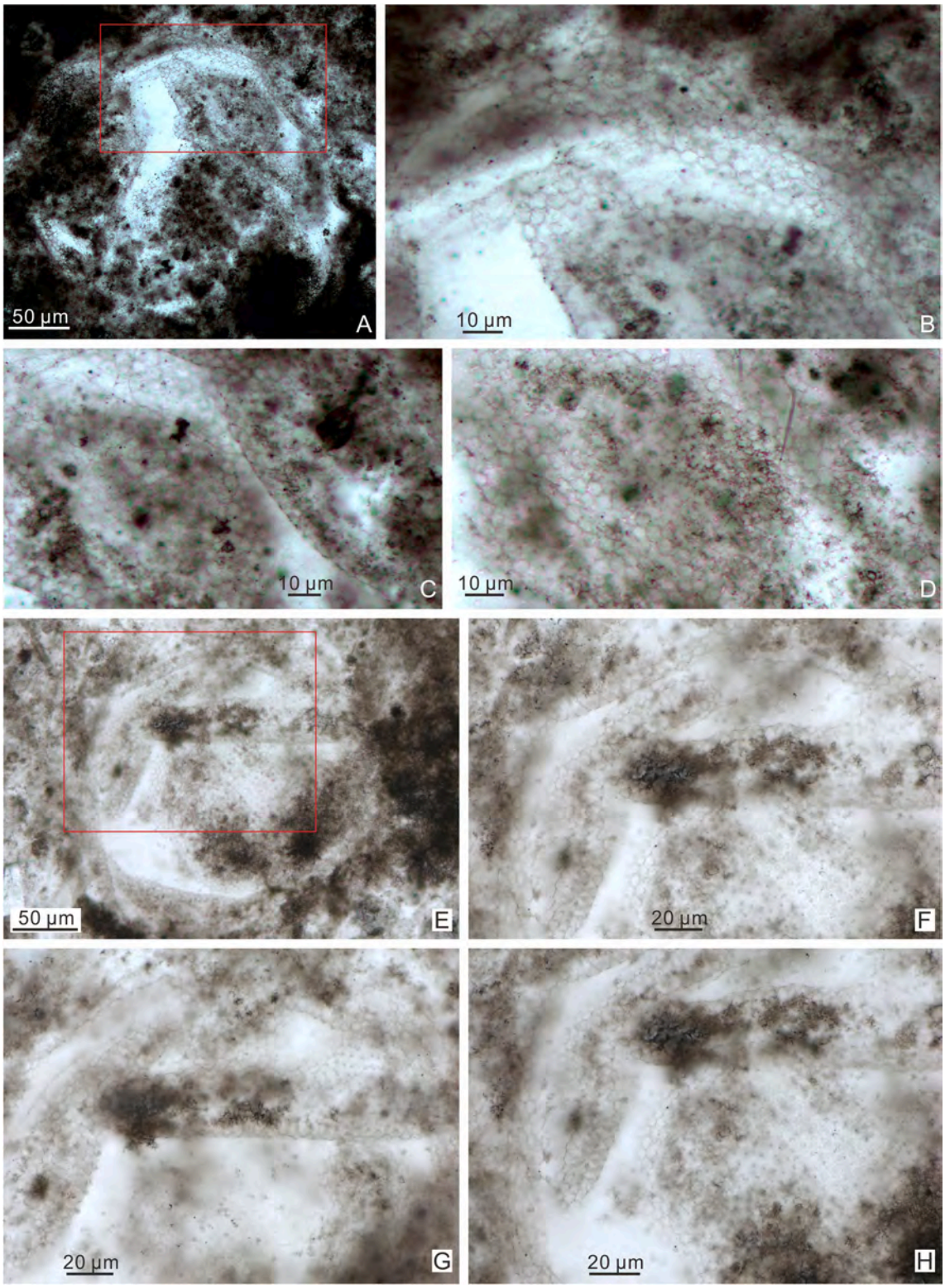

Fig. 31. *Mengeosphaera angusta*? Liu et al., 2014a. (A–D) LHG2-d2-3.1 m-7–17 (25.2 × 71.1). (B–D) Magnified views of area marked by rectangle in (A) at different focal levels. (E–H) 21LHC-1–37 m-10p-4 (18.4 × 100.9). (F–H) Magnified views of area marked by rectangle in (E) at different focal levels, showing details of process morphology and reticulation pattern.

of *M. minuscula*. Considering that the pooled size distribution of *M. inornata* and *M. minuscula* appear to be bimodal (Fig. 30), it is possible that these represent two distinct species. However, the Lianhuacun population is dominated by specimens greater than 400 μm in diameter. From a population point of view, we tentatively identify the Lianhuacun specimens as *M. inornata*. We note, however, that *M. inornata* is a morphospecies with few diagnostic features and thus may include multiple biological species. One specimen identified as *M. minuscula* (Fig. 11J of Anderson et al., 2019) in the Khesen Formation bears a single large process, thus it may not belong to the genus

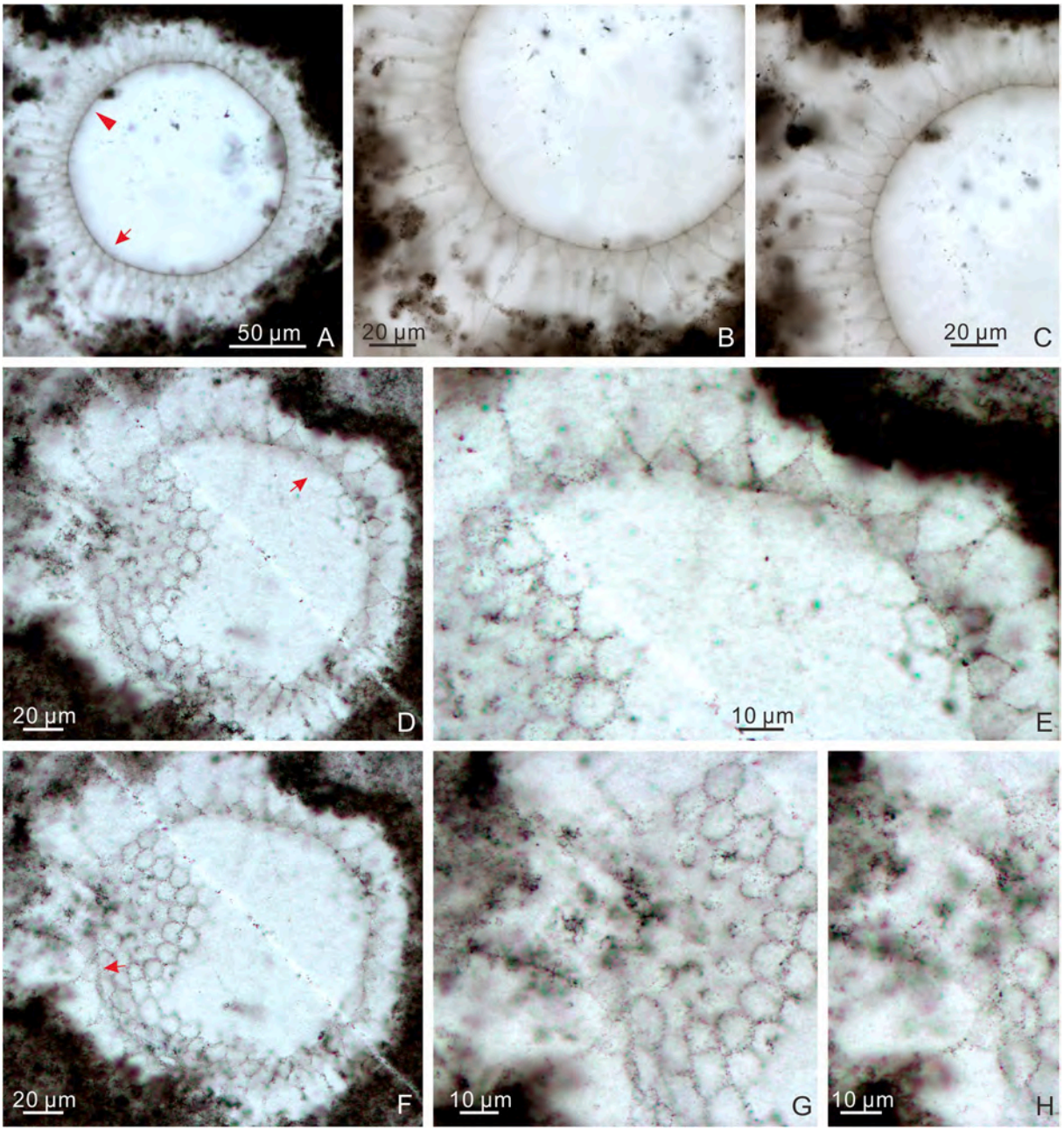

Fig. 32. *Mengeosphaera chadianensis* (Chen and Liu, 1986) Xiao et al., 2014. (A–C) 21LHC-1–41.4 m-1p-1 (6.8 × 111.5). (B–C) Magnified views of areas in (A) marked by arrow and arrowhead, respectively. (D–H) LHG2-d2-3.1 m-3p-25 (29.2 × 77.8). (D, F) Different views of the same specimen. (E) Magnified view of area marked by arrow in (D). (G–H) Magnified views of areas marked by arrow in (F) at different focal levels.

Megasphaera.

A two-layered envelope enclosing a single internal body is apparent in some specimens (e.g., Fig. 29A, C, F; Fig. 2A in Xiao and Schiffbauer, 2009; Fig. 3d in Zhang and Zhang, 2017). Although a taphonomic artifact cannot be excluded, such structures are similar to diapause cysts of some extant invertebrates, which also have a thick and multilayered envelope (Xiao and Knoll, 2000; Cohen et al., 2009).

Occurrence: The Ediacaran Doushantuo Formation in the Shennongjia (this paper), Baokang (Yang et al., 2020; Yin et al., 2009c), Zhangcunping (Ouyang et al., 2019; Ye et al., 2015), and Yangtze Gorges areas (Ouyang et al., 2021; Xie et al., 2008) of Hubei Province, the Weng'an (e.g., Chen and Liu, 1986; Xiao and Knoll, 2000; Xiao et al., 2014; Xue et al., 1995) and Songlin areas (Shang et al., 2019) of Guizhou Province, the Shangrao area of Jiangxi Province (Zhou et al., 2002), and the Zhangjiajie area of Hunan Province (Nie et al., 2017; Ouyang et al., 2017; Shang and Liu, 2020), South China; the Ediacaran Dengying Formation in the Zhenba area of Shaanxi Province (Zhang and Zhang, 2017), South China.

Genus *Mengeosphaera* Xiao et al., 2014.

Type species: *Mengeosphaera chadianensis* (Chen and Liu, 1986) Xiao et al., 2014.

Mengeosphaera angusta? Liu et al., 2014a.

Fig. 31.

Synonymy:

? 2014a *Mengeosphaera angusta* Liu et al., pp. 83, 87, 90, fig. 50.1–50.6, 51.1.

Material: Two well-preserved and two poorly preserved specimens.

Description: Medium-sized spheroidal vesicle, bearing numerous small and closely distributed biform processes that are basally attached. Processes have an inflated basal expansion, whose width is comparable

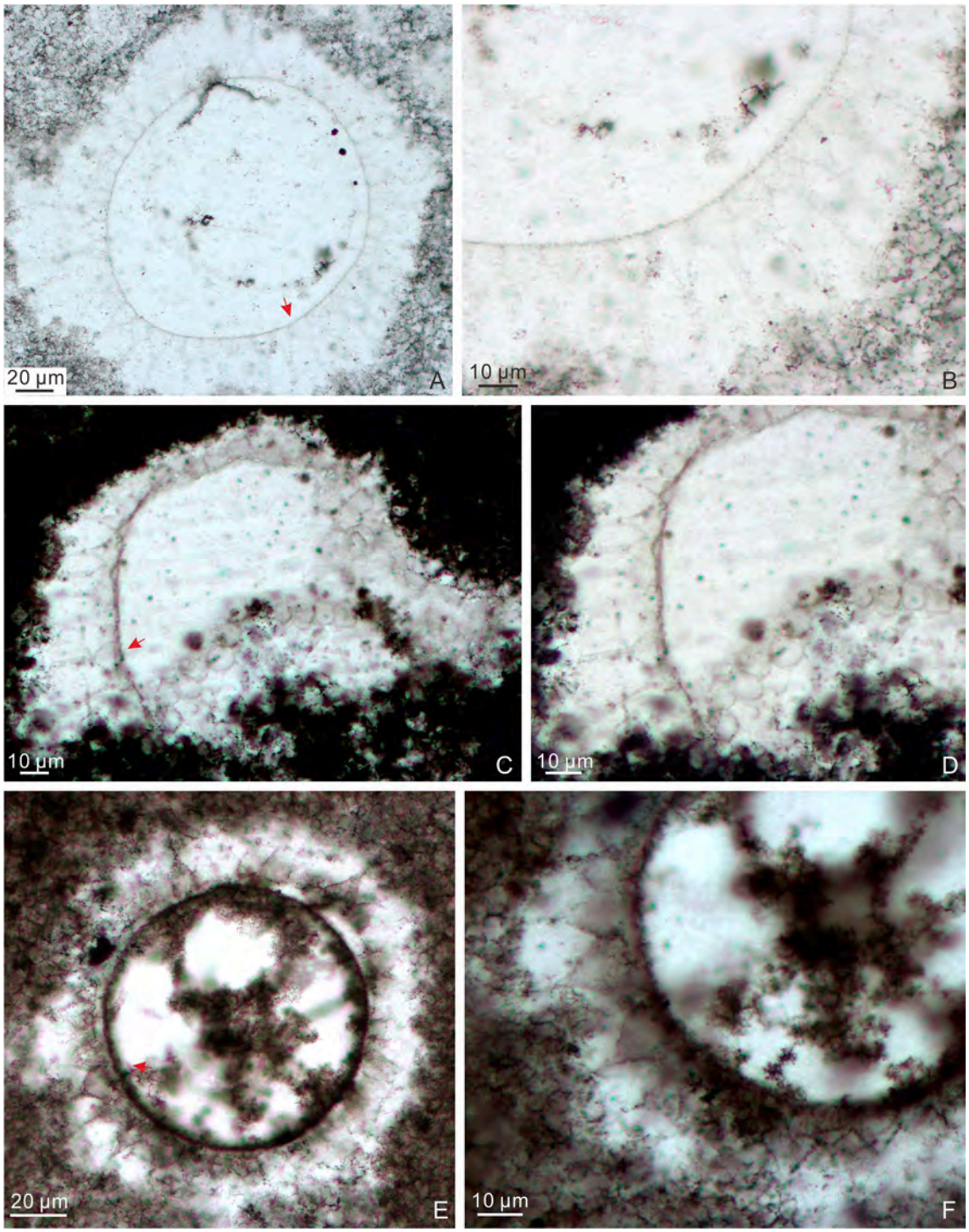

Fig. 33. *Mengeosphaera chadianensis* (Chen and Liu, 1986) Xiao et al., 2014. (A–B) LHG2-d2-2.1 m-7–1 (25.8 × 72.8). (C–D) LHG-d2-50 cm-5–1 (24.2 × 68). (E–F) LHG2-d2-3.1 m-3p-36 (31.5 × 77.2). (B, D, F) Magnified views of areas marked by arrows in (A, C, E), respectively.

to height. Processes are in contact at the base, resulting a regular penta-hexagonal reticulate pattern on the vesicle surface. Apical spine conical and thin, but its full length is difficult to measure because of poor preservation. Processes hollow and communicate openly with the vesicle interior.

Dimensions: Vesicle diameter 223.9–227.1 μm; processes basal expansion 3.5–5.2 μm in width and 3.1–5.8 μm in height.

Remarks: In several *Mengeosphaera* species, including *M. augusta*, *M. latibasis*, and *M. reticulata*, the basal expansion of the processes can impose a reticulate pattern on the vesicle surface. Among these three species, *M. reticulata* is unique in having basally separate processes, each of which sits in a polygonal field defined by ridges (Xiao et al., 2014). *M. latibasis* and *M. augusta* are similar in vesicle size and process density; indeed, Liu and Moczydłowska (2019) commented that these two species may be synonymous. However, we follow Liu et al., (2014a) in distinguishing these two species on the basis of their different process morphologies: the basal expansion of the processes is obtuse (wider than long) in *M. latibasis* but triangular (as wide as long) in *M. augusta*. The specimens in our collection are most similar to *M. augusta* in vesicle diameter and process shape, but the basal expansion of their processes is

Table 5
Compilation of size range of selected specimens of *Mengeosphaera chadianensis* from published literature.

Reference	Synonymy	Specimen number	Vesicle diameter (μm)	process length (μm)	process basal width (μm)	process basal height (μm)	apical spine width (μm)	apical spine length (μm)	pocess length/ vesicle diameter
Chen and Liu, 1986	*Meghystrichosphaeridium chadianensis*	pl. II, Figs. 2, 4–5.	500–800						
Yuan et al., 1993	Unnamed acritarchs	pl. 2, Figs. 4–7	85–200	~30					
Yin and Xue, 1993	Spine-spheroidal acritarchs	pl. 1, figs. c, d, f	200–500						
Yuan and Hofmann, 1998	*Meghystrichosphaeridium wenganensis*	Fig. 10C, 10D.	100	25–30	12				
Zhang et al., 1998	*Meghystrichosphaeridium chadianensis*	figs. 3.6, 10.1–10.4	150–700	25–40	8–10				
Xiao et al., 1999	*Meghystrichosphaeridium chadianensis*	pl. 1, Figs. 1–2	> 500	15–20	10				
Yin et al., 1999	Unnamed acritarchs	pl. 1, figs. AG, pl. 2, figs. E–G	100–500	10–40	5–25				
Zhou et al., 2001	*Meghystrichosphaeridium chadianensis*	pl. 1, Figs. 1–8 (partim)	150–700	25–100	8–75				
Zhou et al., 2002	*Meghystrichosphaeridium chadianensis*	pl. 2, Fig. 5	~280	~70	~10				
Xie et al., 2008	*Meghystrichosphaeridium chadianensis*	pl. 1, Figs. 6–7	> 530		18.5–28	12–17	1.9–2.2	12.5–18	
Xiao et al., 2014	*Mengeosphaera chadianensis*	fig. 25.1–25.8	150–700	20–40	10–30				
Ouyang et al., 2015	*Mengeosphaera chadianensis*	pl. II, Figs. 5–8			10–25	11–20		18–28	
Liu and Moczydłowska, 2019	*Mengeosphaera chadianensis*	fig. 69	145–240	13–23	6–10				5.4–11.7%
Shang et al., 2019	*Mengeosphaera chadianensis*	Fig. 14C–E	~320	29–36	11–13	10–15	1–1.5	19–22	~10%
Yang et al., 2020	? *Mengeosphaera chadianensis*	Fig. 2G–H	260–300		36–48	17–19		23–33	

slightly smaller than *M. augusta* specimens described in Liu et al. (2014a). In addition, the very long apical spine relative to the basal expansion of processes is an important feature of *M. augusta*, but this feature is not easily confirmed in the current specimens because of their poorly preserved apical spines. Thus, these specimens are provisionally placed in *M. augusta*.

Occurrence: The Ediacaran Doushantuo Formation in the Shennongjia area of Hubei Province, South China (this paper).

Mengeosphaera chadianensis (Chen and Liu, 1986) Xiao et al., 2014. Figs. 32–33.

Synonymy:

1986 *Meghystrichosphaeridium chadianensis* Chen and Liu, pp. 51–52, pl. II, Figs. 2, 4–5.

2014 *Mengeosphaera chadianensis* (Chen and Liu, 1986) Xiao et al., pp. 39, 41, fig. 25.1–25.8, and synonyms therein.

2015 *Mengeosphaera chadianensis* (Chen and Liu, 1986) Xiao et al., 2014; Ouyang et al., pp. 217–218, pl. II, Figs. 5–8.

2017 *Mengeosphaera chadianensis*; Ouyang et al., Fig. 9L–M.

2019 *Mengeosphaera chadianensis* (Chen and Liu, 1986) Xiao et al., 2014; Liu and Moczydłowska, pp. 129–132, fig. 69.

2019 *Mengeosphaera chadianensis* (Chen and Liu, 1986) Xiao et al., 2014; Shang et al., p. 25, Fig. 14C–E.

? 2020 *Mengeosphaera chadianensis* (Chen and Liu, 1986) Xiao et al., 2014; Yang et al., p. 6, Fig. 2G–J.

2021 *Mengeosphaera chadianensis* (Chen and Liu, 1986) Xiao et al., 2014; Ouyang et al., Fig. 16G–J.

Material: Thirteen well-preserved and 38 poorly preserved specimens.

Description: Small to medium-sized, circular or deformed vesicle (originally spheroidal) with abundant and densely arranged biform processes (with 40–60 closed spaced processes per circumferential view). Biform processes consist of a basal expansion and an apical spine. Basal expansion inflated, conical to domical in shape, and its width comparable to or wider than length. Apical spine thin, tapering gradually to a pointed or blunt tip. Processes hollow, communicate freely with vesicle cavity, and basally joined or slightly separated.

Dimensions: Vesicle 94.4–148.7 μm in diameter; processes 20.4–57.9 μm in total length (or 18.1–41.2% of vesicle diameter); basal expansion 7.4–17.5 μm in width and 7.0–39.3 μm in height; apical spine ~ 1.0–3.3 μm wide and 9.3–49.4 μm long.

Remarks: Xiao et al. (2014) erected the genus *Mengeosphaera* to accommodate those acanthomorphic taxa with biform processes. A total of 19 species of *Mengeosphaera* have since been established (Liu and Moczydłowska, 2019; Liu et al., 2014a; Shang et al., 2019; Xiao et al., 2014). These species are differentiated from each other by overall vesicle shape, vesicle size, as well as process morphology, density, and relative size (Liu and Moczydłowska, 2019), although some of these species show morphological overlap and they may have been over-split. Previously published specimens of *M. chadianensis* have a wide size range (Table 5): vesicle 85–800 μm in diameter, processes 10–100 μm in length (typically 20–40 μm) or 5.4–11.7% of vesicle diameter, basal expansion 5–30 μm in width and 10–20 μm in height, apical spine 1–2.2 μm in maximum width, and apical spine 12.5–33 μm in length.

Present specimens fit the diagnosis of *Mengeosphaera* because of their hollow, closely arranged, and prominently biform processes that consist of an inflated basal expansion and a much thinner apical spine. They differ from *M. bellula* and *M. minima* in their greater vesicle diameter and process size, from *M. constricta*, *M. flammelata*, and *M. stegosauriformis* in their distinct process morphology, from *M. angusta*, *M. latibasis*, *M. lunula*, and *M. uniformis* in their smaller apical spine length relative to the basal expansion height. Our specimens are most similar to *M. chadianensis* in overall shape and process dimensions, although their process length, as measured relative to vesicle diameter, is greater.

Yang et al. (2020) illustrated two specimens of *Mengeosphaera chadianensis*. One of the specimens (Yang et al., 2020; their Fig. 2G–H) shows the presence of conical structures within their biform processes. These conical structures appear to be internal cores or internal plugs within the processes, giving an impression that the processes are bilayered. Xiao et al. (2014) noted the presence of internal cores in the processes of *Mengeosphaera* sp. (their fig. 28.1–28.10; see also Yuan and

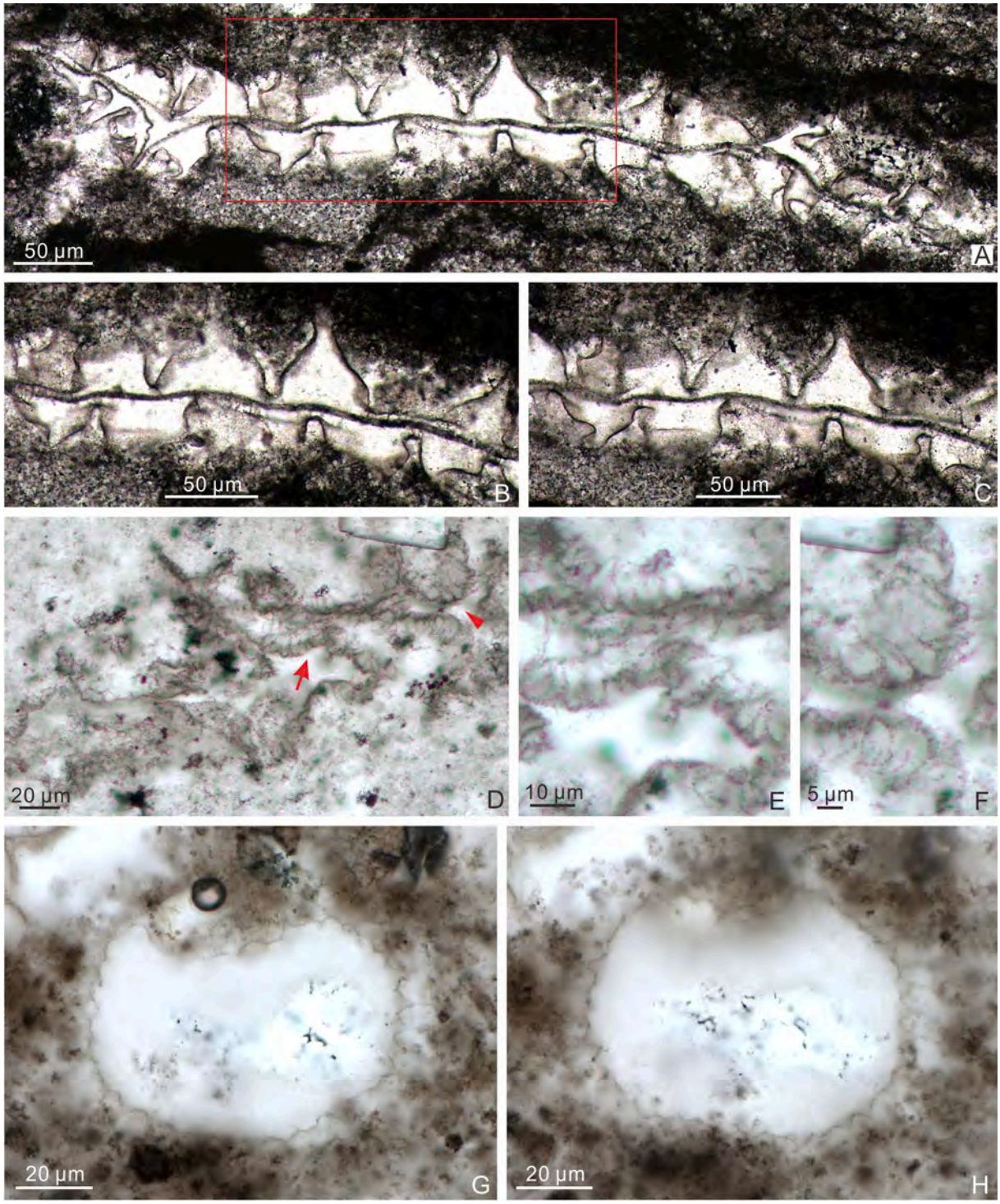

Fig. 34. (A–C) *Mengeosphaera constricta* Liu et al., 2014a; LHG2-d2-3.1 m-23–5 (29.3, NR). (B–C) Magnified views of area marked by rectangle in (A) at different focal levels, showing details of constriction at the base of processes. (D–F) *Mengeosphaera gracilis* Liu et al., 2014a; LHG-d2-4.5 m-3–1 (26.5 × 73.3). (E–F) Magnified views of areas in (D) marked by arrow and arrowhead, respectively, showing biform processes with a deflated basal expansion. (G–H) *Mengeosphaera minima* Liu et al., 2014a; 21LHC-1–39.5 m-3c-2 (16.8 × 106), different views of the same specimen.

Hofmann, 1998; their Fig. 11A–B), and commented that they may be taphonomic artifacts related to organic degradation. On the other hand, Ouyang et al. (2021; their Fig. 17C–F) illustrated the presence of one or two nested domal structures within the processes of *Mengeosphaera matryoshkaformis* and regarded them as biological features. Indeed, Ouyang et al (2021) identified some specimens of *Mengeosphaera* sp. (Xiao et al., 2014; their fig. 28.1–28.6) as *M. matryoshkaformis*, and favored a biological origin for the internal structures in the processes of *Mengeosphaera* sp. (fig. 28.1–28.10 of Xiao et al., 2014; Fig. 11A–B of Yuan and Hofmann, 1998) and *Mastosphaera changyangensis* (pl. 3, Figs. 6–7 of Yin, 1999). Similarly, Liu and Moczydłowska (2019) also regarded the inner core as a diagnostic feature, but they transferred some specimens of *Mengeosphaera* sp. (Xiao et al., 2014; their fig. 28.1–28.8) to *Distosphaera*? *corniculata*; this transfer is problematic

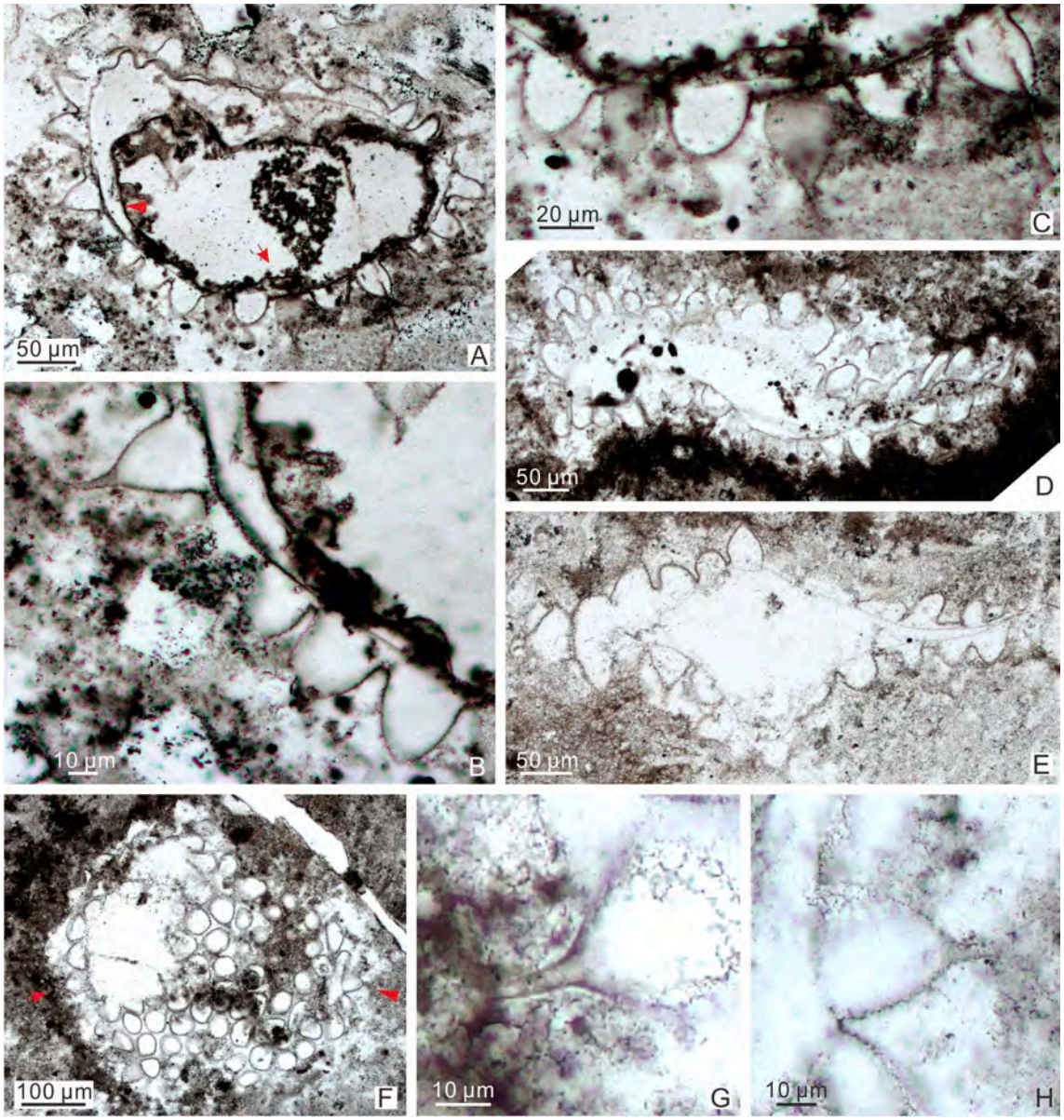

Fig. 35. *Mengeosphaera mamma* sp. nov. (A–C) holotype, LHG-d3 + 30 cm-1–17 (36.3 × 76.1). (B–C) Magnified views of areas in (A) marked by arrowhead and arrow, respectively. (D) LHG2-d2-3.1 m-2p-29 (25.3 × 77.2). (E) LHG-d2-3.7 m-2–1 (18 × 71.1). (F–H) LHG-d3 + 80 cm-6–18 (33.2 × 78.3). (G–H) Magnified views of areas in (F) marked by arrow and arrowhead, respectively.

because *Distosphaera*? *corniculata* does not have biform processes. Pending on the confirmation of the biological vs. taphonomic origin of the internal cores (perhaps with more specimen to assess the consistency of this feature), one of the two specimens illustrated as *Mengeosphaera chadianensis* in Yang et al. (2020; their Fig. 2G–H) may be retained in or excluded from this species. As to the other specimen of *M. chadianensis* illustrated in Yang et al. (2020; their Fig. 2I–J), it has a nearly straight triangular basal expansion and may be more appropriately identified as *Mengeosphaera triangularis* Liu et al., 2014a. As a side note, Liu and Moczydłowska (2019) transferred *M. triangularis* to the genus *Tanarium* and created a new combination *Tanarium triangularis* (*sic*; the species epithet was incorrectly inflected).

Occurrence: *M. chadianensis* is a unique species of South China. It has been reported from the Ediacaran Doushantuo Formation in the Shennongjia (this paper), Baokang (Yang et al., 2020), and Yangtze Gorges areas of Hubei Province (e.g., Liu and Moczydłowska, 2019; Ouyang et al., 2015, 2021; Xie et al., 2008), the Chadian area of Shanxi Province (Chen and Liu, 1986; Xiao et al., 1999), the Shangrao area of Jiangxi Province (Zhou et al., 2002), the Weng'an (e.g., Xiao et al., 2014; Zhang et al., 1998a) and Songlin areas (Shang et al., 2019) of Guizhou Province, and the Zhangjiajie area of Hunan Province (Ouyang et al., 2017).

Mengeosphaera constricta Liu et al., 2014a.

Fig. 34A–C.

Synonymy:

2014a *Mengeosphaera constricta* Liu et al., pp. 95–96, figs. 51.4, 56.1–56.6, 57.1–57.6, 58.1–58.10.

Material: Six adequately and 10 poorly preserved specimens.

Description: Large compressed vesicle, originally spheroidal, bearing abundant closely arranged biform processes. Process basal expansion inflated, conical, slightly wider than long or as wide as long, and constricted at the base. Process apical spine conical and distally tapering to a blunt end, which is often not preserved. Processes are basally separated by a small gap. Processes very large, hollow, and communicate freely with vesicle interior.

Dimensions: Vesicle completely compressed, hence vesicle diameter uncertain. Processes 31.6–63.7 μm in overall length; basal expansion

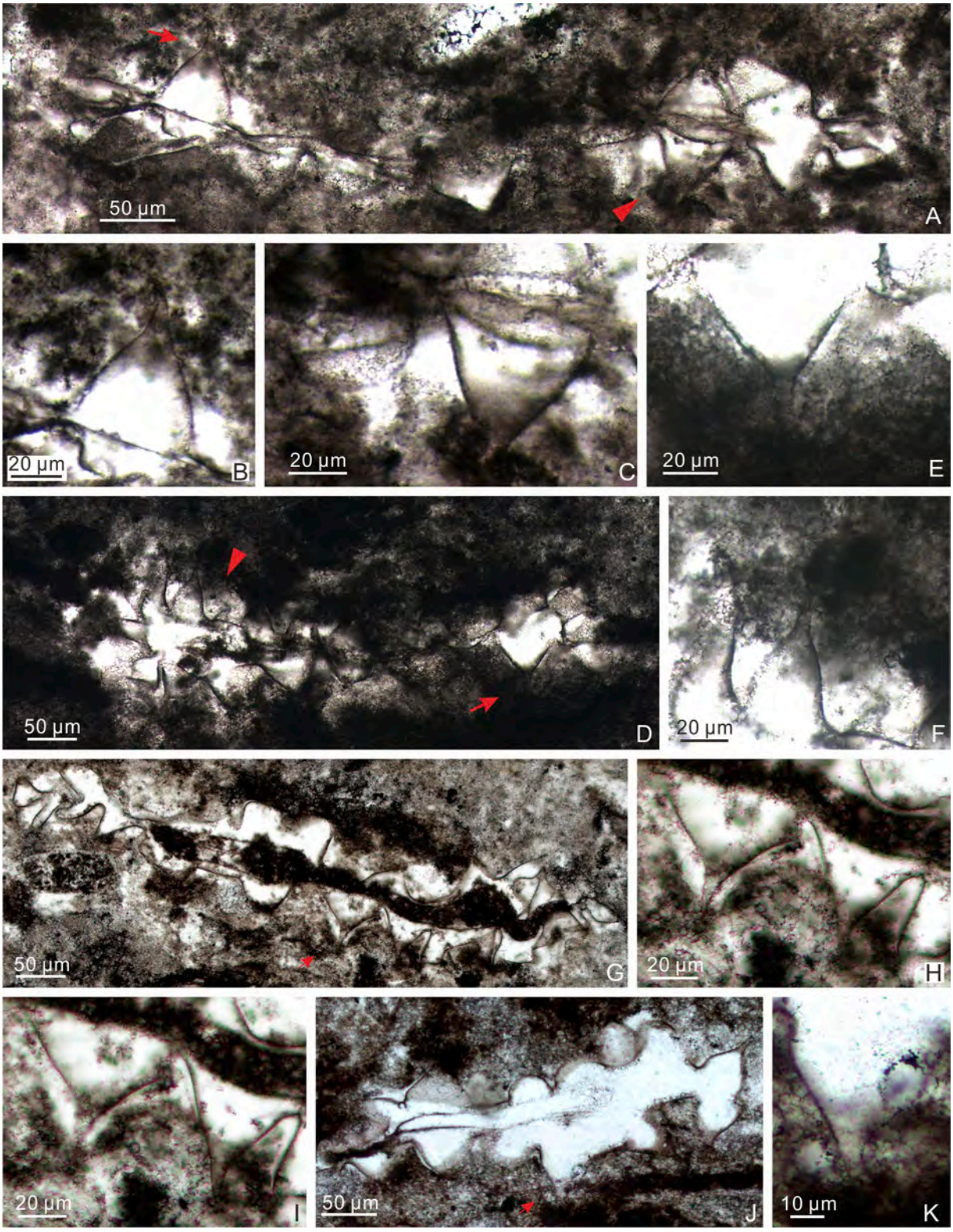

Fig. 36. *Mengeosphaera mamma* sp. nov. (A–C) LHG2-d2-3.1 m-44–16 (40.8, NR). (B–C) Magnified views of areas in (A) marked by arrow and arrowhead, respectively. (D–F) LHG2-d2-3.1 m-4-Z-3 (32.0, NR). (E–F) Magnified views of areas in (D) marked by arrow and arrowhead, respectively. (G–I) LHG2-d2-3.1 m-2c-34 (21.8 × 78.8). (H–I) Magnified views of area marked by arrow in (G) at different focal levels. (J–K) LHG-d2-2 m-1–1 (22.7 × 72.8). (K) Magnified view of area marked by arrow in (J).

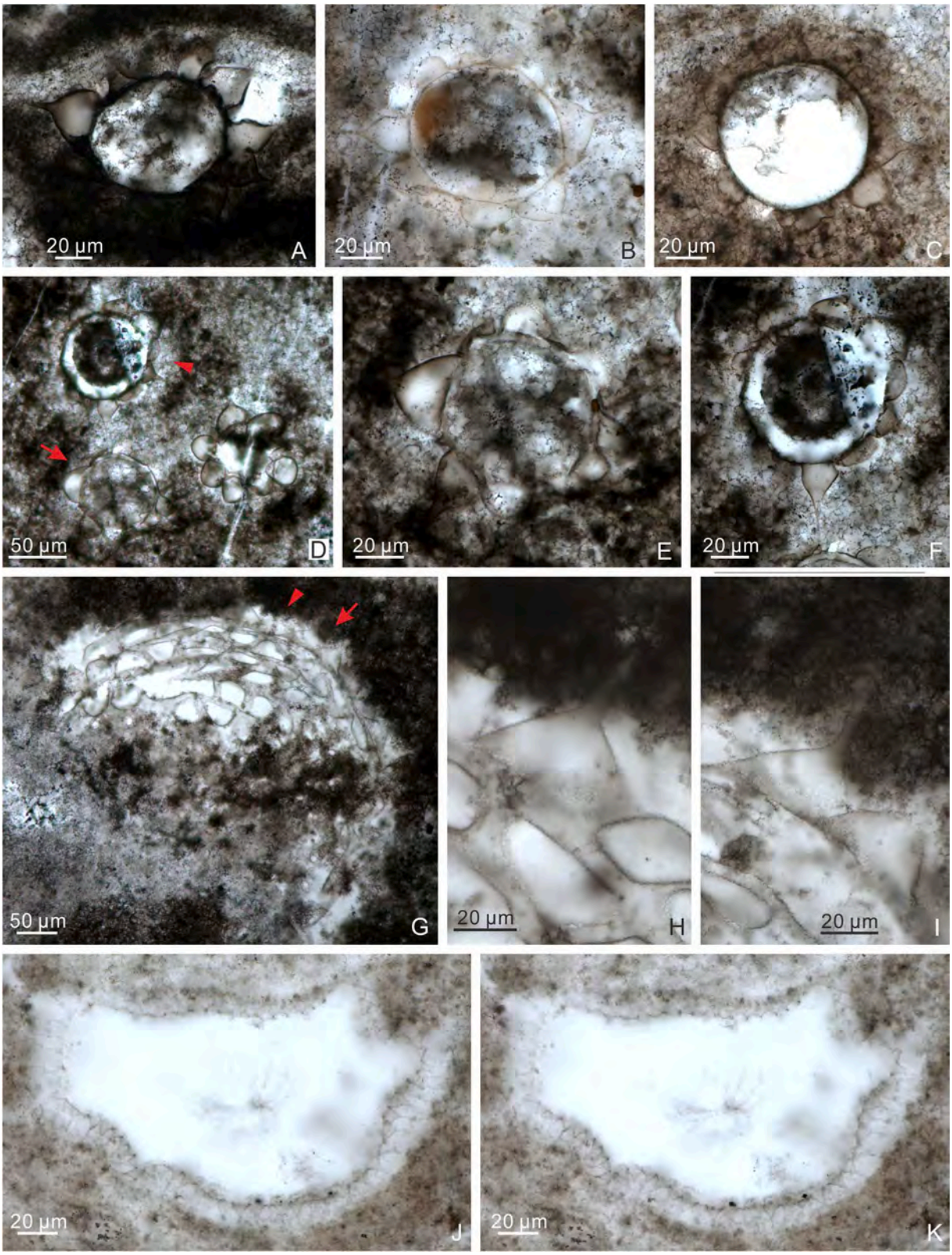

Fig. 37. A–F, *Mengeosphaera stegosauriformis* Liu et al., 2014a. (A) 21LHC-1–47 m-3c-2 (14.4 × 95). (B) 21LHC-1–47 m-4p-6 (10 × 94). (C) 21LHC-1–47 m-21c-1 (12.7 × 93.5). (D–F) 21LHC-1–47 m-4p-4 (6.4 × 96). (E–F) Magnified views of areas in (D) marked by arrow and arrowhead, respectively. (G–I) *Mengeosphaera* sp. 1; 21LHC-1–36.1 m-7p-3 (7.8 × 99.7). (H) Magnified view of area marked by arrowhead in (G) at a different focal level. (I) Magnified view of area marked by arrow in (G). (J–K) *Mengeosphaera* sp. 2; 21LHC-1–32.8 m-5c-4 (1 × 99.8), different views of the same specimen.

35.6–61.5 μm in maximum width and 22.8–37.5 μm in length or height, with 5.4–8.3 μm deep basal constriction; apical spine incompletely preserved, about 6.5–10.5 μm wide and 18.6–26.2 μm long (only the preserved portion was measured); process spacing up to 4.4–9.2 μm, with 18–25 processes per circumferential view.

Remarks: The present specimen has large biform processes with a recognizable basal constriction, conforming to the diagnosis of *M. constricta*. The processes in our specimens show a degree of variation in the shape and size range, which may have been caused by taphonomic alteration because their vesicles are often compressed (e.g., 34A). Liu and Moczydłowska (2019) considered *M. spicata* as a synonym of *M. constricta* without providing justification.

Occurrence: The Ediacaran Doushantuo Formation in the Shennongjia (this paper) and Yangtze Gorges areas (Liu et al., 2014a) of Hubei Province, South China.

Mengeosphaera gracilis Liu et al., 2014a.

Fig. 34D–F.

Synonymy:

2014a *Mengeosphaera*? *gracilis* Liu et al., pp. 96–97, figs. 51.6, 60.1–60.10.

2019 *Mengeosphaera gracilis* Liu et al.; Liu and Moczydłowska, pp. 132–133, fig. 71.

2019 *Mengeosphaera gracilis* Liu et al.; Shang et al., p. 25, Fig. 14F–G.

2020 *Mengeosphaera gracilis* Liu et al.; Shang and Liu, pp. 158–159, Fig. 6F–L.

2021 *Mengeosphaera gracilis* Liu et al.; Ouyang et al., 16 K–M.

2022 *Mengeosphaera gracilis* Liu et al.; Xiao et al., Fig. 25.

Material: Three poorly preserved specimens.

Description: Deformed vesicle (originally spheroidal) bearing numerous closely arranged biform processes. Basal expansion obtusely conical to slightly deflated. Apical spine very thin, filamentous, flexible, and terminated with a sharp-pointed tip. Processes are hollow and freely communicate with the vesicle cavity.

Dimensions: Process 11.3–16.6 μm in overall length; basal expansion

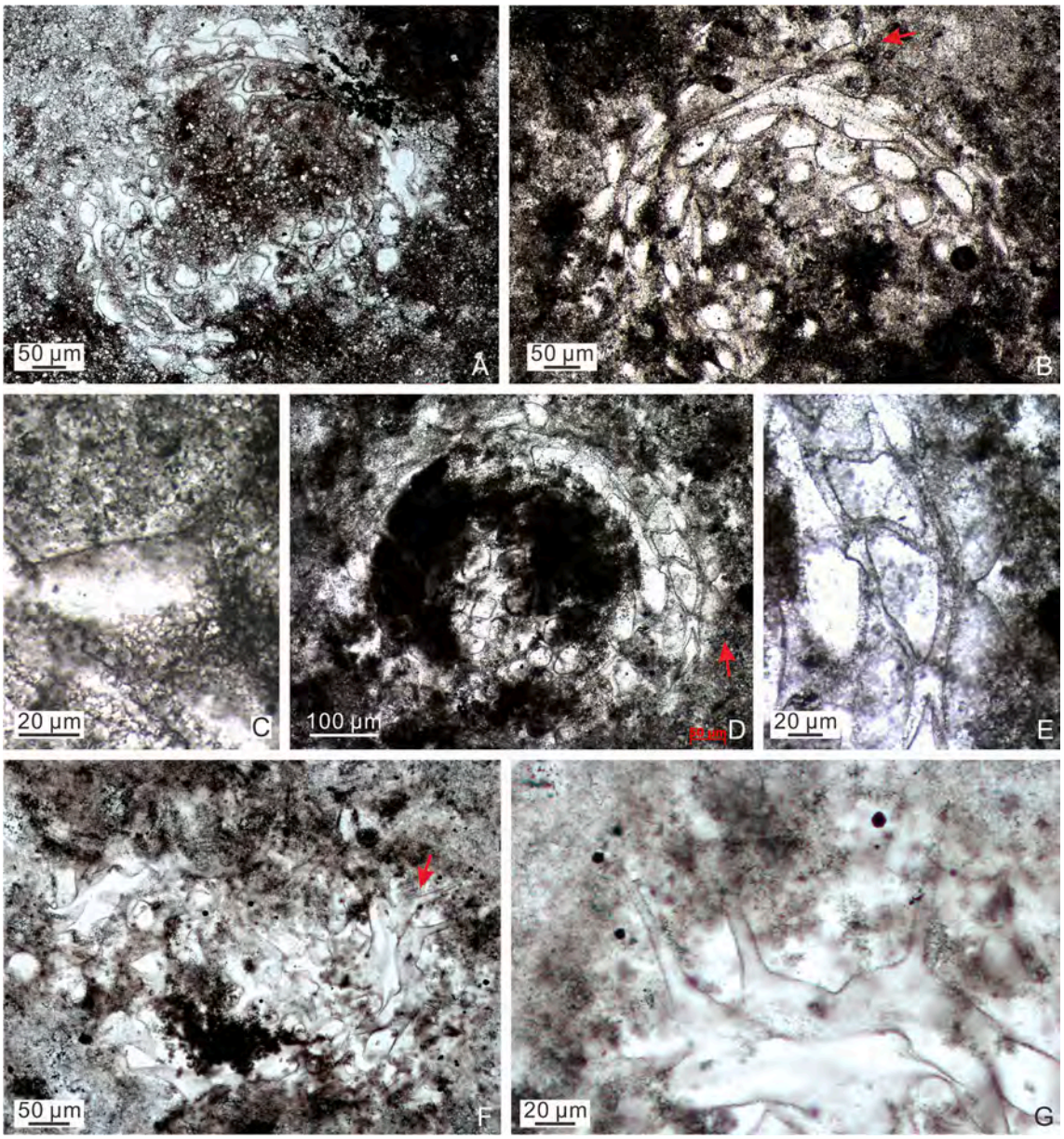

Fig. 38. (A–E) *Mengeosphaera* sp. 1. (A) LHG2-d2-3.1 m-3p-58 (40.0 × 73.0). (B–C) LHG2-d2-3.1 m-4-H-1 (35.8, pc). (C) Magnified view of area marked by arrow in (B). (D–E) LHG2-d2-3.1 m-4-H-8 (26.5, pc). (E) Magnified view of area marked by arrow in (D). (F–G) *Mengeosphaera* sp. 3; LHG2-d2-2 m-5–3 (21.4 × 80.9). (G) Magnified view of area marked by arrow in (F).

~ 5.8 μm in width and 2.2–3.0 μm in height; apical spine < 1 μm in width and 9.1–13.6 μm in estimated length.

Remarks: Our specimens are placed in *M. gracilis* based on their small biform processes with a deflated basal expansion and a thin apical spine. *M. gracilis* is somewhat similar to *Cavaspina basiconica* in process morphology, with both taxa characterized by hollow processes with an expanded base and an apical spine, but the basal expansion in *M. gracilis* is relatively larger and wider (holotype: basal width 7.0–7.8 μm and basal height 3.1–3.9 μm in *M. gracilis*; Liu et al., 2014a vs. ~ 3.2 μm and ~ 2.1 μm in *C. basiconica* measured from illustrations in Moczydłowska et al., 1993).

Occurrence: The Ediacaran Doushantuo Formation in the Shennongjia (this paper) and Yangtze Gorges areas (Liu and Moczydłowska, 2019; Liu et al., 2014a; Ouyang et al., 2021) of Hubei Province, the Zhangjiajie area of Hunan Province (Shang and Liu, 2020), and the Songlin area of Guizhou Province (Shang et al., 2019), South China; and Ediacaran Krol A Formation in northern India (Xiao et al., 2022).

Mengeosphaera mamma sp. nov.

Figs. 35–36.

Synonymy:

2021 *Mengeosphaera* sp. 2; Ouyang et al., Fig. 17H, L.

Holotype: The specimen illustrated in Fig. 35A–C, thin section LHG-d3 + 30 cm-1–17 (36.3 × 76.1).

Etymology: Species name derived from Latin *mamma* (breast), with reference to the biform process with an inflated breast-like basal expansion supporting a conical apical spine.

Locus typicus: The Ediacaran Doushantuo Formation at the Lianhuacun section, Shennongjia area of Hubei Province, South China.

Stratum typicum: Chert nodules in thin to medium bedded dolostones of unit 4, Doushantuo Formation.

Material: Twelve adequately preserved and 31 poorly preserved specimens.

Diagnosis: Large vesicle (originally spheroidal) bearing a moderate number of biform processes with a basal expansion and a relatively short apical spine with a blunt tip. Basal expansion large, inflated, domical in shape, variably spaced, and its width comparable to or slightly greater than length. Apical spine cylindrical to conical, tapers slightly toward a distal end that is often not preserved, not fully captured in thin section (Fig. 35D–E), or taphonomically curved (Fig. 35B, 36B). Processes are often basally joined or separated by a narrow but variable distance. Processes hollow and communicate freely with vesicle cavity.

Dimensions: Holotype: vesicle size 314.8 × 174.7 μm or 269.7 μm in diameter (calculated from circumference); basal expansion 20.9–31.1 μm in width and 20.8–31.7 μm in height; apical spine 3.0–5.1 μm in width and 6.2–17.4 μm in length; process spaced at 3.7–13.1 μm. Other specimens: vesicle 276.5–450.1 μm in diameter; basal expansion 21.4–69.7 μm in width and 22.4–57.3 μm in height; apical spine 3.4–7.4 μm in width and 6.7–23.9 μm in preserved length; space between adjacent processes ranges from near zero to about 38.8 μm.

Remarks: The current specimens are strongly deformed and show considerable variations in process size and shape between or within specimens. However, they have large biform processes with a strongly inflated basal expansion and a relatively short broad apical spine; these features are stable characters and warrant a new species. Nine other species of *Mengeosphaera* exhibit biform process with an inflated basal expansion, including *M. angusta*, *M. bellula*, *M. chadianensis*, *M. constricta*, *M. latibasis*, *M. spicata*, *M. spinula*, *M. stegosauriformis*, and *M. uniformis*. *Mengeosphaera mamma* sp. nov. differs from *M. angusta*, *M. bellula*, *M. latibasis*, *M. spinula*, and *M. uniformis* in that the latter five species have processes whose apical spine is thin (<1.5 μm in width) and longer than its basal expansion. It is different from *M. constricta* and *M. stegosauriformis* in that the latter two species have processes with a basal constriction and smaller vesicle diameters (100–155 μm in *M. constricta* and 42–65 μm in *M. Stegosauriformis*; Liu et al., 2014a). Further, the new species can be distinguished from *M. spicata* because the latter species has smaller vesicle size (60–180 μm in diameter; Liu et al., 2014a) and basally contacting processes. *M. chadianensis* has vesicle and process sizes somewhat similar to *M. mamma*, but its processes are more closely and regularly arranged on the vesicle (Xiao et al., 2014). A single specimen described *Mengeosphaera* sp. 2 in Ouyang et al. (2021; their Fig. 17H, L) fits the diagnosis of *M. mamma* in having large, inflated, and broadly conical processes.

Occurrence: The Ediacaran Doushantuo Formation in the Shennongjia (this paper) and Yangtze Gorges areas (Ouyang et al., 2021) of Hubei Province, South China.

Mengeosphaera minima Liu et al., 2014a.

Fig. 34G–H.

Synonymy:

2014a *Mengeosphaera minima* Liu et al., p. 101, figs. 51.8, 63.1–63.6, and synonyms therein.

Material: One well-preserved specimen and one poorly preserved specimen.

Description: Small spheroidal vesicle bearing abundant closely and evenly spaced processes. Processes hollow and biform, with a conical base and a thin apical filament. Processes basally joined and communicate openly with vesicle interior.

Dimensions: One specimen (Fig. 34G–H): vesicle ~ 74.0 μm in diameter; processes 12.6 μm in length (17.0% of vesicle diameter); basal part of processes 5.5–6.8 μm wide and 3.2–5.1 μm long; distal part of processes ~ 1.0–1.2 μm wide and 7.3–9.5 μm long; ~30 processes in circumferential view. The other specimen: vesicle diameter 74.4 μm, processes basal width 5.8–6.9 μm and basal height 4.3–5.1 μm; processes apical spine cannot be measured due to poor preservation.

Remarks: Our specimens are most similar to *M. minima* in overall shape, process density, and the proportion of process length to vesicle dimater, although they have slightly larger vesicles.

Occurrence: The Ediacaran Doushantuo Formation in the Shennongjia (this paper) and Yangtze Gorges areas (Liu et al., 2014a; also listed in Ouyang et al., 2021; illustrated as *Meghystrichosphaeridium chadianensis* in Xiao, 2004 and Yin et al., 2011b) of Hubei Province, South China.

Mengeosphaera stegosauriformis Liu et al., 2014a.

Fig. 37A–F.

Synonymy:

2014a *Mengeosphaera stegosauriformis* Liu et al., p. 103, figs. 51.12, 67.1–67.4.

Material: Seven well-preserved specimens and 11 poorly preserved specimens.

Description: Small spheroidal vesicle, bearing several large biform processes. Basal expansion inflated, hemispherical, or onion-like, generally wider than high, and slightly constricted at base. Apical spine acutely conical with a blunt tip. Processes hollow and freely communicate with vesicle interior.

Dimensions: vesicle 55.3–77.2 μm in diameter; processes 22.4–41.7 μm in preserved length (40.6–60.0% of vesicle diameter); basal expansion 16.9–39.5 μm wide and 11.0–24.0 μm long, with basal constriction 1.0–5.0 μm deep; well-preserved apical spine 2.0–5.9 μm wide and 12.9–24.4 μm long; about 6–12 processes present in circumferential view.

Remarks: M. stegosauriformis can be differentiated from other *Mengeosphaera* species by its small vesicle size, proportionally large processes with basal constrictions, and low process density.

Occurrence: The Ediacaran Doushantuo Formation in the Shennongjia (this paper) and Yangtze Gorges areas (Liu et al., 2014a) of Hubei Province, South China.

Mengeosphaera sp. 1.

Fig. 37G–I, 38A–E.

Material: Nine adequately preserved specimens and 12 poorly preserved specimens.

Description: Large spheroidal vesicle bearing large, densely and evenly distributed, biform processes that are basally joined. Basal expansion wide, mostly inflated (but can be straight), obtusely domical or conical in shape, and much wider than long (with width twice as

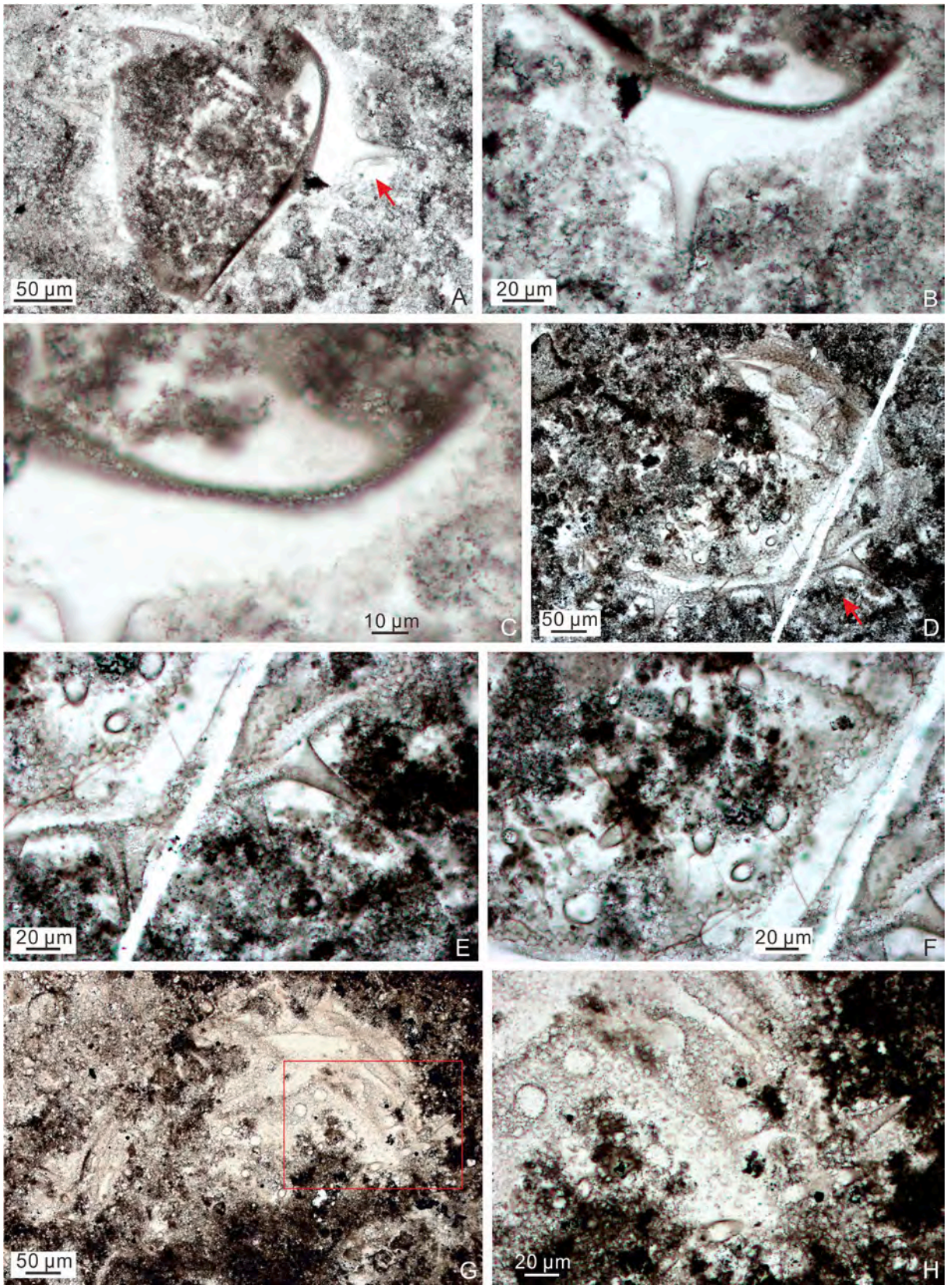

Fig. 39. (A–C) *Sinosphaera asteriformis* Liu et al., 2014a; LHG2-d2-2.1 m-2–11 (19.5 × 65). (B–C) Magnified views of area marked by arrow in (A) at different magnifications. (D–H) *Sinosphaera rupina* Zhang et al., 1998a, emend. Liu et al., 2014a. (D–F) LHG-d2-60 cm-5–1 (23.2 × 77.9). (E–F) Magnified views of area marked by arrow in (D). (G–H) LHG-d2-80 cm-1–13 (23.8 × 84.4). (H) Magnified view of area marked by rectangle in (G).

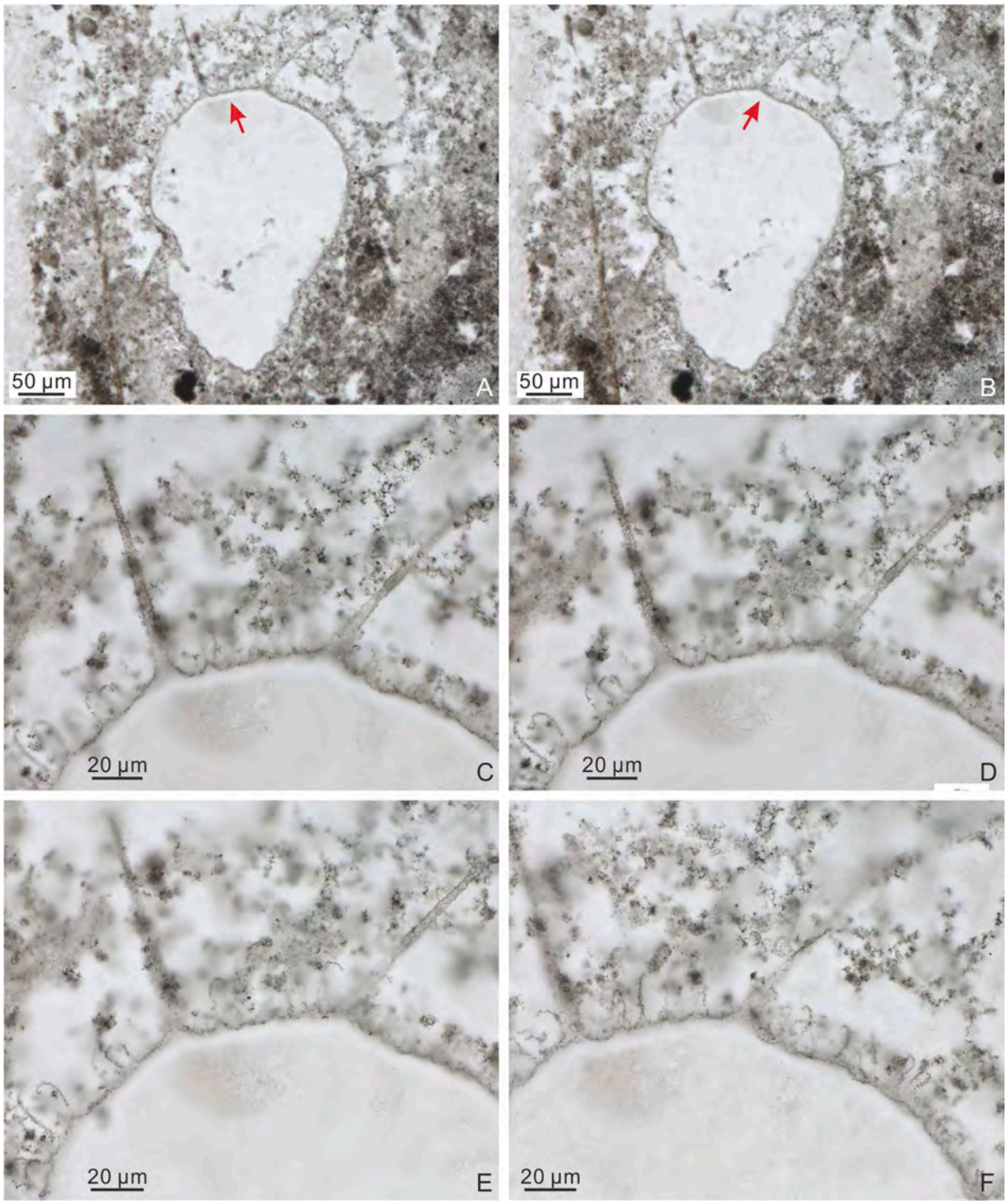

Fig. 40. *Sinosphaera exilis* sp. nov. holotype: 21LHC-1–45.6 m-20c-1 (5.5 × 89.2). (A–B) Different views of the same specimen. (C–E) Magnified views of area marked by arrow in (A), showing two types of processes at different focal levels. (F) Magnified view of area marked by arrow in (B), showing details of small processes.

length). The footprint of processes on vesicle wall ranges from circular, elliptical, triangular, to lozenge in shape. Apical spine cylindrical to conical, and tapers slightly toward a blunt distal end or a swollen clavate end (Fig. 37I). Processes hollow and communicate freely with vesicle cavity.

Dimensions: Vesicle 434.8–720.1 μm in diameter. Basal expansion 41.4–116.5 μm in width and 23.5–76.9 μm in height; apical spine 2.1–8.2 μm in maximum width and 10.4–31.9 μm in preserved length.

Remarks: In most specimens, the processes are cut at the base, showing the more or less even distribution of the basal expansions, which can be circular (Fig. 38A), elliptical (Fig. 38B), triangular (Fig. 37H–I, 38C), or lozenge (Fig. 38E) in shape. Most processes do not preserve an apical spine (Fig. 38A–B, D), probably due to taphonomic loss. Among published *Mengeosphaera* species, *M. latibasis*, *M. stegosauriformis*, and *M. uniformis* have processes whose basal expansion is inflated and wider than long, but they are much smaller than the current specimens in both vesicle size and process size. Our specimens can be differentiated from other *Mengeosphaera* species by its large processes with a very wide, inflated basal expansion and a relatively short broad apical spine. These specimens are provisionally placed

in an open nomenclature because of their incompletely preserved apical spine of their process.

Occurrence: The Ediacaran Doushantuo Formation in the Shennongjia area of Hubei Province, South China (this paper).

Mengeosphaera sp. 2.

Fig. 37J–K.

Material: One adequately preserved specimen.

Description: Medium-sized spheroidal vesicle bearing numerous hollow, homomorphic, densely distributed and basally joined, biform processes. Basal expansion conical in shape, roughly as wide as high. Apical

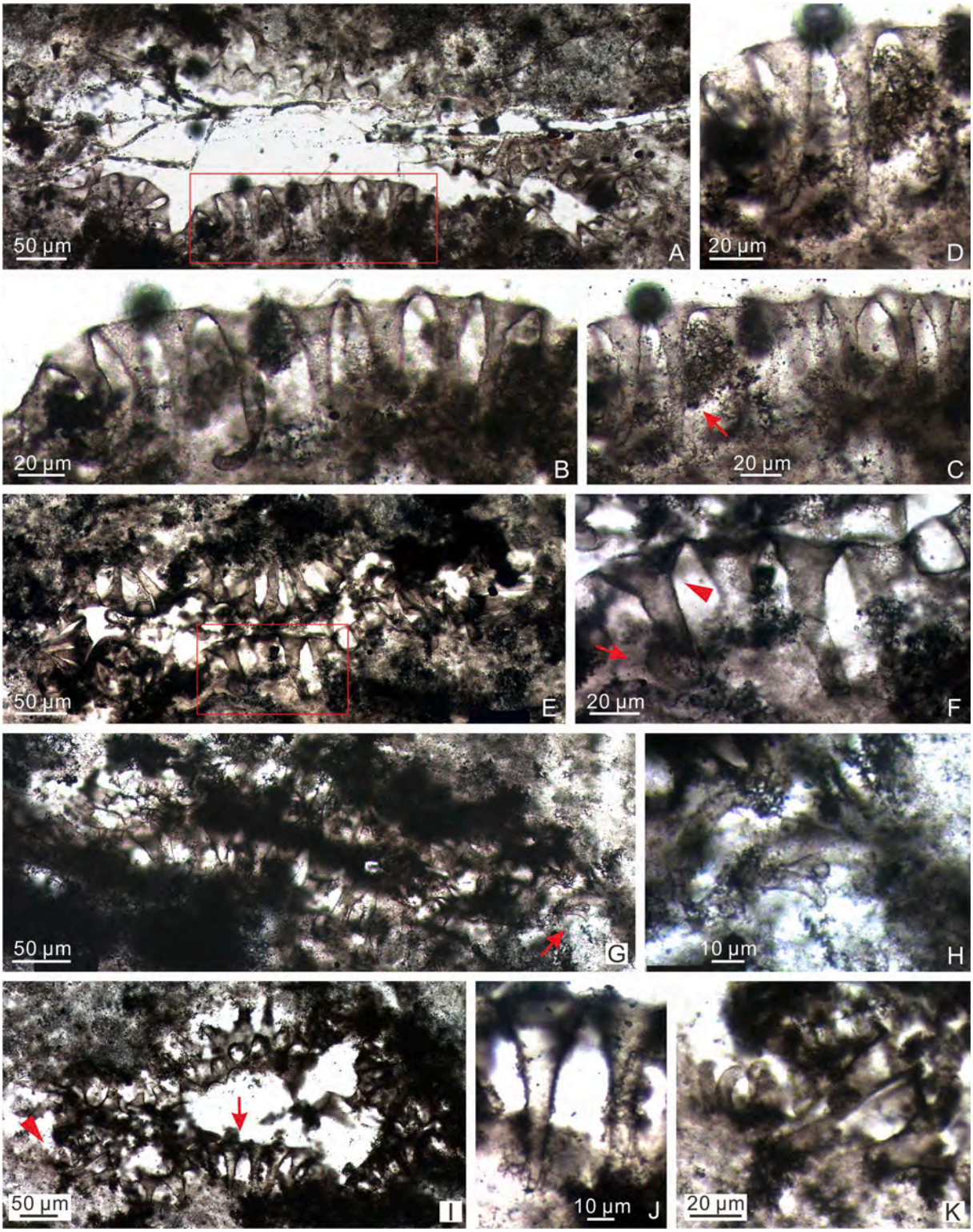

Fig. 41. *Tanarium columnatum* sp. nov. (A–D) holotype, LHG2-d2-2 m-19–1 (28.5, NR). (B–C) Magnified views of area marked by rectangle in (A) at different focal levels. (D) Magnified view of area marked by arrow in (C). (E–F) paratype, LHG2-d2-2 m-40–5 (43.9, NR). (F) Magnified view of area marked by rectangle in (E), showing details of process base (arrowhead) and termination (arrow). (G–H) LHG2-d2-2 m-10–6 (33, NR). (H) Magnified view of area marked by arrow in (G), showing blunt termination of processes. (I–K) LHG2-d2-2 m-8–2 (30, NR). (J–K) Magnified views of areas in (I) marked by arrow and arrowhead, respectively.

spine thin, distally tapering to a sharp tip. Processes open directly to vesicle cavity.

Dimensions: Vesicle diameter ~ 158.4 μm (estimated from circumference measurement); processes 15.6–21.3 μm in preserved length (9.8–13.4% of vesicle diameter); basal expansion 6.8–8.0 μm in width and 6.2–9.2 μm in height (~1.0 in basal width/height ratio); apical spine about 1.0 μm wide and 5.9–14.9 μm long; approximately 65 processes present in circumferential view of vesicle.

Remarks: The diagnostically biform processes of the current specimen identify it with the genus *Mengeosphaera*. It can be distinguished from other *Mengeosphaera* species by its relatively smaller vesicle size and a conical basal expansion that is approximately as wide as high. Our

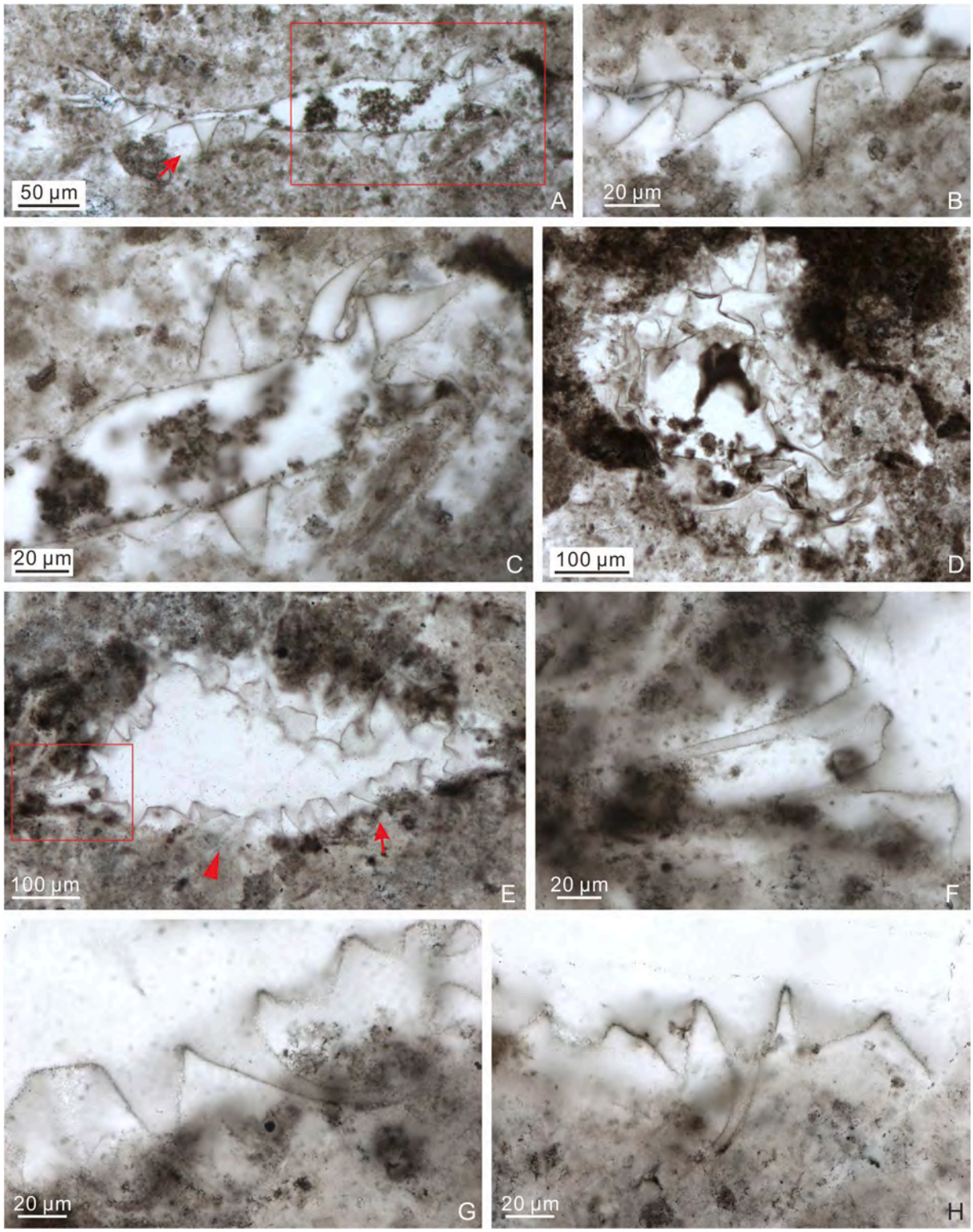

Fig. 42. *Tanarium conoideum* Kolosova, 1991, emend. Moczydłowska et al., 1993. (A–C) 21LHC-1–32.8 m-5c-7 (1.5 × 99.5). (B–C) Magnified views of areas in (A) marked by arrow and rectangle, respectively. (D) 21LHC-1–45.6 m-4p-5 (16 × 95). (E–H) 21LHC-1–48 m-8c-3 (13.3 × 102). (F–H) Magnified views of areas in (E) marked by rectangle, arrow, and arrowhead, respectively.

specimen is most similar to *M. gracilis* and *M. triangularis*, but *M. gracilis* has slightly larger vesicle, greater process density, and a conical basal expansion that is wider than high (~2.1 in width/height ratio; Liu et al., 2014a), and *M. triangularis* has relatively lower process density and much larger and longer processes. With only one specimen at hand, it is provisionally placed in an open nomenclature of *Mengeosphaera*.

Occurrence: The Ediacaran Doushantuo Formation in the Shennongjia area of Hubei Province, South China (this paper).

Mengeosphaera sp. 3.

Fig. 38F–G.

Material: One adequately and seven poorly preserved specimens.

Description: Large (originally) spheroidal vesicle bearing a moderate number of large biform processes with a basal expansion and a very long and gradually tapering apical spine. The basal expansion is obtuse and slightly inflated.

Dimensions: Vesicle diameter ~ 364.0 μm; full length of processes was not measured because of incomplete preservation; basal expansion 40.2–69.6 μm wide and 18.3–30.2 μm high; apical spine 5.2–14.7 μm in maximum width and 57.5–105.0 μm in preserved length.

Remarks: The current specimens belong to *Mengeosphaera* because of their biform processes. However, the apical spine of their processes is broad, extremely long, and tapers gradually, thus different from other published *Mengeosphaera* species. Our specimens are most similar to *M. triangularis*, but the latter has much smaller processes that have a somewhat deflated basal expansion. They are somewhat similar to *M. mamma* (Figs. 35–36), but can be differentiated by their obtuse basal expansion and much longer apical spines. Their processes are also somewhat similar to the large processes in *Duospinosphaera biformis* (Fig. 22), but their apical spines are much longer and they lack the small processes that are characteristic of bimorphic acanthomorphs such as *D. biformis*. At the present, they are provisionally placed in open nomenclature, possibly representing new species of *Mengeosphaera*.

Occurrence: The Ediacaran Doushantuo Formation in the Shennongjia area of Hubei Province, South China (this paper).

Genus *Sinosphaera* Zhang et al., 1998a, emend. Xiao et al., 2014.

Type species: *S. rupina* Zhang et al., 1998a, emend. Liu et al., 2014a.

Sinosphaera asteriformis Liu et al., 2014a.

Fig. 39A–C.

Synonymy:

2014a *Sinosphaera asteriformis* Liu et al., pp. 105–106, figs. 72.1, 73.1–73.6.

Material: One deformed but moderately preserved specimen.

Description: Large but incompletely preserved vesicle (originally spheroidal) bearing bimorphic processes. Small processes abundant, conical to denticle, densely distributed and basally joined. Large processes long, conical, taper gradually, sparsely distributed (three per circumferential view), and scattered among small processes. Both small and large processes are hollow and communicate openly with vesicle cavity.

Dimensions: Small processes 4.8–7.4 μm wide at base and 4.6–6.7 μm long; large processes 21.9–28.8 μm wide at base and 68.9–79.9 μm in preserved length (full length unknown due to incomplete preservation of process tips).

Remarks: S. asteriformis is different from other *Sinosphaera* species in its distinctively sparse large processes interspersed among numerous small processes on the vesicle surface.

Occurrence: The Ediacaran Doushantuo Formation in the Shennongjia (this paper) and Yangtze Gorges areas (Liu et al., 2014a) of Hubei Province, South China.

Sinosphaera exilis sp. nov.

Fig. 40.

Holotype: The specimen illustrated in Fig. 40, thin section 21LHC-1–45.6 m-20c-1 (5.5 × 89.2).

Etymology: From Latin *exilis*, with reference to the large processes of the new species that are slender relative to those of other *Sinosphaera* species.

Locus typicus: The Ediacaran Doushantuo Formation at the Lianhuacun section, Shennongjia area of Hubei Province, South China.

Stratum typicum: Chert nodules in thin to medium bedded dolostones of unit 4, Doushantuo Formation.

Material: One adequately preserved specimen and two poorly preserved specimens.

Diagnosis: Large spheroidal vesicle with two kinds of hollow processes arising from the outer surface of vesicle wall. Large processes slender, conical, very long, few in numbers, sparsely and irregularly distributed among small processes, and taper gradually toward a pointed distal end. Small processes short, thin, biform (with a slightly inflated basal expansion supporting a filamentous apical spine), and densely arranged. Both large and small processes freely communicate with vesicle interior.

Dimensions: Holotype: vesicle diameter 263.9 μm; small processes 22.1–27.3 μm in overall length, ~1.0–3.0 μm in basal spacing, basal expansion 5.4–5.6 μm in width and 1.5–3.3 μm in length, apical spine 0.8–1.2 μm in width and 18.2–20.9 μm in length; large processes 89.5–99.9 μm in maximum length, 10.7–11.2 μm in basal width, and 51.6–139.5 μm in spacing; four to six large processes in circumferential view. Other specimens: vesicle diameter 502.1–532.7 μm (estimated from circumference measurement); small processes 23.1–38.5 μm in length, 5.4–12.5 μm in basal spacing, basal expansion 5.1–6.8 μm in width and 3.0–4.3 μm in height, apical spine ~ 1.0–1.5 μm in width and 20.6–35.5 μm in length; large processes 21.9–61.9 μm in preserved length and 13.5–14.6 μm in basal width; two to four large processes in circumferential view.

Remarks: The new species fits the diagnosis of *Sinosphaera* in its hollow bimorphic processes. Apical spine of small processes is occasionally but not consistently curved toward the distal end (Fig. 40C–D). *Sinosphaera exilis* sp. nov. differs from *S. asteriformis*, *S. rupina*, and *S. speciosa* in that the latter three species have basally joined domical small processes and shorter, relatively more densely and regularly distributed large processes. The current species is most similar to *S. variabilis*, but its small processes are smaller and its large processes are more sparsely arranged, fewer in numbers (2–6 vs. ~ 20 per circumferential view), and narrower in basal width (10.7–14.6 μm in *S. exilis* sp. nov. vs. 30–14.6 μm in *S. variabilis*; Xiao et al., 2014).

Occurrence: The Ediacaran Doushantuo Formation in the Shennongjia area of Hubei Provinces, South China (this paper).

Sinosphaera rupina Zhang et al., 1998a, emend. Liu et al., 2014a.

Fig. 39D–H.

Synonymy:

1998a *Sinosphaera rupina* Zhang et al., pp. 38, 40, fig. 11.4–11.10.

2014a *Sinosphaera rupina* Zhang et al., 1998, emend. Liu et al., pp. 106–107, 109, figs. 72.2, 73.7–73.9, 74.1–74.7, and synonyms therein.

non 2016 *Sinosphaera rupina* Zhang et al., 1998, emend. Liu et al., 2014a; Prasad and Asher, p. 54, pl. VII, Figs. 3–5.

Material: Three well-preserved and two poorly preserved specimens.

Description: Large spheroidal vesicle bearing bimorphic processes. Small processes homomorphic, conical to domical, short, basally joined, and densely arranged. Large processes conical, long, moderate in numbers (approximately 20–30 large processes in circumferential view), and sparsely distributed among small processes. Both small and large processes are hollow and communicate freely with vesicle cavity.

Dimensions: Vesicle diameter 411.4–488.1 μm; small processes 2.5–6.1 μm wide at base and 3.4–6.8 μm long; large processes 8.5–31.6 μm wide at base, 22.9–113.5 μm long, and spaced at 7.1–15.9 μm.

Remarks: Our specimens belong to *Sinosphaera* because of their distinct bimorphic processes. *S. rupina* is characterized by a moderate number of large processes whose basal width is more than twice that of small processes. In comparison, *S. speciosa* (Zhou et al., 2001) Xiao et al., 2014 has relatively fewer large processes whose basal width is less than twice that of small processes. Our specimens are morphologically similar to but relatively smaller in vesicle size than *S. rupina* recorded in the Yangtze Gorges area (Liu et al., 2014a). Specimens illustrated as

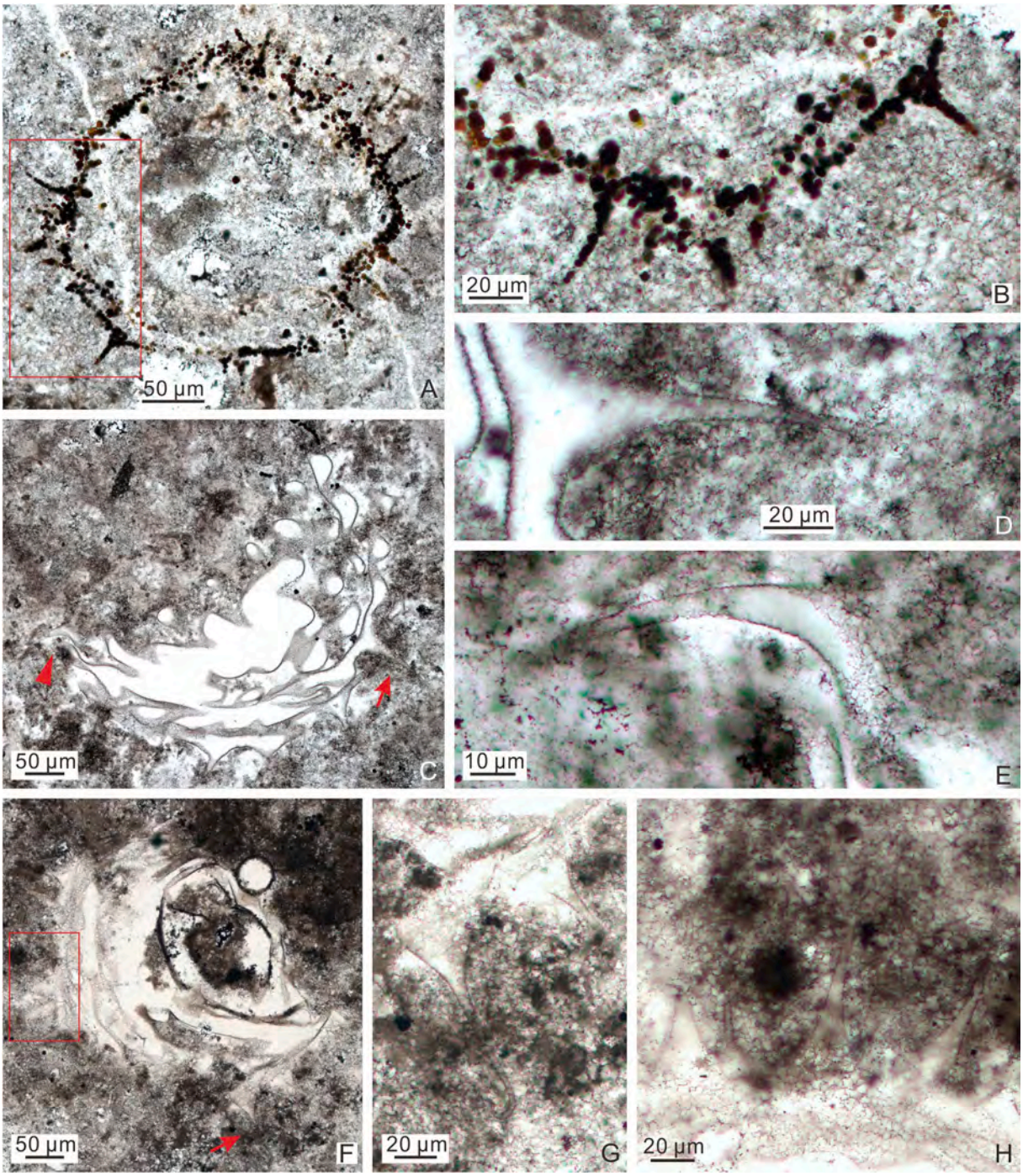

Fig. 43. (A–E) *Tanarium conoideum* Kolosova, 1991, emend. Moczydłowska et al., 1993. (A–B) LHG-d2-2 m-1–2 (21.1 × 83.1). (B) Magnified view of area marked by rectangle in (A). (C–E) LHG2-d2-3.1 m-2p-65 (18.7 × 64.2). (D–E) Magnified views of areas in (C) marked by arrow and arrowhead, respectively. (F–H) *Tanarium cuspidatum* (Liu et al., 2014a) Liu and Moczydłowska, 2019; LHG-d2-80 cm-1–6 (16.3 × 72.9). (G–H) Magnified views of areas in (F) marked by arrow and rectangle, respectively.

S. rupina in Prasad and Asher (2016; their pl. VII, Figs. 3–5) do not have the characteristic bimorphic processes and thus should be excluded from the genus *Sinosphaera*.

Occurrence: The Ediacaran Doushantuo Formation in the Shennongjia (this paper) and Yangtze Gorges areas (Liu et al., 2014a) of Hubei Province, South China.

Genus *Tanarium* Kolosova, 1991, emend. Moczydłowska et al., 1993.

Type species: *Tanarium conoideum* Kolosova, 1991, emend. Moczydłowska et al., 1993.

Tanarium columnatum sp. nov.

Fig. 41.

Holotype: The specimen illustrated in Fig. 41A–D, thin section LHG2-d2-2 m-19–1.

Paratype: The specimen illustrated in Fig. 41E–F, thin section LHG2-d2-2 m-40–5.

Etymology: Species name derives from the Latin *columnatus*, with the reference to the robust and long conical processes of this species.

Locus typicus: The Ediacaran succession in the Lianhuacun section, Shennongjia area of Hubei Province, South China.

Stratum typicum: Chert nodules in thin to medium bedded dolostones

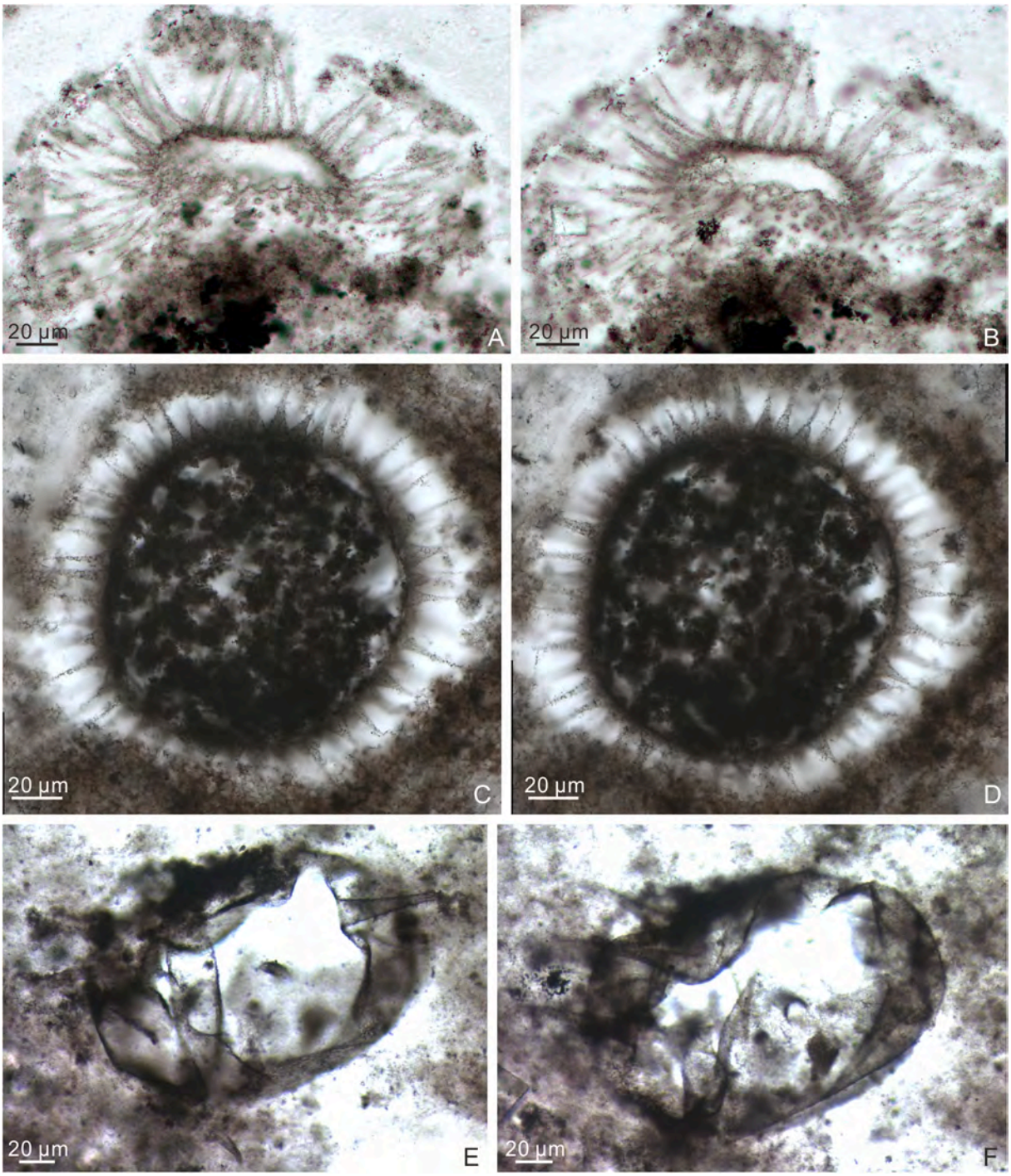

Fig. 44. (A–B) *Tanarium gracilentum* (Yin in Yin and Liu, 1988) Ouyang et al., 2021; LHG2-d2-3.1 m-3p-13 (28.7 × 80.4), different views of the same specimen. (C–D) *Tanarium muntense* Grey, 2005; 21LHC-1–37.4 m-7p-1 (10.3 × 104.4), different views of the same specimen. (E–F) *Tanarium paucispinosum* Grey, 2005; LHG2-d2-3.1 m-18-H-27 (33, NR), different views of the same specimen.

of unit 4 of the Ediacaran Doushantuo Formation.

Material: Six well-preserved and 12 moderately preserved specimens.

Diagnosis: Large spheroidal vesicle bearing abundant densely and evenly distributed processes that are basally contacted or separated by a narrow gap. Processes large, long, robust, thick, elongate conical in overall shape, and gradually taper to a blunt or round end. Some processes exhibit a somewhat deflated basal expansion. The termination of processes is often curved, bent, or truncated. Processes are of more or less equal size within specimens. They are hollow and directly communicate with the vesicle interior.

Dimensions: Holotype: vesicle diameter 462.7 μm (estimated from circumference measurement); process length ~ 66.0–97.2 μm; process basal width 15.1–29.0 μm; process apical width ~ 5.0 μm. Other specimens: vesicle diameter 279.3–376.8 μm (estimated from circumference measurement); process length 33.9–98.3 μm; process basal width 18.2–39.9 μm; process apical width 8.8–14.5 μm.

Remarks: The current specimens are characterized by long and robust processes that more or less gradually taper toward a blunt distal end. Although some of the processes have a slightly deflated basal expansion, most of them are not clearly biform in nature. Thus, they are placed in

Tanarium rather than *Mengeosphaera*. The processes of *T. columnatum* are somewhat similar to those of *Asterocapsoides* species, but they are relatively longer. This new species can be distinguished from other *Tanarium* species by its thick, robust, and large processes with a blunt termination. Morphologically this species is somewhat similar to *T. digitiforme*. However, the latter species has smaller vesicles (107–165 μm) and fewer processes that are narrower in basal width (3–15 μm) and shorter in length (6.5–31 μm) (Sergeev et al., 2011; Xiao et al., 2014). In addition, *T. digitiforme* has more stiff and straight processes than those in *T. columnatum* sp. nov.

Occurrence: The Ediacaran Doushantuo Formation in the Shennongjia area of Hubei Province, South China (this paper).

Tanarium conoideum Kolosova, 1991, emend. Moczydłowska et al., 1993.

Fig. 42, 43A–E.

Synonymy:

1991 *Tanarium conoideum* Kolosova, p. 57, fig. 5.1–15.3.

1993 *Tanarium conoideum* Kolosova, 1991, emend. Moczydłowska et al., p. 514, 516, text-Fig. 10C–D.

non 2012 *Tanarium conoideum* Kolosova, 1991, emend. Moczydłowska et al., 1993; Moczydłowska and Nagovitsin, pp. 18–19, Fig. 8K.

2014 *Tanarium conoideum* Kolosova, 1991, emend. Moczydłowska et al., 1993; Xiao et al., pp. 51, 53, fig. 33.1–33.6, and synonyms therein.

2014a *Tanarium conoideum* Kolosova, 1991, emend. Moczydłowska et al., 1993; Liu et al., p. 109, figs. 76.2, 77.1–77.6.

2015 *Tanarium conoideum*; Golubkova et al., Fig. 2c.

non 2016 *Tanarium conoideum* Moczydłowska et al.; Prasad and Asher, p. 56, pl. VII, Fig. 8.

2019 *Tanarium conoideum* Kolosova, 1991, emend. Moczydłowska et al., 1993; Shang et al., p. 26, Fig. 16A–E.

non 2020 *Tanarium conoideum* Kolosova, 1991, emend. Moczydłowska et al., 1993; Yang et al., pp. 6–7, Fig. 2K.

2020 *Tanarium conoideum* Kolosova, 1991, emend. Moczydłowska et al., 1993; Vorob'eva and Petrov, pp. 374–375, pl. I, Fig. 15.

Material: Six well-preserved specimens and 16 poorly preserved specimens.

Description: Large spheroidal vesicle bearing a small number of conical processes. Processes relatively large, long, straight or slightly curved, slightly expanded at bases and distally taper to a blunt

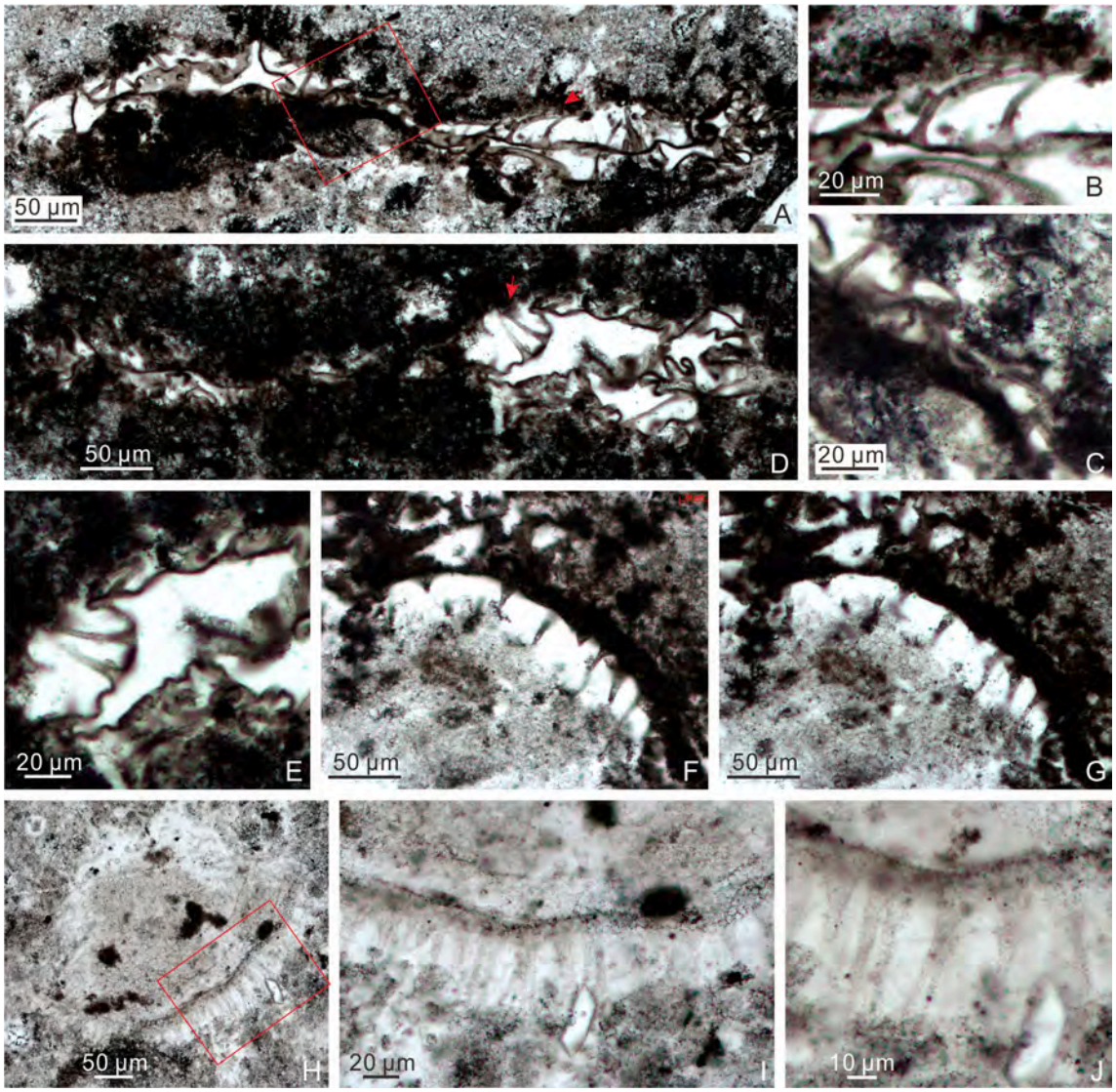

Fig. 45. (A–G) *Tanarium pluriprotensum* Grey, 2005. (A–C) LHG-d2-60 cm-6–4 (21.6 × 73.8). (B–C) Magnified views of areas in (A) marked by arrow and rectangle, respectively. (D–E) LHG-d2-60 cm-10–11 (24.5 × 73.7). (E) Magnified view of area marked by arrow in (D). (F–G) LHG-d3 + 60 cm-1–6 (23.7 × 77.3), different views of the same specimen. (H–J) *Tanarium* sp.; LHG2-d2-2.1 m-2–1 (20.5 × 68.5). (I–J) Magnified views of area marked by rectangle in (H) at different magnifications.

termination. Processes hollow and openly communicate with the vesicle cavity.

Dimensions: Vesicle diameter 226.2–432.3 μm; processes 28.5–140.6 μm in preserved length (or 12.3–37.2% of vesicle diameter), 12.8–52.3 μm in basal width, and up to 15.1–24.5 μm in spacing.

Remarks: T. conoideum is characterized by typical long and relatively large conical processes. It differs from *T. cuspidatum* (Liu et al., 2014a) Liu and Moczydłowska, 2019 by its gradually tapering conical processes without an obvious basal expansion. Several specimens, previously illustrated under *T. conoideum* by Moczydłowska and Nagovitsin (2012) and Prasad and Asher (2016), contain thin and short processes and do not conform to the diagnosis of *T. conoideum*. In addition, a specimen described as *T. conoideum* in Yang et al. (2020) has abundant, proportionally short, and densely distributed processes, some of which have a basal expansion, and this specimen is here excluded from *T. conoideum*.

Occurrence: The Ediacaran Doushantuo Formation in the Shennongjia (this paper) and Yangtze Gorges areas (Liu et al., 2014a) of Hubei Province, the Weng'an (Xiao et al., 2014) and Songlin areas (Shang et al., 2019) of Guizhou Province, South China; and Ediacaran succession in Siberia (Kolosova, 1991; Moczydłowska, 2005; Moczydłowska et al., 1993; Sergeev et al., 2011; Vorob'eva and Petrov, 2020).

Tanarium cuspidatum (Liu et al., 2014a) Liu and Moczydłowska, 2019.

Fig. 43F–H.

Synonymy:

2014a *Mengeosphaera*? *cuspidata* Liu et al., p. 96, figs. 51.5, 59.1–59.6.

2017 *Mengeosphaera*? *cuspidata*; Ouyang et al., Fig. 9I–K.

2019 *Tanarium cuspidatum* (Liu et al., 2014a) Liu and Moczydłowska, p. 145, fig. 80.

2019 *Tanarium cuspidatum* (Liu et al., 2014a) Liu and Moczydłowska; Shang et al., pp. 26–27, Fig. 16F–G.

Material: Six adequately preserved and 11 poorly preserved specimens.

Description: Large spheroidal vesicle with elongate conical processes. Processes are very long, large, with a widened and often deflated basal expansion that more or less gradually tapers to a slender termination. Processes are basally joined or separated by a small gap and occasionally curved at the apical end (Fig. 43G). Processes hollow and communicate freely with the cavity interior.

Dimensions: Vesicle ~ 383.8 μm in diameter; processes 87.2–113.5 μm in length or 22.7–29.6% of vesicle diameter; basal expansion 23.9–44.3 μm in width and 17.1–24.3 μm in height; apical spine 7.0–8.1 μm in maximum width.

Remarks: The overall morphology of our specimen is similar to the holotype of *T. cuspidatum*.

Occurrence: The Ediacaran Doushantuo Formation in the Shennongjia (this paper) and Yangtze Gorges areas (Liu and Moczydłowska, 2019; Liu et al., 2014a) of Hubei Province, the Zhangjiajie area of Hunan Province (Ouyang et al., 2017), and the Songlin area of Guizhou Province (Shang et al., 2019), South China.

Tanarium gracilentum (Yin in Yin and Liu, 1988) Ouyang et al., 2021.

Fig. 44A–B.

Synonymy:

2021 *Tanarium gracilentum* (Yin in Yin and Liu, 1988) Ouyang et al., p. 35, Fig. 19H–J, and synonyms therein.

Material: Two adequately preserved specimens.

Description: Small to medium-sized spheroidal vesicle bearing numerous densely and regularly distributed elongate processes that are nearly cylindrical or taper slightly toward a pointed distal termination. Processes narrow, long, stiff, and without a basal expansion. Processes are basally separated by a small gap. They are hollow and freely communicate with vesicle interior.

Dimensions: Vesicle diameter 90.2–119.6 μm; process length 45.7–50.1 μm (39.3–55.5% of vesicle diameter); process basal width 4.4–7.8 μm; distance between processes 3.3–4.3 μm.

Remarks: This species was redefined and emended by Ouyang et al. (2021) to emphasize its hollow, long, nearly cylindrical, and densely distributed processes, which differentiate *T. gracilentum* from other *Tanarium* species. Morphologically this species is somewhat similar to *T. pluriprotensum* and *T. pycnacanthum*. However, *T. gracilentum* tend to have straight and apparently more rigid processes than the latter species. Moreover, *T. pluriprotensum* has lower process density and somewhat more widely separate processes (Fig. 45A–G) whereas *T. pycnacanthum* has much thinner, more flexible, and more densely arranged processes. Regardless, if *T. gracilentum* were considered synonymous with either *T. pycnacanthum* or *T. pluriprotensum*, it takes priority over the latter species. Thus, we choose the place our specimens in *T. gracilentum*.

Occurrence: The Ediacaran Doushantuo Formation in the Shennongjia (this paper) and Yangtze Gorges areas (Awramik et al., 1985; Ouyang et al., 2019, 2021) of Hubei Province, and the Shangrao area of Jiangxi Province (Zhou et al., 2002), South China.

Tanarium muntense Grey, 2005.

Fig. 44C–D.

Synonymy:

2005 *Tanarium*? *muntense* Grey, pp. 316–318, Fig. 45F, 208F, 233A–B, D, 234A, C–F, 236.

2019 *Tanarium muntense* Grey; Liu and Moczydłowska, pp. 147, 149, fig. 82, and synonyms therein.

Material: One well-preserved specimen.

Description: Medium-sized spheroidal vesicle bearing numerous, hollow, homomorphic, densely arranged and basally joined, conical processes which rapidly taper from a conical base to a sharply pointed tip. Processes freely communicate with vesicle cavity.

Dimensions: Vesicle diameter ~ 126.7 μm; process length 24.5–33.1 μm or 19.3–26.1% of vesicle diameter; process basal width 7.7–9.0 μm.

Remarks: The present specimen is similar to *T. muntense* in overall morphology and size dimensions. It differs from *T. gracilentum* in shorter process length and narrower basal width.

Occurrence: The Ediacaran Doushantuo Formation in the Shennongjia (this paper) and Yangtze Gorges areas (Liu and Moczydłowska, 2019) of Hubei Province, South China; and Ediacaran succession in Australia (Grey, 2005; Willman and Moczydłowska, 2011) and Siberia (Moczydłowska and Nagovitsin, 2012).

Tanarium paucispinosum Grey, 2005.

Fig. 44E–F.

Synonymy:

2005 *Tanarium paucispinosum* Grey, pp. 318–320, Fig. 45G, 208G, 237A–E, 239.

2019 *Tanarium paucispinosum* Grey; Liu and Moczydłowska, pp. 149, 151, fig. 83.

2021 *Tanarium paucispinosum* Grey; Liu et al., fig. 4.7.

Material: One well-preserved specimen.

Description: Medium-sized spheroidal vesicle bearing a few slender and elongate processes that gradually taper from a conical base to a sharp-pointed tip. Processes hollow and directly communicate with the vesicle cavity.

Dimensions: Vesicle diameter ~ 186.9 μm; processes 46.2–80.6 μm in length (24.7–43.1% of vesicle diameter) and 12.8–19.4 μm in basal width; 4–8 processes per circumferential view.

Remarks: The specimen described here fits the diagnosis of *T. paucispinosum*. We note the processes in our specimen have a somewhat larger and broader base than those of *T. paucispinosum* described in Grey (2005), but they lie with the size range of this species given in Liu and Moczydłowska (2019).

Tanarium paucispinosum is similar to *T. conoideum* (as defined by the holotype, pl. 5, Figs. 1–2 of Kolosova, 1991) in their sparsely distributed processes. When *T. paucispinosum* was established (Grey, 2005), no comparison was made with *T. conoideum*. It is possible that these two species are synonymous, in which case *T. conoideum* takes priority. At the present, we refrain from a formal synonymization of these two

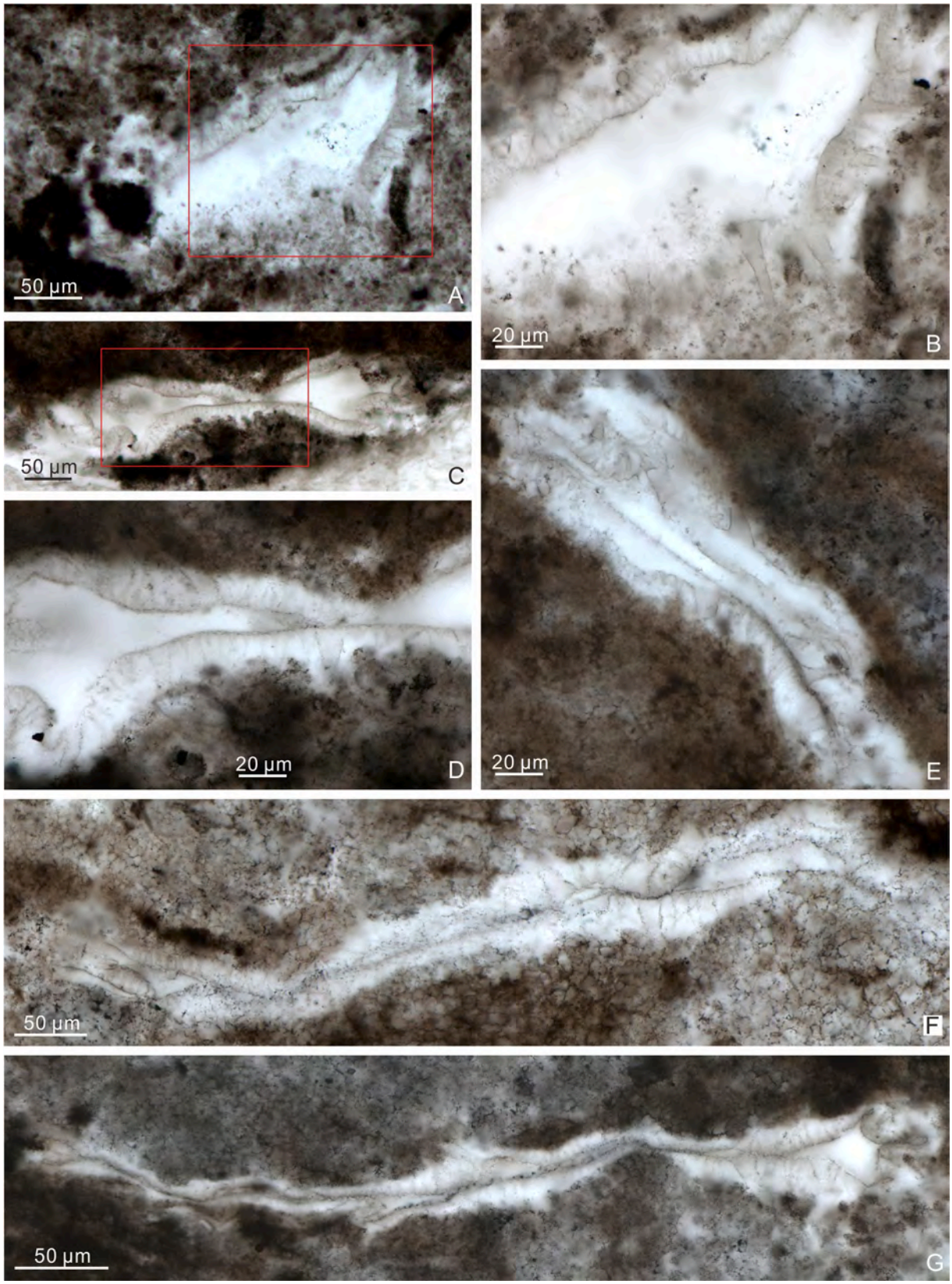

Fig. 46. *Tanarium varium* Liu et al., 2014a. (A–B) 21LHC-1–32.8 m-8c-11 (5.8 × 113.3). (B) Magnified view of area marked by rectangle in (A) at a different focal level, showing details of heteromorphic processes. (C–D) 21LHC-1–39.5 m-2c-20 (13.3 × 99.6). (D) Magnified view of area marked by rectangle in (C). (E) 21LHC-1–39.5 m-3c-26 (13.5 × 96). (F) 21LHC-1–39.5 m-3c-11 (16.3 × 112.4). (G) 21LHC-1–39.5 m-3c-28 (12.5 × 103).

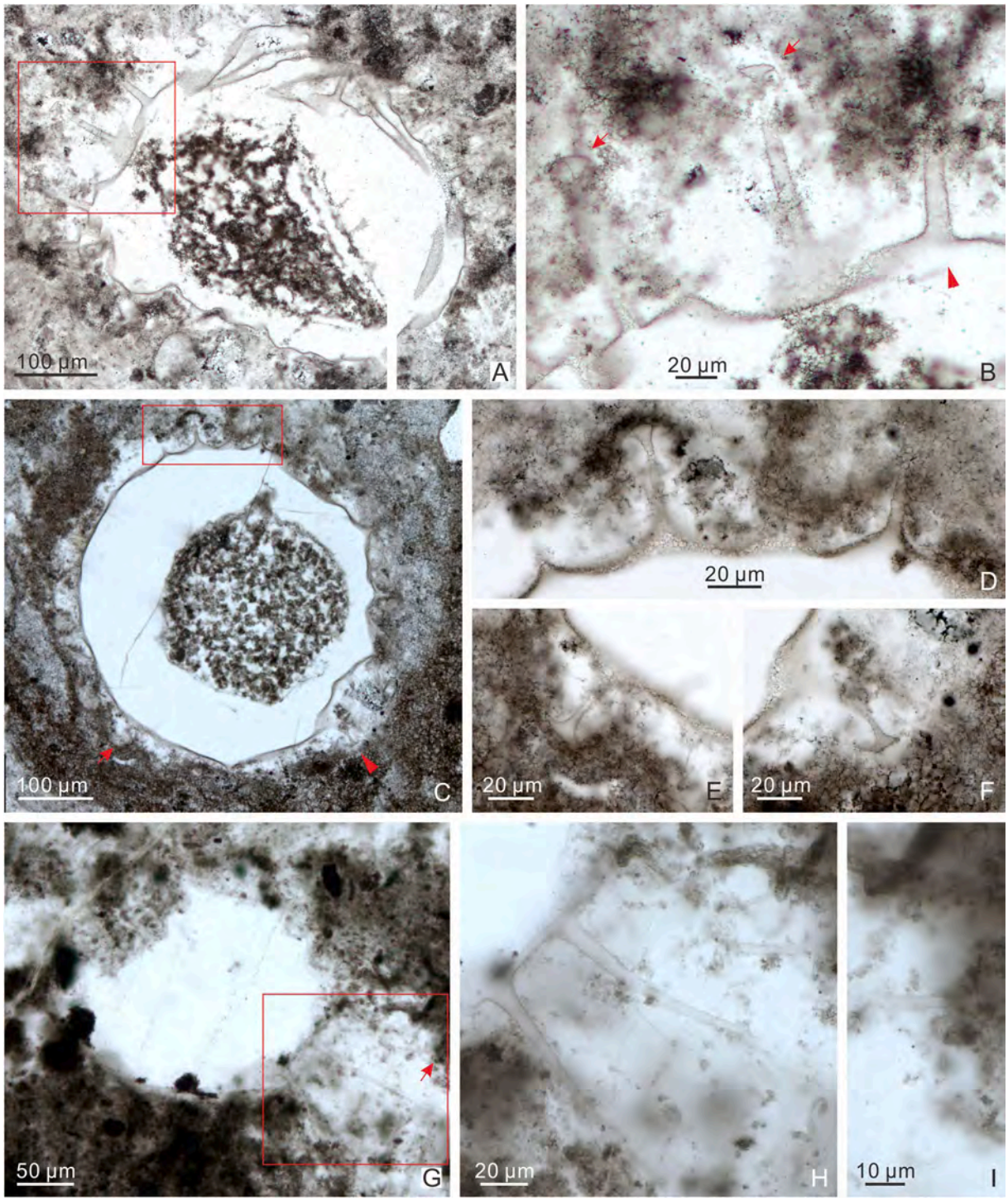

Fig. 47. (A–F) *Urasphaera capitalis* Nagovitsin and Moczydłowska *in* Moczydłowska and Nagovitsin, 2012. (A–B) LHG2-d2-2 m-3–1 (24.8 × 68.2). (B) Magnified view of area marked by rectangle in (A), showing base (arrowhead) and termination (arrows) of processes. (C–F) 21LHC-1–35.2 m-7p-2 (15 × 109). (D–F) Magnified views of areas in (C) marked by rectangle, arrow, and arrowhead, respectively. (G–I) *Urasphaera* cf. *capitalis* Nagovitsin and Moczydłowska *in* Moczydłowska and Nagovitsin, 2012; 21LHC-1–39.5 m-6p-5 (1.9 × 102). (H–I) Magnified views of areas in (G) marked by rectangle and arrow, showing extremely long processes and a shield-like termination of a process, respectively.

species, pending restudy of the type materials.

Occurrence: The Ediacaran Doushantuo Formation in the Shennongjia (this paper), Changyang (Liu et al., 2021), and Yangtze Gorges areas (Liu and Moczydłowska, 2019) of Hubei Province, South China; and Ediacaran succession in Australia (Grey, 2005).

Tanarium pluriprotensum Grey, 2005.

Fig. 45A–G.

Synonymy:

2005 *Tanarium pluriprotensum* Grey, pp. 320–322, Fig. 45H, 208H, 240A–D, 241A–B, 244.

2008 *Tanarium pluriprotensum* Grey; Willman and Moczydłowska, p. 527, Fig. 14A–F.

2011 *Tanarium pluriprotensum* Grey; Willman and Moczydłowska, p. 27, pl. V, Figs. 1–5.

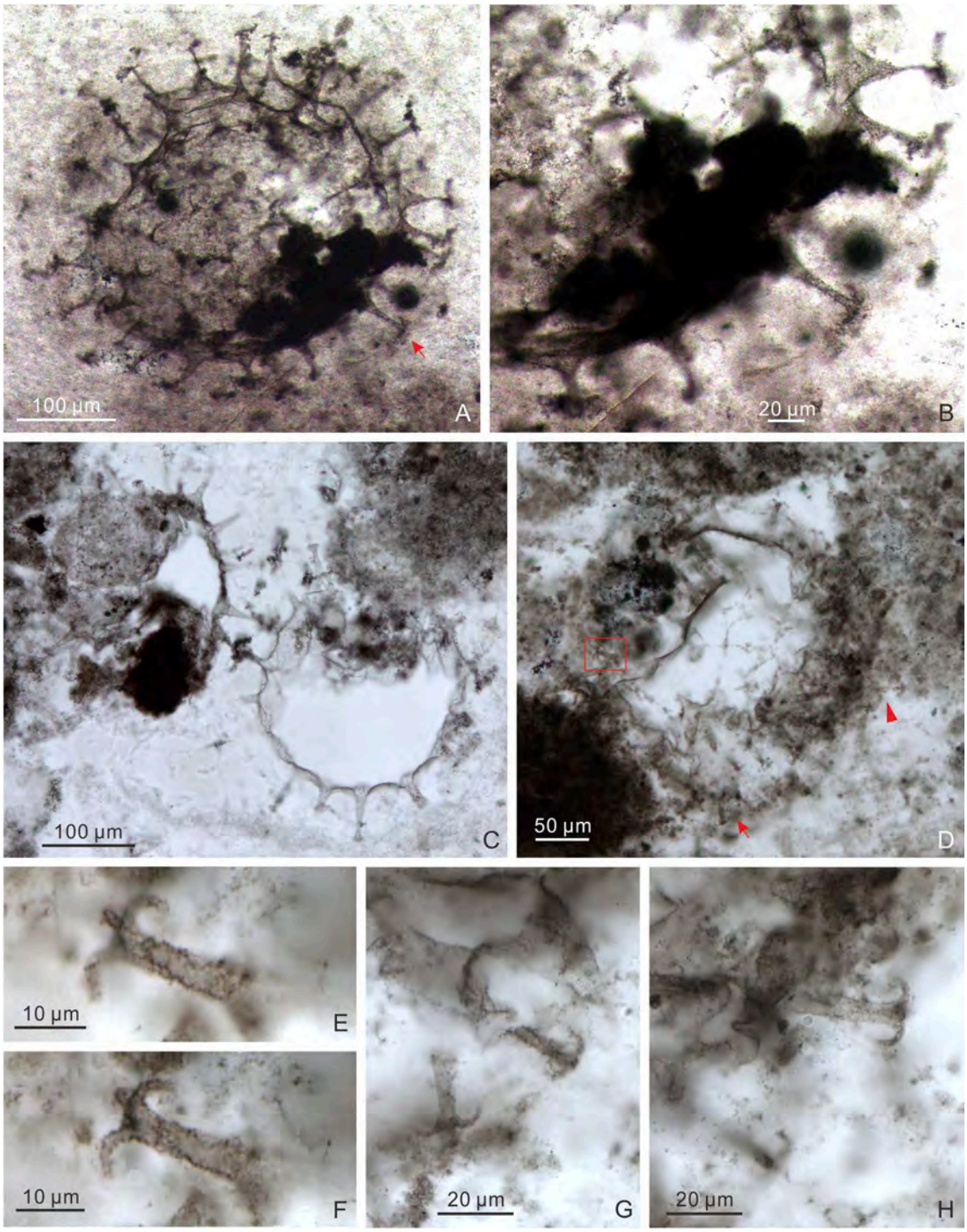

Fig. 48. (A–C) *Urasphaera fungiformis* Liu et al., 2014a. (A–B) LHG2-d2-3.1 m-9-H-7. (B) Magnified view of area marked by arrow in (A). (C) 21LHC-1–35.4 m-1p-3 (15.6 × 99.8). (D–H) *Variomargosphaeridium floridum* Nagovitsin and Moczydłowska *in* Moczydłowska and Nagovitsin, 2012; 21LHC-1–41.4 m-1p-2 (10 × 109.5). (E–F) Magnified views of areas marked by rectangle in (D) at different focal levels, showing branches of process termination. (G–H) Magnified views of areas in (D) marked by arrow and arrowhead, respectively.

non 2013 *Tanarium pluriprotensum* Grey; Liu et al., Fig. 13A. (=*Tanarium pycnacanthum*).

2019 *Tanarium pluriprotensum* Grey; Ouyang et al., Fig. 12I.

2019 *Tanarium pluriprotensum* Grey; Shang et al., p. 27, Fig. 17D–E.

2020 *Tanarium pluriprotensum* Grey; Vorob'eva and Petrov, p. 375, pl. I, Figs. 1–2.

2021 *Tanarium pluriprotensum* Grey; Ouyang et al., Fig. 19P–Q.

Material: Four moderately preserved specimens with collapsed vesicles and four poorly preserved specimens.

Description: Collapsed vesicle (originally spheroidal) bearing narrow conical processes. Processes heteromorphic, long, slender, slightly widened at the base, and taper towards a sharply pointed tip. Processes are basally separated and widely distributed. They are hollow and freely communicate with the vesicle cavity.

Dimensions: Vesicle diameter is uncertain due to incomplete preservation and deformation. Process length 53.9–72.0 μm (the full length of

processes in our specimens is difficult to assess because the apical end is often poorly preserved); process basal width 7.1–13.3 μm; space between processes 10.0–30.0 μm; about 25–34 processes are estimated to be present per circumferential view.

Remarks: This species is distinguished by its long, slender, and basally separate processes. It is different from *T. araithekum* in its larger vesicle and processes. It is somewhat similar to *T. conoideum* but the processes of the latter have a wider basal expansion and are more sparsely distributed. As pointed out in Liu et al. (2014a), a specimen illustrated as *T. pluriprotensum* in Liu et al. (2013; their Fig. 13A) is better assigned to *T. pycnacanthum* because it has a smaller vesicle and thinner processes.

Occurrence: The Ediacaran Doushantuo Formation in the Shennongjia (this paper), Zhangcunping (Ouyang et al., 2019), and Yangtze Gorges areas (Ouyang et al., 2021) of Hubei Province, and the Songlin area of Guizhou Province (Shang et al., 2019), South China; Ediacaran

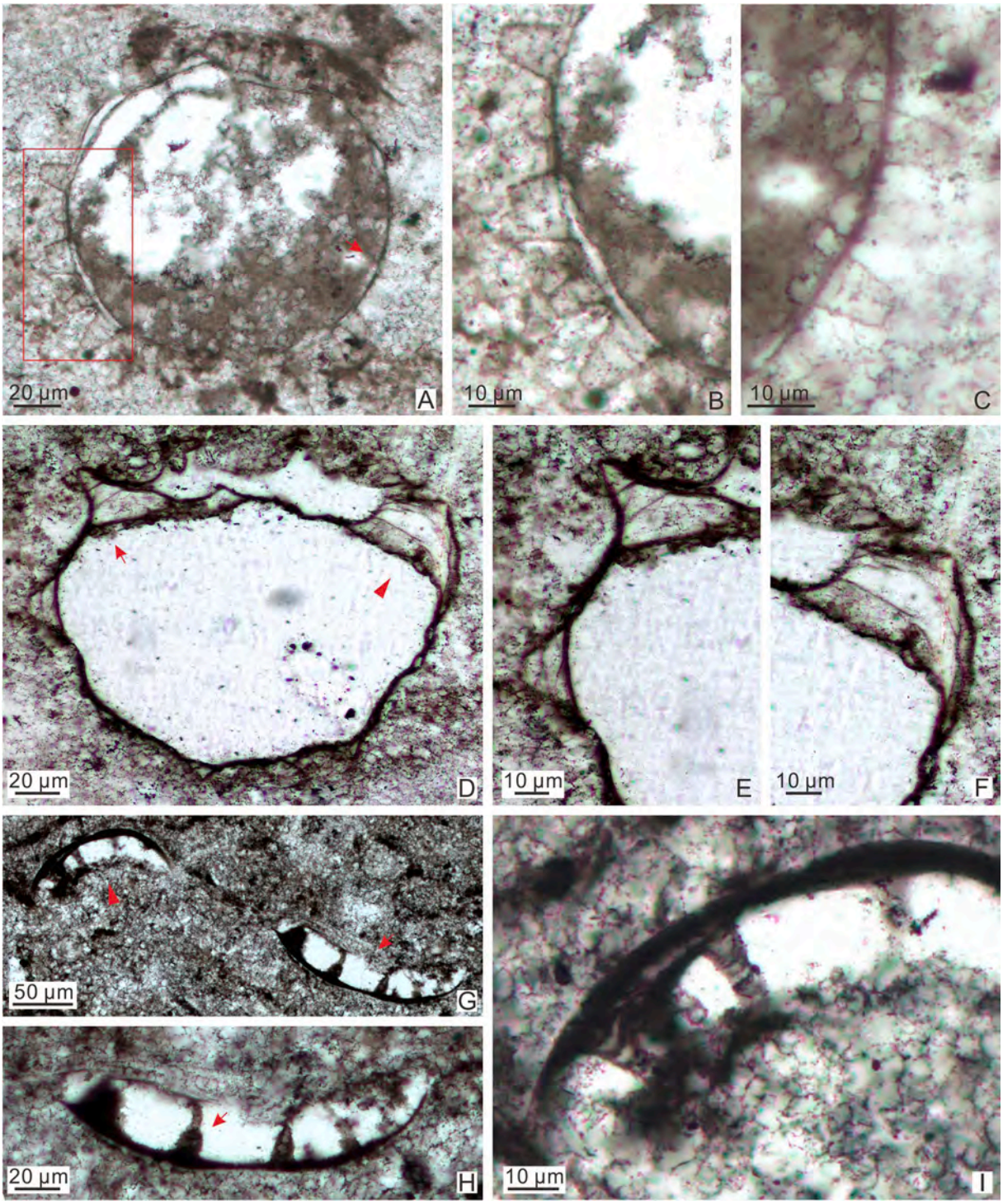

Fig. 49. (A–C) *Weissiella brevis* Xiao et al., 2014, emend. Ouyang et al., 2021; LHG-UD-n-6–1 (19.7 × 75.9). (B–C) Magnified views of areas in (A) marked by rectangle and arrow, respectively. (D–F) *Weissiella* cf. *grandistella* Vorob'eva et al., 2009b; LHG-d2-2 m-4–1 (19 × 78). (E–F) Magnified views of areas in (D) marked by arrow and arrowhead, respectively. (G–I) *Weissiella* cf. *brevis* Xiao et al., 2014, emend. Ouyang et al., 2021; LHG-d3 + 70 cm-3–1 (22 × 71.3). (H–I) Magnified views of areas in (G) marked by arrow and arrowhead, respectively, with arrow in (H) denoting a putative biform process.

strata in Australia (Grey, 2005; Willman and Moczydłowska, 2008, 2011) and Siberia (Vorob'eva and Petrov, 2020).

Tanarium varium Liu et al., 2014a.

Fig. 46.

Synonymy:

2014a *Tanarium varium* Liu et al., p. 119, figs. 76.9, 85.1–85.8, 86.1–86.6.

2017 *Tanarium varium* Liu et al.; Nie et al., pp. 377–378, Fig. 7.

Material: Eight moderately preserved specimens and 29 poorly preserved specimens.

Description: Medium-sized to large compressed vesicle (originally spheroidal) bearing abundant tubular to slightly tapering processes that are heteromorphic, variable in width and length, straight or slightly bent, and taper apically to form a blunt tip. Some processes lack the terminal part due to poor preservation. Processes densely spaced but basally separated. They are hollow and communicate openly with vesicle interior.

Dimensions: Vesicle 149.8–287.9 μm in diameter (calculated from circumference measurement); processes 9.0–62.7 μm in preserved length and 2.1–20.8 μm in basal width; processes spacing 1.0–3.0 μm, with 50–100 processes in circumferential view.

Remarks: The specimens described here are characterized by highly variable and gradually tapering tubular processes, which fit the diagnosis of *T. varium*, although some specimens are beyond the size range of vesicle diameter from Yangtze Gorges area (260–500 μm; Liu et al., 2014a).

Occurrence: The Ediacaran Doushantuo Formation in the Shennongjia (this paper) and Yangtze Gorges areas (Liu et al., 2014a; also listed in Ouyang et al., 2021) of Hubei Province, and the Zhangjiajie area of Hunan Province (Nie et al., 2017; Ouyang et al., 2017), South China.

Tanarium sp.

Fig. 45H–J.

Material: One partially but adequately preserved specimen.

Description: Large spheroidal vesicle, bearing numerous closely spaced processes. Processes conical, long, slender, slightly expanded at base and gradually taper distally. Processes are hollow and communicate freely with vesicle cavity.

Dimensions: Vesicle ~ 319.7 μm in diameter (estimated from circumference measurement); preserved process length 55.0–57.1 μm; process basal width 12.3–16.1 μm; process apical width 3.5–4.5 μm.

Remarks: The long, hollow, conical processes of the present specimen are in accordance to the diagnosis of the genus *Tanarium*. Indeed, the specimen is somewhat similar to *T. gracilentum* in process morphology, but its processes are much thicker. It also resembles *T. pluriprotensum* in overall shape, but its processes are more densely distributed and are in contact basally. Thus, it is placed in an open nomenclature.

Occurrence: The Ediacaran Doushantuo Formation in the Shennongjia area of Hubei Province, South China (this paper).

Genus *Urasphaera* Nagovitsin and Moczydłowska *in* Moczydłowska and Nagovitsin, 2012.

Type species: *Urasphaera capitalis* Nagovitsin and Moczydłowska *in* Moczydłowska and Nagovitsin, 2012.

Urasphaera capitalis Nagovitsin and Moczydłowska *in* Moczydłowska and Nagovitsin, 2012.

Fig. 47A–F.

Synonymy:

2012 *Urasphaera capitalis* Nagovitsin and Moczydłowska; Moczydłowska and Nagovitsin, pp. 20–21, Fig. 7G–J.

Material: Three well preserved specimens and eight poorly preserved specimens.

Description: Large spheroidal vesicle bearing sparsely and unevenly distributed processes that have a capitate termination. Processes arise straightly from the vesicle wall, nearly cylindrical and with an inconspicuously widened base, and then taper distally to form a constricted waist just below with an inflated, shield-like, and capitate apical expansion. Processes hollow and communicate openly with the vesicle cavity.

Dimensions: Vesicle diameter 294.3–422.5 μm; overall length of processes cannot be measured precisely as the basal and apical parts are rarely preserved in the same process, but is up to 63.1–86.2 μm according to our best estimate; processes 6.8–15.7 μm in basal width; constricted waist 3.1–4.3 μm in width and 4.5–7.1 μm below apex; apical expansion 14.2–17.1 μm in width.

Remarks: Although most processes are incomplete, each specimen in our collection preserves a few cylindrical processes with a capitate apex, thus conforming to the diagnosis of *U. capitalis*. However, the processes in our specimens are slightly longer than those in the holotype from the Ura Formation of Siberia (Moczydłowska and Nagovitsin, 2012).

Occurrence: The Ediacaran Doushantuo Formation in the Shennongjia area (this paper) of Hubei Province, South China and the Ediacaran strata in Siberia (Moczydłowska and Nagovitsin, 2012).

Urasphaera cf. *capitalis* Nagovitsin and Moczydłowska *in* Moczydłowska and Nagovitsin, 2012.

Fig. 47G–I.

Synonymy:

cf. 2012 *Urasphaera capitalis* Nagovitsin and Moczydłowska; Moczydłowska and Nagovitsin, pp. 20–21, Fig. 7G–J.

Material: A single poorly preserved specimen.

Description: Large spheroidal vesicle bearing a small number of widely distributed processes. Processes extremely long, nearly straight, more or less cylindrical, and gradually taper to a capitate apex. Processes hollow and openly directly into vesicle interior.

Dimensions: Vesicle diameter ~ 233.9 μm; the full length of processes is difficult to be measured due to poor preservation, but its preserved length can be 96.1–111.7 μm long; processes 16.1–17.4 μm in basal width; constricted waist ~ 3.0 μm in width and ~ 2.5 μm below apex; apical expansion ~ 9.1 μm in width.

Remarks: The present specimen is most similar to *U. capitalis* in having more or less straight processes with a shield-like apical expansion but without a basal expansion. However, our specimen has much longer processes that are far beyond the size range of *U. capitalis* (Moczydłowska and Nagovitsin, 2012). Since there is only one moderately preserved specimen, we tentatively identify it as an open nomenclature, *Urasphaera* cf. *capitalis*.

Occurrence: The Ediacaran Doushantuo Formation in the Shennongjia area of Hubei Province, South China (this paper).

Urasphaera fungiformis Liu et al., 2014a.

Fig. 48A–C.

Synonymy:

2013 *Gyalosphaeridium pulchrum* Zang *in* Zang and Walter, 1992a; Liu et al., Fig. 13G.

2014a *Urasphaera fungiformis* Liu et al., p. 119, figs. 87.1–87.7, 88.1–88.4, 89.1.

2017 *Urasphaera fungiformis* Liu et al.; Ouyang et al., Fig. 8G–8 J.

2017 *Urasphaera fungiformis* Liu et al.; Nie et al., pp. 379–380, Fig. 9.

Material: Three well-preserved and two moderately preserved specimens.

Description: Large spheroidal vesicle bearing a moderate number of regularly arranged processes. Processes are homomorphic, conical in overall shape, and have a broad basal expansion and a relatively thin shield-like apical expansion. Processes hollow and communicate directly with the vesicle interior.

Dimensions: Vesicle diameter 220.6–319.6 μm; processes 44.2–67.3 μm in length, 18.5–26.7 μm in basal width, 3.1–5.1 μm in apical width just below apical shield, and 29.0–48.4 μm in spacing; apical shield 13.4–18.9 μm in width and 2.8–3.7 μm in thickness.

Remarks: Present specimens closely resemble the holotype of *U. fungiformis* in overall morphology (Liu et al., 2014a), although their processes are much longer.

Occurrence: The Ediacaran Doushantuo Formation in the Shennongjia (this paper) and Yangtze Gorges areas (Liu et al., 2014a) of Hubei Province, and the Zhangjiajie area of Hunan Province (Nie et al., 2017;

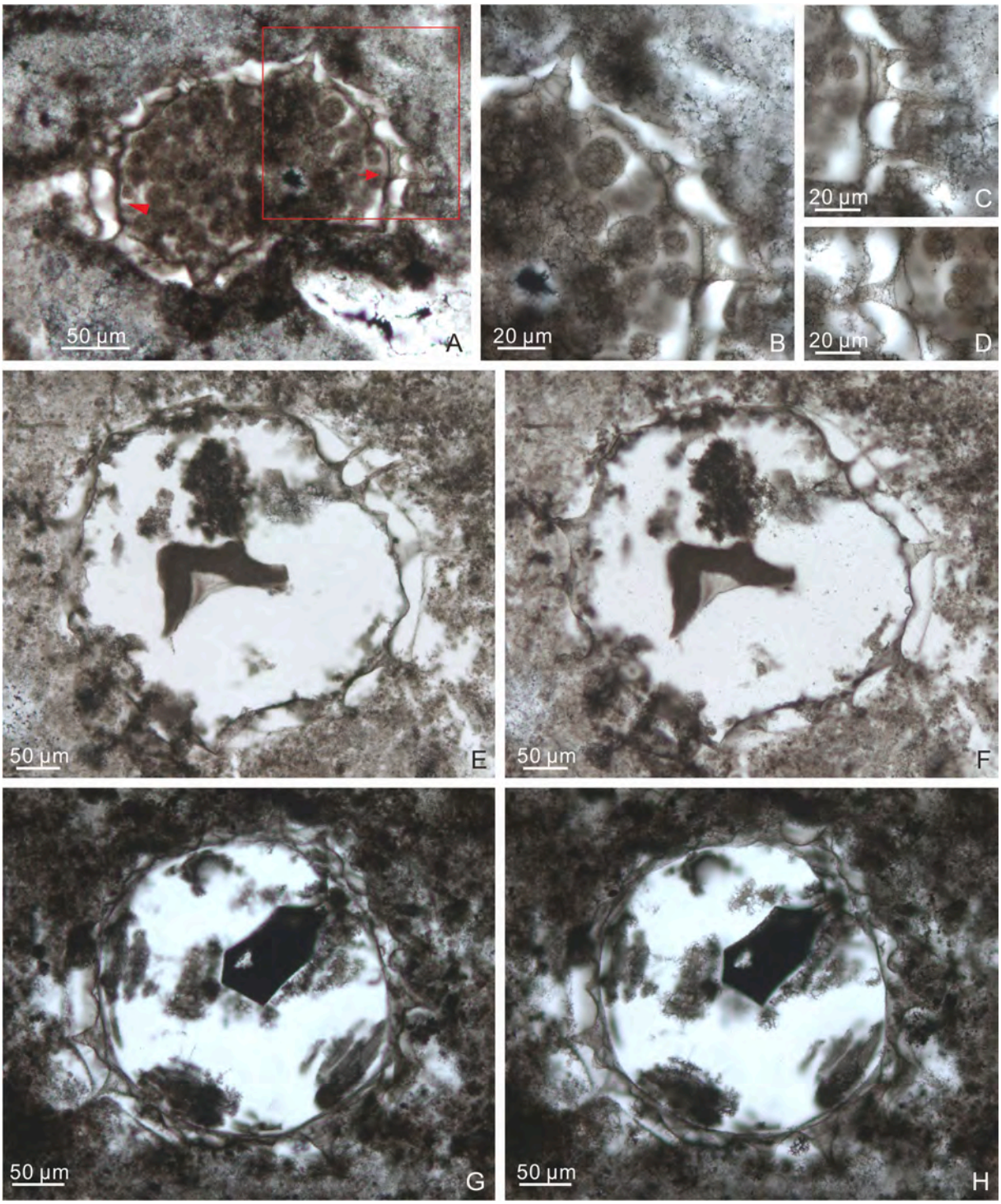

Fig. 50. *Weissiella concentrica* sp. nov. (A–D) holotype, 21LHC-1–43.7 m-2c-18 (17.5 × 98.3). (B–C) Magnified views of areas in (A) marked by rectangle and arrow, respectively. (D) Magnified view of area marked by arrowhead in (A) at a different focal level. (E–F) 21LHC-1–36.1 m-18p-1 (12.3 × 100), different views of the same specimen. (G–H) 21LHC-1–35.4 m-24p-2 (11.6 × 92.5), different views of the same specimen.

Ouyang et al., 2017), South China.

Genus *Variomargosphaeridium* Zang *in* Zang and Walter, 1992a, emend. Xiao et al., 2014.

Type species: *Variomargosphaeridium litoschum* Zang *in* Zang and Walter, 1992a.

Variomargosphaeridium floridum Nagovitsin and Moczydłowska *in* Moczydłowska and Nagovitsin, 2012.

Fig. 48D–H.

Synonymy:

2012 *Variomargosphaeridium floridum* Nagovitsin and Moczydłowska *in* Moczydłowska and Nagovitsin, pp. 21–22, Fig. 9A–I.

2014a *Variomargosphaeridium floridum* Nagovitsin and Moczydłowska *in* Moczydłowska and Nagovitsin; Liu et al., p. 128, figs. 91.1–91.10, 92.1–92.7, 93, and synonyms therein.

Material: One adequately preserved specimen.

Description: Large collapsed spheroidal vesicle, covered with a moderate number of hollow, widely arranged, largely cylindrical, and apically branching processes. The basal-middle part of the processes

slightly tapers or remains straight, whereas the very distal end bifurcates into four small, thin, short, and adbasally bent branchlets. Processes communicate freely with vesicle cavity.

Dimensions: Vesicle diameter 187.6 × 248.8 μm; processes 33.3–39.2 μm in preserved length and 16.5–21.3 μm in basal width; overall apical crown of branchlets 17.3–22.7 μm wide; branchlets 1.0–1.3 μm wide and 9.0–12.1 μm long.

Remarks: The specimen described here is characterized more or less

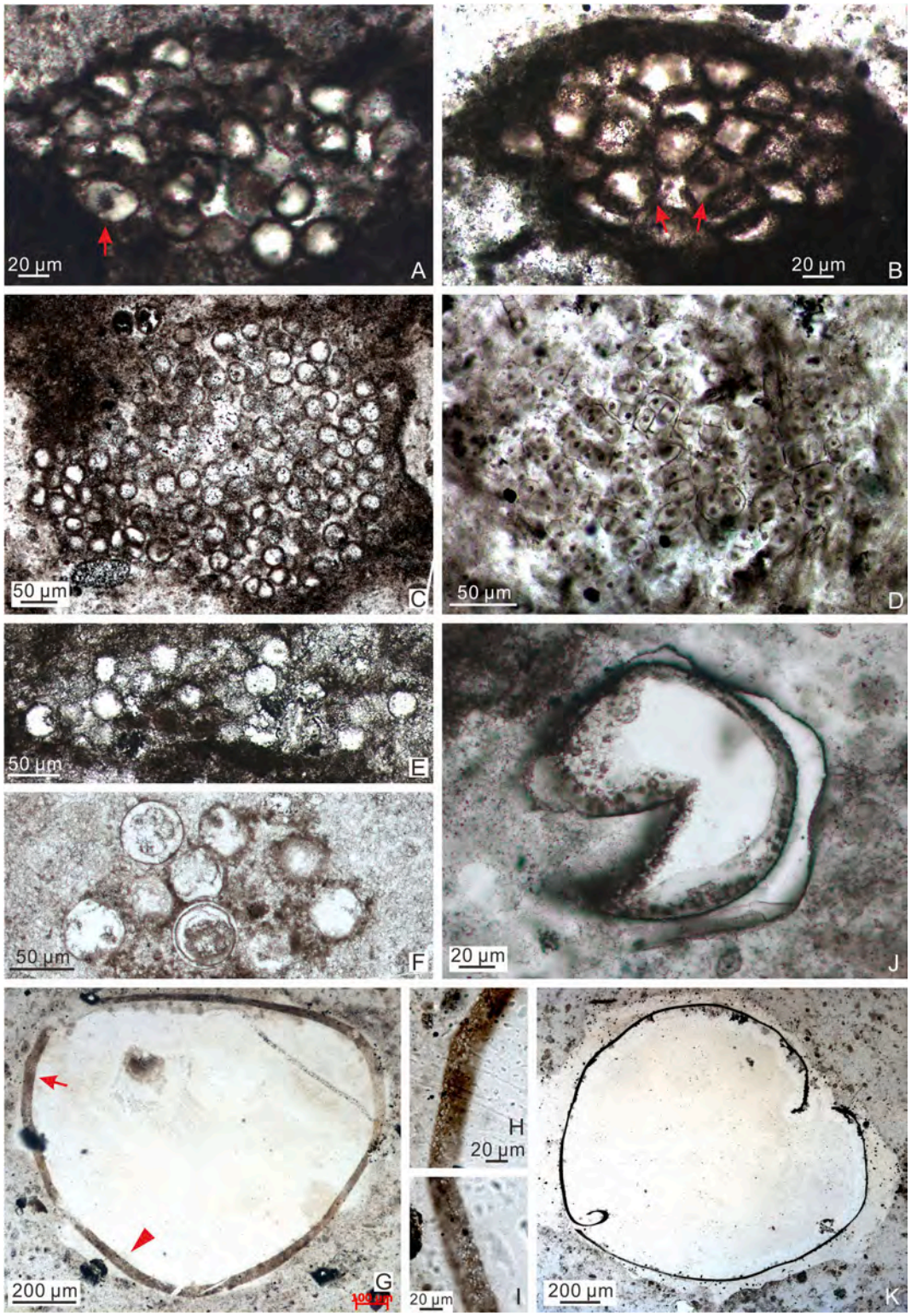

Fig. 51. (A–C) *Leiosphaeridia crassa* (Naumova, 1949) Jankauskas *in* Jankauskas et al., 1989. (A) LHG-d2-2 m-4–1 (22.9 × 79). (B) LHG2-d2-3.1 m-45–1 (41.7, NR). Arrows in (A–B) marking darker spots. (C) LHG2-d2-3.1 m-2p-52 (31.4 × 66.5). (D) *Gloeodiniopsis* sp.; LHG2-d2-3.1 m-18-H-22 (39.2, NR). (E–F) *Leiosphaeridia minutissima* Naumova, 1949, Jankauskas *in* Jankauskas et al., 1989. (E) LHG2-d2-3.1 m-27–1. (F) LHG-d2-4.3 m-2–29 (20.4 × 65). (G–I) *Granitunica* sp.; LHG-d3 + 1.2 m-2–1. (H–I) Magnified views of areas in (G) marked by arrow and arrowhead, respectively. (J) *Schizofusa* sp.; LHG2-d2-2 m-7–1 (26.6 × 77.5). (K) *Osculosphaera* sp.; LHG-d3 + 1.2 m-7c-1 (33 × 82).

by cylindrical processes with a distal crown of about four branchlets, which is a diagnostic feature of *V. floridum*.

Occurrence: The Ediacaran Doushantuo Formation in the Shennongjia (this paper) and Yangtze Gorges areas (Liu et al., 2013, 2014a) of Hubei Province, South China; and Ediacaran strata in Siberian (Golubkova et al., 2010; Moczydłowska and Nagovitsin, 2012; Sergeev et al., 2011; Vorob'eva et al., 2008).

Genus *Weissiella* Vorob'eva et al., 2009b.

Type species: *Weissiella grandistella* Vorob'eva et al., 2009b.

Weissiella brevis Xiao et al., 2014, emend. Ouyang et al., 2021.

Fig. 49A–C.

Synonymy:

2014 *Weissiella brevis* Xiao et al., p. 61, fig. 38.1–38.12.

2021 *Weissiella brevis* Xiao et al., 2014, emend. Ouyang et al., p. 40, Fig. 6C, D, 23A–N, and synonyms therein.

2022 *Weissiella brevis* Xiao et al., 2014, emend. Ouyang et al.; Xiao et al., Fig. 28.

Material: Two adequately and one poorly preserved specimen.

Description: Medium-sized spheroidal vesicle bearing a moderate number of unevenly distributed processes that are widely separated at base. Processes small, slightly conical, and terminally rounded or truncated. Process interior is divided by transverse cross-walls. Processes hollow but separated from the vesicle cavity.

Dimensions: Vesicle diameter 137.1–190.3 μm; processes 11.6–18.6 μm in length or 8.5–11.5% of vesicle diameter, 7.7–16.8 μm in basal width, and 4.3–19.4 μm in spacing; internal cross-walls ~ 3.0 μm in spacing.

Remarks: Weissiella was first erected by Vorob'eva et al. (2009b) to receive a distinct population of acanthomorphic acritarchs with processes internally divided by transverse cross-walls. This genus contains two published species: *W. grandistella* and *W. brevis*, which can be distinguished by their different vesicle diameter and relative process length. Considering that the two species of *Weissiella* are statistically different in vesicle diameter, the ratio of process basal width to vesicle diameter, and the ratio of process length to vesicle diameter, we follow Ouyang et al. (2021) to regard them as two distinct species of *Weissiella*. Current specimens are similar to the holotype of *W. brevis* in process morphology and size, although they have a lower process density.

Occurrence: The Ediacaran Doushantuo Formation in the Shennongjia (this paper), Zhangcunping (Ouyang et al., 2019), and Yangtze Gorges areas (Liu and Moczydłowska, 2019; Ouyang et al., 2015, 2021) of Hubei Province, and the Weng'an (Xiao et al., 2014) and Songlin areas (Shang et al., 2019) of Guizhou Province, South China; Ediacaran succession in India (Shukla and Tiwari, 2014; Xiao et al., 2022).

Weissiella cf. *brevis* Xiao et al., 2014, emend. Ouyang et al., 2021.

Fig. 49G–I.

Synonymy:

cf. 2014 *Weissiella brevis* Xiao et al., p. 61, fig. 38.1–38.12.

cf. 2021 *Weissiella* cf. *grandistella*; Ouyang et al., pp. 40–41, Fig. 24A–H.

Material: One moderately preserved specimen.

Description: Incompletely preserved vesicle bearing small and sparsely distributed processes. Processes are conical or cylindrical in morphology but their terminations are generally not well preserved. They are hollow and internally divided by cross-walls. Some processes seem to be biform, with a slightly expanded base and a cylindrical tip (arrow in Fig. 49H). This apparently biform feature may be a taphonomic artifact because of the differential degradation of the basal vs. apical part of the processes.

Dimensions: Processes 17.5–27.5 μm in preserved length, 8.7–14.0 μm in basal width, and 22.8–30.5 μm in spacing; internal cross-wall spacing 1.6–3.2 μm.

Remarks: Current specimen is similar to *W. brevis* in process size and shape. However, its processes are fewer in number and unevenly distributed. Thus, it is tentatively placed in an open nomenclature.

Occurrence: The Ediacaran Doushantuo Formation in the Shennongjia area of Hubei Province, South China (this paper).

Weissiella cf. *grandistella* Vorob'eva et al., 2009b.

Fig. 49D–F.

Synonymy:

cf. 2009b *Weissiella grandistella* Vorob'eva et al., pp. 183, 185, fig. 10.1, 10.1a–f.

2021 *Weissiella* cf. *grandistella*; Ouyang et al., pp. 40–41, Fig. 24A–H, and synonyms therein.

Material: Four poorly preserved specimens.

Description: Medium-sized spheroidal vesicle bearing a few large processes. Processes are hollow, conical, and have a broad base and a rounded or blunt end. Processes interior contain transverse cross-walls that are flat or distally convex. Only three processes are observed and they are heteromorphic in terms of size and morphology.

Dimensions: Vesicle diameter 149.9–209.4 μm (calculated from circumference measurement); one completely process is 28.7 μm in length or 19.1% of vesicle diameter; processes 25.6–55.0 μm in basal width or 17.1–36.7% of vesicle diameter; internal cross-wall spacing 3.4–11.9 μm.

Remarks: Current specimens resemble *W. grandistella* in their overall process morphology. However, they differ from the holotype of *W. grandistella* in having sparse, irregularly distributed, and heteromorphic processes. In addition, our specimens are smaller in vesicle and process sizes. Our specimens lie within the size range of *Weissiella* cf. *grandistella* from the Yangtze Gorges area described in Ouyang et al. (2021); for comparison, specimens illustrated in Ouyang et al. (2021) have a vesicle diameter of 95–194 μm, process length of 26.8–113.2 μm, and process basal width of 13.3–53.8 μm.

Occurrence: The Ediacaran Doushantuo Formation in the Shennongjia (this paper) and the Yangtze Gorges areas (Liu and Moczydłowska, 2019; Liu et al., 2013, 2014a, b; Ouyang et al., 2021) of Hubei Province, South China.

Weissiella concentrica sp. nov.

Fig. 50.

Holotype: The specimen illustrated in Fig. 50A–D, thin section 21LHC-1–43.7 m-2c-18 (17.5 × 98.3).

Etymology: From Latin *concentrica*, with reference to the presence of two concentric walls.

Locus typicus: The Ediacaran Doushantuo Formation at the Lianhuacun section, Shennongjia area of Hubei Province, South China.

Stratum typicum: Chert nodules in thin to medium bedded dolostones of unit 4, Doushantuo Formation.

Material: Three fairly well-preserved specimens and one poorly preserved specimen.

Diagnosis: Medium-sized to large spheroidal vesicle bearing two concentric walls and a small number of conical processes with internal cross-walls. Processes widely separated and irregularly arranged on the inner wall, and penetrate a single-layered outer wall. Processes widened at base and gradually taper to a cylindrical apical spine with a blunt or pointed tip. Processes interior contain flat or distally convex transverse cross-walls. Bifurcate apical spines occasionally present on an expanded base (Fig. 50C). Multiple spheroidal internal bodies of variable size are preserved within the vesicle cavity of some specimens (Fig. 50A).

Dimensions: The holotype: inner wall diameter 185.8 μm; processes 44.7–82.6 μm in length or 24.1–44.5% of vesicle diameter, 15.4–31.5 μm in basal width, and 3.1–5.3 μm in apical width; basal spacing between processes 13.4–36.3 μm; spacing between internal cross-walls up to 1.8–5.1 μm; distance between inner and outer walls 11.0–20.9 μm. Other specimens: inner wall diameter 185.6–397.8 μm; processes 52.4–89.6 μm in length or 19.2–22.5% of vesicle diameter, 23.84–46.7 μm in basal width, and 2.4–6.1 μm in apical width; basal spacing between processes 17.0–55.5 μm; spacing between internal cross-walls up to 3.7–12.5 μm; distance between inner and outer walls 22.3–35.4 μm.

Remarks: W. concentrica sp. nov. is similar to *W. grandistella* in its process morphology, size, and density, but differs in the presence of an outer wall. The outer wall is single-layered, thin, smooth, and

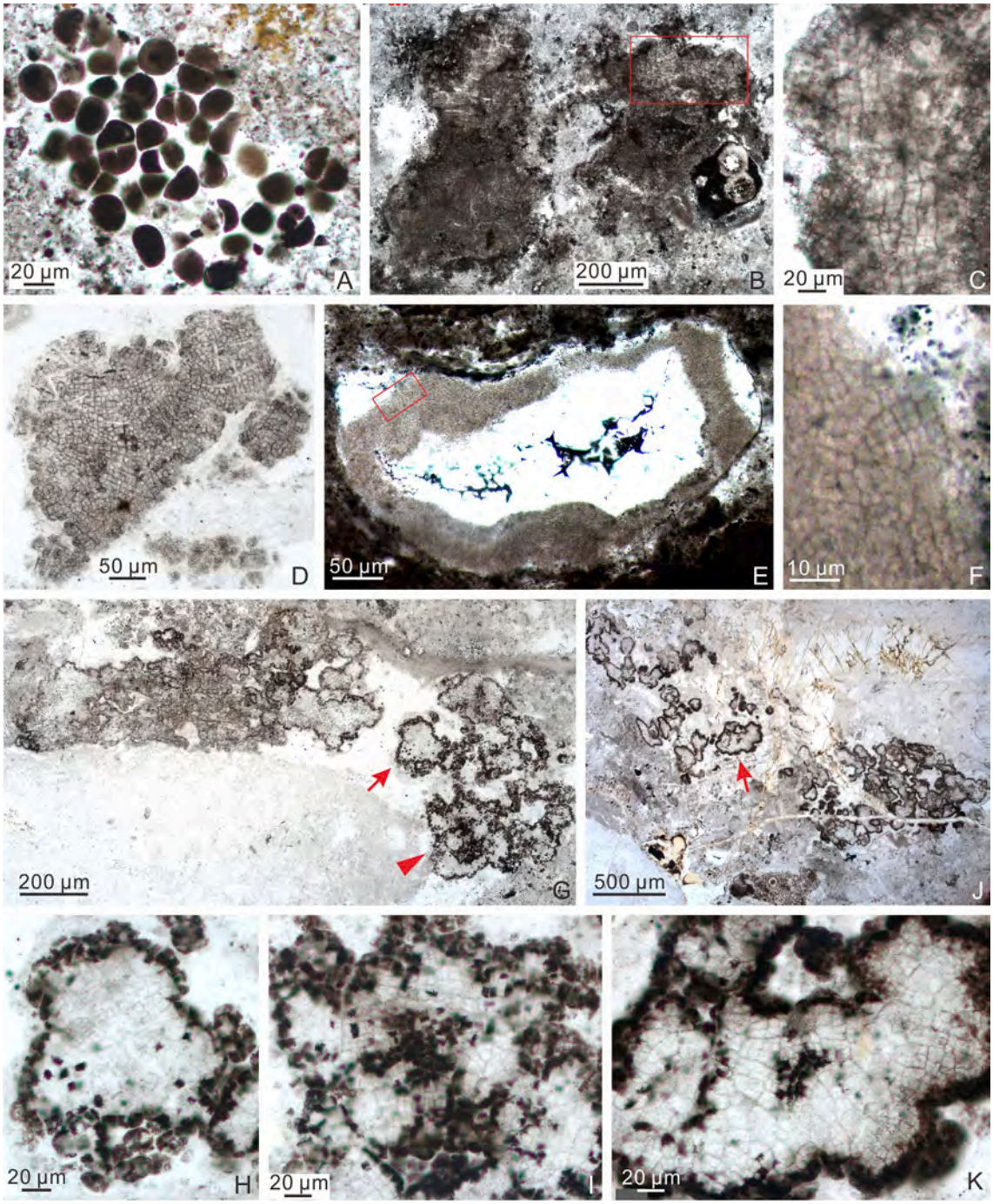

Fig. 52. (A) *Archaeophycus yunnanensis* (Song in Luo et al., 1982) Dong et al., 2009; LHG2-d2-2.9 m-4–1 (18.2 × 73). (B–F) *Sarcinophycus* sp. (B–C) LHG2-d2-2 m-7–4 (18.2 × 70.7). (C) Magnified view of area marked by rectangle in (B) with a rotation. (D) LHG-d2-4.3 m-5–26 (34.8 × 75.8). (E–F) LHG2-d2-3.1 m-44–6 (44.6, NR). (F) Magnified view of area marked by rectangle in (E) with a rotation. (G–K) *Sarcinophycus papilloformis* Xiao, 2004. (G–I) LHG-d2-4.3 m-5–29 (29 × 73.3). (H–I) Magnified views of areas in (G) marked by arrow and arrowhead, respectively. (J–K) LHG-d2-4.5 m-2–2 (32.8 × 68). (K) Magnified view of area marked by arrow in (J).

penetrated by processes. The consistent presence of an outer wall in multiple specimens strongly indicate its biological origin, rather than a taphonomic artifact related to the accumulation of organic particles. The outer wall consists of a coherent organic layer rather than aggregates of organic particles. In addition, it is penetrated by widely separate processes, unlike accumulation of organic particles, which tend to occur at the distal end of densely arranged processes with a uniform length. Liu and Moczydłowska (2019, p. 163) also mentioned the presence of a thin outer wall in their collection of *W. grandistella*, although no illustrations were provided; their specimens may represent additional occurrence of *W. concentrica*. It is possible that *W. concentrica* and *W. grandistella* may be taxonomically conspecific if the latter species had an outer wall but was subsequently lost taphonomically. However, as numerous specimens of *W. grandistella* have been reported from a number of Ediacaran successions and there is no vestige of an outer membrane in all illustrated specimens, we deem the lack of an outer membrane a biological feature. Thus, *W. concentrica* and *W. grandistella* are regarded as distinct species.

Two specimens illustrated as *Weissiella* sp. in Ouyang et al. (2015; pl. IV, Figs. 8–13) but subsequently synonymized with *Weissiella brevis*

(Ouyang et al., 2021) appear to have a multilamellate vesicle wall (generally 2–3 layers) and dumbbell-shaped processes, but they do not have a distinct outer wall and hence are different from *W. concentrica* sp. nov.

Occurrence: The Ediacaran Doushantuo Formation in the Shennongjia area of Hubei Provinces, South China (this paper).

Sphaeromorphs.

Genus *Granitunica* Liu et al., 2014a.

Type species: *Granitunica mcfaddeniae* Liu et al., 2014a.

Granitunica sp.

Fig. 51G–I.

Material: Four adequately preserved specimens.

Description: Large sphaeromorph bearing a very thick vesicle wall with a granular texture.

Dimensions: Vesicle diameter 578.4–1483.4 μm; vesicle wall thickness 21.3–98.0 μm.

Remarks: The current specimens are most similar to, but have much larger vesicles and thicker vesicle walls than *G. mcfaddeniae* from the Ediacaran Doushantuo Formation of Yangtze Gorges area (Liu et al., 2014a).

Occurrence: The Ediacaran Doushantuo Formation in the Shennongjia area of Hubei Province, South China (this paper).

Genus *Leiosphaeridia* Eisenack, 1958, emend. Downie and Sarjeant, 1963, emend. Turner, 1984.

Type species: *Leiosphaeridia baltica* Eisenack, 1958.

Leiosphaeridia crassa (Naumova, 1949) Jankauskas *in* Jankauskas et al., 1989.

Fig. 51A–C.

Synonymy:

1949 *Leiotriletes crassa* Naumova, p. 54, pl. I, Figs. 5–6, pl. II, Figs. 5–6.

1989 *Leiosphaeridia crassa* (Naumova, 1949) emend. Jankauskas; Jankauskas et al., pp. 75–76, pl. IX, Figs. 5–10.

1992b *Leiosphaeridia crassa* (Naumova, 1949) emend. Jankauskas; Zang and Walter, pp. 289, 291–292, pl. IX, figs. A–K, pl. XII, fig. K, pl. XIV, figs. E, H, and synonyms therein.

1994 *Leiosphaeridia crassa* (Naumova, 1949) Jankauskas; Butterfield et al., pp. 40–42, Fig. 16F, 23 K.

2005 *Leiosphaeridia crassa* (Naumova, 1949) Jankauskas *in* Jankauskas et al.; Grey, pp. 179–182, figs. 63A–C, 64A–D, 65–66.

Material: Abundant specimens in thin sections.

Description: Small spheroidal vesicles with a thick and smooth wall. Individuals are typically aggregated in clusters. Vesicles occasionally contain a darker spot in the center (arrows in Fig. 51A–B).

Dimensions: Vesicle diameter 19.6–39.1 μm; wall thickness ~ 3.3–4.3 μm.

Remarks: Species of *Leiosphaeridia* are very common in Precambrian strata. They can be distinguished mainly by vesicle size and vesicle wall thickness (Butterfield et al., 1994). *L. crassa* is characterized by a thick-walled vesicle smaller than 70 μm in diameter.

Occurrence: Abundant in Proterozoic strata.

Leiosphaeridia minutissima (Naumova, 1949) Jankauskas *in* Jankauskas et al., 1989.

Fig. 51E–F.

Synonymy:

1949 *Leiosphaeridia minutissima* Naumova, pl. I, Fig. 1.

1989 *Leiosphaeridia minutissima* (Naumova, 1949) emend. Jankauskas; Jankauskas et al., pp. 79–80, pl. IX, Figs. 1–4, 11.

2019 *Leiosphaeridia minutissima* (Naumova, 1949) Jankauskas *in* Jankauskas et al.; Shang et al., p. 24, Fig. 21A, and synonyms therein.

Material: Dozens of well-preserved specimens.

Description: Small spheroidal vesicles with a thin and smooth wall. Vesicles are preserved individually or in clusters.

Dimensions: Vesicle diameter 14.2–37.5 μm; wall thickness ~ 1 μm.

Remarks: Current specimens fit the diagnosis of *L. minutissima* based on their wall thickness and vesicle size.

Occurrence: A long-ranging species in the Proterozoic and Paleozoic.

Genus *Osculosphaera* Butterfield *in* Butterfield et al., 1994, emend. Liu et al., 2014a.

Type species: *Osculosphaera hyaline* Butterfield *in* Butterfield et al., 1994, emend. Liu et al., 2014a.

Osculosphaera sp.

Fig. 51K.

Material: One well-preserved specimen and one moderately preserved specimen.

Description: Large spheroidal vesicles with one or two invaginated

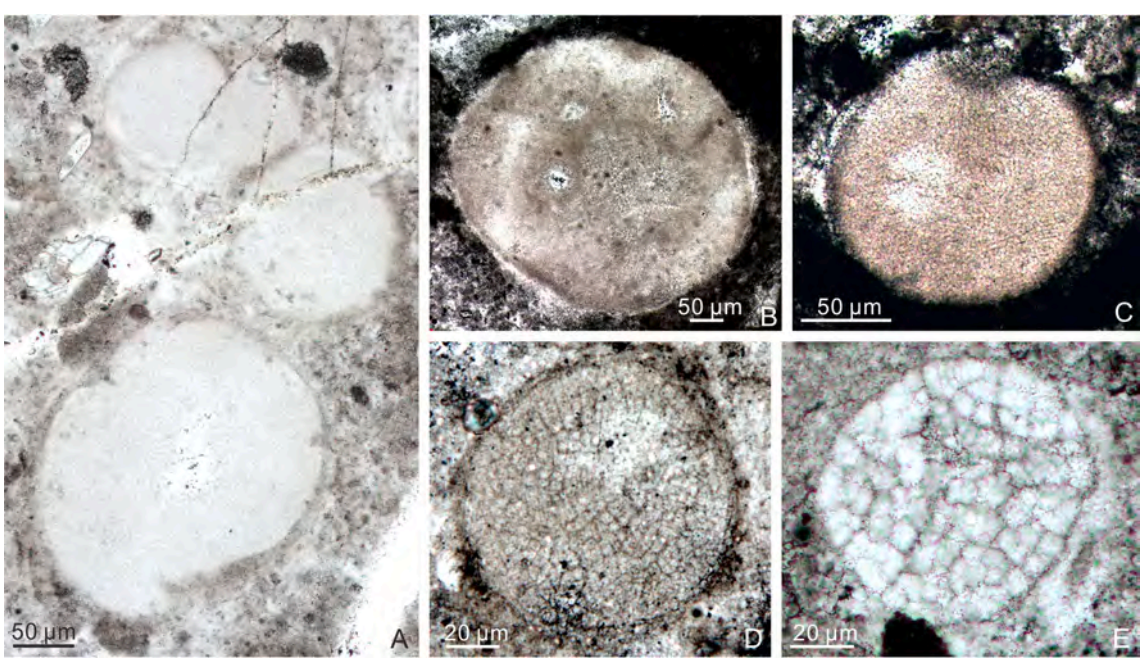

Fig. 53. (A–C) *Wengania exquisita* Zhang et al., 1998a. (A) LHG2-d2-2 m-2–12 (24.0 × 73.0). (B) LHG2-d2-3.1 m-4-H-3 (32.6, NR). (C) LHG2-d2-3.1 m-11–1 (36.9, NR). (D) *Wengania globosa* Zhang, 1989, emend, Zhang et al., 1998; LHG2-d2-2 m-2–22 (104.1 × 15.0). (E) *Wengania minuta* Xiao, 2004; LHG2-d2-3.1 m-3p-66 (24.5 × 61.9).

apertures defined by an inwardly directed oral collar.

Dimensions: The two specimens in our collection are 1407.8 μm and 1420.0 μm in vesicle diameter, respectively. The better-preserved specimen in our collection (Fig. 51K) bears two apertures, which are 46.4 μm and 223.6 μm in aperture diameter, and 175.0 μm and 168.0 μm in collar length.

Remarks: Our specimens are similar to *O. arcelliformis* in overall morphology, but they are much larger in vesicle size and aperture diameter. For comparison, the vesicle diameter and aperture diameter of *O. arcelliformis* are 76–165 μm and 2.5–14 μm, respectively. We note that the specimen illustrated in Fig. 51J could be a large *Schizofusa* vesicle that is cut near the apices of a V-shaped split. This uncertainty, along with the limited material, led us to place our specimens in an open nomenclature.

Occurrence: The Ediacaran Doushantuo Formation in the Shennongjia area of Hubei Province, South China (this paper).

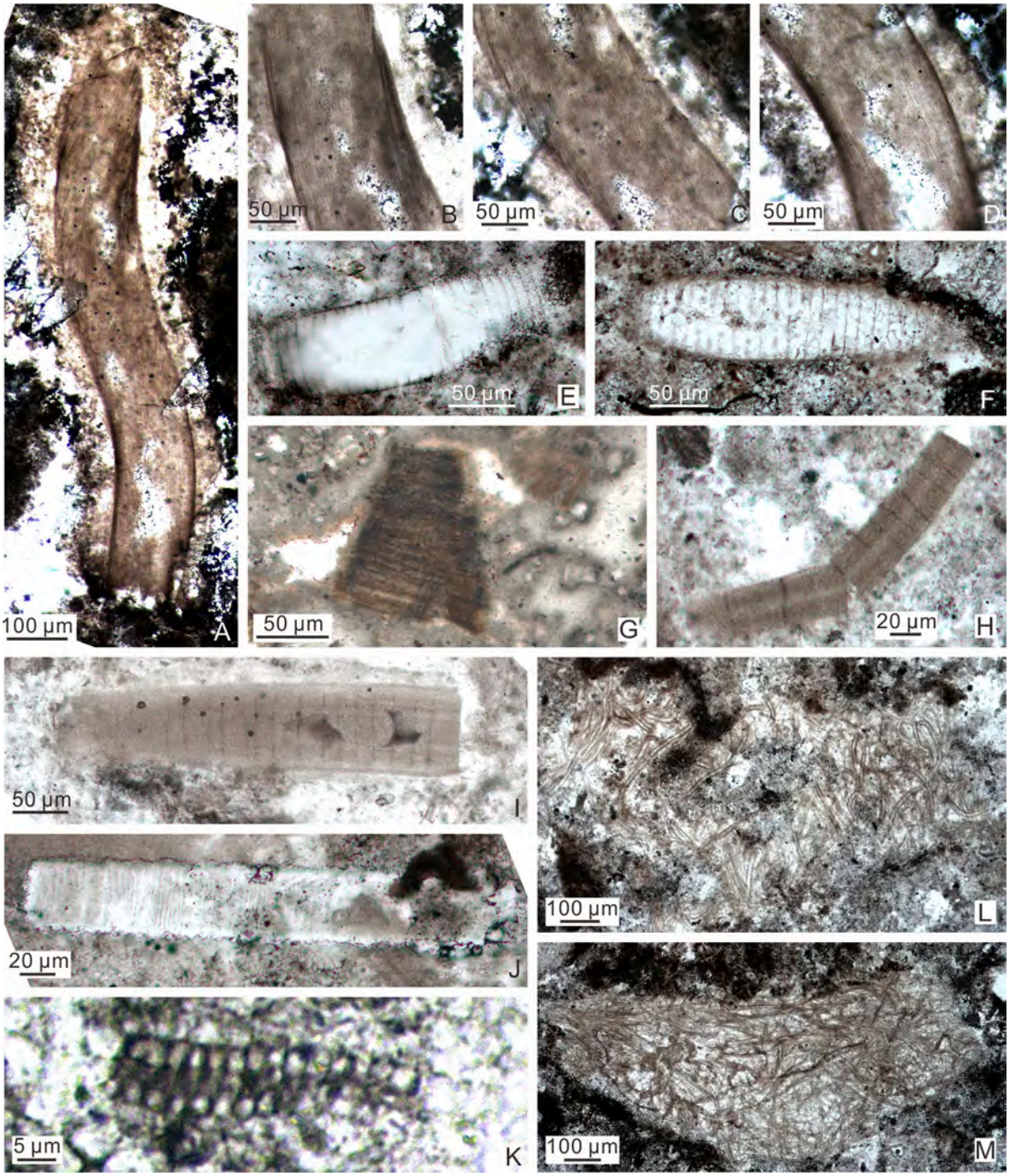

Fig. 54. (A–D) *Jixiania retorta* sp. nov. holotype: LHG2-d2-3.1 m-18-H-25 (37.5, NR). (B–D) Magnified views of (A) from top to bottom, respectively. (E–F) *Oscillatoriopsis majuscula* Knoll et al., 1988, emend. (E) LHG2-d2-2 m-2–4 (21.8 × 78). (F) LHG-d2-60 cm-7–1 (17 × 80.5). (G) *Botominella lineata* Reitlinger, 1959; LHG-1 + 0.8 m-n-2–2 (21.5 × 69.7). (H–I) *Salome hubeiensis* Zhang, 1986. (H) LHG2-d2-3.1 m-1p-3 (24.8 × 80). (I) LHG2-d2-2 m-5–9 (25 × 75). (J) *Oscillatoriopsis* sp.; LHG-d2-3.4 m-2–1 (25.7 × 77.4). (K) *Obruchevella minor* Zhang, 1984b; LHG2-d2-3.1 m-12-H-1. (L–M) *Siphonophycus* spp. (L) LHG2-d2-3.1 m-7–26 (29 × 78.3). (M) LHG2-d2-3.1 m-4p-6 (17.6 × 76.5).

Genus *Schizofusa* Yan, 1982.

Type species: *Schizofusa sinica* Yan, 1982.

Schizofusa sp.

Fig. 51J.

Material: One well-preserved specimen.

Description: Medium-sized spheroidal vesicle bearing a deep slit-like medial split that cuts into one half of the vesicle. Vesicle is surrounded by a flexible outer membrane.

Dimensions: Vesicle diameter ~ 140.1 μm; aperture 67.3 μm wide ad 73.9 μm deep; vesicle wall ~ 1.9 μm thick, outer membrane ~ 2.2 μm thick, and they are separated from each other by a gap up to 23.3 μm.

Remarks: The current specimen fits the diagnosis of *Schizofusa* because its medial split, but it can be differentiated from other *Schizofusa* species by its distinct membrane. It would be identified as *S. zangwenlongii* if the outer membrane had not been preserved. The specimen is somewhat similar to *Osculosphaera membranifera*, but it is characterized by a medial split rather than an aperture with an outwardly directed collar.

Occurrence: The Ediacaran Doushantuo Formation in the Shennongjia area of Hubei Province, South China (this paper).

Multicellular algae thalli.

Genus *Sarcinophycus* Xiao and Knoll, 1999.

Type species: *Sarcinophycus radiatus* Xiao and Knoll, 1999.

Sarcinophycus papilloformis Xiao, 2004.

Fig. 52G–K.

Synonymy:

2004 *Sarcinophycus papilloformis* Xiao, pp. 395–397, Fig. 2.

2010 *Sarcinophycus papilloformis* Xiao; Chen et al., fig. 2.8.

2015 *Sarcinophycus papilloformis* Xiao; Ye et al., p. 51, pl. III, Figs. 7–8.

2019 *Sarcinophycus papilloformis* Xiao; Ouyang et al., Fig. 6C–D.

Material: Five moderately preserved specimens.

Description: Large thalli consisting of tightly packed cell packets in thallus interior and poorly preserved papillate or conical protuberances in thallus periphery. Cells are generally cuboidal in overall shape. Thallus periphery is much darker in color than thallus interior.

Dimensions: The maximum dimension of thalli 577.7–1049.0 μm; cells diameter 3.0–10.0 μm, typically ~ 6.0 μm.

Remarks: The genus *Sarcinophycus* and the type species *S. radiatus* were originally established on the basis of material extracted from Doushantuo phosphorites in the Weng'an area (Xiao and Knoll, 1999), and a second species, *S. papilloformis*, was subsequently reported from Doushantuo chert nodules in South China (Chen et al., 2010; Ouyang et al., 2019; Xiao, 2004; Ye et al., 2015). The type species is diagnosed by nested sarcinoidal cell packets that are arranged in radiating rays, whereas *S. papilloformis* is characterized by sarcinoidal cell packets organized in parallel rows and the presence of conical or papillate protuberance in thallus periphery. The current specimens exhibit the defining characters of *S. papilloformis* and like the type material (fig. 2.1 of Xiao, 2004), their thallus periphery is dark in color, probably because of the accumulation of organic matter.

Occurrence: The Ediacaran Doushantuo Formation in the Shennongjia (this paper), Zhangcunping (Ouyang et al., 2019; Ye et al., 2015), and Yangtze Gorges areas (Chen et al., 2010; Xiao, 2004) of Hubei Province, South China.

Sarcinophycus sp.

Fig. 52B–F.

Material: Five adequately and four poorly preserved specimens.

Description: Multicellular thalli consisting of thousands of tightly arranged cell packets. Individual cells are cuboidal and have a relatively uniform size of 2.3–6.4 μm.

Remarks: In our specimens, the cells are densely packed but they are not clearly organized to form radial or parallel rows, and the thallus margin is poorly preserved, making it difficult to assign our specimens to an existing species of *Sarcinophycus*.

Occurrence: The Ediacaran Doushantuo Formation in the Shennongjia area of Hubei Province, South China (this paper).

Genus *Wengania* Zhang et al., 1998a.

Type species: *W. globosa* Zhang, 1989, emend. Zhang et al., 1998a.

Wengania exquisita Zhang et al., 1998a.

Fig. 53A–C.

Synonymy:

1998a *Wengania exquisita* Zhang et al., p. 45, fig. 15.1–15.4.

2015 *Wengania exquisita* Zhang et al.; Ye et al., p. 52, pl. III, Figs. 11–12, and synonyms therein.

2019 *Wengania exquisita* Zhang et al.; Ouyang et al., p. 178, Fig. 6F.

2020 *Wengania exquisita* Zhang et al.; Yang et al., p. 16, Fig. 5J–K.

2021 *Wengania exquisita* Zhang et al.; Ouyang et al., Fig. 8E–F.

Material: Thirty-three adequately preserved specimens.

Description: Circular or elliptical (originally spheroidal) thalli bearing thousands of relatively small cells that are tightly and irregularly organized.

Dimensions: Maximum thallus diameter 79.9–464.1 μm; cell diameter 2.0–4.0 μm.

Remarks: Three species of *Wengania* have been named on the basis of their different thallus size, cell diameter, and cell arrangement: *W. exquisita* (thallus diameter 40.0–400.0 μm, cell diameter 2.0–4.0 μm, irregular cell arrangement), *W. globosa* (thallus diameter 55.0–750.0 μm, cell diameter 3.0–15.0 μm, regular cell arrangement into rows and columns), and *W. minuta* (thallus diameter 44.0–200.0 μm, cell diameter 3.0–8.0 μm, irregular cell arrangement). The current specimens are best described under *W. exquisita* because of their relatively small cells that are tightly and irregularly packed.

Occurrence: The Ediacaran Doushantuo Formation in the Shennongjia (this paper), Zhangcunping (Ouyang et al., 2019; Ye et al., 2015; Zhou et al., 2005), Yangtze Gorges (Liu et al., 2014a; Ouyang et al., 2021), and Baokang areas (Yang et al., 2020; Zhou et al., 2004) of Hubei Province, and the Weng'an area of Guizhou Province (Yuan et al., 2002; Zhang et al., 1998a), South China.

Wengania globosa Zhang, 1989, emend. Zhang et al., 1998a.

Fig. 53D.

Synonymy:

1989 *Wengania globosa* Zhang, p. 129, Fig. 13A–C.

2015 *Wengania globosa* Zhang, 1989, emend. Zhang et al., 1998; Ye et al., pp. 51–52, Figs. 9–10, and synonyms therein.

2019 *Wengania globosa* Zhang; Ouyang et al., Fig. 6E.

2019 *Wengania globosa* Zhang, 1989, emend. Zhang et al., 1998; Shang et al., p. 31, Fig. 20I.

2020 *Wengania globosa* Zhang, 1989, emend. Zhang et al., 1998; Yang et al., p. 16, Fig. 5L–Q.

2021 *Wengania globosa* Zhang, 1989, emend. Zhang et al., 1998; Ouyang et al., Fig. 8D.

Material: Six adequately preserved specimens.

Description: Circular (originally spheroidal) thallus consisting of polyhedral or cuboidal cells that are regularly arranged in columns.

Dimensions: Thallus diameter 107.2 μm; cell diameter 3.6–5.7 μm.

Remarks: Our specimen fits the diagnosis of *W. globosa* in morphology and size range.

Occurrence: The Ediacaran Doushantuo Formation in the Shennongjia (this paper), Zhangcunping (Ouyang et al., 2019; Ye et al., 2015; Zhou et al., 2005), Yangtze Gorges (Ouyang et al., 2021) and Baokang areas (Yang et al., 2020; Zhou et al., 2004) of Hubei Province, the Weng'an (Yuan et al., 1993; Zhang, 1989; Zhang et al., 1998a) and Songlin areas (Shang et al., 2019) of Guizhou Province, and the Mianxian area of Shanxi Province (Xiao et al., 1999), South China.

Wengania minuta Xiao, 2004.

Fig. 53E.

Synonymy:

2004 *Wengania minuta* Xiao, pp. 397, 399, fig. 3.1–3.6.

2005 *Wengania minuta* Xiao; Zhou et al., pl. I, fig. f–g.

2010 *Wengania minuta* Xiao; Chen et al., fig. 2.10.

2017 *Wengania minuta* Xiao; Nie et al., p. 385, fig. 12.8.

2019 *Wengania minuta* Xiao; Ouyang et al., Fig. 6G.

2021 *Wengania minuta* Xiao; Ouyang et al., Fig. 8A–C.

Material: Five adequately preserved specimens.

Description: Circular (originally spheroidal) thallus consisting of spheroidal or polyhedral cells that are irregularly arranged.

Dimensions: Thallus diameter 79.0 μm; cell diameter 6.5–7.4 μm.

Remarks: The current specimen is very similar to *W. minuta* in overall shape and size range.

Occurrence: The Ediacaran Doushantuo Formation in the Shennongjia (this paper), Zhangcunping (Chen et al., 2010; Ouyang et al., 2019; Zhou et al., 2005), and Yangtze Gorges (Ouyang et al., 2021; Xiao, 2004) of Hubei Province, and the Zhangjiajie area of Hunan Province (Nie et al., 2017), South China.

Cyanobacteria.

Genus *Archaeophycus* Wang et al., 1983.

Type species: *Archaeophycus yunnanensis* (Song *in* Luo et al., 1982) Dong et al., 2009.

Archaeophycus yunnanensis (Song *in* Luo et al., 1982) Dong et al., 2009.

Fig. 52A.

Synonymy:

1982 *Tretraphycus yunnanensis* Song; Luo et al., p. 216, pl. 31, Figs. 3–4.

2019 *Archaeophycus yunnanensis* (Song *in* Luo et al., 1982) Dong et al., 2009; Shang et al., pp.30–31, Fig. 20A–B, and synonyms therein.

2020 *Archaeophycus yunnanensis* (Song *in* Luo et al., 1982) Dong et al., 2009; Yang et al., pp. 10–11, Fig. 4A–B.

2021 *Archaeophycus yunnanensis* (Song *in* Luo et al., 1982) Dong et al., 2009; Ouyang et al., Fig. 7A–B.

Material: Dozens of well-preserved specimens.

Description: Individual spheroidal or subspheroidal cells that are packed to form dyads and tetrads, which further aggregate loosely to form a cluster. Cells are not surrounded by sheaths.

Dimensions: Cell diameter 12–23.7 μm; cluster size 24.2–49.3 μm; cell wall thickness ~ 1 μm.

Remarks: Archaeophycus yunnanensis has been variously interpreted as a cyanobacterium (Zhang, 1985), a possible bangiophyte (Zhang et al., 1998a), or a green alga (Xiao and Knoll, 1999; Yuan et al., 2002).

Occurrence: The Ediacaran Doushantuo Formation in the Shennongjia (this paper), Zhangcunping (Ouyang et al., 2019; Ye et al., 2015; Zhou et al., 2005), Yangtze Gorges (Ouyang et al., 2021; Zhang, 1985), and Baokang areas (Yang et al., 2020; Zhou et al., 2004) of Hubei Province, the Weng'an (Yuan and Hofmann, 1998; Yuan et al., 1993; Zhang et al., 1998a) and Songlin areas (Shang et al., 2019) of Guizhou Province, and the Zhangjiajie area of Hunan Province (Hawkins et al., 2017; Nie et al., 2017), South China; the early Cambrian Zhujiaqing Formation in eastern Yunnan, South China (Luo et al., 1982; Wang et al., 1983), Yanjiahe Formation in the Yangtze Gorges area, South China (Dong et al., 2009), Yurtus Formation in the Asku area of Tarim Basin, northwestern China (Dong et al., 2009); the uppermost Khesen Formation in northern Mongolia (Anderson et al., 2017a, 2019), which is considered terminal Ediacaran in age although it contains Cambrian-age detrital zircons (Anttila and Macdonald, 2020); and the Lower Cambrian Kyrshabakta (Berkuta Member) and Chulaktau formations of South Kazakhstan (Schopf et al., 2015).

Botominella lineata Reitlinger, 1959.

Fig. 54G.

Synonymy:

1959 *Botominella lineata* Reitlinger, p. 25, pl. 10, Figs. 1–7.

2019 Gen. et sp. indet., Shang et al., p. 32, Fig. 21C.

2021 *Botominella lineata* Reitlinger; Sharma et al., p. 6, Fig. 5J–K, 7A, and synonyms therein.

2022 *Botominella lineata* Reitlinger; Xiao et al., fig. 32.1–32.2.

Material: Twelve moderately preserved specimens.

Description: Straight or slightly curved trichome-like structure with closely distributed transverse septum-like structures. One of our specimens has a truncated conical shape, possibly representing an oblique section of a short and curved specimen.

Dimensions: Trichome-like structure 50.0–120.0 μm in diameter and up to 196.0 μm in length; septum-like structures 2.1–6.6 μm in thickness and ~ 1.0–5.0 μm in spacing.

Remarks: Present specimens are somewhat similar to *Oscillatoriopsis* sp. (Fig. 54J) described above, but have a much larger diameter and much narrower cells. Our specimens, as well as the specimen illustrated in Shang et al. (2019; their Fig. 21C), are better identified as *Botominella lineata* on the basis of their similarity in extremely flat or narrow septum-like structures.

Occurrence: The Ediacaran Doushantuo Formation in the Shennongjia area (this paper) of Hubei Province, and the Songlin area of Guizhou Province (Shang et al., 2019), South China; Ediacaran Krol A Formation in northern India (Sharma et al., 2021; Xiao et al., 2022); lower Cambrian Pestrocventnaya Formation of Siberia (Reitlinger, 1959); and lower Cambrian Kyrshabakta (Berkuta Member) and Chulaktau formations of South Kazakhstan (Schopf et al., 2015).

Genus *Gloeodiniopsis* Schopf, 1968, emend. Knoll and Golubic, 1979.

Type species: *Gloeodiniopsis lamellosa* Schopf, 1968, emend. Knoll and Golubic, 1979.

Gloeodiniopsis sp.

Fig. 51D.

Material: Two well-preserved specimens.

Description: Spheroidal to ellipsoidal cells enclosed in a smooth envelope or sheath. Cells commonly occur as monads, dyads, and tetrads, and they can form nested cell packets surrounded by a common sheath. A dark organic body is present in some cells.

Dimensions: Cells approximately 11.4–18.2 μm in diameter; external envelopes generally 35.1–36.2 μm in diameter and ~ 0.5–1.0 μm in thickness; internal bodies about 3.5 μm in diameter.

Remarks: Gloeodiniopsis closely resembles the modern cyanobacterial genus *Chroococcus*.

Occurrence: Widely distributed in Proterozoic strata.

Genus *Jixiania* Yan, 1986, emend. Miao et al., 2021.

Type species: *Jixiania lineata* Yan, 1986.

Jixiania retorta sp. nov.

Fig. 54A–D.

Holotype: The specimen illustrated in Fig. 54A–D, thin section LHG2-d2-3.1 m-18-H-25 (37.5, pc).

Etymology: Species name derived from Latin *retorta*, with reference to the twisted longitudinal striations of the species.

Locus typicus: The Ediacaran Doushantuo Formation at the Lianhuacun section, Shennongjia area of Hubei Province, South China.

Stratum typicum: Chert nodules in thin to medium bedded dolostones of unit 4, Doushantuo Formation.

Material: One incompletely but well-preserved specimen.

Diagnosis: Slightly curved tubular structure with well-developed and densely distributed longitudinal striations on the outer wall. Outer wall is thin and dark in color. Longitudinal striations are straight or slightly twisted along the length of the fossil, discontinuous, and mostly parallel to one another. Neither end of the fossil is preserved.

Dimensions: Diameter 132.1 μm; preserved length ~ 980.1 μm; outer wall thickness 2.5–4.6 μm; striation thickness 0.5–1.0 μm; striations spaced at 0.9–3.7 μm.

Remarks: Based on fossil material from the Mesoproterozoic Xiamaling Formation near Tianjin, North China, Yan (1986) established the genus *Jixiania* as unbranched tubes with longitudinally arranged parallel striations. Our specimen fits the diagnosis of *Jixiania* but differs from its type species *J. lineata* in having twisted and discontinuous longitudinal striations. Although represented by only a single specimen, its morphology is so distinct and clearly preserved. Hence, formal description of the specimen as new species of *Jixiania* is warranted. *Jixiania* is considered to be a filamentous metaphyte due to its complex morphology and large size (Javaux and Knoll, 2017; Miao et al., 2021; Vorob'eva et al., 2015; Yan, 1986), but this interpretation remains to be

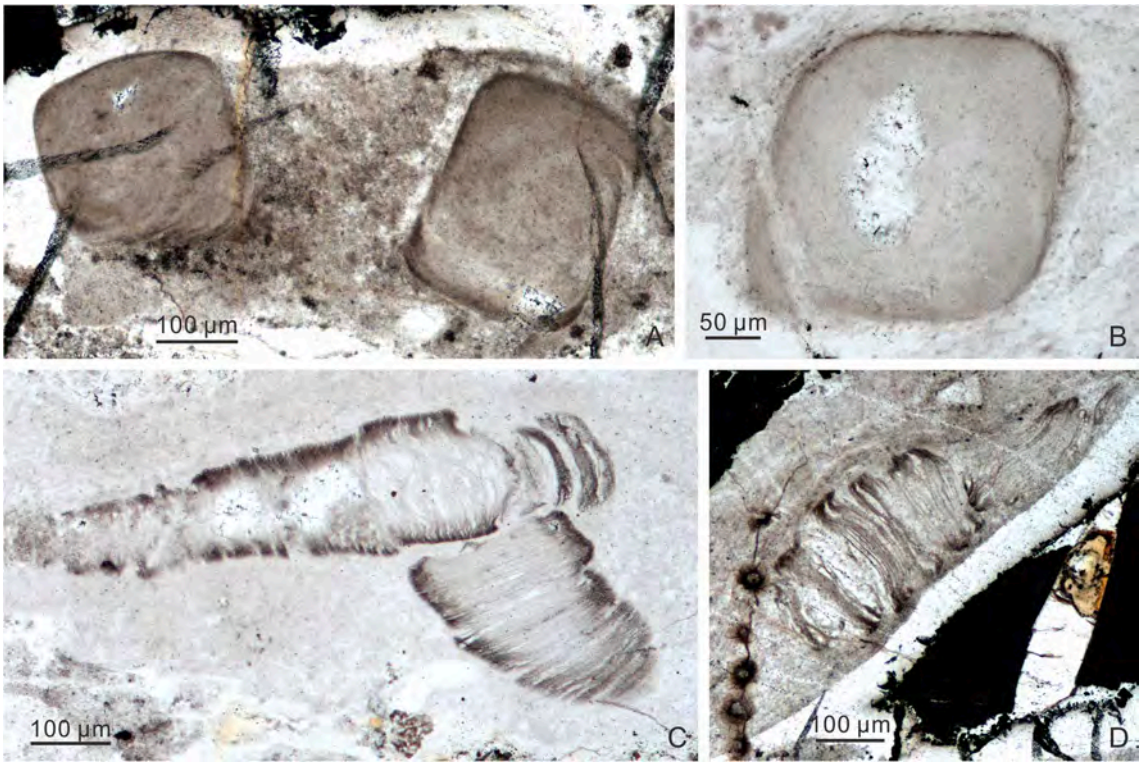

Fig. 55. (A–B) *Quadratitubus orbigoniatus* Xue et al., 1992, emend. Liu et al., 2008. (A) LHG-d3 + 30 cm-2–8 (66 × 31.4). (B) SLHG-d2-1.5 m-1–1 (23 × 71.3). (C–D) *Sinocyclocyclicus guizhouensis* Xue et al., 1992, emend. Liu et al., 2008. (C) SLHG-d2-2.5 m-1–1 (19.3 × 70.3). (D) LHG-d3 + 30 cm-2–13.

confirmed and the possibility of cyanobacterial sheath cannot be ruled out with confidence.

Occurrence: The Ediacaran Doushantuo Formation in the Shennongjia area of Hubei Province, South China (this study).

Genus *Obruchevella* Reitlinger, 1948, emend. Yakshchin and Luchinina, 1981.

Type species: *Obruchevella delicata* Reitlinger, 1948.

Obruchevella minor Zhang, 1984b.

Fig. 54K.

Synonymy:

1984b *Obruchevella minor* Zhang, p. 449, pl. I, Figs. 1–6.

2015 *Obruchevella minor* Zhang; Ye et al., pp. 53–54, pl. IV, Figs. 10–11, and synonyms therein.

2020 *Obruchevella minor* Zhang; Yang et al., pp. 11–12, Fig. 4C–G.

2021 *Obruchevella minor* Zhang; Ouyang et al., Fig. 7I.

Material: One well-preserved and one poorly preserved specimen.

Description: Hollow, aseptate, cylindrical filament tightly wound into a helix with closely spaced spires.

Dimensions: The specimen has a tube diameter of 2.0–2.4 μm and a helix diameter of 9.3 μm. The helix is 38.8 μm in length.

Occurrence: The Ediacaran Doushantuo Formation in the Shennongjia (this paper), Zhangcunping (Ye et al., 2015), Yangtze Gorges (Ouyang et al., 2021; Zhang, 1984b), and Baokang areas (Yang et al., 2020; Zhou et al., 2004) of Hubei Province, South China; Late Precambrian strata in the Suining area of Jiangsu Province, North China (Liu et al., 1984); early Cambrian Zhujiaqing Formation in the Meishucun area of Yunnan Province (Song, 1984), South China.

Genus *Oscillatoriopsis* Schopf, 1968, emend. Butterfield et al., 1994.

Type species: *Oscillatoriopsis obtusa* Schopf, 1968, emend. Butterfield et al., 1994.

Oscillatoriopsis majuscula Knoll et al., 1988, emend.

Fig. 54E–F.

Synonymy:

1988 *Oscillatoriopsis majuscula* Knoll et al., p. 277, Fig. 11a.

2015 *Oscillatoriopsis* sp.; Ouyang et al., fig. 3.2.

2021 Unnamed trichome with flat and regular septa; Ouyang et al., Fig. 7H.

Material: Two moderately preserved specimens.

Emended diagnosis: A species of *Oscillatoriopsis* with trichomes consisting of cells 25.0–100.0 μm in cell diameter and 2.0–13.0 μm in cell length.

Dimensions: The two specimens in our collection are 248.1 μm and 261.3 μm in preserved trichome length, 71.0 μm and 70.5 μm in cell diameter, and 6.4–12.8 μm in cell length. The ratio of cell length to cell diameter is about 0.1–0.2.

Remarks: Butterfield et al. (1994) recognized four *Oscillatoriopsis* species based on their cell diameters: *O. vermiformis* 1–3 μm, *O. obtusa* 3–8 μm, *O. amadeus* 8–14 μm, and *O. longa* 14–25 μm. Knoll et al. (1988) established *O. majuscula* to accommodate *Oscillatoriopsis* specimens with larger cell diameter. However, with only one specimen from the Paleoproterozoic Duck Creek Dolomite in Western Australia, the original diagnosis limited *O. majuscula* to specimens with cells approximately 63 μm wide and 6–11 μm long (Knoll et al., 1988). Our material fits the diagnosis of *O. majuscula* except their slightly greater cell diameter. Thus, the diagnosis of *O. majuscula* is emended here to accommodate specimens with larger sizes. One of the two specimens in our collection is apparently spindle-shaped in thin section (Fig. 54F), but this is likely a tangential cut of a curved cylindrical trichome. Our specimens are somewhat similar to the genera *Sinocyclocyclicus* Xue et al., 1992 and *Megathrix* Yin, 1987 in the presence of regular cross-walls inside a cylindrical tube or a trichome. However, the latter two genera have incomplete cross-walls that are interspersed between complete ones.

A specimen identified as *Oscillatoriopsis* sp. in Ouyang et al. (2015; their fig. 3.2, ~ 48.1 μm in cell width and 5.6–11.1 μm in cell length) and unnamed specimens illustrated in Ouyang et al. (2021; their Fig. 7H, 31.2–46.1 μm in cell width and 2.8–10.4 μm in cell length) are characterized by uniseriate trichome with flat and regular spaced cross walls. They are morphologically similar to our specimens and fit in the

emended diagnosis of *O. majuscula*.

Occurrences: The Ediacaran Doushantuo Formation in the Shennongjia (this paper) and Yangtze Gorges areas (Ouyang et al., 2015, 2021) of Hubei Province, South China; and the Paleoproterozoic Duck Creek Dolomite, western Australia (Knoll et al., 1988).

Oscillatoriopsis sp.

Fig. 54J.

Material: One incompletely preserved specimen.

Description: Unbranched, uniseriate cellular trichome with cell length considerably less than cell diameter. Cells are variable in length. Cross cell walls thin, straight or slightly curved, continuous (but can be discontinuous due to poor preservation).

Dimensions: Specimen 266.2 μm in preserved length and 44.5 μm in diameter; cross-walls spaced at 1.6–3.9 μm.

Remarks: The present specimen is somewhat similar to *O. majuscula* in having a large cell diameter. However, its irregular cross-walls and extremely low cell length/diameter ratios (0.04–0.09) make it distinct from *O. majuscula*; thus, it is provisionally placed in the genus *Oscillatoriopsis* as an open nomenclature.

Occurrence: The Ediacaran Doushantuo Formation in the Shennongjia area of Hubei Province, South China (this paper).

Genus *Salome* Knoll, 1982.

Type species: *Salome svalbardensis* Knoll, 1982.

Salome hubeiensis Zhang, 1986.

Fig. 54H–I.

Synonymy:

1986 *Salome hubeiensis* Zhang, pp. 33–34, pl. I, Figs. 2, 6, pl. II, Figs. 2, 5.

2019 *Salome hubeiensis* Zhang; Shang et al., p. 32, Fig. 21D, and synonyms therein.

2021 *Salome hubeiensis* Zhang; Ouyang et al., Fig. 7L–M.

2021 *Salome hubeiensis* Zhang; Sharma et al., Fig. 5E–I.

Material: A large number of well-preserved specimens in both cross and longitudinal sections.

Description: Thick, multilamellate sheaths with a large and variable diameter and irregularly spaced transverse markings.

Dimensions: Multilamellate sheath 38.4–80.8 μm in outer diameter and 29.9–50.6 μm in inner diameter. Transverse markings irregularly arranged at a spacing of 5.0–105.2 μm. Sheath length 211.3–1407.6 μm.

Remarks: The genus *Salome* is characterized by a thick and multilamellate sheath with transverse markings. Three species of *Salome* have been established and they can be differentiated on the basis of sheath diameter. The outer sheath diameter of *S. nunavutensis* and *S. svalbardensis* is < 40 μm (Butterfield, 2001) and 23–65 μm (Knoll, 1982), respectively, while *S. hubeiensis* has a larger and variable diameter that can be up to 200 μm (e.g., Liu et al., 2014a; Shang et al., 2019; Zhang, 1986). Based on this distinction, the current specimens are identified as *S. hubeiensis*.

Occurrence: The Ediacaran Doushantuo Formation in the Shennongjia (this paper), Zhangcunping (Ouyang et al., 2019), and Yangtze Gorges areas (Zhang, 1986; Zhang et al., 1998a; Liu et al., 2014a; Ouyang et al., 2021) of Hubei Province, the Zhangjiajie area of Hunan Province (Nie et al., 2017), and the Songlin area of Guizhou Province (Shang et al., 2019), South China; the Ediacaran Shuurgat Formation of Zavkhan Terrane in south-western Mongolia (Anderson et al., 2017b); the Ediacaran Krol 'A' succession of Lesser Himalaya, India (Sharma et al., 2021).

Genus *Siphonophycus* Schopf, 1968, emend. Knoll et al., 1991.

Type species: *Siphonophycus kestron* Schopf, 1968.

Siphonophycus spp.

Fig. 54L–M.

Material: Thousands of well-preserved specimens of Doushantuo Formation.

Description: Un-branched, nonseptate, smooth-walled tubular filaments that are often folded, twisted, or aggregated in clusters.

Remarks: Siphonophycus likely represent cyanobacterial sheaths and several morphospecies are recognized on the basis of sheath diameter (Knoll et al., 1991; Butterfield et al., 1994; Buick and Knoll, 1999; Tang et al., 2013). Five species are present in our collection: *S. septatum* (1–2 μm in width), *S. robustum* (2–4 μm in width), *S. typicum* (4–8 μm in width), *S. kestron* (8–16 μm in width) and *S. solidum* (16–32 μm in width).

Tubular microfossil.

Genus *Quadratitubus* Xue et al., 1992, emend. Liu et al., 2008.

Type species: *Quadratitubus orbigoniatus* Xue et al., 1992, emend. Liu et al., 2008.

Quadratitubus orbigoniatus Xue et al., 1992, emend. Liu et al., 2008.

Fig. 55A–B.

Synonymy:

1992 *Quadratitubus orbigoniatus* Xue et al., p. 534, pl. 2, Fig. 10a, 10b.

2014a *Quadratitubus orbigoniatus* Xue et al., 1992, emend. Liu et al., 2008; Liu et al., p. 135, fig. 116.1–116.4, and synonyms therein.

2019 *Quadratitubus orbigoniatus* Xue et al.; Sun et al., Fig. 3G–K.

Material: Seven adequately preserved specimens.

Description: Tubular structure with a square to rectangular cross section and rounded corners. Tube interior is subdivided by both complete and incomplete transverse cross-walls, although they are not captured in transverse cross section of the specimens.

Dimensions: Each side of tube 223.8–295.3 μm in width; outer wall thick 3.7–5.1 μm.

Remarks: Liu et al. (2008) provided a detailed description of five species of tubular microfossils from the Ediacaran Doushantuo Formation in the Weng'an area. Among which, *Q. orbigoniatus* is distinguished from other tubular fossils by its square transverse cross section and a thin outer wall. The current specimens are observed in transverse cross-sections and thus transverse cross-walls are not captured in the thin section. They are slightly wider than *Q. orbigoniatus* from the Doushantuo Formation at Weng'an (typically 160–250 μm in width; Liu et al., 2008), but are otherwise similar.

Occurrence: The Ediacaran Doushantuo Formation in the Shennongjia (this paper) and Yangtze Gorges areas (Liu et al., 2010, 2014a; Yin et al., 2009a) of Hubei Province, and the Weng'an area of Guizhou Province (Li et al., 2003; Liu et al., 2007, 2008; Sun et al., 2019; Xue et al., 1992; Yin et al., 2007a), South China.

Genus *Sinocyclocyclicus* Xue et al., 1992, emend. Liu et al., 2008.

Type species: *Sinocyclocyclicus guizhouensis* Xue et al., 1992, emend. Liu et al., 2008.

Sinocyclocyclicus guizhouensis Xue et al., 1992, emend. Liu et al., 2008.

Fig. 55C–D.

Synonymy:

1992 *Sinocyclocyclicus guizhouensis* Xue et al., p. 533, pl. 2, Figs. 4–6.

2014a *Sinocyclocyclicus guizhouensis* Xue et al., 1992, emend. Liu et al., 2008; Liu et al., pp. 135–136, figs. 116.5–116.8, 117.1–117.6, and synonyms therein.

2019 *Sinocyclocyclicus guizhouensis* Xue et al.; Sun et al., Fig. 3A–F.

Material: Seven adequately preserved specimens and three poorly preserved specimens.

Description: Unbranching cylindrical tubes with transverse cross-walls. Tubes can be curved and have poorly preserved outer wall. Both complete and incomplete cross-walls are observed inside tubes. Cross-walls straight or strongly curved.

Dimensions: Tubes 272.7–748.6 μm in preserved length and 164.6–207.8 μm in diameter; complete cross-wall spacing 3.0–7.5 μm.

Remarks: It is difficult to distinguish *Q. orbigoniatus* and *S. guizhouensis* based on longitudinal sections alone, as both are characterized by the presence of complete and incomplete cross-walls inside tubes (Liu et al., 2008). Our specimens are identified as *S. guizhouensis* because they have a round or conical end (Fig. 55C, probably representing oblique cuts of cylindrical tubes) and show no evidence of square cross-sections when observed under the microscope with adjusted focus levels.

Occurrence: The Ediacaran Doushantuo Formation in the Shennongjia (this paper) and Yangtze Gorges areas (Liu et al., 2009c, 2010, 2014a; Yin et al., 2009a) of Hubei Province, and the Weng'an area of Guizhou Province (Li et al., 1997, 2003; Liu et al., 2007, 2008; Sun et al., 2019; Xiao et al., 2000; Xue et al., 1992; Yin et al., 2007a), South China.

Declaration of Competing Interest

The authors declare that they have no known competing financial interests or personal relationships that could have appeared to influence the work reported in this paper.

Acknowledgements

This work was supported by Fundamental Research Funds for National Natural Science Foundation of China (41902004, 41802206), the Central Universities (CUGCJ1816, CUG 2106101) to China University of Geosciences (Wuhan), National Postdoctoral Program for Innovative Talents (BX20180278), China Postdoctoral Science Foundation (2018M642946, 2021M692980), State Key Laboratory of Palaeobiology and Stratigraphy (Nanjing Institute of Geology and Palaeontology, CAS) (No. 213125), Hubei Key Laboratory of Paleontology and Geological Environment Evolution (PEL-202003), and State Key Laboratory of Biogeology and Environmental Geology (GBL201709). S.X. was supported by the National Science Foundation (EAR-2021207). We thank Haodong Gu and Yang Yu for discussion of petrography and regional geology. We thank Prof. Leiming Yin and an anonymous reviewer for constructive comments.

Appendix A. Supplementary data

Supplementary data to this article can be found online at https://doi.org/10.1016/j.precamres.2022.106691.

References

An, Z., Tong, J., Ye, Q., Tian, L., Zhao, X., Liu, S., Mou, Z., 2018. Stratigraphic Division and Correlation of Ediacaran Doushantuo Formation in Zhangcunping Area, Yichang. Hubei Province. Earth Science 43 (7), 2206–2221.
An, Z., Jiang, G., Tong, J., Tian, L., Ye, Q., Song, H., Song, H., 2015. Stratigraphic position of the Ediacaran Miaohe biota and its constrains on the age of the upper Doushantuo delta ^{13}C anomaly in the Yangtze Gorges area, South China. Precambrian Research 271, 243–253.
Anderson, R.P., Macdonald, F.A., Jones, D.S., McMahon, S., Briggs, D.E.G., 2017a. Doushantuo-type microfossils from latest Ediacaran phosphorites of northern Mongolia. Geology 45, 1079–1082.
Anderson, R.P., McMahon, S., Bold, U., Macdonald, F.A., Briggs, D.E.G., 2017b. Palaeobiology of the early Ediacaran Shuurgat Formation, Zavkhan Terrane, southwestern Mongolia. Journal of Systematic Palaeontology 15, 947–968.
Anderson, R.P., McMahon, S., Macdonald, F.A., Jones, D.S., Briggs, D.E.G., 2019. Palaeobiology of latest Ediacaran phosphorites from the upper Khesen Formation, Khuvsgul Group, northern Mongolia. Journal of Systematic Palaeontology 17, 501–532.
Anttila, E.S.C., Macdonald, F.A., 2020. Cryogenian to early Cambrian evolution of the phosphorite-bearing Khovsgol basion, Mongolia. Geological Society of America Abstracts with Programs 52 (6). https://doi.org/10.1130/abs/2020AM-359065.
Awramik, S.M., McMenamin, D.S., Yin, C., Zhao, Z., Ding, Q., Zhang, S., 1985. Prokaryotic and eukaryotic microfossils from a Proterozoic/Phanerozoic transition in China. Nature 315, 655–658.
Buick, R., Knoll, A.H., 1999. Acritarchs and microfossils from the Mesoproterozoic Bangemall Group, northwestern Australia. Journal of Paleontology 73, 744–764.
Butterfield, N.J., 2001. Paleobiology of the late Mesoproterozoic (ca. 1200 Ma) Hunting Formation, Somerset Island, arctic Canada. Precambrian Research 111, 235–256.
Butterfield, N.J., Chandler, F.W., 1992. Paleoenvironmental distribution of Proterozoic microfossils, with an example from the Agu Bay Formation, Baffin Island. Palaeontology 35, 943–957.
Butterfield, N.J., Knoll, A.H., Swett, K., 1994. Paleobiology of the Neoproterozoic Svanbergfjellet Formation, Spitsbergen. Fossils and Strata 34, 1–84.
Chen, B., Hu, C., Mills, B.J.W., He, T., Andersen, M.B., Chen, X., Liu, P., Lu, M., Newton, R.J., Poulton, S.W., Shields, G.A., Zhu, M., 2022. A short-lived oxidation event during the early Ediacaran and delayed oxygenation of the Proterozoic ocean. Earth and Planetary Science Letters 577, 117274.
Chen, L., Xiao, S., Pang, K., Zhou, C., Yuan, X., 2014. Cell differentiation and germ-soma separation in Ediacaran animal embryo-like fossils. Nature 516, 238–241.
Chen, M., Liu, K., 1986. The geological significance of newly discovered microfossils from the upper Sinian (Doushantuo age) phosphorites. Scientia Geologica Sinica 1, 46–53.
Chen, S., Yin, C., Liu, P., Gao, L., Tang, F., Wang, Z., 2010. Microfossil assemblage from chert nodules of the Ediacaran Doushantuo Formation in Zhangcunping, Northern Yichang, South China. Acta Geologica Sinica (Chinese Edition) 84, 70–77.
Cohen, P.A., Knoll, A.H., Kodner, R.B., 2009. Large spinose microfossils in Ediacaran rocks as resting stages of early animals. Proceedings of the National Academy of Sciences of the United States of America 106, 6519–6524.
Cohen, P.A., Macdonald, F.A., 2015. The Proterozoic record of eukaryotes. Paleobiology 41, 610–632.
Condon, D., Zhu, M., Bowring, S., Wang, W., Yang, A., Jin, Y., 2005. U-Pb ages from the Neoproterozoic Doushantuo Formation, China. Science 308, 95–98.
Dong, J., Zhang, S., Jiang, G., Shao, Q., Li, H., Shi, X., Liu, J., 2008. Early diagenetic growth of carbonate concretions in the upper Doushantuo Formation in South China and their significance for the assessment of hydrocarbon source rock: Science in China Series D: Earth Sciences 51, 1330–1339.
Dong, L., Xiao, S., Shen, B., Zhou, C., Li, G., Yao, J., 2009. Basal Cambrian microfossils from the Yangtze Gorges area (South China) and the Aksu area (Tarim Block, northwestern China). Journal of Paleontology 83, 30–44.
Downie, C., Sarjeant, W.A.S., 1963. On the interpretation and status of some hystrichosphere genera. Palaeontology 6, 83–96.
Eisenack, A., 1958. *Tasmanites* Newton 1875 und *Leiosphaeridia* n. gen. aus Gattungen der Hystrichosphaeridea. Palaeontographica Abteilung A 110, 1–19.
Evitt, W.R., 1963. A discussion and proposals concerning fossil dinoflagellates, hystrichospheres, and acritarchs. Proceedings of the National Academy of Sciences.
Golubkova, E.Y., Raevskaya, E.G., Kuznetsov, A.B., 2010. Lower Vendian microfossil assemblages of East Siberia: Significance for solving regional stratigraphic problems. Stratigraphy and Geological Correlation 18, 353–375.
Golubkova, E.Y., Zaitseva, T.S., Kuznetsov, A.B., Dovzhikova, E.G., Maslov, A.V., 2015. Microfossils and Rb-Sr age of glauconite in the key section of the Upper Proterozoic of the northeastern part of the Russian plate (Keltmen-1 borehole). Doklady Earth Sciences 462, 547–551.
Grazhdankin, D., Nagovitsin, K., Golubkova, E., Karlova, G., Kochnev, B., Rogov, V., Marusin, V., 2020. Doushantuo-Pertatataka-type acanthomorphs and Ediacaran ecosystem stability. Geology 48, 708–712.
Grey, K., 2005. Ediacaran palynology of Australia. Memoirs of the Association of Australasian Palaeontologists 31, 1–439.
Grey, K., Willman, S., 2009. Taphonomy of Ediacaran acritarchs from Australia: Significance for taxonomy and biostratigraphy. Palaios 24, 239–256.
Gu, H., Hu, J., An, Z., Ye, Q., Sun, S., Zhang, Z., Li, C., 2021. Sedimentary characteristics of the Doushantuo Formation in Shennongjia area and its implications for the "Western Hubei Trough". Earth Science—Journal of China University of. Geosciences 46, 2958–2972.
Hawkins, A.D., Xiao, S., Jiang, G., Wang, X., Shi, X., 2017. New biostratigraphic and chemostratigraphic data from the Ediacaran Doushantuo Formation in intra-shelf and upper slope facies of the Yangtze platform: Implications for biozonation of acanthomorphic acritarchs in South China. Precambrian Research 300, 28–39.
Jankauskas, T.V., Mikhailova, N.S., Hermann, T.N., 1989. Mikrofossilii Dokembriya SSSR [Precambrian Microfossils of the USSR]. Nauka, Leningrad.
Javaux, E.J., Knoll, A.H., 2017. Micropaleontology of the lower Mesoproterozoic Roper Group, Australia, and implications for early eukaryotic evolution. Journal of Paleontology 91, 199–229.
Javaux, E.J., Knoll, A.H., Walter, M.R., 2001. Morphological and ecological complexity in early eukaryotic ecosystems. Nature 412, 66–69.
Jiang, G., Kaufman, A.J., Christie-Blick, N., Zhang, S., Wu, H., 2007. Carbon isotope variability across the Ediacaran Yangtze platform in South China: implications for a large surface-to-deep ocean $\delta^{13}C$ gradient. Earth and Planetary Science Letters 261, 303–320.
Jiang, G., Shi, X., Zhang, S., Wang, Y., Xiao, S., 2011. Stratigraphy and paleogeography of the Ediacaran Doushantuo Formation (ca. 635–551 Ma) in South China. Gondwana Research 19, 831–849.
Joshi, H., Tiwari, M., 2016. *Tianzhushania spinosa* and other large acanthomorphic acritarchs of Ediacaran Period from the Infrakrol Formation, Lesser Himalaya, India. Precambrian Research 286, 325–336.
Knoll, A.H., 1982. Microfossils from the late Precambrian Draken Conglomerate, NY Friesland, Svalbard. Journal of Paleontology 56, 755–790.
Knoll, A.H., 1984. Microbiotas of the late Precambrian Hunnberg Formation, Nordaustlandet, Svalbard. Journal of Paleontology 58, 131–162.
Knoll, A.H., 1992. Vendian microfossils in metasedimentary cherts of the Scotia Group, Prins Karls Forland, Svalbard. Palaeontology 35, 751–774.
Knoll, A.H., Golubic, S., 1979. Anatomy and taphonomy of a Precambrian algal stromatolite. Precambrian Research 10, 115–151.
Knoll, A.H., Strother, P.K., Rossi, S., 1988. Distribution and diagenesis of microfossils from the lower Proterozoic Duck Creek Dolomite, Western Australia. Precambrian Research 38, 257–279.
Knoll, A.H., Swett, K., Mark, J., 1991. Paleobiology of a Neoproterozoic tidal flat/lagoonal complex: The Draken Conglomerate Formation, Spitsbergen. Journal of Paleontology 65, 531–570.
Kolosova, S.P., 1991. Pozdnedokembriyskie shipovatie mikrofossilii vostoka sibirkoy platformi [Late Precambrian acanthomorphic acritarchs from the eastern Siberian Platform]. Algologiya [Algologia] 1, 53–59.
Li, G., Xue, Y., Zhou, C., 1997. Late Proterozoic tubular fossils from the Doushantuo Formation of Weng'an, Guizhou, China. Palaeoworld 7, 29–37.

Liu, H., Qi, S., Fan, J., Guo, W., Pei, M., Huang, D., Cheng, L., Bian, M., Liu, L., Zhao, Y., Zhang, J., 2021. An acritarch assemblage from the Lower Ediacaran Doushantuo Formation in Changyang. Hubei Province. Journal of Stratigraphy 45 (1), 19–28.
Liu, P., Yin, C., Chen, S., Tang, F., Gao, L., 2009a. New data of phosphatized globular fossils from Weng'an biota in the Ediacaran Doushantuo Formation and the problem concerning their affinity. Acta Geoscientica Sinica 30, 457–464.
Liu, P., Xiao, S., Yin, C., Tang, F., Gao, L., 2009b. Silicified tubular microfossils from the upper Doushantuo Formation (Ediacaran) in the Yangtze Gorges area, South China. Journal of Paleontology 83, 630–633.
Liu, P., Moczydłowska, M., 2019. Ediacaran microfossils from the Doushantuo Formation chert nodules in the Yangtze Gorges area, South China, and new biozones. Fossils and Strata 65, 1–172.
Liu, P., Xiao, S., Yin, C., Chen, S., Zhou, C., Li, M., 2014a. Ediacaran acanthomorphic acritarchs and other microfossils from chert nodules of the upper Doushantuo Formation in the Yangtze Gorges area, South China. Journal of Paleontology 72 (supplement to No 1), 1–139.
Liu, P., Xiao, S., Yin, C., Zhou, C., Gao, L., Tang, F., 2008. Systematic description and phylogenetic affinity of tubular microfossils from the Ediacaran Doushantuo Formation at Weng'an, South China. Palaeontology 51, 339–366.
Liu, P., Yin, C., Chen, S., Tang, F., Gao, L., 2010. Affinity, distribution and stratigraphic signification of tubular microfossils from Ediacaran Doushantuo Formation in South China. Acta Palaeontologica Sinica 49, 308–324.
Liu, P., Yin, C., Chen, S., Tang, F., Gao, L., 2012. Discovery of *Ceratosphaeridium* (Acritarcha) from the Ediacaran Doushantuo Formation in Yangtze Gorges, South China and its biostratigraphic implication. Bulletin of Geosciences 87, 195–200.
Liu, P., Yin, C., Chen, S., Tang, F., Gao, L., 2013. The biostratigraphic succession of acanthomorphic acritarchs of the Ediacaran Doushantuo Formation in the Yangtze Gorges area, South China and its biostratigraphic correlation with Australia. Precambrian Research 225, 29–43.
Liu, P., Yin, C., Tang, F., Gao, L., Wang, Z., 2007. Progresses and questions on studying metazoan fossils of the Weng'an biota. Geological Review 53, 728–735.
Liu, P., Yin, C., Gao, L., Tang, F., Chen, S., 2009c. New material of microfossils from the Ediacaran Doushantuo Formation in the Zhangcunping area, Yichang, Hubei Province and its zircon SHRIMP U-Pb age. Chinese Science Bulletin 54, 1058–1064.
Liu, P., Chen, S., Zhu, M., Li, M., Yin, C., Shang, X., 2014b. High-resolution biostratigraphic and chemostratigraphic data from the Chenjiayuanzi section of the Doushantuo Formation in the Yangtze Gorges area, South China: Implication for subdivision and global correlation of the Ediacaran System. Precambrian Research 249, 199–214.
Liu, X., Liu, Z., Zhang, L., 1984. Late Precambrian algal assemblage in Suining, Jiangsu Province. Acta Micropalaeontologica Sinica 1, 171–182.
Li, Y., Zhang, X.L., Guo, J.F., Ding, L.F., Han, J., Shu, D.G., 2003. New materials of phosphatized cylindrical and tabulate microfossils from the Neoproterozoic Doushantuo Formation at Weng'an, Guizhou, South China. Acta Palaeontologica Sinica 42, 200–207.
Luo, H., Jiang, Z., Wu, X., Song, X., Ouyang, L., 1982. The Sinian-Cambrian Boundary in Eastern Yunnan. China. People's Publishing House of Yunnan, Kunming, Yunnan.
McFadden, K.A., Huang, J., Chu, X., Jiang, G., Kaufman, A.J., Zhou, C., Yuan, X., Xiao, S., 2008. Pulsed oxidation and biological evolution in the Ediacaran Doushantuo Formation. Proceedings of the National Academy of Sciences of the United States of America 105, 3197–3202.
McFadden, K.A., Xiao, S., Zhou, C., Kowalewski, M., 2009. Quantitative evaluation of the biostratigraphic distribution of acanthomorphic acritarchs in the Ediacaran Doushantuo Formation in the Yangtze Gorges area, South China. Precambrian Research 173, 170–190.
Miao, L., Moczydłowska, M., Zhu, M., 2021. A diverse organic-walled microfossil assemblage from the Mesoproterozoic Xiamaling Formation. North China. Precambrian Research 360 (3), 106235.
Moczydłowska, M., 2005. Taxonomic review of some Ediacaran acritarchs from the Siberian Platform. Precambrian Research 136, 283–307.
Moczydłowska, M., Nagovitsin, K.E., 2012. Ediacaran radiation of organic-walled microbiota recorded in the Ura Formation, Patom Uplift, East Siberia. Precambrian Research 198–199, 1–24.
Moczydłowska, M., Vidal, G., Rudavskaya, V.A., 1993. Neoproterozoic (Vendian) phytoplankton from the Siberian Platform, Yakutia. Palaeontology 36, 495–521.
Moczydłowska, M., Willman, S., 2009. Ultrastructure of cell walls in ancient microfossils as a proxy to their biological affinities. Precambrian Research 173, 27–38.
Muscente, A.D., Hawkins, A.D., Xiao, S., 2015. Fossil preservation through phosphatization and silicification in the Ediacaran Doushantuo Formation (South China): a comparative synthesis. Palaeogeography Palaeoclimatology Palaeoecology 434, 46–62.
Nagovitsin, K.E., Kochnev, B.B., 2015. Microfossils and biofacies of the Vendian fossil biota in the southern Siberian Platform. Russian Geology and Geophysics 56, 584–593.
Narbonne, G.M., Xiao, S., Shields, G.A., 2012. The Ediacaran Period. In: Gradstein, F.M., Ogg, J.G., Schmitz, M., Ogg, G. (Eds.), Geological Time Scale 2012. Elsevier, Oxford, pp. 413–435.
Naumova, S.N., 1949. Spory nizhnego kembriya (Spores from the Lower Cambrian). Izvestiya Akademii Nauk SSSR, Seriya Geologicheskaya 1949 (4), 49–56.
Nie, X., Liu, H., Dong, L., 2017. Ediacaran microfossils from the Doushantuo Formation of the Siduping section, Zhangjiajie, Hunan Province, China. Acta Palaeontologica Sinica 34, 369–389.
Ouyang, Q., Guan, C., Zhou, C., Xiao, S., 2017. Acanthomorphic acritarchs of the Doushantuo Formation from an upper slope section in northwestern Hunan Province, South China, with implications for early-middle Ediacaran biostratigraphy. Precambrian Research 298, 512–529.
Ouyang, Q., Zhou, C., Xiao, S., Guan, C., Chen, Z., Yuan, X., Sun, Y., 2021. Distribution of Ediacaran acanthomorphic acritarchs in the lower Doushantuo Formation of the Yangtze Gorges area, South China: evolutionary and stratigraphic implications. Precambrian Research 353, 106005.
Ouyang, Q., Zhou, C., Guan, C., Wang, W., 2015. New microfossils from the Ediacaran Doushantuo Formation in the Yangtze Gorges area, South China, and their biostratigraphic implications. Acta Palaeontologica Sinica 54, 207–229.
Ouyang, Q., Zhou, C., Xiao, S., Chen, Z., Shao, Y., 2019. Acanthomorphic acritarchs from the Ediacaran Doushantuo Formation at Zhangcunping in South China, with implications for the evolution of early Ediacaran eukaryotes. Precambrian Research 320, 171–192.
Prasad, B., Asher, R., 2016. Record of Ediacaran complex acanthomorphic acritarchs from the Lower Vindhyan succession of the Chambal Valley (east Rajasthan), India and their biostratigraphic significance. Journal of the Palaeontological Society of India 61, 29–62.
Reitlinger, E.A., 1948. Kembriiskie foraminiferi Yakutii (Cambrian Foraminifera of Yakutia). Byulletin' Moskovskogo Obshchestva Ispyatatelej Prirody, Otdelenie Geologii 23, 77–81.
Reitlinger, E.A., 1959. Atlas of Microscopic Organic Remains and Problematica of Ancient Deposits of Siberia. Academiya Nauk SSSR, Moscow 62, pp in Russian.
Rooney, A.D., Cantine, M.D., Bergmann, K.D., Gómez-Pérez, I., Baloushi, B.A., Boag, T. H., Busch, J.F., Sperling, E.A., Strauss, J.V., 2020. Calibrating the coevolution of Ediacaran life and environment. Proceedings of the National Academy of Sciences 117 (29), 16824–16830.
Schopf, J.W., 1968. Microflora of the Bitter Springs Formation, Late Precambrian, central Australia. Journal of Paleontology 42, 651–688.
Schopf, J.W., Sergeev, V.N., Kudryavtsev, A.B., 2015. A new approach to ancient microorganisms: taxonomy, paleoecology, and biostratigraphy of the Lower Cambrian Berkuta and Chulaktau microbiotas of South Kazakhstan. Journal of Paleontology 89, 695–729.
Schwid, M.F., Xiao, S., Hiatt, E.E., Fang, Y., Nolan, M., 2020. Iron phosphate in the Ediacaran Doushantuo Formation of South China: A previously undocumented marine phosphate sink. Palaeoecology Palaeoclimatology Palaeoecology 560, 109993.
Sergeev, V.N., Knoll, A.H., Vorob'eva, N.G., 2011. Ediacaran microfossils from the Ura Formation, Baikal-Patom Uplift, Siberia: taxonomy and biostratigraphic significance. Journal of Paleontology 85, 987–1011.
Shang, X., Liu, P., 2020. Acritarchs from the Ediacaran Doushantuo Formation at the Tianping section in Zhangjiajie area of Hunan Province, South China and their biostratigraphic significance. Journal of Stratigraphy 44 (2), 150–162.
Shang, X., Liu, P., Moczydlowska, M., 2019. Acritarchs from the Doushantuo Formation at Liujing section in Songlin area of Guizhou Province, South China: Implications for early-middle Ediacaran biostratigraphy. Precambrian Research 334, 105453.
Sharma, M., Tiwari, M., Ahmad, S., Shukla, R., Shukla, B., Singh, V., Pandey, S.K., Ansari, A., Shukla, Y., Kumar, S.P., 2016. Palaeobiology of Indian Proterozoic and Early Cambrian Successions— Recent Developments. Proceedings of the Indian National Science Academy 82 (3), 559–579.
Sharma, M., Shukla, Y., Sergeev, V.N., 2021. Microfossils from the Krol 'A' of the Lesser Himalaya. Additional supporting data for its early Ediacaran age. Palaeoworld, India in press.
Shukla, R., Tiwari, M., 2014. Ediacaran acanthomorphic acritarchs from the Outer Krol Belt, Lesser Himalaya, India: Their significance for global correlation. Palaeoworld 23, 209–224.
Song, X., 1984. *Obruchevella* from the Early Cambrian Meishucunian Stage of the Meishucun section, Jinning, Yunnan, China. Geological Magazine 121, 179–183.
Sun, W., Yin, Z., Donoghue, P., Liu, P., Shang, X., Zhu, M., 2019. Tubular microfossils from the Ediacaran Weng' an Biota (Doushantuo Formation, South China) are not early animals. Palaeoworld 28, 469–477.
Tang, Q., Pang, K., Xiao, S., Yuan, X., Ou, Z., Wan, B., 2013. Organic-walled microfossils from the early Neoproterozoic Liulaobei Formation in the Huainan region of North China and their biostratigraphic significance. Precambrian Research 236, 157–181.
Tang, Q., Pang, K., Yuan, X., Wan, B., Xiao, S., 2015. Organic-walled microfossils from the Tonian Gouhou Formation, Huaibei region, North China Craton, and their biostratigraphic implications. Precambrian Research 266, 296–318.
Tiwari, M., Knoll, A.H., 1994. Large acanthomorphic acritarchs from the Infrakrol Formation of the Lesser Himalaya and their stratigraphic significance. Journal of Himalayan Geology 5, 193–201.
Tiwari, M., Pant, C.C., 2004. Neoproterozoic silicified microfossilsin Infrakrol Formation of Lesser Himalaya, India. Himalayan Geology 25, 1–21.
Turner, R.E., 1984. Acritarchs from the type area of the Ordovician Caradoc Series, Shropshire, England. Palaeontographica Abteilung B 190, 87–157.
Veis, A.F., Vorob'eva, N.G., Golubkova, E.Y., 2006. The early Vendian microfossils first found in the Russian Plate: Taxonomic composition and biostratigraphic significance. Stratigraphy and Geological Correlation 14, 368–385.
Vidal, G., 1990. Giant acanthomorph acritarchs from the upper Proterozoic in southern Norway. Palaeontology 33, 287–298.
Vidal, G., Moczydłowska-Vidal, M., 1997. Biodiversity, speciation, and extinction trends of Proterozoic and Cambrian phytoplankton. Paleobiology 23, 230–246.
Vorob'eva, N.G., Petrov, P.Y., 2020. Microbiota of the Barakun Formation and Biostratigraphic Characteristics of the Dal'nyaya Taiga Group: Early Vendian of the Ura Uplift (Eastern Siberia). Stratigraphy and Geological Correlation 28, 365–380.
Vorob'eva, N.G., Sergeev, V.N., Knoll, A.H., 2009a. Neoproterozoic microfossils from the margin of the East European Platform and the search for a biostratigraphic model of lower Ediacaran rocks. Precambrian Research 173, 163–169.

Vorob'eva, N.G., Sergeev, V.N., Knoll, A.H., 2009b. Neoproterozoic microfossils from the northeastern margin of the East European Platform. Journal of Paleontology 83, 161–196.
Vorob'eva, N.G., Sergeev, V.N., Chumakov, N.M., 2008. New finds of early Vendian microfossils in the Ura Formation: Revision of the Patom Supergroup Age, middle Siberia. Doklady Earth Sciences 419A, 411–416.
Vorob'eva, N.G., Sergeev, V.N., Petrov, P.Y., 2015. Kotuikan Formation assemblage: A diverse organic-walled microbiota in the Mesoproterozoic Anabar succession, northern Siberia. Precambrian Research 256, 201–222.
Wang, F., Zhang, X., Guo, R., 1983. The Sinian microfossils from Jinning, Yunnan, Southwest China. Precambrian Research 23, 133–175.
Wang, Z., Wang, J., Suess, E., Wang, G., Chen, C., Xiao, S., 2017. Silicified glendonites in the Ediacaran Doushantuo Formation (South China) and their potential paleoclimatic implications. Geology 45 (2), 115–118.
Willman, S., Moczydłowska, M., 2008. Ediacaran acritarch biota from the Giles 1 drillhole, Officer Basin, Australia, and its potential for biostratigraphic correlation. Precambrian Research 162, 498–530.
Willman, S., Moczydłowska, M., 2011. Acritarchs in the Ediacaran of Australia - Local or global significance? Evidence from the Lake Maurice West 1 drillcore. Review of Palaeobotany and Palynology 166, 12–28.
Willman, S., Moczydłowska, M., Grey, K., 2006. Neoproterozoic (Ediacaran) diversification of acritarchs: A new record from the Murnaroo 1 drillcore, eastern Officer Basin, Australia. Review of Palaeobotany and Palynology 139, 17–39.
Woltz, C.R., Porter, S.M., Agić, H., Dehler, C.M., Junium, C.K., Riedman, L.A., Hodgskiss, M.S.W., Wörndle, S., Halverson, G.P., 2021. Total organic carbon and the preservation of organic-walled microfossils in Precambrian shale. Geology 49, 556–560.
Xiao, S., 2004. New multicellular algal fossils and acritarchs in Doushantuo chert nodules (Neoproterozoic, Yangtze Gorges, South China). Journal of Paleontology 78, 393–401.
Xiao, S., Knoll, A.H., 1999. Fossil preservation in the Neoproterozoic Doushantuo phosphorite Lagerstätte, South China. Lethaia 32, 219–240.
Xiao, S., Knoll, A.H., 2000. Phosphatized animal embryos from the Neoproterozoic Doushantuo Formation at Weng'an, Guizhou, South China. Journal of Paleontology 74, 767–788.
Xiao, S., Knoll, A.H., Zhang, L., Hua, H., 1999. The discovery of *Wengania globosa* in Doushantuo phosphorites in Chadian, Shaanxi Province. Acta Micropalaeontologica Sinica 16, 259–266.
Xiao, S., McFadden, K.A., Peek, S., Kaufman, A.J., Zhou, C., Jiang, G., Hu, J., 2012. Integrated chemostratigraphy of the Doushantuo Formation at the northern Xiaofenghe section (Yangtze Gorges, South China) and its implication for Ediacaran stratigraphic correlation and ocean redox models. Precambrian Research 192–195, 125–141.
Xiao, S., Narbonne, G.M., 2020. The Ediacaran Period. In: Gradstein, F.M., Ogg, J.G., Schmitz, M.D., Ogg, G.M. (Eds.), Geologic Time Scale 2020 (Volume 1). Elsevier, Oxford, pp. 521–561.
Xiao, S., Schiffbauer, J.D., 2009. Microfossil phosphatization and its astrobiological implications. In: Seckbach, J., Walsh, M. (Eds.), From Fossils to Astrobiology. Springer-Verlag, New York, pp. 89–117.
Xiao, S., Schiffbauer, J.D., McFadden, K.A., Hunter, J., 2010. Petrographic and SIMS pyrite sulfur isotope analyses of Ediacaran chert nodules: Implications for microbial processes in pyrite rim formation, silicification, and exceptional fossil preservation. Earth and Planetary Science Letters 297, 481–495.
Xiao, S., Yuan, X., Steiner, M., Knoll, A.H., 2002. Macroscopic carbonaceous compressions in a terminal Proterozoic shale: A systematic reassesment of the Miaohe Biota, South China. Journal of Paleontology 76, 347–376.
Xiao, S., Zhang, Y., Knoll, A.H., 1998. Three-dimensional preservation of algae and animal embryos in a Neoproterozoic phosphorite. Nature 391, 553–558.
Xiao, S., Zhou, C., Liu, P., Wang, D., Yuan, X., 2014. Phosphatized acanthomorphic acritarchs and related microfossils from the Ediacaran Doushantuo Formation at Weng'an (South China) and their implications for biostratigraphic correlation. Journal of Paleontology 88, 1–67.
Xiao, S., Narbonne, G.M., Zhou, C., Laflamme, M., Grazhdankin, D.V., Moczydlowska-Vidal, M., Cui, H., 2016. Towards an Ediacaran Time Scale: Problems, Protocols, and Prospects. Episodes 39, 540–555.
Xiao, S., Yuan, X., Knoll, A.H., 2000. Eumetazoan fossils in terminal Proterozoic phosphorites? Proceedings of the National Academy of Sciences, U.S.A., 97, 13684–13689.
Xiao, S., Jiang, G., Ye, Q., Ouyang, Q., Banerjee, D.M., Singh, B.P., Muscente, A.D., Zhou, C., Hughes, N.C., 2022. Integrated acritarch biostratigraphy and $\delta^{13}C$ chemostratigraphy of the early Ediacaran Krol A Formation, Lesser Himalaya, northern India. Journal of Paleontology. https://doi.org/10.1017/jpa.2022.7.
Xie, G., Zhou, C., McFadden, K.A., Xiao, S., Yuan, X., 2008. Microfossils discovered from the Sinian Doushantuo Formation in the Jiulongwan section, East Yangtze Gorges area, Hubei Province, South China. Acta Palaeontologica Sinica 47, 279–291.
Xue, Y., Tang, T., Yu, C., 1992. Discovery of the oldest skeletal fossils from upper Sinian Doushantuo Formation in Weng'an, Guizhou, and its significance. Acta Palaeontologica Sinica 31, 530–539.
Xue, Y., Tang, T., Yu, C., Zhou, C., 1995. Large spheroidal chlorophyta fossils from the Doushantuo Formation phosphoric sequence (late Sinian), central Guizhou, South China. Acta Palaeontologica Sinica 34, 688–706.
Yakshchin, M.S., Luchinina, V.A., 1981. Novye dannye po iskopaemym vodorosliam semeistva Oscillatoriaceae (Kirchn.) Elenkin [New data on fossil algae in Family Oscilliatoriacea (Kirchn.) Elenkin]. In: Meshkova, N.P., Nikolaeva, I.V. (Eds.), Pogranichnye otlozhenyia Dokembryia i Kembryia Cibirskoi platformi.
Yan, Y., 1982. *Scizofusa* from the Chuanlinggou Formation of Changcheng System in Jixian County. Bulletin, Tianjin Institute of Geology and Mineral Resources 6, 1–7.
Yan, Y., 1986. The tubular algal fossils from the Xiamaling Formation in Jixian County. Bulletin of Tianjin Institute of Geology and Mineral Resources 16, 165–169.
Yang, C., Rooney, A.D., Condon, D.J., Li, X., Grazhdankin, D.V., Bowyer, F.T., Hu, C., Macdonald, F.A., Zhu, M., 2021. The tempo of Ediacaran evolution. Science advances 7, eabi9643.
Yang, L., Pang, K., Chen, L., Zhong, Z., Yang, F., 2020. New materials of microfossils from the Ediacaran Doushantuo Formation in Baizhu phosphorite deposit, Baokang, Hubei provience. Acta Palaeontologica Sinica 37, 1–20.
Ye, Q., Tong, J., An, Z., Hu, J., Tian, L., Guan, K., Xiao, S., 2019. A systematic description of new macrofossil material from the upper Ediacaran Miaohe Member in South China. Journal of Systematic Palaeontology 17, 183–238.
Ye, Q., Tong, J., An, Z., Tian, L., Zhao, X., Zhu, S., 2015. Phosphatized fossil assemblage from the Ediacaran Doushantuo Formation in Zhangcunping area, Yichang, Hubei Province. Acta Palaeontologica Sinica 54, 43–65.
Yin, C., Tang, F., Liu, P., Gao, L., Wang, Z., Chen, S., 2009a. New advances in the study of biostratigraphy of the Sinian (Ediacaran) Doushantuo Formation in South China. Acta Geoscientica Sinica 30, 421–432.
Yin, C., 1999. Microfossils from the Upper Sinian (Late Neoproterozoic) Doushantuo Formation in Changyang, western Hubei, China. Continental Dynamics 4, 1–18.
Yin, C., Liu, G., 1988. Micropaleofloras. In: Zhao, Z., Xing, Y., Ding, Q., Liu, G., Zhao, Y., Zhang, S., Meng, X., Yin, C., Ning, B., Han, P. (Eds.), The Sinian System of Hubei. China University of Geosciences Press, Wuhan, pp. 170–180.
Yin, C., Liu, P., Awramik, S.M., Chen, S., Tang, F., Gao, L., Wang, Z., Riedman, L.A., 2011a. Acanthomorph biostratigraphic succession of the Ediacaran Doushantuo Formation in the East Yangtze Gorges, South China. Acta Geologica Sinica (English Edition) 85, 283–295.
Yin, C., Liu, P., Chen, S., Tang, F., Gao, L., Wang, Z., 2009b. Acritarch biostratigraphic succession of the Ediacaran Doushantuo Formation in the Yangtze Gorges. Acta Palaeontologica Sinica 48, 146–154.
Yin, C., Liu, P., Gao, L., Tang, F., Chen, S., 2009c. New data of phosphatized microfossils from the Doushantuo Formation in Baizhu, Baokang County, Hubei Province, and their stratigraphic implications. Acta Geoscientica Sinica 30, 447–456.
Yin, C., Liu, Y., Gao, L., Wang, Z., Tang, F., Liu, P., 2007a. Phosphatized Biota in Early Sinian (Ediacaran) – Weng'an Biota and Its Environment. Geological Publishing House, Beijing.
Yin, L., 1987. Microbiotas of latest Precambrian sequences in China, in: Nanjing Institute of Geology and Palaeontology Academica Sinica (Ed.), Stratigraphy and Palaeontology of Systemic Boundaries in China: Precambrian–Cambrian Boundary (1). Nanjing University Press, Nanjing, pp. 415–494.
Yin, L., Zhu, M., Knoll, A.H., Yuan, X., Zhang, J., Hu, J., 2007b. Doushantuo embryos preserved inside diapause egg cysts. Nature 446, 661–663.
Yin, L., Wang, D., Yuan, X., Zhou, C., 2011b. Diverse small spinose acritarchs from the Ediacaran Doushantuo Formation, South China. Palaeoworld 20, 279–289.
Yuan, X., Hofmann, H.J., 1998. New microfossils from the Neoproterozoic (Sinian) Doushantuo Formation, Weng'an, Guizhou Province, southwestern China. Alcheringa 22, 189–222.
Yuan, X., Wang, Q., Zhang, Y., 1993. Late Precambrian Weng'an Biota from Guizhou, southwest China. Acta Micropalaeontologica Sinica 10, 409–420.
Yuan, X., Xiao, S., Yin, L., Knoll, A.H., Zhou, C., Mu, X., 2002. Doushantuo Fossils: Life on the Eve of Animal Radiation. China University of Science and Technology Press, Hefei, China.
Zang, W., Walter, M.R., 1992a. Late Proterozoic and Cambrian microfossils and biostratigraphy, Amadeus Basin, central Australia. The Association of Australasia Palaeontologists Memoir 12, 1–132.
Zang, W., Walter, M.R., 1992b. Late Proterozoic and Early Cambrian microfossils and biostratigraphy, northern Anhui and Jiangsu, central-eastern China. Precambrian Research 57, 243–323.
Zhang, Y., 1989. Multicellular thallophytes with differentiated tissues from late Proterozoic phosphate rocks of South China. Lethaia 22, 113–132.
Zhang, Y., Yin, L., Xiao, S., Knoll, A.H., 1998a. Permineralized fossils from the terminal Proterozoic Doushantuo Formation, South China. Journal of Paleontology 72 (supplement to No. 4), 1–52.
Zhang, Y., Yuan, X., Yin, L., 1998b. Interpreting Late Precambrian microfossils. Science 282, 1783.
Zhang, Y., Zhang, X., 2017. New *Megasphaera*-like microfossils reveal their reproductive strategies. Precambrian Research 300, 141–150.
Zhang, Y., Pufahl, P.K., Du, Y., Chen, G., Liu, J., Chen, Q., Wang, Z., Yu, W., 2019. Economic phosphorite fromthe Ediacaran Doushantuo Formation, South China, and the Neoproterozoic-Cambrian Phosphogenic Event. Sedimentary Geolody 388, 1–19.
Zhang, Z., 1984a. A new microphytoplankton species from the Sinian of western Hubei Province. Acta Botanica Sinica 26, 94–98.
Zhang, Z., 1984b. On the occurrence of *Obruchevella* from the Doushantuo Formation (late Sinian) of western Hubei and its significance. Acta Palaeontologica Sinica 23 (4), 447–451.
Zhang, Z., 1985. Coccoid microfossils from the Doushantuo Formation (Late Sinian) of South China. Precambrian Research 28, 163–173.
Zhang, Z., 1986. New material of filamentous fossil cyanophytes from the Dushantuo Formation (Late Sinian) in the eastern Yangtze Gorges. Scientia Geologica Sinica 21, 30–37.
Zhou, C., Brasier, M.D., Xue, Y., 2001. Three-dimensional phosphatic preservation of giant acritarchs from the terminal Proterozoic Doushantuo Formation in Guizhou and Hubei provinces, South China. Palaeontology 44, 1157–1178.

Zhou, C., Chen, Z., Xue, Y., 2002. New microfossils from the late Neoproterozoic Doushantuo Formation at Chaoyang phosphorite deposit in Jiangxi Province, South China. Acta Palaeontologica Sinica 41, 178–192.
Zhou, C., Xiao, S., 2007. Ediacaran $\delta^{13}C$ chemostratigraphy of South China. Chemical Geology 237, 89–108.
Zhou, C., Xie, G., McFadden, K., Xiao, S., Yuan, X., 2007. The diversification and extinction of Doushantuo-Pertatataka acritarchs in South China: Causes and biostratigraphic significance. Geological Journal 42, 229–262.
Zhou, C., Xie, G., Xiao, S., 2005. New fossils from the Neoproterozoic Doushantuo Formation at Zhangcunping, Hubei Province. In: The 9th National Meeting and the 21st Annual Meeting of the Chinese Paleontological Society, pp. 15–16.
Zhou, C., Yuan, X., Xiao, S., Chen, Z., Xue, Y., 2004. Phosphatized fossil assemblage from the Doushantuo Fromation in Baokang, Hubei Province. Acta Micropalaeontologica Sinica 21, 349–366.
Zhou, C., Xiao, S., Wang, W., Guan, C., Ouyang, Q., Chen, Z., 2017a. The stratigraphic complexity of the middle Ediacaran carbon isotopic record in the Yangtze Gorges area, South China, and its implications for the age and chemostratigraphic significance of the Shuram excursion. Precambrian Research 288, 23–38.
Zhou, C., Li, X., Xiao, S., Lan, Z., Ouyang, Q., Guan, C., Chen, Z., 2017b. A new SIMS zircon U-Pb date from the Ediacaran Doushantuo Formation: age constraint on the Weng'an biota. Geological Magazine 154 (6), 1193–1201.
Zhu, M., Lu, M., Zhang, J., Zhao, F., Li, G., Yuan, A., Zhao, X., Zhao, M., 2013. Carbon isotope chemostratigraphy and sedimentary facies evolution of the Ediacaran Doushantuo Formation in western Hubei, South China. Precambrian Research 225, 7–28.
Zhu, M., Zhang, J., Yang, A., 2007. Integrated Ediacaran (Sinian) chronostratigraphy of South China. Palaeogeography Palaeoclimatology Palaeoecology 254, 7–61.